Development of aptasensors for malaria using *Plasmodium falciparum* Glutamate dehydrogenase as target antigen.

A thesis

Submitted by

Naveen Kumar Singh

For the award of the degree

Of

Doctor of Philosophy

Department of Biosciences and Bioengineering

Indian Institute of Technology Guwahati

Guwahati – 781039, Assam, India

January, 2019

INDIAN INSTITUTE OF TECHNOLOGY GUWAHATI

Department of Biosciences and Bioengineering

Guwahati - 781039

STATEMENT

I do hereby declare that the matter embodied in this thesis is the result of investigations carried out by me in the Department of Biosciences and Bioengineering, Indian Institute of Technology Guwahati, Assam, India, under the guidance of Prof. Pranab Goswami.

In keeping with the general practice of reporting scientific observations, due acknowledgements have been made wherever the work described is based on the findings of other investigators.

January, 2019

Naveen Kumar Singh

INDIAN INSTITUTE OF TECHNOLOGY GUWAHATI

Department of Biosciences and Bioengineering

Guwahati - 781 039, India

Phone: +91-361-2582202(Office)

Fax: +91-361-2582249 (Office)

E-mail: pgoswami@iitg.ernet.in

Pranab Goswami, PhD

Professor (Higher Academic Grade)

CERTIFICATE

It is certified that the work described in this thesis, entitled "**Development of aptasensor for malaria using *Plasmodium falciparum* Glutamate dehydrogenase as target antigen**", performed by Naveen Kumar Singh for the award of degree of Doctor of Philosophy is an authentic record of the results obtained from the research work carried out under my supervision, in the Department of Biosciences and Bioengineering, Indian Institute of Technology Guwahati India. The results embodied in this thesis have not been submitted to any other University or Institute for the award of any degree.

Prof. Pranab Goswami, Ph.D

(Supervisor)

Acknowledgement

This PhD work presented here would not have been possible without the support of many people and I am truly indebted and thankful to all those who have contributed their time and effort throughout my journey of completing PhD.

I would like to extend my deepest gratitude towards my thesis advisor ***Prof. Pranab Goswami*** for mentoring me to think like a researcher and teaching me to never lose my patience. His esteemed guidance, advice and encouragement at every step has helped me to propel my work in a fruitful direction. His optimism and down to earth nature has kept me grounded and made this journey much bearable and memorable. I would also like to thank him for the well-equipped laboratory, vast resources and dedicated work culture that has made working in his laboratory a pleasant experience.

I would also like to extend my gratitude towards my doctoral committee members ***Dr. Biplab Bose*** , ***Dr. S. P Kanaujia***, and ***Dr. A. K Saikia*** for their critical assessments and valuable suggestions that helped me focus on the weaker areas of my research.

I gratefully acknowledge ***Dr. Pedro Estrela,*** University of Bath, Bath, U. K for providing me his guidance and allowing me to work in his lab. I would also like to thank, ***Dr Pawan, Dr Sunil, Dr. Wong, Dr. Shiva Serife, Jahnavi, Emily, Bryony*** **and** ***Ben***, for making Biosensor (C3B) lab a perfect work environment. Indeed, it has become my second lab like home, all because of you people.

During this work I had great time with our research group who have helped me as well as cheered me during my hard days. I would like to give my warm thanks to my fellow lab members ***Phurpa***, ***Lightson***, ***Sharbani, Priyanki, Pooja, Abdul, Vinay, Smita, Caraline*** and ***Mrinal bhaiya*** for their constant support professionally and emotionally.

Special thanks to my seniors ***Mitun***, ***Babina, Priyamvada***, ***Ankana***, ***Santhosh, Madhuri***, ***Urimla***, ***Seeraj*** and ***Reddy Bhaiya*** for guiding me well around the laboratory. Also to my beloved juniors, ***Torsha***, ***Farhan***, ***Anil***, ***Naveen*** and ***Sanjay*** to brighten up my days with their youthful energy.

Along with this I wish to extend my appreciation to the staff members of ***Dept. BSBE***, ***CIF*** and ***COE*** for their technical support.

I would also like to acknowledge my friends and seniors from BITS Pilani, who have always brightened my days, enriched my career and cheered my heart during hard days. I would like to especially thank to seniors ***Dr. Zerna, Dr. Gagandeep, Dr. Panchsheela, Dr. Isha, Dr. Kuldeep, Dr. Mithlesh*** and ***Dr. Gurpreet kaur*** for sharing and providing constant support during stressed phases of PhD. I would also like to thanks my friends from BITS ***Shubhendu, Saif, Amarto, Soumya*** **and** ***Shubha*** who gave me the best memories of my life in BITS and made me realize what friends for life are meant.

I also want to appreciate constant support of my friends in IIT Guwahati ***Himali***, ***Tripathi, Ankur, Vikky, Naresh, Rishi, Anupama, JK*** and ***Dr. Mohitosh***, who cherished my life with happiness and support during rough time and I shared numerous memories, parties and moments of both happiness and sadness with them. You people are among the few connected to me by soul. I want to take this opportunity to thank you all for the best of times we have had together and also that I owe you people big time for making my time here at IIT an all the more memorable.

My love to the Department of BSBE, IIT Guwahati the locus of my nostalgia that has given the shape and charge to my dreams of becoming a researcher in the field of science. My journey as a M. tech. student and scholar in the Department of BSBE has been a tough game, a great experience and a pleasant memory. The indelible mark that has been etched

on boy is there to remain forever. Maybe, a part of the boy inside has now transformed into a man, a professional, a better human being. Cheers to the department.

At the very end, I express my profound debt to my family members, to ***Papa***, ***Maa*** who kept on encouraging me to pursue this path. A Ph.D is simultaneous and intensely solipsistic and collective exercise. Without the help of these people and many more whom I had not been able to mention, this research would have been impossible. Thank you for sharing my journey.

Naveen Kumar Singh
January, 2019

Table of Contents

Abstract

The current investigation focuses on the development of specific aptamer against *Plasmodium falciparum* glutamate dehydrogenase (*Pf*GDH) with an aim of developing novel malaria diagnostic platforms well-endowed with efficient biosensing parameters such as sensitivity, specificity and stability. For generating specific aptamer against *Pf*GDH, we selected recombinant *Pf*GDH as target antigen and human glutamate dehydrogenase (*H*GDH) as control protein. Both these proteins were cloned and expressed in BL21 (DE3) pLysS bacterial cells. The structural and functional integrity of the expressed proteins were confirmed by various physical and enzymatic methods. We performed systemic evaluation of ligand by exponential enrichment (SELEX) technique and developed a novel specific ssDNA aptamer (NG3) against *Pf*GDH. The *Pf*GDH binding affinity of the developed aptamer as discerned by circular dichroism (CD) and surface plasmon resonance spectroscopy (SPR) were 0.5 ± 0.04 μM, 79.16 ± 1.58 nM, respectively. The specificity of the 90 mer long aptamer towards the target was confirmed by gel electrophoresis and CD studies. The presence of two quadruplex forming regions, two big and four small stem loop structures of aptamer with a ΔG of -7.99 kcal mole^{-1} were deduced by computational studies. The developed aptamer was utilized in four different independent approaches for detection of *Pf*GDH in serum samples. (A) Protein induced fluorescence enhancement based detection of *Pf*GDH (B) Development of capacitive aptasensor for *Pf*GDH (C) Development of aptaFET sensor based and extended gate field effect transistor for *Pf*GDH detection and lastly (D) Instrument based or instrument free detection of *Plasmodium* lactate dehydrogenase (*P*LDH) and *Pf*GDH in serum samples following optical transduction principles.

(A) *Protein induced fluorescence enhancement based detection of PfGDH*

In this approach spherical carbon dots (Cdots) of size 2 - 4 nm were synthesized by pyrolysis method using L-Glutamate as a substrate. The synthesised Cdots were covalently allied to the amine modified aptamer. The Cdot with a band gap of 2.8 eV and a quantum yield of 34 % produced fluorescence at ~ $\lambda_{410\ nm}$ when excited at $\lambda_{320\ nm}$. The quantum yield of Cdot-aptamer assembly was increased upto 40 % in presence of the *Pf*GDH in solution. A linear relationship with a dynamic range of 0.5 nM to 25 nM (R^2 = 0.98) and a limit of detection (LOD) of 0.48 nM was discerned between the fluorescence intensity of the Cdots-aptamer conjugate and the concentration of *Pf*GDH. The method could detect *Pf*GDH with an LOD of 2.85 nM in diluted serum sample. This novel simple, sensitive and specific protein induced

fluorescence enhancement based detection of *Pf*GDH has a great potential to develop as a method for malaria detection.

(B) *Development of capacitive aptasensor for PfGDH*

A highly sensitive and selective capacitive aptasensor for detecting *Pf*GDH, directly in human serum samples was developed. The thiolated aptamer was used for the development of an aptasensor against *Pf*GDH using a non-Faradaic electrochemical impedance based signal transduction technique by monitoring the capacitance response at a frequency of 2 Hz. The aptasensor exhibited a wide dynamic range of 100 fM - 100 nM. The LOD obtained for the aptasensor were 0.43 pM in buffer and 0.77 pM in serum samples. The developed aptasensor exhibited low interferences from other predominant malarial biomarkers, namely, *P*LDH and Histidine rich protein-II (HRP-II) in spiked serum samples. This *Pf*GDH aptasensor with label free detection capability has great application potential for diagnosis of asymptotic malaria and monitoring the regression of malaria during treatment regime with antimalarial drugs.

(C) *Development of aptaFET sensor based on extended gate field effect transistor for PfGDH detection*

There has been a continuous strive to develop portable, stable, sensitive and low cost detection system for malaria to meet the demand of effective screening actions in developing countries where the disease is most endemic. In this work an aptamer-based field effect transistor (aptaFET) biosensor was developed by using an extended gate field effect transistor with inter-digitated gold microelectrodes (IDµE) for the detection of *Pf*GDH in serum samples. The NG3 was used in the aptaFET to capture the target protein. The intrinsic surface net charge of the captured protein led to change in gate potential of the aptaFET device, which could be correlated to the concentration of the protein. This biosensor exhibited a sensitive response in broad dynamic range of 100 fM - 10 nM with limits of detection of 16.7 pM and 48.6 pM in spiked buffer and serum samples, respectively. The high selectivity of the biosensor for *Pf*GDH was verified by testing relevant analogous human and parasitic proteins on the device. Overall, the results validated the application potential of the developed aptaFET for diagnosis of both symptomatic and asymptomatic malaria.

(D) *Instrument based and instrument free detection of Plasmodium lactate dehydrogenase (PLDH) and PfGDH in serum samples following optical transduction principles.*

In this work we have developed simple tests for malaria diagnosis based on capture of *P*LDH and *Pf*GDH parasitic enzymes from serum with the help of P38 and NG3 aptamer decorated magnetic beads, respectively. The captured *P*LDH and/or *Pf*GDH target enzymes were confirmed by resazurin dye based couple reaction, which was initiated by the transformed co-factors (APAD/ NADP) of the captured *P*LDH and *Pf*GDH enzymes. The tests have potential for pan specific (*P. vivax*, *P. malaria* etc.) and species specific *P. falciparum* detection of malaria based on selective capture of *P*LDH and *Pf*GDH biomarkers, respectively. This method offers dual approach, one is instrument based (Fluorescence or UV-Vis spectrophotometer) method while the other one is an instrument free optical method for point of care (POC) application. For the point of care instrument free diagnostic approach, a routine medical syringe, prefabricated with magnet and surface functionalized paper wick was used to produce *in-situ* noise free colorimetric response over paper wick. The developed methods exhibited LOD in picomolar range and could detect each of the target enzymes (*P*LDH, *Pf*GDH) in a broad linear dynamic range of 1 pM – 100 nM in undiluted serum conditions. The developed methods are simple and sensitive bearings potential to generate a low cost quantitative malaria diagnostic device.

List of Abbreviations

ACT	Artemisinin combination therapy
AFM	Atomic force microscopy
AgNP	Silver nanoparticle
AKD	Alkyl Ketene Dimer
ANG	Angipoietin
AO	Acridine orange
APAD	3-Acety pyridine adenine dinucleotide
APADH	3-Acety pyridine adenine dinucleotide hydrate
ATP	Adenosine triphosphate
Au	Gold
AuNP	Gold nanoparticle
BSA	Bovine serum albumin
BB	Binding buffer
CD	Circular Dichroism
Cdot	Carbon dot
CDC	Centers for disease control and prevention
CM	Cerebral malaria
COE	Centre for instrument facility
CPE	Constant phase element
CSF	Cerebrospinal fluid
CV	Cyclic voltammetry
CXCL	Chemokine interferon inducible protein
DBT	Department of biotechnology

DNA	Deoxyribonucleic acid
DMSO	Dimethyl sulfoxide
Dl	Double layer
DSP	Dithiobis(succinimidyl propionate)
DTT	Dithiothreitol
EDTA	Ethylenediaminetetraacetic acid
EIS	Electrochemical impedance spectroscopy
EgFET	Extended gate field effect transistor
ELISA	Enzyme linked immunosorbent assay
EMSA	Electrophoretic mobility shift assay
EPO	Erythropoietin
FACS	Fluorescence activated cell sorting
FCM	Flow cytometry
FET	Field effect transistor
FTIR	Fourier transform infrared spectroscopy
FRET	Fourier resonance energy transfer
G6PD	Glucose 6-phosphate dehydrogenase
GO	Graphene oxide
GS	Glutathione
GSAgNPs	Glutathione coated silver nanoparticles
GSK	GlaxoSmithKline
GTS	Giemsa thick smear
GTTS	Giemsa thick and thin smear
HEPES	(4-(2-hydroxyethyl)-1-piperazineethanesulfonic acid)

His	Histidine
HisRPs	Histidine rich proteins
HGDH	Human glutamate dehydrogenase
HLDH	Human lactate dehydrogenase
HPLC	High performance liquid chromatography
HRP-II	Histidine rich protein II
HSA	Human serum albumin
ICAM	Intracellular adhesion molecule
ICT	Immunochromatography tests
IFA	Immunofluorescence antibody testing
IHEC	Institute human ethics committee
IL	Interleukin
IPTG	Isopropyl β-D-1-thiogalactopyranoside
iRBC	Infected red blood cells
IgM	Mouse monoclonal antibody
ITC	Isothermal titration calorimetry
LAMP	Loop mediated isothermal amplification
LB	Luria Bertani
LDH	Lactate dehydrogenase
LDMS	Laser desorption mass spectrometry
LOD	Limit of detection
LSPR	Localized surface plasmon resonance
mAb	Monoclonal antibody
MB	Magnetic bead

MM	Mild malaria
MP	Microparticle
MQ	Milli-Q
MVI	Malaria Vaccine Initiative
MWCNT	Multiwalled carbon nanotube
NAD	Nicotinamide adenine dinucleotide
NADH	Nicotinamide adenine dinucleotide reduced
NADP	Nicotinamide adenine dinucleotide phosphate
Ni-NTA	Nickel Nitrilotriacetic acid
OD	Optical density
ORF	Open reading frame
PES	Phenazine etho sulphate
PAGE	Polyacrylamide gel electrophoresis
PBS	Phosphate buffered saline
PCR	Polymerase chain reaction
PDB	Protein data bank
PIFE	Protein induced fluorescence enhancement
*Pf*EMP1	*P. falciparum* erythrocyte membrane protein 1
*Pf*GDH	*Plasmodium falciparum* glutamate dehydrogenase
*Pf*LDH	*Plasmodium falciparum* lactate dehydrogenase
PmLDH	*Plasmodium malariae* lactate dehydrogenase
POC	Point of care
PLIP	Protein-ligand interaction profile
PVDF	Polyvinylidene fluoride

QBC	Quantitative buffy coat
QD	Quantum dots
RBC	Red blood cell
RDT	Rapid diagnostic test
RMSD	Root mean square deviation
RNA	Ribonucleic acid
RSD	Relative standard deviation
RT	Room temperature
SAM	Self assembled monolayer
SB	Starting blocking buffer
SD	Standard deviation
SDS	Sodium dodecyl sulfate
SELEX	Systematic evolution of ligands by exponential enrichment
SERS	Surface enhanced raman spectroscopy
SAHRP	Small histidine-alanine-rich protein
sFas	Soluble Fas ligand
SM	Severe malaria
SPR	Surface plasmon resonance
ssDNA	Single stranded DNA
sTNF-R	Soluble tumour necrosis factor receptor
TAE	Tris acetate EDTA
TBE	Tris borate EDTA
TEM	Transmission electron microscopy
TSS	Transformation and storage solution

USD	United States dollars
UV	Ultra violet
V_{gs}	Gate to source voltage
V_{ds}	Drain to source voltage
WB	Western blot
WHO	World health organization
μPAD	Microfluidic paper based analytical device
XRD	X-ray diffraction spectroscopy

List of Symbols

%	Percent
~	Approximately
<	Lesser than
=	Equal to
>	Greater than
≥	Greater than equal to
°C	Degree Celsius
C_{dl}	Double layer capacitance
µA	Microampere
µcal	Microcalorie
µg	Micrograms
µl	Microliter
µM	Micromolar
µmole	Micromole
2D	Two dimensional
3D	Three dimensional
A	Ampere
Å	Angstrom
a.u.	Arbitrary units
bp	Basepair
cal	Calorie
cm	Centimeter
Da	Dalton

ε	Extinction coefficient
fM	Femto molar
g	Grams
h	Hour
I_d	Drain current
Hz	Hertz
Ka	Association constant
kb	Kilobasepair
kcal	Kilocalorie
Kd	Dissociation constant
kDa	Kilodalton
kHz	Kilohertz
kV	Kilovolt
L	Liter
M	Molarity
mA	Milliampere
mdeg	Millidegree
mg	Milligrams
min	Minute
ml	Milliliter
mM	Millimolar
mm	Millimeter
mV	Millivolt
mV	Millivolt

Mw	Molecular weight
MΩ	Mega ohm
N	Normality
n	No. of binding sites
ng	Nanograms
nM	Nanomolar
nm	Nanometer
Nmole	Nanomole
Pg	Picograms
Pm	Picomolar
pmole	Picomole
R^2	Regression coefficient
R_{ct}	Charge transfer resistance
Rpm	Revolutions per minute
Rs	Solution resistance
S	Second
T	Temperature
V	Volt
V_{th}	Threshold voltage
v/v	Volume/volume
w/v	Weight/volume
Wt	Weight
X	Times concentrated
g	Centrifugation speed in RCF

Zw	Warburg impedance
ΔG	Change in free energy
ΔH	Change in enthalpy
ΔS	Change in entropy
λ	Lambda (unit of wavelength)
λ_d	Debye length
τ	Fluorescence lifetime
Ω	Ohm

List of Figures

List of Tables

INTRODUCTION

Somewhere, Something incredible
is waiting to be known.

- Carl Sagan

Introduction

Malaria is a third leading cause of death globally in the category of infectious disease. A total 216 million cases of malaria were detected from 91 countries in the year of 2016. Nearly 89 % of the cases were reported from African region, and rest of the cases were mostly from South East Asian countries and Mediterranean region (World Malaria Report, 2017). Among the South East Asian countries, ~ 75 % of the malaria cases were reported from India. Again, out of the total cases from India, 80 % were reported from remote and village locations. A continuous effort has been made over the last few decades to eradicate malaria as evident from the intensive research and development (R&D) activities on various aspects of therapy and diagnosis of this vector borne disease. Malaria caused by *Plasmodium falciparum* species is the most dreaded one causing highest rates of morbidity and mortality (World malaria report 2016). One of the growing challenges encountered in the malaria eradication programme is the rise of multi drug resistance (MDR) *Plasmodium* strains, mostly, belonging to the species *P. falciparum*. The first drug resistance was reported in Southeast Asia, Oceania and South America during 1950-60. Since then it has been spreading across the globe. There has been a rising concern on the asymptomatic form of malaria as well that occurs due to partial immunity developed against the *Plasmodium* parasite (Lindblade *et al.,* 2013). The asymptomatic form of malaria is not an immediate threat to the patients, but if ignored it may generate inflammatory response, anaemia and muscles impairment (Chen *et al.,* 2016). Furthermore, the asymptomatic populations may act as infectious reservoir in endemic as well as non-endemic locations. In the recent past, a vaccine named as Mosquirix™ also known as RTS,S/AS01 was developed by PATH Malaria vaccine initiative and Glaxo SmithKline (GSK) with the support from the Bill and Melinda Gates foundation. However, the effectiveness of the vaccine could not be properly validated so far. For monitoring and curbing the disease, efficient diagnostic methods and tools are essential.

There are many malaria diagnosis methods supported by microscopy, PCR, ELISA, LAMP etc. in the laboratory settings available. These methods are though reliable and sensitive, they are time consuming, instrument dependent, expensive and require skilled manpower. There is a great demand for a portable, reliable and inexpensive malaria diagnostic sensor or kit with an additional capability to distinguish the disease causing parasite species, particularly *P. falciparum*, for using in point of care (POC) and resource limited environments. This will cater timely treatment of the patients with appropriate

medicine for this life-threatening disease occurring mostly in tropical countries with poor healthcare facilities. There are several portable diagnostic kits developed for using in POC settings. Among these kits, the lateral flow format based rapid detection tests (RDTs) are widely used in POC and malaria endemic remote locations. Although these antibody-based RDTs have substantially reduced the clinical burden on malaria diagnosis, the tests suffers from many drawbacks among which, non-quantitative, limited species differentiation capability, poor performance in hot and humid climate, and variability of results are prominent which prompted to explore more efficient low cost portable detection system for malaria (Mouatcho and Goldring, 2013).

Based on an intensive literature survey we identified four critical issues, reliable biomarker, stable recognition molecule, sensitive signal transduction system, and low cost fabrication technology that ought to be addressed for developing a portable device, which can surpass the drawbacks of the currently available RDTs. In order to develop an efficient malaria diagnosis test, a deep understanding on various malaria biomarkers is essential. Most of the RDTs currently available in the global market target either pan malaria biomarker *P*LDH or species specific biomarker *Pf*HRP-II (Jain *et al* 2014). However, there is a rising frequency of HRP II gene deletions primarily in Amazon regions and in many African countries that demand a test for non-HRP II *P. falciparum*-specific targets (Bharti *et al.* 2016). In this regard *Pf*GDH (EC no. 1.4.1.4; PlasmoDB accession no.PF3D7_1416500) may be projected as an alternative malaria biomarker for specific detection of the *P. falciparum*-specific antigen. The strength of this *Pf*GDH biomarker is founded by the fact that the host counterpart of this enzyme, the human glutamate dehydrogenase (*H*GDH), is not present in the human erythrocyte where *Pf*GDH is released by the parasite. Moreover, it has some distinctive structural, compositional and functional features from the *H*GDH. This homo-hexameric protein (Mw 49.5 kDa per subunit) shares only 23 % overall amino acid sequence identity with HGDH and 69 % match with *Plasmodium vivax* GDH. *Pf*GDH is present in soluble form throughout the sexual and asexual stages of the parasite development and is present in significant quantity in the blood serum of the malaria patients (Dominguez and Acosta, 1996).

Various antigen recognition systems as alternative to the existing antibodies for POC malaria diagnosis have been reported (Chakma., *et al*. 2016; Lee., *et al.* 2014; Gulka *et al.,* 2014). Each of these methods however, has its own merits and demerits such as, low specificity, poor sensitivity and technical complexities in the analysis. Among the new generation of biorecognition systems, aptamers have drawn special attentions owing to

their certain properties that fair well over the conventional antibody based systems for developing biosensors and bio detection systems. The advantages commonly being attributed to aptamers over antibodies are their easy synthesis, thermal stability, high shelf life, scope for chemical modification to enhance the target selectivity, and wider target range from metal ions to bacterial cells (Hicke and Stephens, 2000). The nucleic acid aptamers are single-stranded oligonucleotides that are selected through an enrichment technique from a pool of oligonucleotide library in presence of the target following a widely acclaimed process called SELEX (Dirkzwager *et al.,* 2016).

In regards to the signal transduction methods we have explored four different approaches. The most important requirement for precise measurement of analytes concentration is the generation of measurable noise free signal from specific bio-recognition event. The specific interaction of target with sensing probe could be transduced to various signal forms among which, the optical signal systems one emerging as a method of choice in the field of biosensor due to their simplicity, simple operation, high sensitivity, scope for real-time analysis of the target in complex mixtures, and requirement of small sample volumes (Yue *et al.,* 2015). Recently, the fluorescence based optical transduction system are imbuing with portable sensors and biosensor owing to the technological improvements in miniaturization of the fluorescence monitoring devices (Malica and Kirk, 2006). On the other hand, the electrochemical transduction systems are always getting preference for commercial application due to their label free detection capabilities, rapid response time and high sensitivity for biosensing application. The capacitance based transduction platform come under the non-faradaic electrochemical impedance spectroscopy. It is a label free approach based on interfacial capacitance developed over the electrode surface as a consequence of surface charge associated with the recognition event (Berggren *et al*., 2001). The capacitance based transduction platform do not require any external redox probe, permitting direct measurement of the target molecule in the sample that makes it a potential system for POC applications (Arya *et al.,* 2018; Luo *et al.,* 2013).

The field effect transistor (FET) is another example of redox free system with non-faradaic electrochemical measurement, which is simple to monitor the reaction occurring between solution and electrode surface based on native charge of the target analytes (Park *et al.,* 2012). Over the last few years, application of FET as transduction platform has received enormous attention for diagnosis of various disease (Aliakbarinodehi *et al.,* 2017). The major driving force for application of FET as sensing device are their high

sensitivity, rapid response time, small size, and established cheap fabrication technology to produce the device in large scale at low cost. In a further development the extended gate field effect transistor (EgFET) has been introduced to enhance the sensitivity and stability of FET for the application of biological sample (Kaisti, 2017). In EgFET, the gate of the sensing chip is extended and immersed to the solution during measurement process, which offer an advantage to easy modification of the gate surface for sensing applications and help to keep dry the transistor region to avoid it malfunction.

In view of the above challenges and projected plans, we conducted a systematic study with the following specific objectives:

1. Preparation and characterization of *Pf*GDH biomarker and all the relevant control proteins through conventional molecular biology techniques and methods**.**
2. Development ssDNA aptamer against *Pf*GDH and their characterizations.
3. Development of *Pf*GDH aptasensors following optical (absorption and fluorescence), capacitive and FET-based signal transduction principles.
4. Detection of pan malaria and *P. falciparum* species based dual detection system for both laboratory settings and portable format.

This thesis has been subdivided into seven chapters as briefly described below. At the end of the chapters, a section describing the overall conclusion from the thesis and a critical evaluation of the work with the scope for future work has been included.

Chapter 1: Literature review

This chapter discusses the recent progress and status of malaria detection methods, with special focus on *Pf*GDH targeted detection. Various conventional malaria detection methods are described and compared these methods with more recent detection platforms to identify the important gaps to be bridged for developing efficient products of practical use.

Chapter 2: Cloning, expression, purification and characterization of *Pf*GDH.

To develop efficient malaria sensor, *Pf*GDH as marker protein and its human counterpart as control protein were cloned, expressed purified and characterized. The cloned ORFs were confirmed through restriction digestion and electrophoresis. The purity and integrity

of expressed proteins were validated through various techniques such as, western blot, enzyme kinetics, circular dichroism spectroscopy and analytical ultracentrifugation studies. A detailed account on the basic findings is incorporated in this chapter.

Chapter 3: Development of aptamer specific for *Pf*GDH and its characterization.

In this chapter, development of specific ssDNA aptamers against *Pf*GDH was accomplished by the process of SELEX, including counter-SELEX against HGDH. The secondary and 3D structures of the evolved aptamer candidates were determined through computational and spectroscopic study. The selected candidates were further investigated to explore their specificity using different tools and techniques such as, EMSA, CD, SPR and docking studies.

Chapter 4: Development of aptamer based fluorometric detection of *Pf*GDH.

This chapter entails the development of a fluorometric assay based on protein induced fluorescence enhancement phenomenon by using carbon dots (Cdots) synthesized from L glutamate through pyrolysis. The synthesised Cdots were characterised through various techniques and then these were covalently attached to the amine modified aptamers. The constructed Cdot-aptamer was used as sensing element for detection of *Pf*GDH in human serum. An effort has been made to elucidate the principle mechanism involved in the detection phenomenon.

Chapter 5: Development of capacitive aptasensor for detection of *Pf*GDH.

The content in this chapter describes the fabrication of aptasensor over gold electrode with thiol modified aptamer/MCH and its application for the non-faradic impedance spectroscopic based detection of *Pf*GDH. The sensor fabrication was characterized with the help of electrochemical and microscopic techniques.

Chapter 6: Development of aptamer–FET based detection of *Pf*GDH.

This chapter includes fabrication of thiol modified aptamer over interdigitated gold electrodes. The fabricated sensor was characterised by electrochemical impedance spectroscopy (EIS) and atomic force microscopy (AFM) studies. The fabricated interdigitated gold micro electrode (IDμE) was connected with extended gate of n type

metal oxide semiconductor (nMOSFET). The design and procedure for aptaFET measurement has been discussed in details. Specificity of the developed sensor was cross checked in the presence of different analogous and homologues proteins.

Chapter 7: Development of laboratory and portable format based detection system for pan malaria and *P. falciparum* species.

Herein, we report a novel detection strategy for pan malaria and *P. falciparum* species using a dye based reaction catalysed by the biomarker enzymes *P*LDH and *Pf*GDH, respectively. For the detection, two ssDNA aptamers specific to the corresponding *P*LDH and *Pf*GDH were used. The aptamer-captured enzymes were detected through a substrate dependent reaction that offers signals in the form of fluorescence intensity, absorption, and pixel intensity. The detection approach could therefore be customized to spectrophotometer-based laboratory technique and instrument-free device. A detailed account on the developed technique and device and their advantages for malaria diagnosis are discussed in this chapter.

Conclusion and future directions of research

This section summarizes the work to reach a logical conclusion. Along with the concluding statements a critical evaluation on the works embodied in this thesis has been included in this section. Additionally, the scope of augmenting the work for translating the proposed proof of concepts to technologically viable products has also been discussed at the end.

Chapter 1

Review of Litrature

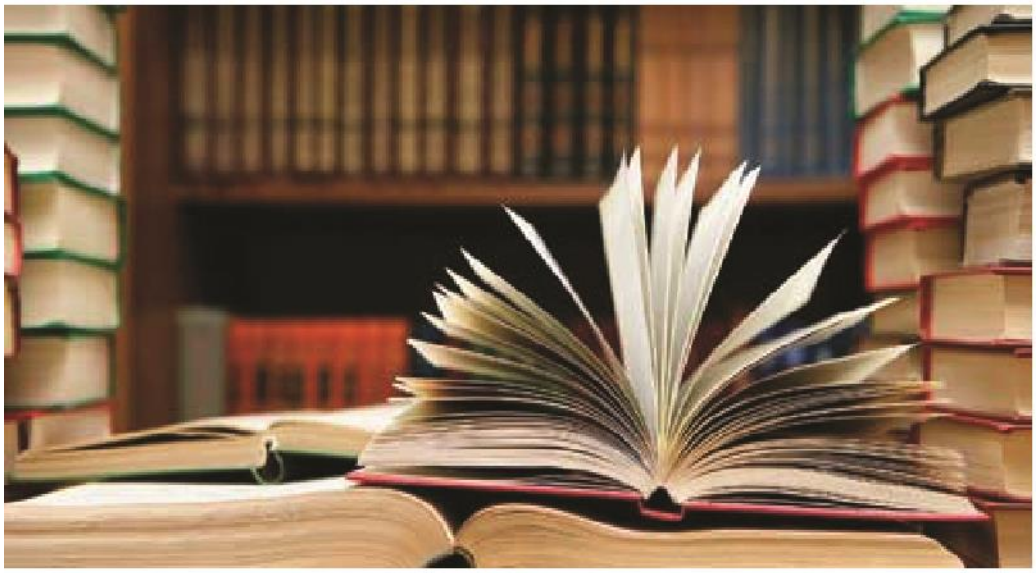

Research is to see what everybody else has seen, and to think what nobody else has thought.

- Albert S Gyorgyi

Chapter 1

Review of Literature

1.1 Overview

Malaria is a public health challenge for most of the countries located in the tropical and subtropical regions of the world (Bhatt *et al.,* 2015). Its prevalence in these countries is mostly contributed by their hot and humid climate and poor economic conditions (Sachs and Malaney, 2002). Malaria is an arthropod born disease and caused by the protozoan parasite. It is transmitted by the nibble of more than thirty species of female anopheles mosquito. The causative agent belongs to *Plasmodium* genus. More than 120 species of *Plasmodium* genus are known out of which five species; *P. falciparum, P. vivax, P. malariae, P. ovale,* and *P. knowlesi* are recognized as human contagious parasites. Among these, *P. falciparum* led malaria is the most lethal one and is responsible for most malaria related death (McKenzie *et al.,* 2005). According to the national vector born disease control and prevention (NVBDCP), India report on malaria (2016-17), 1.2 million cases of *P. falciparum* infection have been reported in India out of which ~7.65 % cases were found in North East region alone. The high level of malaria in these regions is mostly attributed to geographical location and conditions such as, high humidity, moderate temperature and dense forest, which are conducive for the growth and proliferation of the mosquito.

The typical symptom of malaria includes episodes of high fever followed by shudders and rigors, which are repeated every 24 h in *knowlesi*, 48 h in *falciparum, ovale, vivax* and 72 h in case of *malariae* infection. The malaria life cycle can be divided into two categories: the asexual cycle in human and sexual cycle in mosquito (Figure 1.1). The disease spread among humans with bite of female infected mosquito. Before sucking human blood it injects sporozoites along with saliva in human to prevent blood from clotting. The sporozoites after getting into blood stream invade the liver hepatocytes within 45 minutes of the bite and proliferate into merozoites. The single sporozoite from falciparum species can be proliferate into 40,000 merozoites within six days of infection in hepatocyte. In case of *P. falciparum* infection, more number of merozoites release into the blood as compared to *P. vivax* infection. The hypnozoites stage may be formed during *P. vivax* and *P. ovale* infections from sporozoites, which can stay dormant in hepatocytes for long time and later, enter into the asexual life cycle as merozoites. Besides this, *P. vivax*

hypnozoites stay dormant in the liver and may cause reappearance of the disease (Centers for disease control and prevention, 2016).

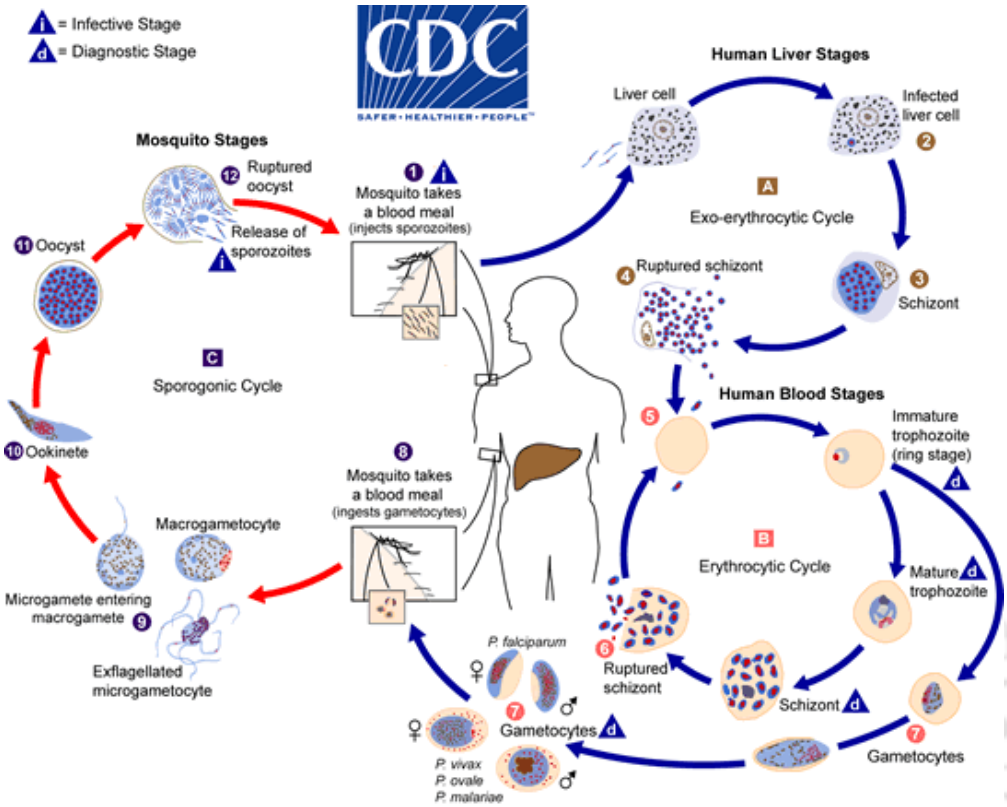

Figure 1.1: Life cycles of the malaria parasite. Source https:// www.cdc.gov/malaria/ about/biology/index.html.

At the beginning of intra-erythrocytic stage, merozoites enter into the erythrocytes. The invaded red blood cells (RBCs) start producing *Pf*EMP1 (*P. falciparum* erythrocyte membrane protein 1) on the erythrocyte membrane surface within 12 h of invasion, thus avoiding the removal of infected RBCs (iRBCs) by the spleen. The iRBC with surface protein (*Pf*EMP-1) have tendency to form rosette formation. The confiscation of iRBCs lead to injured endothelial cells (ECs) and disturbs blood flow and lactic acidosis, causing tissue hypoxia. These mechanisms are responsible for organ-specific syndromes such as, placental and cerebral malaria, which occur in the placenta, and brain, respectively. The major consequence of malaria infection is anemia caused due to hemolysis of infected and uninfected RBCs, often accompanied by impaired erythropoiesis. The lysis of iRBCs, which release the toxic hemozoin particles and merozoites, cause fever and shudders in the infected person. The released merozoites have a divided fate; most of merozoites invade fresh RBCs and develop into ring stage, traphozoites, which further mature into

schizont stage of parasites, on the other hand some of them develop into male and female gametocytes and are ingested up by mosquitoes during a blood feeding (Miller *et al*., 2013). The release of hemozoin into human blood after rapturing the infected RBC activated cytokine responsible for malaria symptoms.

Selective diagnosis of *P. falciparum* malaria is important from the points of proper therapy avoiding indiscriminate use of drugs. Notably, overuse and indiscriminate use of drugs have been ascribed responsible for the emergence of anti-malarial drug resistance strains of *P. falciparum*. Alarmingly, this particular species has developed resistance to artemisinin, which is one of the most widely used anti-malarial drugs (WHO, World Malaria Report, 2015). The precise early diagnosis and prompt medical care with suitable antimalarial drugs are the major technical constituents of the global strategy to control malaria as per WHO guidelines. For malaria treatment several antimalarial drugs are available which can be classified according to their stage of action during parasitic development inside host.

I. Schizonticides for causal prophylaxis: This class of drug act on schizont stage which present inside liver cells and accountable to initiate erythrocytic stage of development in human. The blocking of this stage, further progression of parasite development can be hypothetically prevented. Since it is difficult to predict the infection before on set of clinical symptoms, this type of therapy is more hypothetical than real-world application. The drugs Pyrimethamine and Primaquine are fall under this category.

II. Schizonticides for preventing relapse: This class of drugs act on the hypnozoites stage of *P. vivax* and *P. ovale* commonly present inside liver hepatocytes cells. This stage is accountable for relapse of symptoms on renaissance of dormant hypnozoites. The drugs tafenoquine, Krintafel and Primaquine phosphate commonly used to eradicate hypnozoites.

III. Blood Schizonticides: Inside red blood cells repetitive cycle of parasitic development take place with predefined periodicity. The end of each cycle release multiple new parasite in blood flow after rapturing of RBC, bring onset of malaria symptoms. The blood Schizonticides class of drug act on above mention stage of parasite and thereby help in termination of clinical attacks due malaria infection. These are the most imperative drugs for malaria treatment. The common schizonticides drug such as

chloroquine, quinine, mefloquine, halofantrine, pyrimethamine, sulfadoxine, sulfones, tetracyclines etc. were used by doctors.

IV. Gametocytocides: These drugs act on the sexual stage of the parasite development which take place in the blood and thus inhibit the transmission of infection to the mosquito. The chloroquine and quinine have shown gametocytocidal activity against *P. vivax and P. malariae*, but not for *P. falciparum*. However primaquine has shown gametocytocidal activity against all *Plasmodium* species, including *P. falciparum*.

V. Sporontocides: This class of drug blocks the progression of oocysts development in mosquito therefore prevent, transmission of parasite. The primaquine and chloroguanide commonly used for sporontocidal activity.

In conclusion, currently very few effective drugs are available to target hypnozoites stage of infection; among them only 8-aminoquinolines drug family is highly effective on this target. Unfortunately, the drugs from this family are not safe for populations with glucose-6-phosphate dehydrogenase (G6PD) deficiency, which paradoxically is also a common deficiency in malaria prone area (Uthman *et al*., 2014). Consequently, there is a great demand for new non-toxic therapeutic agents that target this crypto stage of the parasite life cycle, to abolish the recurrence of *P. vivax* and *P. ovale* infections.

The severity of malaria caused by *P. falciparum* can be understood by the fact that out of the total number of cases, more than 50 % malaria deaths were due to the infection caused by this species (Robert, 2015). There are several reasons that make *P. falciparum* infection lethal such as: i) the rate of proliferation of sporozoites into merozoites is very high as compared to other species, for example single sporozoites released upto 40000 merozoites within 12 h of infection in blood, ii) rapid hemolysis of iRBC leads to rapid clinical deterioration within 3-7 days of infection (Trampuz *et al.,* 2003), iii) the parasite causes alteration in morphology of iRBC and developed knob like structure over the cell surface leading to it adherence to the endothelial lining of blood vessels and gets sequestrated into various organ thereby evading removal by the spleen, iv) the cyto adherence in microvessels cause blockage of nutrients and oxygen to various organs causing tissue hypoxia and apoptosis. If this occurs in cerebral vessels the patient's condition worsen leading to cerebral malaria.

Through these information, we conclude that there is an urgency to develop rapid, sensitive, specific and low cost portable detection techniques for malaria detection caused by the different *Plasmodium* species, especially *P. falciparum*. For efficient diagnosis of malaria caused by *P. falciparum* infection we need to have a strong knowledge about the biomarkers and released kinetics that are specific to this plasmodium species. The currently available malaria diagnostic methods such as, thin and thick smear microscopy, quantitative buffy coat (QBC), polymerase chain reaction (PCR), enzyme linked immune sorbent assay, rapid diagnostic tests (RDTs) and other non-conventional methods suffer from many limitations. In the subsequent sections we shall discuss about the different biomarkers of *P. falciparum* and their detection methods developed until now.

1.2 Biomarker for Malaria Diagnosis

A biomarker is an indicative of any kind to determine variations for biochemical, molecular or cellular alternations in biological samples that can specify pathological, biological or therapeutic responses (Hulka *et al.*, 1991). Till date there has been no well recognised classification system to categorize different biomarkers. However scientists have tried to classify them into three different categories i.e Type 0, Type 1, Type 2 to bring clarity into matter (Frank and Hargreaves, 2003). In type 0 biomarkers are based on the usual history of disease and associate with clinical outcomes. The type 1 biomarkers normally define the biological effect of a therapeutic intervention. The type 2 biomarkers are like 'surrogacy' markers where a surrogate point has been indicated as a biomarker intended to substitute for a clinical end point, the latter being a typical or variable that imitates how a patient feels, survives or functions.

For diagnosis of malaria both broad spectrum specific as well as, species specific biomarkers have enormous importance. To diagnose pan malaria disease, broad spectrum specific biomarker(s) needs to be targeted without discriminating among the disease causing parasite species. While, the species specific biomarkers help to diagnose the selective species such as, *P. falciparum*. Notably, malaria has higher dominance in African continent regions and many *P. falciparum* infected individuals suffered from asymptomatic form of malaria (Dal-Bianco *et al.*, 2007). The occurrence of these asymptomatic infections can be as high as 52 % of the total number of malaria cases. A malaria patient suffering from asymptomatic malaria act as parasite reservoir and help to

spread the disease. The potential malaria biomarkers commonly discussed in the literature has been listed in table 1.1.

Table 1.1: List of potential malarial biomarkers along with their some critical information.

Plasmodium Biomarker	Molecular properties	Locations	Significant features	References
Glutamate dehydrogenase	Homo hexameric, Mw ~49.5 kDa per subunit, NADP or NAD used as cofactor	Present in parasitic cytoplasm; in human, present in iRBC and Serum	Structurally and sequentially different from its human counterparts, Act as redox enzyme release NADPH/NADH and NH_4^+.	Wagner *et al.,*(1998); Roth *et al.*, (1990)
Lactate dehydrogenase	Homo tetrameric, Mw ~34 kDa per subunit, NAD used as cofactor	Cytoplasmic protein in parasite; present inside iRBC and serum	Sequentially different from host protein and rate of utilization of APAD is higher than host protein. Presence of amino acid DKEWN in all *plasmodium* species.	Brown *et al.*, (2004); Dunn *et al.*, (1996); Shoemark *et al.*, (2007)
Histidine rich protein-II	Mw ~35 kDa	Released in human blood, Cerebro spinal fluid, urine in abundance	The repeats of unique tandem sequence (Ala-His-His-Ala-Ala-Asp). Present in 3_{10} α helix conformation when bound with heam. 3_{10}-helix conformation when attached to heme.	Wellems and Howard, (1986); Schneider and Marletta, (2005)
Aldolase	Present in homotetrameric form, subunit Mw~40 kDa	Present inside parasite cytoplasm, iRBC and serum	Show high diversity in sequence and enzyme kinetics compare to host aldolase; detectable in case of high parasitimia.	Döbeli *et al.*, (1990); Tjitra *et al.*, (1999); Eisen and Saul, (2000)
Hemozoin	β-haematin, Mw 4.9 kDa	Present inside digestive vacuole of parasite	Consists of Fe(III) PPIX centro symmetric dimmers linked through H- bonds.	Pagola *et al.*, (2000); Solomonov *et al.*, (2007)
Hypoxanthine-guanine phosphoribosyl transferase	Present in homo tetrameric form, subunit Mw 26 kDa,	Present in parasitic cytoplasm	Involve in parasite purine metabolism, Similar protein found in human but have potential to use as biomarker	Queen *et al.*, (1988).
Topoisomerase-I	Mw ~104 kDa	Present in patient's saliva in detectable amount.	Involve in over winding or under winding of DNA, Enzymatically active in high salt concentration (0.5M NaCl)	Tesauro *et al.*, (2012) Hede *et al.*, (2018)

1.2.1 Serological Biomarkers

Cerebral malaria is the most lethal form of malaria and is primarily associated with *P. falciparum* infection. It can cause death within 24-72 hours if proper medical healthcare is not provided (Lucchi *et al*., 2011). The progression of normal malaria into cerebral malaria (CM) or severe malaria can be identified by taking advantage of initial relevant immunologically serological biomarkers. It would help to separate febrile patient into categories: those who seem to develop cerebral malaria and another group who are likely to develop mild or severe malaria (MM or SM). However till date no distinctive biomarker has been reported for CM, even though some studies have revealed a noticeable relationship between severity of CM and different host proteins such as, chemokine interferon inducible proteins CXCL 10 and CXCL4 (Armah *et al*., 2007; Olszewski and Llinás, 2011).

The higher expression level of these proteins was observed in many CM patients. Moreover numerous other CM serological biomarkers have been identified such as, higher expression level in many fold of soluble tumour necrosis factor receptor (sTNF-R) and soluble Fas ligand that were observed in case of CM neuropathy (Armah *et al*., 2007). For the identification of suitable serological biomarker for CM, John and co-workers monitored twelve different cytokines and chemokines in CSF and serum levels of infected CM patient and normal healthy person as control (John *et al.*, 2008). They observed elevated levels of interleukin 1 receptor antagonist (IL-1ra), Interleukin 8 (IL-8) and TNF. It should be kept in mind that the level of these proteins (IL, TNF) also gets elevated after infection with other pathogen such as virus, bacteria and in cancer disease condition. The deregulations of endothelial growth factors such as angiopoietin –I, II (ANG-I, ANG-II) are also found in CM and the ratio of ANG-II: ANG-I could be used for accurately differentiate between CM and MM patients (Lovegrove *et al*., 2009; Conroy *et al*., 2009).

The complement system is present in our body to support the antibodies to facilitate elimination of antigens, which were also found under malaria condition. The suppressed level of C3 protein of complementary system was observed in SM and MM patients compared to normal healthy controls (Wenish *et al*., 1997; Olszewski and Llinás, 2011). The plasma membrane get fragmented under various physiological stress conditions, these are known as microparticles (MPs) or microvesicles (MV) (Freyssinet, 2003) and have also been related with pathophysiology condition of malaria (Haest, 1982). A case

study was performed by Corners and group (Conners *et al*., 2004) with Malawian children suffering from CM, uncomplicated and severe malaria caused by *P. falciparum* amongst whom different levels of endothelial origin MPs were found in the plasma. The fluorescent activated cell sorting study was performed and found that the platelet origin MP increased during CM stage and subsequently reduced after treatment the patient, which indicate it can be used as a relevant biomarker for CM diagnosis (Mfonkeu *et al*., 2010). The immunofluorescence is generally used for detection of serological biomarkers but they are hard to use as a reliable malaria biomarker. For example, CXCR3 and its legends were elevated during several neurological disease conditions such as *Toxoplasma gondii* (Olszewski and Llinás, 2011), West Nile virus (Klein *et al*., 2005; Zhang *et al*., 2008), and HIV infections (Sui *et al*., 2004). Nevertheless, detection of these markers signifies great importance to detect CM, after malaria infection is confirmed through using a well-known antigenic biomarker.

1.2.2 Antigenic Malaria Biomarker

1.2.2.1 Aldolase: It is a key enzyme of glycolysis pathway, it catalyses the conversion of fructose 1,6 bisphosphate into glyceraldehyde 3 phosphate (G3P) and dihydroxy acetone phosphate (DHAP) (Srivastava *et al*., 1990). The aldolase is present in soluble active form inside parasitic cytoplasm and its insoluble inactive form is associated with membrane (Knapp and Kupper., 1990). This enzyme is homotetrameric in nature with each subunit of 40 kDa (Döbeli *et al.,* 1990). It shows 50-60 % sequence similarity with other host aldolase protein (Kim *et al*., 1998). Upon infection by *Plasmodium* the glucose uptake of the erythrocyte has been reported to increase up to 50 fold. To utilize this excess absorbed glucose, aldolase level increased upto 70 fold in comparison of normal RBC (Srivastav *et al.,* 1990). Thus, this enzyme is suitable for drug target and has potential as a malaria biomarker. There have been numerous studies performed on inhibition of *P. falciparum* aldolase through several entrants such as rabbit antibodies, phosphorothioate, a 19- residue synthetic peptide, and antisense oligo deoxynucleotides (Döbeli *et al.,* 1990; Shear *et al.,* 1999). The RDTs based on combination of aldolase and *Pf*HRP-II were used for species identification (*P. vivax* and *P. falciparum* respectively) along with malaria diagnosis (Tjitra *et al.,* 1999; Eisen & Saul, 2000). However, many drawbacks are associated with aldolase based RDTs like, poor sensitivity and stability. Lee and co-worker performed an genetic diversity study on this enzyme and found that amino acid sequences in aldolase are highly conserved, signifying that antigenic diversity

is not responsible for low sensitivity of this biomarker based detection (Lee *et al.,* 2006a).

1.2.2.2 Hemozoin: During intra erythrocytic cycles, *Plasmodium* parasite feeds into the host haemoglobin (Hb) and release free amino acid to regulate osmotic pressure (Lew *et al.,* 2003). After the digestion of globin from Hb, toxic haematin is released (Omodeo-Sale *et al.,* 2005), which further react with oxygen resulting in the formation of brownish yellow inert hemozoin pigment (Fitch and Kanjananggulpan, 1987). Hemozoin is an insoluble microcrystalline disposable product formed from the polymerization of free heme by species of blood-feeding parasites, such as, *Rhodnius prolixus* (Oliveira *et al.,* 1999), *Schistosoma mansoni* (Chen *et al.,* 2001) and *Plasmodium spp*. (Francis *et al.,* 1997). The crystal structure of hemozoin was explored by Slater and co-workers. It was found that it contain polymer of heme covalently linked with central ferric ion of one heme and carboxylic side chain oxygen of another heme (Slater *et al.,* 1991). Further X-ray diffraction study confirmed that its structure is similar to synthetic β-haematin (Pagola *et al.,* 2000). The different morphology of hemozoin crystals has been used to distinguish different species of parasites (Noland *et al*., 2003). Hemozoin crystals are paramagnetic in nature and hence show cotton-mouton effect in the presence of an external magnetic field which corresponds linearly to the hemozoin concentration. Based on this concept an *in-vivo* diagnostic method using a magneto-optic fingertip probe was developed (Newman *et al.,* 2008a; Newman *et al.,* 2010b). Recent studies have shown that hemozoin have the potential to be used as a novel biomarker and new methods based on this have been developed for efficient malaria diagnosis (Pirnstill and Cote, 2015; Garrett *et al.,* 2015; Lukianova-Hleb *et al.,* 2014; Rebelo *et al.,* 2013). The major challenge associated with these malaria diagnoses is that the clinical samples which consist of young ring stage parasite which don't have detectable amount of hemozoin crystal (Delahunt *et al.,* 2014). Thus, hemozoin based methods are often not satisfactory when compared to RDTs or PCR based malaria diagnosis (Mens *et al.,* 2010)

1.2.2.3 *Plasmodium* Topoisomerase I: This is large 104 kDa monomeric protein with highly conserved DNA binding site and C terminal catalytic site linked through each other with non-conserved hydrophilic region. It has 64 % similarity with human topoisomerase-I (Cheesman, 2000). Topoisomerases are enzymes that regulate the overwinding or underwinding of DNA. The winding problem of DNA arises due to the intertwined nature of its double-helical structure during DNA replication and transcription. In order to prevent and correct these types of topological problems caused

by the double helix, topoisomerases bind either single-stranded or double stranded DNA and produce nick in the phosphate backbone of the DNA and remove the supercoil. The *Pf* topoisomerase has contrasting feature in comparison of human topoisomerase and *Pf* topoisomerase activity was reported in presence of high salt concentration (upto 0.5 M of NaCl). This specific characteristic of *Pf* Topoisomerase was used to develop Rolling circle enhance enzyme activity detection (REEAD) system for potential use of future POC diagnosis for malaria (Tesauro *et al*., 2012; Hede *et al.,* 2018; Givskov *et al.,* 2016). Various drug targeting *Pf* topoisomerases have been developed to overcome drug resistance problem, among them phosphorothioate antisense oligodeoxynucleotides (ODNs) with nanoparticle has shown promising results (Foger *et al.,* 2006).

1.2.2.4 Hypoxanthine-guanine phosphoribosyl transferase (HGPRT): Most of the *Plasmodium* parasites don't have de novo purine nucleotide synthesis pathways; they solely depend on salvage pathway of preformed purine from host system (Ullaman and Carter., 1995; Sherman, 1979). The HGPRT belongs to transferase class of enzyme, and catalyses the conversion of guanine to guanine monophosphate and hypoxanthin to ionosin monophosphate. The HGPRT enzymatic activity is essential for survival of the parasite. Inhibition of this enzyme stops the parasitic growth. It has central role in parasite purine synthesis (Keough *et al.,* 1999). The HGPRT is active in homotetrameric form and subunit mass is 26 kDa. The *Pf*HGPRT share 76 % similarity and 44 % sequence identity with human HGPRT. Besides this high degree of sequence similarity and identity, the parasitic enzyme substrate specificity is different from the host enzyme. For example, the *Pf*HGPRT has higher capabilities to catalyse the phosphoribosylation of xanthine, in addition to hypoxanthine and guanine (Queen *et al.,* 1988). These differences made this *Pf*HGPRT as novel target for drug and sensor development for malaria diagnosis.

1.2.2.5 Histidine rich protein (HRP): HRP was first discovered in cytoplasmic granules from avian malaria parasite *Plasmodium lophurae*. This protein contains a upto 73 % of histidine amino acid. Since then it incited interest to understand structure and function of this protein (Kilejian, 1974). There are three main types of HRPs associated with *P. falciparum* and these are named according to their order of discovery (Howard *et al.,* 1986). The HRP-I is knob associated protein and present in knob^{+} strain which help in adhesion of iRBC with endothelium of blood vessels (Pologe *et al.,* 1987). The HRP-II is the most important biomarker for *P. falciparum* and associated with both Knob^{+}/Knob^{-}

strain of the parasite, the most lethal form of malaria. This protein is involved in heme detoxification and form hemozoin after the Hb digestion (Leech *et al*., 1984; Lynn *et al.*, 1999). The HRP-II has the potential to be used as a vaccine against malaria and projected as a suitable antigenic target (Kilejian, 1978). Synthesized by *P. falciparum*, *Pf*HRP-II is a 35 kDa protein consisting mostly of histidine, alanine and aspartic acid. There are 18 tripeptides (Ala-His-His), 3 pentapeptides (Ala-His-His-Ala-Ala) and 33 hexapeptides (Ala-His-His-Ala-Ala-Asp). HRP II transports from the parasite, through the host cell cytoplasm, to the culture supernatant *in vitro* (Howard *et al.*, 1986) which also accounts for its presence in the serum, CSF and urine of infected patients (Parra *et al.*, 1991; Valle *et al.*, 1991). *Pf*HRP-II is released in plenty amount in malaria patient which is why it can be used as an antigen biomarker of malaria. The *Pf*HRP-II is a prime target for developing antimalarial drugs and diagnostic test as evident from the large number of publication on this. The *Pf*HRP-II diagnostic assays show more sensitivity and specificity for *P. falciparum* detection compare to aldolase and LDH based detection approach (Iqbal *et al.*, 2002).

Numerous immunosensors targeting *Pf*HRP-II were designed and developed on piezoelectric and electrochemical platforms. The antibodies conjugates with nanomaterials such as, Au nanoparticles and multiwall carbon nanotubes (MWCNTs) (Sharma *et al.*, 2008), magnetic particles (de Souza Castilho *et al.*, 2011), self-assembled monolayers (SAMs) prepared with thioctic acid and 1-dodecanethiol (Sharma *et al.*, 2011a) were used and shown to achieve good results equivalent to commercial available RDTs. However, *Pf*HRP-II has several drawbacks. It is released in copious amount in human blood of malaria patient even after the disease ceased giving false positive results in diagnosis (Mayxay *et al.*, 2001; Kyabayinze *et al.*, 2008). Antigenic variation along with deletion of *Pf*HRP-II gene has been reported from parasites in Amazon regions and in many African, Asian countries (Bharti *et al.* 2016; Palmer *et al.*, 1998; Iqbal *et al.*, 2004; Lee *et al.*, 2006a), which led to false negative result in malaria diagnosis. Moreover, several reports claimed variable results on the use of RDT against *Pf*HRP-II (Mason *et al.*, 2002). The incidence of surfacing deletion and mutation of *Pf*HRP-II gene in the parasite in some regions has cautioned the malaria diagnosis and management sectors globally on the use of this biomarker for specific detection of *Pf* malaria (Kumar *et al.*, 2013; Koita *et al.*, 2012). This created a demand for tests that replaces *Pf*HRP-II with other suitable (*Pf*) specific proteins. The *Pf*HRP-III is not very common as I, and II.

It is a small histdine repeat rich protein (SHARP) and share structure homology with HRP-II. It has been hypothesised that *Pf*HRP-II and *Pf*HRP-III were resulted from duplication and interchromosomal deviation from a single ancestral gene (Kemp *et al.*, 1987). Due to homology in structure, antibody raise against *Pf*HRP-II has cross-reactivity with *Pf*HRP-III (Wellems *et al.*, 1986; Chakma *et al*., 2016).

1.2.2.6 Lactate Dehydrogenase: During the intra erythrocytic cycle of *Plasmodium* parasite, it solely depends on host for growth and replication. It voraciously uses the host glucose and because of this glucose consumption increased upto 100 times by iRBC. Microarray studies revealed that all the enzymes of *P. falciparum* glycolysis pathway are unregulated in many folds during the asexual stage of life cycle (Bozdech *et al.*, 2003). The *P*LDH is the last enzyme of glycolytic pathways which catalyses the inter conversion of pyruvate to lactate and release NAD/NADH as by product (Jensen *et al.*, 1983; Roth *et al.*, 1990). The mRNA level of *P*LDH expression progressively increases at 24-30 h during the intra erythrocytic cycle and after that, it declined to zero level at schizont stage. *P*LDH is a homotetrameric protein with each subunit mass of 38 kDa. It is found in parasitic cytoplasm and is released into human serum and iRBC in active and soluble form. The *P*LDH is a tetrameric protein, consists of two domains, small and big domain. The big domain includes Rossmann fold that bind with NADH cofactor while the catalytic domain is present inside the small domain (Brown *et al.*, 2004).

The *PL*DH have some major structural and enzyme kinetics difference from the human LDH (*H*LDH) which has been exploited for development of drug and detection system for malaria diagnosis. The insertion of five amino acid sequence aspartic acid (D), glutamic acid (E), lysine (K), tryptophan (K) and aspargine (N) was discovered in active site of *P*LDH which is absent in its host counterpart. This insert has been used as a common epitope for detection (Hurdayal *et al.*, 2010; Brown *et al.*, 2004). The *P*LDH shares 29 % sequence identity with HLDH. Besides this, *P*LDH does not show substrate inhibition in presence of high concentration of pyruvate as compared to *H*LDH (Sessions *et al.*, 1997). Another kinetic difference is that rate of utilization of $APAD^+$ (3-acetylpyridine adenine dinucleotide), a synthetic analogue of NAD, by *P*LDH is 200 times higher than that of the HLDH (Dunn *et al.*, 1996; Chaikuad *et al.*, 2005). The LDH protein sequence alignment study reveals ~ 90% sequence identity amongst different *Plasmodium* species indicating that LDHs among different species (i.e *Pf*, *Pv* etc.) are very much similar to each other (Shin *et al.*, 2013; Kim and Searson, 2017). The *P*LDH

is a globally accepted and widely used biomarker for malaria diagnosis (Dunn *et al.*, 1996; Jain *et al.*, 2016).

1.2.2.7 Glutamate dehydrogenase (GDH): It is a pervasive enzyme in the living systems that act as important bridge between carbon and nitrogen metabolism. It is commonly associated in assimilation of ammonia (NADP dependent GDH) and catabolism of glutamate (NAD dependent GDH). The GDH is the most studied enzyme at the structural and biochemical level. *P. falciparum* also expresses three different type of GDH isozyme termed as *Pf*GDH$_a$, *Pf*GDH$_b$ and *Pf*GDH$_c$ according to their order of discovery (Macrae *et al.*, 2013). The genome analysis of *P. falciparum* was revealed that it contains three genes to express two potential NADP/H cofactor dependent GDH (*Pf*GDH$_a$, *Pf*GDH$_b$) and are synthesised inside parasitic apicoplast while localization and specificity for cofactor for the third *Pf*GDH$_c$ has not been determined (Miyashita and Good., 2008; Aparicio *et al.*, 2010). The *Pf*GDH$_a$ is expressed episomally and is exclusively present in the *P. falciparum* cytosol. Fluorescent microscopy showed GDH is not co-localize with parasitic nucleus or mitochondrion, and the fluorescent merged image (figure 1.2.) proves that *Pf*GDH$_a$ is a cytosolic protein (Storm *et al.*, 2011; Avedano *et al.*, 1997).

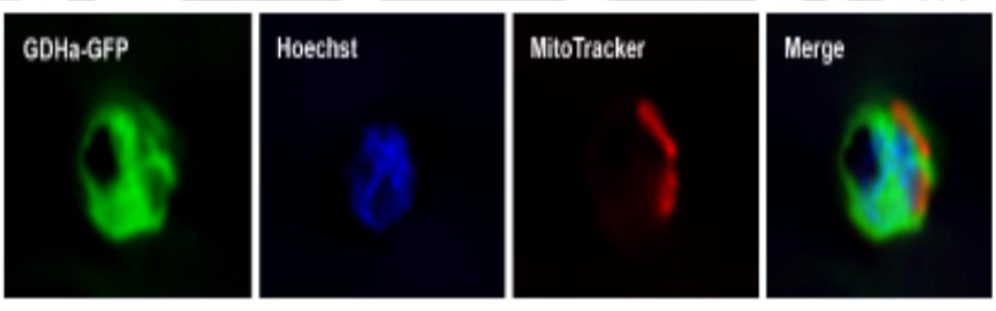

Figure 1.2: Cytosolic localization of *Pf*GDH$_a$-GFP, not present in the nucleus (Hoechst) and not co-localize with the mitochondrion (MitoTracker) (adopted from Storm *et al.*, 2011).

The genome analysis study predicated the location of *Pf*GDH$_a$ but the study performed by Storm and co-workers indicates its presence inside parasitic cytoplasm. However, in plants, during senescence, the location of GDH could be distributed among organelle and cytosol (Kichey *et al.*, 2005). This is contradiction because GDH is a mitochondrial (Rothe *et al.*, 1988) and endoplasmic reticulum (Colon *et al.*, 1986) protein in mammals, plants and yeast (Hudson and Daniel 1993). In human, GDH is expressed widely as

housekeeping gene but it is absent in mature human erythrocytes. However, during *P. falciparum* infection the *Pf*GDH existence was reported in human erythrocytes, plasma, and serum in active and soluble form (Acosta *et al.*, 1998; Siegal *et al.*, 1996). There are two isoform of GDH in human; *H*GDH$_1$ is present inside blood and liver, and HGDH$_2$ is expressed chiefly in brain, testis and retina (Zaganas *et al.*, 2009).

The total size of *P. falciparum* nuclear genome is 22.8 megabases (Mb) and spread among 14 different chromosomes varying in size from ~ 0.643 to 3.29 Mb. The total A+T percentage in genome is 80.6 % and this increases upto 90 % with noncoding introns and intergenic sections (Gardner *et al.*, 2002). Three potential genes encoding *Pf*GDH is present in the genome of *P. falciparum*, out of which two are present over chromosome 14 (PF14_0164 and PF14_0286) encoding *Pf*GDH$_a$ and *Pf*GDH$_b$ respectively and third one is located over chromosome 8 (PF08_0132) expressing *Pf*GDH$_c$ (Hudson and Daniel., 1993). *Pf*GDH$_a$ is a univocal single copy gene and it does not contain any intron on genomic DNA. The open reading frame of gene is 1410 basepair (bp) and expresses 470 long amino acid sequence of protein. The 5' and 3' flanking regions of mRNA of *Pf*GDH$_a$ have 82 % A+T and the coding region display 69 % A+T content. The starting codon (ATG/AUG) position inside the gene is unequivocal since no other starting codon is present inside the open reading frame of the gene. The adenine nucleotide present at -3 and AGT found at position of +4 to +6 are in agreement with eukaryotic consensus sequences around translation initiation site for efficient translation of the protein from gene (Yamauchi, 1991). Beyond the 3' end of *Pf*GDH$_a$ gene, a long adenine polynucleotide region is present in noncoding region of the gene. It may involve as just adenine rich stretch instead of polyadenylation site (Figure 1.3).

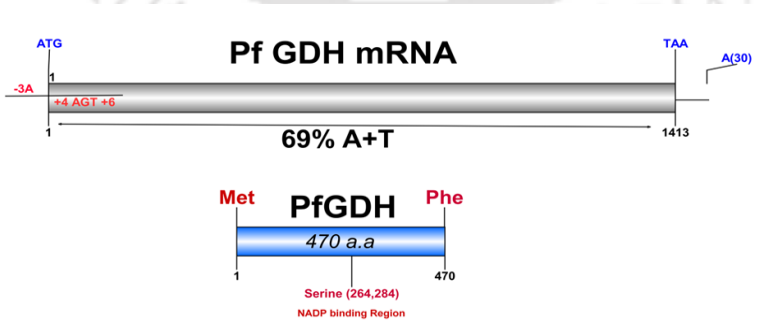

Figure 1.3: Schematic representation of molecular architecture of *Pf*GDH$_a$ mRNA domains and *Pf*GDH$_a$ amino acid.

The occurrence of two serine (S-260, S284) residue in *Pf*GDH$_a$ indicating its specificity towards NADP cofactor. These residues are involved in the formation of H-bond with 2'-phosphate group of NADP and provide extra space for accommodation (Baker *et al*., 1992). The genomic and proteomic details of different isoform of GDH present in *P. falciparum, P. vivex* and human are presented in table 1.2. In human, two isoforms of GDH are present. This enzyme is widely expressed in human with highest level in liver and absent in erythrocytes (Zaganas *et al.,* 2009). Subcellular level *H*GDH is specifically present in mitochondria and in very little amount in the endoplasmic reticulum (ER) of these cells (Schmidt and Schmidt, 1963). The human genome project verified that *H*GDH$_1$ and *H*GDH$_2$ locus on 10q23.3 and Xq24 - q25 sequentially. *H*GDH$_1$ contain 12 intron and 13 exon while *H*GDH$_2$ lacks intron. The intronless nature of *H*GDH$_2$ hypothesize that *H*GDH$_1$ can reversibly be transcribed and subsequently inserted in chromosome X (Shashidharan *et al.,* 1997). The transcript for *H*GDH$_1$ and *H*GDH$_2$ is 2970 bp in size, which is finally translated into protein sequence of 558 amino acid long polypeptide consisting of a cleavable signal sequence region of 53 amino acids (Mavrothlassitis *et al.,*1998) and theoretical molecular weight for both the protein is 57.5 kDa (Nakatani *et al.,* 1987). *Pf*GDH and *H*GDH are catalytically active in homohexameric form (Fischer, 1985). This protein is reversibly post translationally modified by cysteine specific ADP ribosylation (Figure 1.4). It helps in physiological regulation of enzyme activity (Yraola *et al.,* 2001).

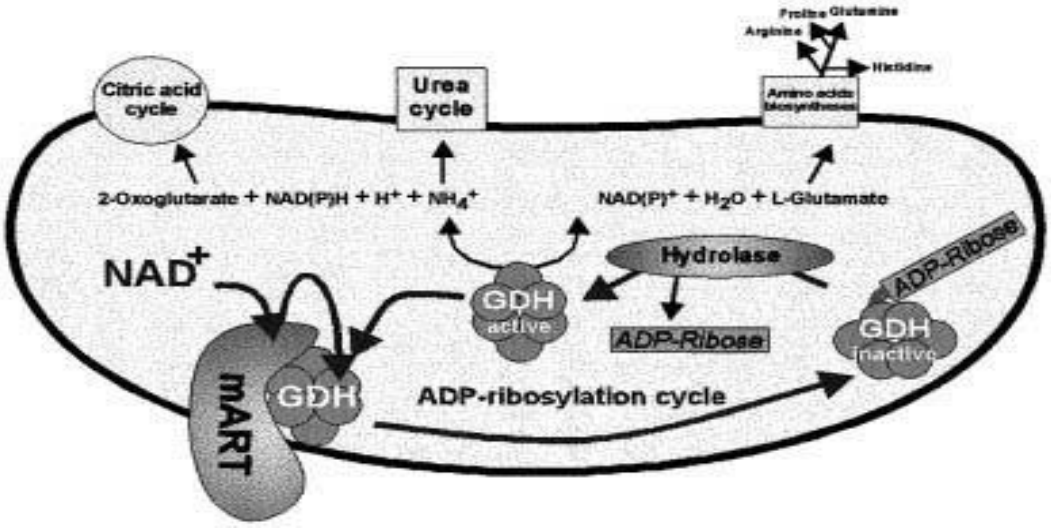

Figure 1.4: Mitochondrion ADP ribosylation regulating GDH activity (mART-mitochondrial ADP ribosylation transferase) (Yraola *et al.,* 2001).

Table 1.2: Genomics and proteomics information of *Plasmodium* GDH and *H*GDH (MW_T Theoretical molecular weight).

UniProt/ PlasmoDB ID/ Protein	Gene (bp)	Amino Acid No.	MW_T	Co factor	Location	Subunits	Signal Sequence
***Pf*GDH$_a$** Q8ILT0/PF3D7_1416500	1410	470	52.5	NADP	Cytosolic	Hexameric	putative No signal peptide
***Pf*GDH$_b$** Q8ILF7/PF3D7_1430700	1452	502	54	NAD^+	Apicoplast	Hexameric	putative No signal peptide
***Pf*GDH$_c$** Q8IAM0/PF3D7_0802000	1397	NA	160	NADP /NAD	Cytosolic	Hexameric	putative No signal peptide
***Pv*GDH$_a$,** A5K164/ PVX_085625	1413	470	49	NADP	Apicoplast Cytoplast	Hexameric	putative No signal peptide
***Pv*GDH$_b$** A5K0U3/PVX_085005	1510	502	54	NADP	Apicoplast Mitochon--drion	Hexameric	Mitochondrial targeting sequence
***Pv*GDH$_c$** A5KCJ5/PVX_093640	1244	NA	NA	NA	NA	NA	putative No signal peptide
HGDH$_1$ P00367	2970	505	57.5	NAD	Mitochon--drion, ER, Cytosol	Hexameric	Mitochondrial targeting sequence,PTM
HGDH$_2$ P49448	2970	505	57.5	NADP	Mitochon--drion, Astrocytes, Cytosol	Hexameric	Mitochondrial targeting sequence,PTM

PTM-post translational modification, ER-endoplasmic reticulam.

The *Pf*GDH$_a$ is a homo hexameric protein, meaning six identical subunit joint together. Each subunit with M_w 49.5 kDa consists of two domains divided by a profound cleft to accommodate cofactor and substrate binding sites (Wagner *et al.,* 1998). The amino acid sequence analysis revealed that *Pf*GDH$_a$ is 77 % different from HGDH$_1$ and differ 35 - 40 % from *P. vivax* GDH (*Pv*GDH). The unligated state 3-D structure of *Pf*GDH$_a$ was resolve by X-ray crystallography at resolution of 2.7 A°. According to crystallographic structure it shows that *Pf*GDH$_a$ contain a special N terminal extension and this extension of enzyme is 30 residues longer than the mature human enzyme. However, the function of this N terminal extension is not yet known (Wagner *et al.,* 1998). This structure is not reported in any other species GDH. Further subunit interaction analysis of *Pf*GDH$_a$ and *H*GDH$_1$ exposed that subunit linked with each other through salt bridge interaction in case of parasitic protein. Whereas, in case of *H*GDH$_1$ these interactions are mainly

hydrophobic linkage (Plaitakis *et al*., 2003; Werner *et al.*, 2005). The crystal structure of *Pf*GDH$_a$ showed that active site of enzyme is in direct contact with the substrate and it occupies residues Lys112 and Ser 401, most likely linked with the γ-carboxylate group of the substrate, whereas Gln133 and Lys136 are supposed to be linked with the α-carboxylate group of glutamate. The amino group form coordinated bond with Gly187 and Asp188 (Werner *et al.*, 2005). Among them two of these residues are different in the human enzyme: the α-carboxylate ligand Gln133 is replaced by Met115 and another amino group ligand Gly187 by Pro171 (Figure 1.5). In addition to these alterations in primary sequence further differences to the mammalian enzymes may occur in the detailed binding of substrate. (Stillman *et al.*, 1993).

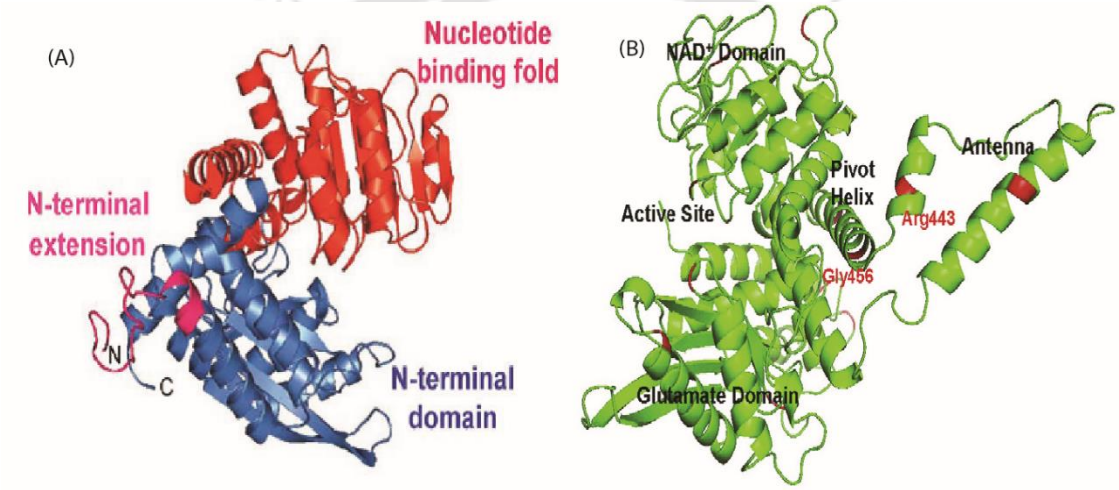

Figure 1.5: (A) *PfGDH$_a$* (Werner *et al.*, 2005) (B) *H*GDH$_1$ (Zaganas *et al.*, 2009) mutually aligned showing the nucleotide-binding fold in red and green in *H*GDH$_1$, the N-terminal domain in blue and the antenna region in the human enzyme in green.

The GDH is universal enzyme that acts as bridge to connect carbon and nitrogen metabolism. It helps in synthesis of two important amino acid glutamine and glutamate which is a vital step for metabolism of cell in all organisms, because it signifies the only way of integrating nitrogen atom into carbon backbones. The inorganic form of nitrogen assimilated in the form of ammonia later transformed into ammonium ions, which is further added as an amino group to glutamine or amino group to glutamate (Figure 1.6). Later these amino acids turn as precursor of amino group and act as donor for the synthesis of various nitrogen containing compounds in the cell. Specifically, amino group of glutamate is utilized in the synthesis of amino sugars, purine, pyrimidine, tryptophan, histidine and aspargine (Santero *et al.*, 2012). The typical tricarboxylic acid cycle (TCA)

is not present in *P. falciparum*, instead it possesses branched TCA cycle for metabolism. It was assumed that the key entry point for ammonia to TCA pathway in parasite is α ketoglutarate formed from glutamate and catalysed by GDH enzyme (Vaidya and Mathur, 2009).

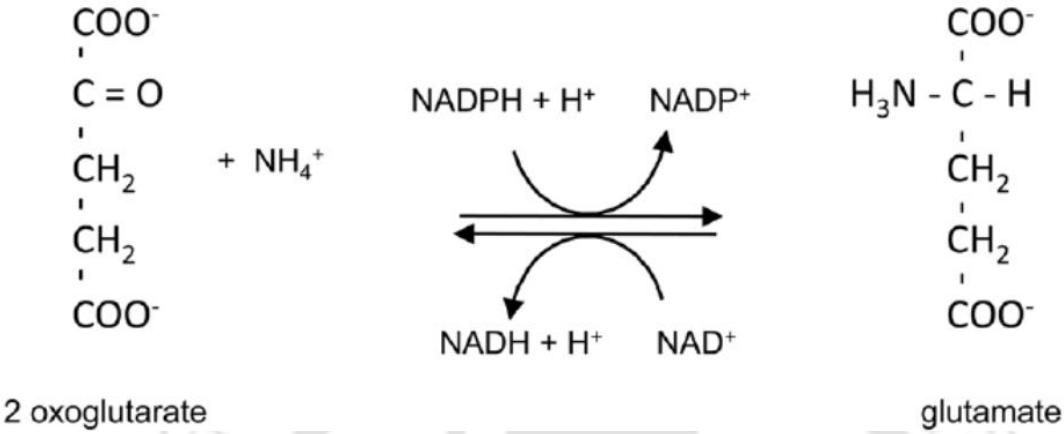

Figure 1.6: Reaction catalysed by GDH.

The *Pf*GDH$_a$ enzymes are present throughout the intra-erythrocytic cycle of the parasite with the maximum expression level in both young and old trophozoites and the segmented stages (Wagner *et al* 1998). Parasitized red cells contain about 10 times more NAD(H) than uninfected red cells, but the NADP(H) content is unchanged (Roth., 1990). In mammalian system, GDH helps in regulation of osmotic balance, high temperature tolerance and also act as neurotransmitter (Nandineni *et al.*, 2004; Consalvi *et al.*,1991; Kelly and Stanley, 2001).

The GDH is involved in catalysis of reversible NAD(P)$^+$ associated oxidative deamination of glutamate as substrate which convert into α-ketoglutarate and ammonia as product in two steps (Smith *et al.*, 1975). The enzymatic reaction mechanism start with formation of Schiff base intimidate between α-ketoglutarate and ammonium ion. This step is important because it introduces the α-carbon atom in stereochemistry of glutamate, further this Schiff base intermediate is protonated, which is performed by the transfer of hydride ion from NADPH and lead to formation of L-glutamate. The GDH is an exclusive enzyme because it efficiently utilizes both NAD$^+$ and NADP$^+$ (Stryer, 2002).

Table 1.3: Comparisons of Michaelis Menten Constant (K_m) for GDH between *Plasmodium* parasite and human origins. (Vander jagat *et al.,* 1989; Zaganas *et al.,* 2005; Cho *et al.,* 1995).

S. No	Substrates	K_m value of *Pf*GDH (mM)	K_m value of *H*GDH (mM)	K_i value *Pf* GDH(µM)	K_i value *H*GDH(µM)
1.	Glutamate	0.29	12.4	-	-
2.	NADP	0.007	1.22	-	-
3.	α-Ketoglutarate	0.69	2.00	-	-
4.	NADH	0.003	0.12	-	-
5.	Isopathalic Acid	-	-	6.2	426

The comparisons of different enzyme kinetic parameters between *P. falciparum* and *H*GDH has made under the Table 1.3, which shows that *Pf*GDH has higher affinity toward glutamate, NADP, α-Ketoglutarate than *H*GDH. There are various specific competitive inhibiters are known, to specifically inhibit the activity of *Pf*GDH without affecting the activity of *H*GDH. These specific inhibiters are isopathalic acid, 2 methyl glutarate and 2, 4 pyridine dicorboxylate (Cunliffe *et al.,* 1983). These inhibitors may play important role in development of effective drug against malaria. The activity of *Pf*GDH is also regulated by adenosine 5'-triphosphate (ATP), guanosine-5'-triphosphate (GTP) as allosteric inhibitors and adenosine 5'-monophosphate (AMP), guanosine-5'-monophosphate (GMP) as allosteric activators (Storm *et al.,* 2011). Further analysis of various kinetic parameters revealed that *Pf*GDH shows higher affinity towards glutamate than to α-ketoglutaric acid. According to chemical kinetics data, *Pf*GDH favor the formation of-ketoglutaric acid and ammonia (Lightfoot *et al.,* 1988).

The analysis of significant points of different isoforms of *Pf*GDH (a,b,c) revealed that *Pf*GDH_a is cytosolic in nature and released in good concentration in blood serum of infected patient. Besides this, X ray crystallographic (3D) structure of *Pf*GDH_a is known, which make it a suitable target among different isoforms of *Pf*GDH for sensing work. Hence, *Pf*GDH_a is represented as *Pf*GDH in the later chapters of the thesis. These findings underline the fact that there are immense sequential, structural and kinetic differences among the two enzymes (*Pf*GDH_a and *H*GDH) that may be used for selective

detection of *Pf*GDH for malaria diagnosis.

1.3 Malaria diagnosis approaches

1.3.1 Conventional malaria diagnosis methods

Microscopy is known as the gold standard for malaria diagnosis. It is still used for sensitive detection of malaria and identification of plasmodium species since 1904 (Fleischer, 2004). Thick smear and thin smear are also widely used techniques for malaria diagnosis. Thin smear is used for species differentiation, while, the thick smear is used for better signal intensity. However, these techniques are associated with some drawbacks such as labour intensive, instrument dependent, required trained staff, low sensitivity (100-200 parasite per μl^{-1}) and time consuming. For the assessment of sensitivities and specificities of various diagnostic methods Bayesian latent class model was used and found that microscopy is not good reference test (Goncalves *et al.,* 2012). To enhance the sensitivity, fluorescent microscopy was introduced using fluorophores such as acridine orange (AO) and benzothio corboxy purine (BCP) for quantitative buffy coat analysis method. Besides microscopy, nucleic acid based molecular techniques are also used such as hybridization PCR, nested PCR (Lee *et al.,* 2012; Morassin *et al.,* 2002), quantitative nucleic acid sequence-based amplification (QT-NASBA) and LAMP (Loop mediated Isothermal amplification) for diagnosis of malaria. LAMP based nucleic acid amplification technique is performed at isothermal condition hence these don't require thermocyclers (Lee *et al.,* 2012). However, these methods are prone to cross contamination while addition of fluorescent dye for visualization of the results. Moreover these techniques cannot be used for amplification of target DNA more than 500 bp size, as this hampers the strand displacement during the process (Lau *et al.,* 2011). Moreover, they suffer from some disadvantages such as time consuming, dependent on expensive instruments and require skilled person with good lab facilities (Ragavan *et al.,* 2018). On positive note, the nucleic acid based techniques are very sensitive as these can detect parasitaemia down to the level of one parasite per microliter of blood samples and provide both quantitative and qualitative information about the disease.

Flow cytommetry (FCM) and automated erythrocytes shortening method are used for detection of hemozoin or double strand DNA (dsDNA) in iRBC. However, the application of dsDNA for malaria detection through FCM suffers from false positive result during the pathological condition due to surge of normoblast and erythroblast in the

blood (Malleret *et al.*, 2011). The laser desorption mass spectroscopy (LDMS) is a suitable technique for small molecule detection (< 1.5 kDa) hence can efficiently detect such as porphyrins, phospholipids and hemozoin. The laser beam lead to vaporization of individual heme molecule from hemozoin, which is later detected by LDMS. However this method may not be useful for species identification and is semi quantitative in nature (Feldman, 2006). Recently, optomagnetic acoustic noninvasive sensor has been developed for malaria diagnosis. A laser beam is applied over patient's skin is absorbed by hemozoin paramagnetic molecule, leading to vibration of the molecules and generating micro bubbles. Later the burst of these micro bubbles are recorded by acoustic sensor. This method is sensitive but cannot be used to differentiate between malaria species (Lukinova *et al.*, 2014).

ELISA is a well-known method for malaria diagnosis and using antibodies as bio recognition molecules against various antigens (*Pf*GDH, *P*LDH and *Pf*HRP-II) (Martin *et al.*, 2009; Dominguez *et al.*, 1996). ELISA is highly sensitivity technique it can detect malaria in short time frame. Despite this, application of ELISA is not a suitable technique for field study is restricted to sophisticated labs and blood bank where large population of sample needs to analyze (Noedl *et al.*, 2006). The conventional methods for malaria diagnosis have been summarized in Table 1.4.

Table 1.4: Assessment of performance factors for different conventional techniques. Part of the table adapted with permission from Tangpukdee *et al*., (2009).

Test type	**Detection principle of the technique**	**Instrument**	**Sensitivity and specificity**	**LOD***	**Detection time (min)**
Blood smears (Giemsa stain)	Variation in morphology of different parasitic species with thick and thin smear	Bright field microscope	Depends on quality of instrument and the skill of the operator	50-100 parasites	30-60
Quantitative buffy coat (QBC)	DNA stained by acridine orange (AO)	fluorescent microscope	Non-specific: (AO stains DNA from all cell types) Sensitivity varying in low parasitaemia level	>5 parasites	<15

RDTs	Detection based on immune Chromatographic assay	Paper fluidics	Moderate at Higher parasitaemia (>100 parasite.μl^{-1}). Variability in result at high temperature and humidity.	50-100 parasites	10-15
PCR	Specific parasitic DNA amplification with amplicon	Thermo cycler	High	≥1 parasites	45-360 depending on the methods
Serological tests	Malaria antigen detection with Primary and secondary antibody	Microplate reader (for ELISA)	Relatively high	N/A	30-60
LAMP	Turbidity detection after specific DNA amplification at isothermal condition	Turbidity meter	High	>5 parasites	<6
Microarrays	DNA hybridization and fluorescent based quantification	DNA chip	High	N/A	<60
Flow cytometry	Detection of hemozoin	Flow cytometer	Variable sensitivity, high specificity	Nonlinear response	<1
Automated blood cell counters	Hemozoin detection in stimulated monocyte	Haematology analysers	Variability in sensitivity and specificity	5-20 parasites	<1
Mass spectrometry	Identification of heme	LDMS	Not able to differentiate between species	100 parasites	<1
Immune chromate-graphic Assay (Li et al., 2005)	Identification of *Pf*GDH antigen with antibody (colour development due to aggregation of AuNP)	Paper fluidics	Not used	Detect *Pf*GDH 2-16 nM	20-30
ELISA (Dominguez and Acosta., 1996)	Target *Pf*GDH as antigen with polyclonal Antibody	96 Well plate reader	N/A	NA	120-180
Dot Blot (Ling et al., 2005)	Target *Pf*GDH as antigen with specific anibody	Nitro cellulose paper	Able to differentiate *Plasmodium* species	N-A	120-180

1.3.2 Rapid Diagnostic tests (RDTs)

The RDTs were developed for quick and instrument free diagnosis of malaria. They are not as sensitive as thick smear but at high parasitic load (1000 - 2000 parasite. μl^{-1} blood) the sensitivity can reach up to > 95 % (Bjorkman and Martensson, 2010). RDTs depend on capture of specific antigen from patient's serum through mono or polyclonal antibodies conjugated with gold nanoparticles or selenium dye containing inside liposome. Secondary monoclonal antibodies immobilized over nitrocellulose (NC) paper act as the immobile phase. The modified antibody-antigen complexes present as the mobile phase travel along the NC paper strip and are captured by monoclonal antibody present and the consequence of this generate a visible colored line (Moody, 2002).

The first RDT developed against *Pf*GDH displayed good sensitivity and specificity (Domenguez and Acosta., 1996). The *Pf*GDH based RDTs when used for clinical trials in China for malaria diagnosis displayed 86.66 % sensitivity and 96.43 % specificity for *P. falciparum* as compare to thick smear test of microscopy (Li *et al.*, 2005). Many RDTs targeting *Pf*GDH and *Pv*GDH have been employed in the malaria endemic areas as fast diagnosis method (Seol *et al.*, 2017). The currently available dipstick can be divided into different classes on the basis of their target biomarkers viz. *Pf*HRP-II, *Pf*GDH (species specific biomarker) and *P*LDH (pan malaria diagnosis). The commercially available RDTs are mostly based on detection of *Pf*HRP-II and *P*LDH proteins. To increase the efficiency of malaria diagnosis through RDTs, simultaneously dual target detection approach has been also developed. The dual immuno chromatographic test based on *Pf*HRP-II and aldolase biomarker was developed to detect the presence of *P. falciparum* and *P. vivax* in the patient's blood, respectively. However aldolase based RDTs suffer from low sensitivity as these can detect parasite only in presence of high parasitic load (Tjitra *et al.*, 1999; Eisen and Saul, 2000). Another field trial study performed with CareStart™ (Access Bio start, Princeton, USA), which targets *Pf*HRP-II and *P*LDH for *P. falciparum* and non-falciparum species infection, respectively. The study reported the efficiency of the system but showed poor sensitivity in detection of *P. malaria* and *P. ovale* infection (Maltha *et al.*, 2010). RDTs offer several advantages such as, instrument free analysis need of only semiskilled operators and it offers short response time (< 30 min) (Wongsrichanalai *et al.*, 2001). Peng and coworkers has developed the Wondfo rapid diagnostic test, which relies on the aggregation of gold nanoparticle modified with monoclonal antibodies (pan and *P. falciparum* specific) and immune chromatographic

assay. It was better in term of response time and sensitivity and the results show 95.49 % sensitivity and 99.53 % specificity compare to microscopy (Peng *et al.,* 2012).

Although RDTs help a lot to curb malaria problem from malaria endemic region where basic medical healthcare facilities are weak, it suffers from various disadvantages. The variability in RDTs results with the variation of temperature, humidity, patient's age, season of the year, and storage condition, along with its short shelf life are the major drawbacks of the RDTs (Abeku *et al.,* 2008). The most common reason for the low performance of RDTs is exposure to high temperature and humidity which are the typical conditions in tropical or subtropical region of world where malaria is prominent (Jorgensen *et al.,* 2006). The major causes of variation are loss of activity of antibody and damage of NC membrane. Chiodini and coworkers studied the temperature sensitivity of RDTs (or Antibody) and observed their efficiency were affected when temperature increased from 25 °C to 60 °C (Chiodini *et al.,* 2007). Moreover, RDTs are not efficient to provide quantitative information on parasitic load, unable to differentiate among species and showing false positive results due to persistent *Pf*HRP-II antigenmia (Mayxay *et al.,* 2001; Kyabayinze *et al.,* 2008) or false negative result due to deletion of HRP-II gene (Palmer *et al.,* 1998; Iqbal *et al.,* 2004; Lee *et al.,* 2006a). There is a rising frequency of HRP II gene deletions primarily in Amazon regions and in many African and Asian countries that demand for a test with non-HRP II *falciparum*-specific targets (Bharti *et al.,* 2016; Gamboa *et al.,* 2010; Maltha *et al.,* 2012; Bendezu *et al.,* 2010). As most RDTs available in the market are HRP-II based for *P. falciparum* identification, they are prone to false positive and false negative results. In regard to this WHO has issued guidelines to take extra precautions while RDTs are used for malaria diagnosis and to search for suitable alternative biomarker for *P. falciparum* identification (World Malaria Report., 2016).

The genetic polymorphism in biomarkers (*Pf*GDH, *Pf*HRP-II, *P*LDH and aldolase) may produce false negative results as observed in global region wise assessment for polymorphism. The high level of polymorphism was reported for *Pf*HRP-II, III genes envisaging that approximately 9 % isolates from Madagascar region were not able to detected parasitaemia at < 250 parasite μl^{-1} (Mariette *et al.,* 2008). The genetic polymorphism was also reported within and across malaria endemic countries (Joshi, 2003). This has led to low efficiency of the test and only 84 % of *P. falciparum* infection in Asia-Pacific are possible to detect at parasitic load < 250 parasite μl^{-1} based on probable regression analysis. Moreover, *Pf*HRP-III is also supposed to play a significant

contribution in the performance of *Pf*HRP-II based detection system (Baker *et al.*, 2005). Which bring a major challenge to distinguish severe form of malaria from other normal febrile illness caused by *P. falciparum* infection based on immuno chromatographic test. Besides of this deletion and polymorphism in *Pf*HRP-II gene, the result produced by *Pf*HRP-II based RDTs have to consider with precaution and further confirmation is require with other diagnostic methods (World Malaria report, 2016). The various scientific reports on performance analysis of different RDTs from different part of world have been published (Chansuda, 2001). In spite of this large number of reports their comparative exploration is, however tough due to variance in demographic, different trial guidelines, their clinical and epidemiological symptoms etc. (Wongsrichanalai *et al.*, 2007). However, a comparative study has been performed for few prominent field trial diagnostic tests on the ground of sensitivity and specificity, as shown in table 1.5. It is clearly reveled from the table that the performances of RDTs significantly vary across different studies. Because of these variations there is a demand for more sensitive, selective, reliable and pragmatic detection method for malaria diagnosis.

Table 1.5: Comparative assessment on sensitive and selective of various prominent dipstick RDTs.

Dipstick	**Standard**	**Region of study**	**Sensitivity (%)**	**Selectivity (%)**	**Reference**
Carestart AccessBio,(Princet-on, USA)	GTTS*	South-western Uganda	95.6	91.5	Fogg *et al.*, (2008)
Vistapan Mitra, (New Delhi, India)	GTTS*	South-western Uganda	91.9	89.6	Fogg *et al.*, (2008)
Parabank Orchid/Zephyr, (Goa, India)	GTTS*	South-western Uganda	84.7	94.3	Fogg *et al.*, (2008)
Paracheck *Pf*, Orchid/Zephyr, (Goa, India)	GTTS*	South-western Uganda	94	87.3	Fogg *et al.*, (2008)
Optimal-IT, DiaMed,(Cressier, Switzerland)	GTS	Gabon Children n	94	97	Mawili-Mboumba *et al.*, (2010)
Acon, Acon Labs, (San Diego, CA)	GTS	Gabon Children under 11 years	94	90	Mawili-Mboumba *et al.*, (2010)
PALUTOP+4 ALL.DIAG,(France)	GTTS* and PCR	Madagascar	95.4	97.1	Rakotonirina *et al.*, (2008)
Optimal-IT, DiaMed,(Cressier, Switzerland)	GTTS* and PCR	Madagascar	75.8	99.0	Rakotonirina *et al.*, (2008)

ParaHIT *Pf* Test, Span Diagnostic Ltd., (Surat, India)	GTTS* and PCR	Tanzania	69.2	100	Nicastri *et al*., (2009)
Malaria *Pf*™, ICT Diagnostics, (South Africa)	GTTS*	Uganda	98	72	Kyabayinze *et al*., (2008)
Paracheck *Pf*, Orchid Biomedical Systems, (Goa, India)	GTTS*	Kenya	91.7	96.7	de Oliveira *et al*., (2009)
Malaria Check_*Pf* test, Cumberland Diagnostics, (USA)	GTS**	Brazil	97.4	88.5	Avila *et al*., (2002)
Makromed Dipstick Assay, Makro medical, (South Africa)	PCR	Cananda	97.0	96.0	Richardson *et al*., (2002)
ParaSight®-F, Becton Dickinson, (USA)	Thin blood smears and QBC	France	94	99	Uguen *et al*., (1995)
ParaSight®-F, Becton Dickinson, (USA)	Microscopy	Iquitos, Peru,and Maesod, Thailand	95	86	Forney *et al*., (2001)
Paracheck *Pf*, Orchid Biomedical Systems,(Goa, India)	Microscopy	India	93	84	Singh *et al*., (2005)
ParaHIT-*Pf*, Span Diagnostics, (Surat, India)	GTS**	Tanzania	90.7	73.5	McMorrow *et al*., (2010)
ParaHIT-*Pf* , Span Diagnostics, (Surat, India)	Microscopy	India	87.5	97	Singh *et al*., (2005)

GTTS*-Giemsa thick and thin smear, GTS**-Giemsa thick smear

1.3.3 Non-antibody based bio recognition molecules for malaria diagnosis.

Over the last decade there has been a continuous strive to replace antibodies and other labile biorecognition elements with stable recognition systems for developing various diagnostic and detection devices (Thiviyanathan and Gorenstein., 2012). Among them, nucleic acid based aptamers are emerging as efficient and viable alternatives to the antibodies. (Yang *et al.,* 1998; Stoltenburg *et al.,* 2012; Marangoni *et al.,* 2015; Radom *et al.,* 2013). Aptamers are able to bind to specific target in 3D conformation and they work on lock-key hypothesis. The particular 3D conformation shape fits well into the binding pocket present over the target or vice versa. Aptamers are generated by SELEX procedure, which consist of selection of probable best binders from a very large oligonucleotide library pool (10^{12}-10^{15} molecules) against the target by iterative procedure

of *in vitro* selection and enrichment as depicted in figure 1.7 (Cho *et al.*, 2009).

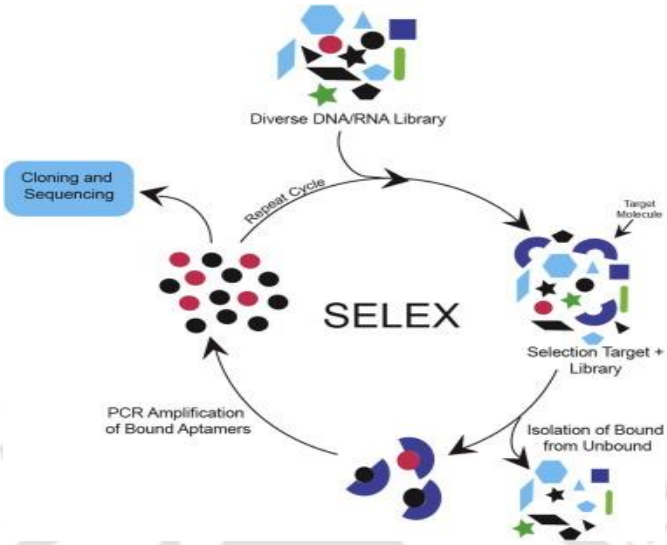

Figure 1.7: A general scheme of SELEX process (adapted from Wu *et al.*, 2016).

The aptamer recognizes and binds with target similar to antigen-antibody interaction. Most of the aptamer-target interactions are govern by intermolecular interaction i.e aromatic rings, hydrogen bonding, π-π stacking, van der Waals and electrostatic interactions between charged groups (Kakoti and Goswami, 2017). The binding affinity of the ssDNA aptamers with their targets is usually lie in the pM to nM range (Kimoto *et al.*, 2013; Kraemer *et al,* 2011; Parekh *et al.*, 2013). Aptamers overcome several limitations of antibodies and offer various advantages over it. They can distinguish the target among large population over subtle structure differences (Xiong *et al.*, 2014; Cho *et al.*, 2009; Ng *et al.*, 2006). For example, theophylline specific aptamer show a 10000 times lower dissociation constant against it target compare to caffeine, which diverges from theophylline by single methyl (CH_3) group at N_7 nitrogen atom. Aptamer are small in size, nonimmunogenic and nontoxic because of which it can easily go into cells, tissue through pores and exhibit fast elimination from human system and are suitable candidate for therapeutic applications (Martinez *et al.*, 2014; Melancon *et al.*, 2014). Besides this, aptamers offer thermal stability, low cost production, functionalization with chemicals and robustness due to phosphodiester backbone (Sun *et al.*, 2015; Potyrailo *et al.*, 2015; McKeague and DeRosa, 2012). The aptamer can be produced economically in a large scale following established chemical protocols. Moreover, there is a scope to enhance the selectivity of the DNA aptamers by chemical modifications (Song *et al.*, 2012). Because of these advantages aptamer are suitable candidate to replace unstable and expensive

antibodies. A comparative study has been performed between aptamer and antibody and summarize in table 1.6.

Table 1.6: Comparison between aptamer and antibody on some critical parameters (part of table adapted from Lee *et al.*, 2008).

	Aptamers	**Antibody**
Cost	Inexpensive	Expensive
Binding affinity	K_d in nM-pM range	K_d in nM-pM range
Specificity	High	High
Synthesis	chemical procedure	*In vitro* biological procedure
Target array	Broad range of targets i.e. ions, small organic, molecules, proteins, whole cells, etc.	Limited: only immunogenic compounds
Batch to batch variation	Not significant	Significant
Chemical modification	Easy and straightforward	Limited
Thermal denaturation	Reversible and stable at RT	Irreversible and unstable at RT
Shelf-life	Very long	Limited

Malaria has dominance in tropic region, hence it requires stable diagnosis platform that can endure high temperature and humid conditions without significant reduction in functionality. Keeping this in view, current trend on malaria research is focused on the development of DNA based sensing platform and other chemical based recognition system (Chakma *et al.*, 2016). There are few reports on development of aptamer-based malaria detection approaches (Cheung *et al.*, 2013; Jain *et al.*, 2016). These are several chemical based recognition systems have also been reported in last few years for malaria detection. Although these chemical detection systems offer some advantages such as fast, simple, stable and low cost diagnosis they are suffering from some drawbacks such as poor sensitivity, specificity and inability to differentiate among various *Plasmodium* species. Recently, Chakma *et al.*, (2016) reported chemical based assay in which they have used hydrophilic tridentate orange color dye murexide (ammonium purpurate) that binds with Ni^{2+} with three coordinated bonds forming pink color compex. The restoration of original color of murexide with competitive substitution of Ni^{2+} from complex in the

presence of *Pf*HRP-II used as detection signal for malaria. In another chemical based approach chemical alternation at membrane of iRBC compare to normal RBC were used as probe for malaria detection. For which array of silver nanorod (AgNR) arranged over glass slide at particular angle used as recognition probe to capture RBC or iRBC from sample and further analyzed through surface enhanced Raman spectroscopy. The different stages of iRBC (trophozoite, schizoid or ring stage of parasite inside RBC) correspond to characteristic Raman peaks, which were significantly different among each other and compare to normal RBC. This system is however incapable to precisely quantify the infection or parasitic load in patient (Chen *et al.*, 2016a). The Buffy coat analysis is another example of chemical based detection method in which acridine orange (AO) dye, a specific binder for deoxyribonucleic acid (DNA) or ribonucleic acid (RNA) used as recognition and reporter probe. This method based on centrifugal stratification of blood components and surrounding beneath the buffy coat was analyzed through fluorescent microscope for quantification and detection of malaria. Albeit this method is quit sensitive and specific but dependent on various instrument that makes it difficult to use in scenario of developing countries (Alias *et al.*, 1996).

1.3.4. Advance techniques and different signal transduction principles applied for malaria diagnosis

Biosensor has revolutionized the field of diagnosis and detections. A schematic presentation of different parts of biosensor is shown in figure 1.8.

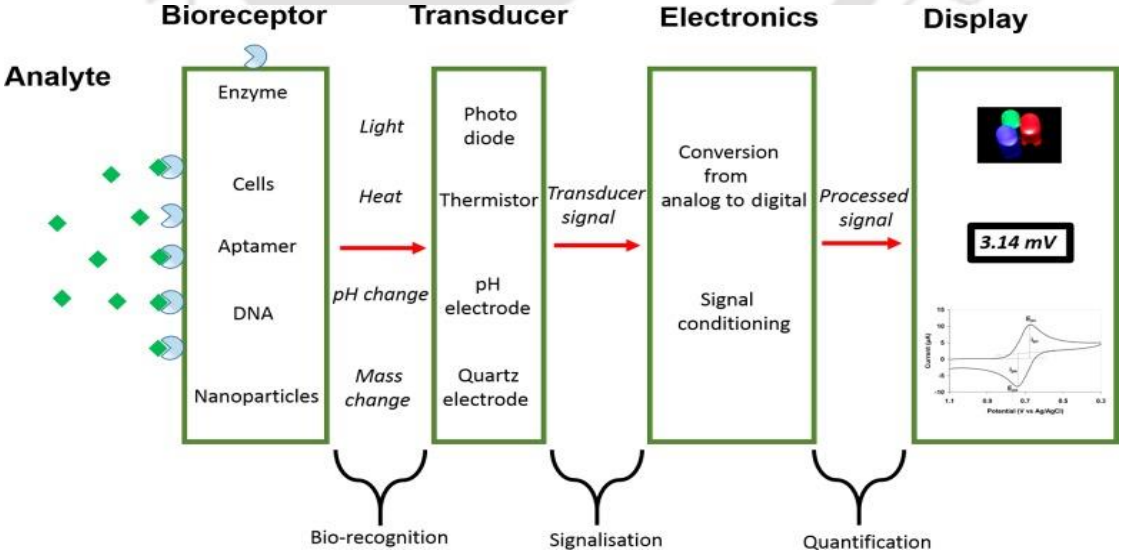

Figure 1.8: Schematic presentation of biosensor parts (Adopted from Bhalla *et al.*, 2016).

The different types of bio recognition elements used for biosensor applications mostly include enzyme, antibody, aptamer, DNA, peptides and cells. The electrochemistry, piezoelectricity, and optical behaviour are commonly used transduction principles in biosensor device. The current trend in biosensor research shows promise towards the development of a rapid, sensitive, stable, reproducible and low cost detection system for various analytes of clinical importance. Practical advantage is that it can be used by semi-skilled person in POC settings or by patients/users themselves. The detection platforms exploited to develop biosensors and diagnostics should complies well with the ASSURED (Affordable, Sensitive, Specific, User-friendly, Rapid and robust, Equipment free and Deliverable to end users) mandate of WHO for application of such diagnostic tools in developing and underdeveloped countries (Kunte and Kunwar, 2011). Most of the proof-of-concepts developed so far for malaria diagnosis are rely on optical principle, while a few of them exploit electrochemical principles such as amperometry, voltammetry (Lee *et al.,* 2012; Miranda *et al.,* 2018). Each of these methods, however, has its own merits and demerits. For POC settings, colorimetric approaches are suitable as they may provide equipment-free detection through naked eyes. Some prominent POC malaria sensors with their respective signal transduction principles, detection platforms and some critical performance factors are included in table 1.7.

The current major research focuses on electrochemical biosensors for developing malaria diagnostic using antibody or aptamer developed against *P*LDH and *Pf*HRP-II. The electrochemical sensor offer great advantages such as rapid response time, high sensitivity, low LOD, miniaturization and easy electrode surface modification for formation of surface assembled monolayer (SAM) to capture broad range of targets (Schmidt and Schaechter, 2011). Electrochemical impedance spectroscopy (EIS), which can be performed via Faradaic or non-Faradaic modes, has recently received enormous interest in the field of biosensors due to its highly sensitive signal transduction feature (Arya *et al.,* 2017; Rohrbach *et al.,* 2012). The Faradaic impedance spectroscopy however, relies on an indirect method where a redox species is used to investigate the biological interaction at the electrode interface (Liu *et al.,* 2012). Hence, the method requires an additional design strategy or step to incorporate the redox species such as ferricyanide or ruthenium complex in the detection device, which intricate the system and thus discourage it for POC applications. In contrast, non-Faradaic EIS measurements do not require any external redox probe, allowing direct measurement of the target molecule in the sample that makes the system suitable for POC applications (Arya *et al.,* 2018; Luo

and Davis, 2013).

Table 1.7: Some selected POC malaria sensors along with their detection principles, sensor platforms and few performance factors.

Technique	Surface/ Electrode	Probe	Detect-ion range	Target Antigen	Respon-se time	LOD	References
Colorimetric	Paper µPAD	Murexi-de dye-Ni Ions	10-100 nM	*Pf*HRP-II	~5 min	30 nM	Chakma *et al.,(* 2016)
Colorimetric	Gold nanoparticle	Aptamer	-	*P*LDH	~10 min	57 pg. μL^{-1}	Cheung *et al.*, (2013)
Colorimetric	Gold nanoparticle	Aptamer	1pM-1µM	*Pf*LDH	~10	1.25 pM	Lee *et al.*, (2014)
Electrochem-ical phone based Immuno-sensor	Poly dimethyl siloxne µPAD	Antibo-dy	10.8-27.5 nM	*Pf*HRP-II	~15 min	432.43 pM	Lillehoj *et al., (*2013)
Colorimetric	Magnetic beads	Antibo-dy	25 nM-2 µM	*Pf*LDH	~45 min	25.7 pM	Markwalter *et al.*, (2016)
Colorimetric	Paper	Aptamer	3.5 nM-35 µM	*Pf*LDH	~45 min	36 pM	Dirkzwager *et al.*, (2016)
Opto-Magnetic	-	-	100 nM-5.0 µM	Hemozoin	~1 min	~2 nM	Newman *et al., (*2008)
Opto Magnetic	Portable optical system (PODs)	-	1-5 $\mu g.mL^{-1}$	Hemozoin	~ 1min	~0.0087µg. mL^{-1}	McBirney *et al.*, (2018)
Immune chromatogra m-phic	Gold nanoparticle	Antibo-dy	2-16 nM	*Pf*GDH	10-20 min	N/A	Li *et al.*, (2005)
Optical (RDT*)	Paper microfluidic	*Pf*HRP-II Antibo-dy	0.7- 91 pM	*Pf*HRP-II	20 Min	23 pM	Jimenez *et al.*, (2017)
		*Pv*LDH Antibo-dy	3.9 pM-39 nM	*Pv*LDH	20 Min	195 pM	Jimenez *et al., (*2017)

* Based on analytical performance of best malaria rapid diagnostic tests (RDTs) in market.

It is based on alteration of electrical double layer properties. The variations in interfacial capacitance, developed by dislocating water molecules and ions away from a bio-

functionalized (such as enzyme, antibody or aptamer) electrode or semiconductor surface after its binding to the target molecule is used for sensor application (Tkac and Davis, 2009). The electric double denotes two parallel layers of charge over metal surface in buffer and are separated be a particular distance. The first layer comprises of positive and/or negative charge due to surface adsorption of ions over metallic electrode through electrostatic interaction or chemisorption. The second layer of counter ions forms against first layer due to columbic interaction and screen the surface charge of the first layer. This system acts as a capacitor when potential is applied, a linear potential drop is obtained between these two layers with constant double layer capacitance (C_{dl}). In 1947 Grahame further improvised this double layer model by introducing three layer model of capacitance (figure 1.9).

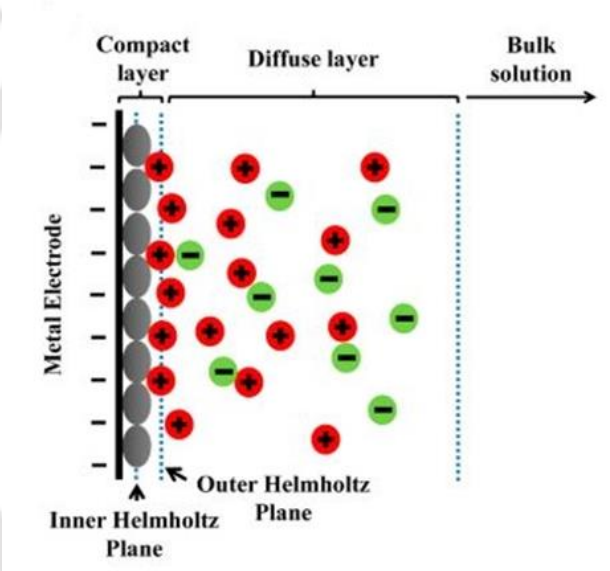

Figure 1.9: The electric double layer model (Liu *et al.*, 2017).

The closest layer to electrode called inner Helmholtz plane (IHP) and formed due to specific absorption of ions, followed by nonspecifically enticed counter solvated ions through ionic interactions called outer Helmholtz plane (OHP) along with this weakly attracted solvated counter ions forms the third layer and referred to as the diffuse layer. Till date this three layer model is a well-accepted model to explain electric double layer system. As depicted in figure 1.9, the two capacitors are connected in series with each other: first is differential capacitance C_{OHP} formed between OHP and IHP. Another capacitance formed between OHP and diffuse layer and termed as $C_{diffuse}$. So overall capacitance is sum of two as equation (i) but in case of biofunctionalized electrode it changed drastically as equation (ii) where C_{SAM} is the capacitance of biofunctionalized

surface over electrode. The target specific interaction at surface of biofunctionalized electrode lead to change in capacitance (equation iii where, εo is the dielectric constant of free space, εr is the dielectric constant of material, A is the area of SAM surface, D is the distance between layers) of system by altering the thickness of double layer and change in dielectric properties between layer interface.

$$1/C_{dl} = 1/C_{OHP} + 1/C_{IHP} \text{..... (i)}$$

$$1/C_{T} = 1/C_{dl} + 1/C_{SAM} \text{ ..... (ii)}$$

$$\text{Capcitance} = \frac{\varepsilon o\ \varepsilon r\ \mathrm{A}}{D} \text{..... (iii)}$$

Since non-faradaic EIS give direct information of specific binding at electrode surface in absence of any label or reagents, and thus noninvasive in nature contrast to Faradic EIS where redox dyes are used. Due to aforementioned advantages non-Faradic EIS have been broadly used for various studies such as detection, of biomarker (Arya *et al.,* 2018), Proteins (Mirsky *et al.,* 1997), Antibody (Rickert *et al.,* 1996), Cell exocytosis (Jayant *et al.,* 2015), DNA (Ma *et al.,* 2006), Ions (Bontiden *et al.,* 1998) and environmental effect on overall cell growth (Lin *et al*., 2015). An electrochemical aptasensor was developed targeting *Pf*LDH with detection limit of 0.10 pM and 0.12 pM for *Pv*LDH and *Pf*LDH respectively (Lee *et al.,* 2012b). The EIS is a desirable detection platform due to it impeccable properties such as high sensitivity (Ohnoa *et al.,* 2013), label free (Min *et al.,* 2008) and redox free (Arya *et al.,* 2018) attributes.

The first miniaturized FET based sensor was developed by Bergveld over silicon layer (Bergveld, 1970). This silicon based FET sensor offers great advantages for development of new detection method because of their small size, rapid response, on chip integration facilities and signal processing scheme with the future prospect of POC devices for field application (Schöning and Poghossian, 2002). The FET based biosensor is an emerging area of sensor research, which comes under the potentiometric spectroscopy. The BioFET can be fabricated from ion selective FET (ISFET) by altering the gate surface or joining it with various types of biological recognition elements (Figure 1.10). In the BioFET device, charge or potential effect is used to measure the recognition events. The FET based system is highly sensitive in nature and display sensitivity in attomolar (10^{-18} M) range in highly complex solutions like serum (Chu *et al.,* 2017; Kim *et al.,* 2013).

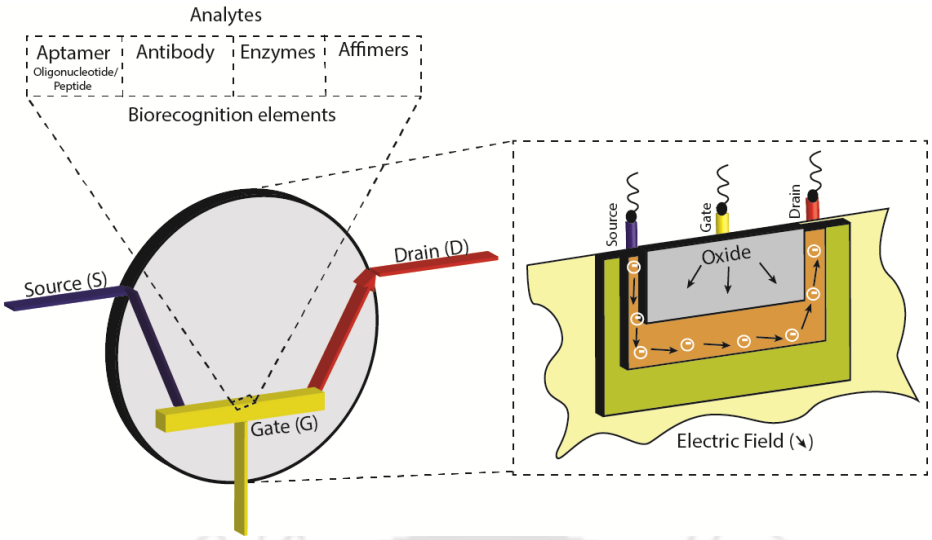

Figure 1.10: Schematic illustration of BioFET.

The extended gate field effect transistor (EgFET) is suitable for detection of series of biological analytes from biological samples. In this method gate is extended away from transistor body and connected through wire system, offering a separation of wet and dry environments. The biofunctionalized sensing electrode act as off-chip extended gate and it is only submerged in solutions. This offers benefits such as a simple and easy electrode fabrication along with post processing steps. The EgFET transfer the signal from high to low resistance environment tangibly near to transducer interface thus circumventing the need for Faraday cage. The EgFET basic detection principle is explained well by Shoorideh and Chui, (2014). The charge present at extended gate electrode surface is in resting phase (σ_0). This surface charge depends on the double layer (C_{dl}) and sensor capacitance (C_{FET}) connected in parallel to each other. The (C_{FET}) capacitance consists of gate oxide capacitance (C_{OX}) and depletion layer capacitance (C_b). The binding interaction at the surface of sensing electrode lead to change in surface potential as displayed in equations (iv, v). The C_b depends on the type of transistor biasing (forward or reverse).

$$\Psi_0 = \Delta\sigma_0/C_{dl} + C_{FET} \ldots\ldots\ldots \text{(iv)}$$

$$\Psi_0 = \Delta\sigma_0/C_{dl} + C_{OX} + C_b \ldots\ldots \text{(v)}$$

In simple words, the change in signal response with binding of the target over sensing surface is defined with underlying physics. First the net charge present over target surface change the oxide electric field and alter the outer surface electrode surface potential. Second the shift in potential change the drain current (I_D) lead to transconductance effect of a FET. Recently this simple design and concept was used for various sensing concepts

as follows. An electrical ELISA was performed with antibody to detect bovine herpes virus (BHV-1) infection (Tarasov *et al.*, 2016). This concept was also used for detection of potassium ions (K^+) in extracellular fluids to check the efficacy of Na^+- K^+ over interdigitated micro electrode (Odijk *et al.*, 2015). An aptamer based reagent free, label free sensor has been developed to detect the tenofovir concentration during drug administration in real time within the therapeutic range (Aliakbarinodehi *et al.*, 2017). A portable integrated device with versatile EgFET platform also has been reported (Kaisti *et al.*, 2016).

Majority of the optical and colorimetric systems are founded on ELISA platform and flow immunoassays principle, respectively. A highly sensitive immunocapture based optical diagnostic method for the detection of *Pf*LDH has been developed by Piper *et al*., (Piper 1999) which showed limit of detection of 50 *plasmodium* parasites μl^{-1}. The aptamer or antibody based capture of *P*LDH malaria biomarker from blood with enhanced sensitivity was developed. It used the enzymatic activity of captured enzyme for generating signal. This helped to reduce the number of false positive signal which may occur due to non-specific binding of aptamer or antibody with serum proteins (Dirkzwager *et al.*, 2016; Markwalter *et al.*, 2015). Recently, twelve aptamers targeting *Pf*LDH were united into a rectangular DNA origami. The captured *Pf*LDH displayed significant enzymatic activity, the target-aptamer complex was observed dynamically using high-speed AFM (Godonoga *et al.*, 2016). In another innovative report, a non-invasive rapid (~ 20 sec) method for malaria detection has been developed. This method was based on transdermal optical excitation with short laser impulse which promotes the formation and bursting of vapor nanobubbles around hemozoin molecules and recorded by acoustic sensor present over the skin (Hleb *et al.*, 2015). The recent advanced methods reported during recent past on detection of various biomarkers for malaria diagnosis are enlisted in table 1.8.

Table 1.8: Some prominent malaria detections based on various methods and there characteristics.

Assay name and Probe	Sensor platform	Biomarker	Range	Detection limit	References
Amperometric (Antibody)	MWCNTs and Au nanoparticles modified SPE	HRP-II	-	8 $ng.ml^{-1}$	Sharma, *et al.*, (2008)
Impedance (Aptamer)	Graphene oxide over GCE	*Pf*LDH	0.5- 10 fM	0.5 fM	Jain *et al.*, (2016)
Amperometric (Antibody)	Gold nanoparticles /alumina sol-gel modified SPE	HRP-II	-		Sharma, *et al.*, (2010)
Amperometry	Ni-coated electrode	Hemoglo-bin	Qualitative (yes/no format)	-	Bhattacharya ., (2011)
Impedance (Aptamer)	Gold electrode	HRP-II	1-500 pM	3.15 pM	Chakma *et al.*, (2018)
Piezoelectric sensor (Antibody)	Quartz crystal	HRP-II	15-60 $ng.ml^{-1}$	12 $ng.ml^{-1}$	Sharma, *et al.*, (2011)
Magneto sensor (Antibody)	Graphite-Epoxy Composite Magneto Electrodes	HRP-II	-	0.36 $ng.ml^{-1}$	Castilho, *et al.*, (2011)
Electrochemical phone based sensors (Antibody)	Polydimethylsiloxne microfluidic chips	HRP-II	-	16 $ng.ml^{-1}$	Lillehoj, *et al.*, (2013)
Carbon Nanofibers sensors (Antibody)	Carbon nanofiber forest grown on glass microballons	HRP-II	0.01–10 $ng.ml^{-1}$	0.025 $ng.ml^{-1}$	Gikunoo *et al.*, (2014)
Self-assembled nanofiber sensor (Aptamer)	Mercaptopropyl phosphonic acid Functionalized copper doped zinc oxide nanofibers	HRP-II	10 $ag.ml^{-1}$-10 $\mu g.ml^{-1}$	6.8 $ag.ml^{-1}$	Brince , *et al.*, (2016)
Enzyme-free electrochemical Sensor (Antibody)	MB, hydrazine and platinum nanoparticles (Pt NPs) on Low electrocatalytic ITO modified glass electrodes	HRP-II	1 $pg.ml^{-1}$- 100 $ng.ml^{-1}$	2.2 $pg.ml^{-1}$	Dutta, *et al.*, (2017)
Enzyme-free electrochemical sensor (Antibody)	Electrochemical-chemical-chemical (ECC) redox cycling signal amplification on (ITO) modified glass electrodes;		10 fg. ml^{-1} – 100 $ng.mL^{-1}$	10 $fg.ml^{-1}$	Dutta, *et al.*, (2017)
Electrochemical sensors (Antibody)	Gold nanoparticles modified gold SPE	HRP-II	-	36 $pg.ml^{-1}$	Hemben, *et al.*, (2017)

Electrochemical sensor (Aptamer)	PvLDH aptamer functionalized gold electrode	*Pf*LDH	-	120.1 fM	Lee *et al*., (2012a)
Magneto-ELISA (Antibody)	Magnetic nanoparticles/ Magnetic beads	HRP-II	0.35-7.81 1.31-62.5 $ng.ml^{-1}$	0.35 and 1.31 ng. ml^{-1} for Magnetic nanoparti-cles/ beads	Castilho, *et al*., (2011)
Immuno-fluorescence chromatographic assay (Antibody)	Fluorescent nanoparticle labelled immune-chromatographic strips	HRP-II	-	25 parasites. μl^{-1}	Kang, *et al*., (2015)
Colorimetric Enzyme amplification assay (Antibody)	Cellulose paper Functionalized by enzyme/metal/polymer conjugated antibody	HRP-II	-	0.32, 0.15, 6.9 , 6.2 nM for paper functional-ized by enzyme / metal/ polymer respectively	Lathwal, *et al*., (2016)
Signal amplification with porphyrin nanoparticles assay (Antibody)	Antibody conjugated TCPP NPs in sandwich Assay	HRP-II	10-1000 pM	2.05±0.003 pM	Gibson, *et al*., (2016)
Bead-based assay (Antibody)	Antibody functionalized polystyrene beads in ELISA format	HRP-II		1 $pg.ml^{-1}$	Rogier, *et al*., (2017)
Fluorescent chromatographic test (Antibody)	Coumarin derived dendrimer	*Pv*LDH		0.1 ng	Song *et al*., (2012)
Colorimetric sensor (Aptamer)	Gold nanoparticle-Aptamer-Salt	*Pf*LDH		57 $pg.\mu l^{-1}$	Cheung *et al*., (2013)
Colorimetric sensor (Aptamer)	AuNP-Aptamer-Cationic polymer PDDA2 and PAH3	*Pv*LDH		8.7 pM and 8.3 pM for PDDA2 and PAH3, respectively	Jeon *et al*., (2013)
Fluorescence-linked immunosorbent assay (Antibody)	Coumarin-derived dendrimer	*Pv*LDH		0.01ng. ml^{-1}	Yeo *et al*., (2014).
Colorimetric sensor (Aptamer)	AuNP-Aptamer-Cationic surfactant	*Pv*LDH		1.25 pM	Lee *et al*., (2014)

Magnetic beads and dye based enzyme assay (Aptamer)	Magnetic microparticle	*Pf*LDH	2 parasites. ml^{-1}	Markwalter *et al.,* (2016)
Fluorescence sensor (Aptamer)	FAM4-aptamer-MoS_2 nanosheets	*Pf*LDH	550 pM	Geldert *et al*., (2016)
Opto acoustic based sensor (Hemozoin)	Laser impulse and acoustic sensor	Hemozoin	0.8 % Parasite-mia	Hleb *et al.*, (2015)

1.3.5 Nanomaterials for malaria diagnostics application

Various types of nanomaterials such as metal nanoparticles, carbon based nanomaterial, quantum dots and nanoclusters are used in the bioanalytical systems due to their diverse physical, chemical and electronic properties. Over the last few years various methods for surface functionalization of nanomaterials have been developed, which facilitate the interaction of biomolecules with nanomaterials for potential sensing applications. These complexes exhibit selectivity, function and provide required chemical or physical properties from the corresponding nanomaterials and biorecognition elements (Guo and Dong 2009). A decent example of this complex is the immobilization of antibody with magnetic micro or nanoparticle to improve the performance of current ELISA system. The magnetic particles facilitate concentration and separation of target from biological fluids and enhance the signal to noise ratio (Markwalter, 2016b). Nanomaterial like graphene oxide (GO), carbon nanotube and zinc oxide nanofibres with excellent electrochemical properties have been modified with aptamer or antibodies for highly sensitive malaria sensor (Jain *et al.,* 2016; Paul *et al.,* 2016; Gikunoo *et al.,* 2014). Apart from this few other nanomaterials based optical system has been developed for sensitive detection of malaria (Jain *et al.,* 2017; Yeo *et al.,* 2014; Guirgis *et al.,* 2012). Over the last several years Cdots achieved remarkable scientific attention in various fields and these are ideal alternative of various existing metal based nanomaterial, offering advantage such as low slung toxicity, biocompatibility, solubility, cheap, easy synthesis, surface functionalization and stability. Few additional features of Cdots make special these materials from other existing fluorometric material. In general, fluorescent carbon dots based sensor includes three approaches. One is direct approach in which association of target analytes directly quench the fluorescence of carbon dots. Different types of metal ions directly detect in broad range through quenching of pristine Cdots which act as sensing material. The functional group and surface charge present over carbon dot directly coordinate with target metal ion. Furthermore, various oxidative analytes could

quench the fluorescence of carbon dots directly, probably through oxidation of carbon dots surface (Sun and Lei, 2017). The second design for Cdots based sensor development is through post modification or functionalization of carbon dots. To increases the sensor specificity and sensitivity specific receptor (aptamer, antibody, dendrimer and chemical reagents) has been conjugated with CDs which facilitate their binding with specific target analyte in different population of analytes (Ding *et al.,* 2015; Muhammadi *et al.,* 2018). The third approach is integration of Cdots with others substrates (fluorophores for FRET application, quenchers, etc.) as sensory materials. For example, first fluorescent carbon dot quenched in the presence of quenching element and fluorescence recovered back. As mention earlier, with addition of metal ions carbon dots fluorescence is quenched. This quenched carbon dot-metal complex could be applied for sensing a range of analytes such as anions. Some dual mode sensor in which more than one analyte detected based on integrating fluorescence quenching and recovery of carbon dot fluorescence. Furthermore, ratiometric sensor also has been developed in which ratio of fluorescence intensities at two or more wavelengths is measured, which is thus more reliable and less interfered (Motaghi *et al.,* 2017).

Carbon based nanomaterial is an emerging class for malaria sensing applications Gikunoo *et al.,* (2014) immobilized carbon nanofibre forest and antibody complex over glass micro balloon due to this it offer extraordinary sensitivity for detection of HRP-II antigen compared to routine ELISA. Recently, quantum dot (CdSd/CdZnS) functionalized with protein G and magnetic bead (MB) decorated with antibody for HRP-II was used detection of malaria. In this approach special cartridge prepared from PDMS with custom design was used which facilitate magnetic bead capture and separation of antigen/antibody/MB complex and quantum dot with protein-G help in fluorescence enhancement (Kim *et al.,* 2017). Among different types of nanomaterials gold nanoparticle (AuNP) is the most prominent nanoparticle and due to their biocompatibility nature it holds great promise for clinical and biological applications (Xiao *et al.,* 2003). The functionalized AuNPs with recognition molecules (antibody, aptamer etc.) find application in diagnosis, therapy (Li *et al.,* 2005; Stoeva *et al.,* 2006) and design of materials (Lee *et al.,* 2007). The advanced materials that have been effectively used for developing aptamer, antibody and other material based malaria detection platforms are summarized in table 1.9.

Table 1.9: Advanced materials used for malaria detection.

Advance material	Probe	Biomarker	Method	Detection limit	References
Coumarin derived dendrimer	Antibody	*Pf*LDH	Fluorescence	0.01ng.ml^{-1}	Yeo *et al.*, (2014)
AuNP, Cy3 Antigen	Antibody	*Pf*Hsp70[1]	Fluorescence	2.4 µg.ml^{-1}	Guirgis *et al.*, (2012)
MB with Dye	Antibody	*Pf*LDH	Optical	21.1 parasites. ml^{-1}	Markwalter *et al.*, (2016a)
MB and enzyme based reporter	Antibody	*P*LDH and HRP-II	Optical	2 parasite. ml^{-1}	Markwalter *et al.*, (2016b)
Magnetic micro and nano beads	Antibody	HRP-II	Electrochemical	0.36 ng. ml^{-1}	De souza *et al.*, (2011)
SAM with thioctic acid and dodecanethiol	Antibody	HRP-II	Piezoelectric	12 ng.ml^{-1}	Sharma *et al.*, (2011a)
Mercaptobenzoic acid with SPR chip	Antbody	HRP-II	SPR	5.6 pg	Sikarwar *et al.*, (2014)
Cu/Zn nanofibre	Antibody	HRP-II	Electrochemical	6 attogram.ml^{-1}	Paul *et al.*, (2016)
Coumarin derived Dendrimer	Antibody	*Pv*LDH	Fluorescence	0.1 ng	Song *et al.*, (2012)
CTAB[2] with AuNP	Aptamer	*P*LDH,	Optical	1.25 and 2.94 pM for *Pv*LDH, *Pf*LDH respectively	Lee *et al.*, (2014)
MB with shell nanorattle	Aptamer	*P.falciparum* gene Art-R	SERS[4]	100 attomole	Ngo *et al.*, (2016)
Quantum dots	Aptamer	18s rRNA	Fluoremetric	-	Chen *et al.*, (2013)
AuNP	Aptamer	MSP[3] 10	optical	12 parasite. µl^{-1}	Alnasser *et al.*, (2016)
FAM-aptamer, MoS_2 nanosheets	Aptamer	*Pf*LDH	Fluorometric	500 pM	Geldert *et al.*, (2016)
PEG[5] 4-Ni-NTA/AuNP	w/o bioprobe	HRP-II	Optical	7.4 nM	Gulka *et al.*, (2015)
-	-	Hemozoin	Magnetic resonance relaxometry	10 parasites. µl^{-1}	Peng *et al.*, (2014)
Murexide dye Ni (II) ions	w/o bioprobe	HRP-II	optical	30 nM	Chakma *et al.*, (2016)

Ni-NTA polystyrene particles	w/o bioprobe	HRP-II	Optical	10 pM	Gulka *et al.*, *(*2014)
Silver nanorod	w/o bioprobe	iRBC	SERS[4]	$1.5\times 10^{7}.ml^{-1}$ iRBC	Chen *et al.*, *(*2016a)
AgNP	w/o bioprobe	Hemozoin	SERS	2.5 parasites. μl^{-1}	Chen *et al.*, *(*2016b)
Gold coated butterfly wings	w/o bioprobe	Hemozoin	SERS	0.0005 % iRBC	Garrett *et al.*, *(*2015)
Silver nanoparticle with MB	w/o bioprobe	Hemozoin	SERS	30 parasites. μl^{-1}	Yuen and Liu, (2012)

[1]heat shock protein 70, [2]Cetyl trimethyl ammonium bromide, [3]Merozoite surface protein, [4] Surface enhanced Raman spectroscopy, [5]Poly ethyl glycol, w/o without.

Chapter 2

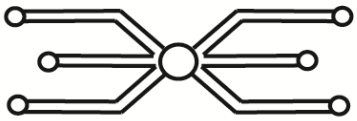

Cloning, Expression, Purification and Characterization of PfGDH, HGDH

Chapter 2

Cloning, expression, purification and characterization of *Plasmodium falciparum* and Human glutamate dehydrogenases

2.1 Overview

The *Pf*GDH (EC no. 1.4.1.4; PlasmoDB accession no. PF3D7_1416500) is projected as an alternative malaria biomarker for detection of the *P. falciparum* target (Wagner *et al.,* 1998; Seol *et al.,* 2017). The strength of *Pf*GDH as a suitable biomarker has been established by the fact that the host counterpart of this target, the *H*GDH, is not present in the human erythrocyte, where the parasite primarily releases *Pf*GDH (Wagner *et al.,* 1998*)*. Moreover, it has some distinctive structural, compositional and functional features from the *H*GDH (Werner *et al.,* 2005; Storm *et al.,* 2011; Zaganas *et al.,* 2012). *Pf*GDH is present in soluble form throughout the sexual and asexual stages of the parasite development and is present in significant quantity in the blood serum of malaria patients (Dominguez and Acosta, 1996). The isoform, *Pf*GDH$_a$ shows many contrasting differences with *H*GDH, that makes it a better target than other isoforms of *Pf*GDH for sensing applications. We used *Pf*GDH$_a$ for our present work, and it is represented as *Pf*GDH in the later sections of this thesis. This chapter includes the results obtained from the studies involving cloning, purification, and characterization of this target protein *Pf*GDH along with the control protein, *H*GDH. We expressed these proteins with His-tag to facilitate their purification and immobilization, which is involved in some experiments in a latter part of this thesis work.

2.2 Experimental procedures

2.2.1 Materials

P. falciparum 3D7 asynchronous cDNA was obtained from American type culture collection (ATCC). The single stranded DNA aptamer library was obtained from IDT (USA). The primers were synthesized from Bioserve (India). Restriction enzymes and Taq Red pcr mix were obtained from New England Biolabs and Sigma Aldrich, respectively. The SYBR Gold (10000X) was procured from Invitrogen (USA). The molecular weight cutoff filters from Sartorius and pGEMT easy vector from Promega

were purchased. The pGEMT clone of *H*GDH was obtained from Genescript Plasmid Repository (USA). The pET28a and pCOLD-II vector were procured from Novagen, and Clontech, respectively. Ni-NTA Hi-Trap column procured from GE healthcare. The polyvinylidene fluoride (PVDF) membrane (Hybond P) was procured from Amersham. The anti-His primary antibody and HRP tagged secondary antibody were obtained from GE healthcare. The 3, 3'-diaminobenzidine (DAB) was obtained from Amresco. The quick ligation and Gel extraction kits were procured from New England Biolabs and Sigma Aldrich respectively. The TA cloning kit obtained from Promega (USA). All other chemicals used in the experiments were of analytical grade. The restriction map of cloning and expression vectors used in this work depicted in figure B1 under the appendix of this thesis.

2.2.2 Primer synthesis

The *Pf*GDH (Gene ID: 14_0164) and *H*GDH (Gene ID: 54537) genes were amplified from *P. falciparum* 3D7 cDNA and *H*GDH Clone in TA vector by using specially designed primers along with prefabricated enzyme restriction sites. The forward and revers primers for *PfGDH gene* were constructed with *BamHI* and *XhoI,* respectively. The *H*GDH *gene* was amplified with forward and reverse primer constructed with *NdeI* and *XhoI* restriction enzyme sites, respectively as depicted in Table A4 (appendix).

2.2.3 Bacterial cell culture

The *E. coli* strains {Dh5α, BL21(DE3) pLysS} were cultured and propagated in Luria Bertani broth and agar (Himedia, India), respectively. The bacterial culture Dh5α, *and* BL21(DE3) pLysS were grown at 37 °C, 180 rpm (in shaker incubator) in the presence of suitable antibiotics (kanamycin, chloramphenicol and ampicillin). The detailed information related to *E. coli* strain and selective media compositions used in this work have been incorporated under table A1 and A2 in appendix section, respectively. Glycerol stock of *E. coli* was prepared and stored in -80 °C for further use.

2.2.4 Nucleic acid quantification

For cloning and other molecular biology purposes, the information on concentration and purity of the DNA is highly desirable. The concentration was assessed by UV-Visible nanodrop spectrophotometer. Before measurement, the blank was set with nuclease free

water at $\lambda_{260\ nm}$, $\lambda_{280\ nm}$ followed by sample measurements at these wavelengths. The ratiometric significant ($\lambda_{260\ nm}$/ $\lambda_{280\ nm}$) values within range of 1.8-2.0 indicate purity of DNA sample. The O.D value of one at λ_{260} nm was considered to signify a concentration of 33 µg. ml^{-1} or 50 µg. ml^{-1} for ssDNA or dsDNA, respectively (Barbas III *et al.*, 2001). Further concentration of DNA was calculated with help of following equation (i):

DNA concentration (µg. ml^{-1}) = $O.D_{260}$ X dilution factor X 50 or 33 µg. ml^{-1}……(i)

2.2.5 Protein quantification

The concentration of proteins were analysed by Bradford assay (Bradford, 1976) at $\lambda_{595\ nm}$ using Coomassie Brilliant Blue (CBB) G-250 as colorimetric dye. Human serum albumin (HSA) was used as standard to construct the calibration plot.

2.2.6 Plasmid DNA isolation

The plasmid DNA present in *E. coli* was isolated through alkaline lysis method (Green and Sambrook, 2012). The compositions of various solutions used in procedure are mentioned in appendix table A3. An *E. coli* colony was isolated from LB agar plate and inoculated in 5 ml LB broth supplemented with suitable antibiotics and kept for overnight growth at 37 °C, 180 rpm in incubator shaker. The overnight grown culture was pelleted by centrifugation at 6000 x g for 5 min at 4 °C. The pelleted cell mass was suspended in 100 µl of chilled solution-I. The cell suspension was lysed with the help of lysis buffer solution-II by gentle mixing the cell suspension in the tube. For which the tube was shaked by inverting 4 - 5 times followed by incubating it in an ice box for 3 - 5 min.

The bacterial cell debris containing genomic DNA or protein was differentially precipitated by adding 150 µl of solution-III, incubated in an ice box for 5 min without shaking followed by centrifugation at 12000 x g for 10 min at 4 °C. The supernatant was carefully (without shaking) transferred into a new centrifuge tube and tris saturated phenol: chloroform: iso-amyl alcohol (25: 24:1 v/v) was added in equal quantity followed by centrifugation at 12000 x g for 10 min at 4 °C. This centrifugation led to separation of aqueous phase from organic phase. The aqueous phase was transferred into a new centrifuge tube, in which 100 % ethanol was added in double the amount for the precipitation of plasmid DNA. The mixture was incubated at -20 °C for 3 - 4 hours and then subjected to 12000 x g for 10 min at 4 °C to precipitate the DNA. The supernatant

was decanted and then washed the DNA precipitate by adding 70 % ethanol followed by centrifugation at 12000 x g for 10 min at 4 °C the washed precipitate was then dried at RT, this procedure was repeated twice. At the end the DNA was suspended in nuclease free water and stored at -20 °C till future use.

2.2.7 Agarose gel electrophoresis

Agarose gel (0.8 - 2 % w/v) solution was prepared in 1 x TAE buffer (table A3, appendix) followed by boiling in microwave oven. For DNA visualization 0.5 mg/ ml ethidium bromide was added when agarose solution temperature drops down to 45 - 55 °C. The DNA sample was blend with 6X DNA loading dye and loaded into the wells. The electrophoresis was performed in 1X TAE buffer at 80 V until the proper separation of the loading dye from the wells achieved. A wide range DNA ladder (Direct load™) was run in one of the wells with samples, wherever required. The DNA bands were visualized over the UV-transilluminator and image was captured through gel documentation (ChemiDoc XRS+ Imaging System, BIORAD).

2.2.8 Gel DNA elution

The specific DNA band in agarose gel after the PCR amplification or restriction digestion was eluted from gels through GenElute™ gel extraction kit (Sigma Aldrich, USA) following the manufacturer's protocol. After the electrophoresis, the gel was visualized over UV- transilluminator and desired DNA band was excised with a surgical blade. The excised gel was solubilized in 300 µl of gel solubilisation solution for every 100 mg of gel by heating in water bath at 50 - 60 °C for 10 min followed by vortexing.

Meanwhile, binding column was prepared by inserting it in 2 ml collection tube followed by centrifugation for 1 min at 12000 x g, after addition of 500 µl of column preparation solution. The solubilized gel was mixed with equal volume of isopropanol, and then the solution was loaded in prepared binding column and centrifuged for 1 min at 12000 x g. The flow through was discarded and column was washed with 700 µl wash buffer followed by centrifugation at 12000 x g for 1 min. This procedure repeated without addition of wash buffer to remove residual ethanol. The bound DNA in the column was eluted with 50 °C preheated nuclease free water through centrifugation at 12000 x g for 1 min to a fresh collection tube.

2.2.9 Polymerase chain reaction (PCR)

The DNA amplification was carried out through PCR using Taq red™ PCR kit. A total 20 - 30 ng DNA was used as template for all kind of PCR reactions. The PCR reaction mixture composition and conditions are mentioned in table A5 (appendix).

2.2.10 Ligation of *PfGDH* and *HGDH* genes with pGEMT easy vectors

The *Pf*GDH and *H*GDH genes amplified with gene specific primers. The amplified bands were eluted with gel elution protocol. The eluted DNA fragments were ligated with pre-linearized pGEMT easy vectors (Promega, USA) by mixing in 1:3 molar ratio with ligation reaction mix. The setup of ligation reaction mixture as described in table A6 (appendix). The reaction mixture was incubated at 4 °C for overnight after mixing with pipette. Following the incubation, ligated DNA (vector + insert) was transformed into competent cells. The positive clones with insert were selected with blue white screening. The clones were then subjected to restriction digestion with appropriate enzymes.

2.2.11 DNA Digestion with restriction enzymes

The PCR amplified or recombinant plasmid fragments were double digested with restriction enzyme. The typical composition of reaction mixture used for a restriction digestion is as included under table A6 (appendix). To separate particular insert from a vector requires digestion with a set of restriction enzymes. The *BamHI/XhoI* restriction digestion in cut smart buffer was performed for *Pf*GDH gene and *NdeI/XhoI* restriction digestion in cut smart buffer was used for *HGDH* gene. The restriction digestion was carried out for 1 h, according to manufacture guidelines. The digested DNA (vector, inserts) was resolved through agarose gel electrophoresis.

2.2.12 Ligation of digested DNA fragments

The desired DNA bands were eluted from agarose gel after the restriction digestion. The insert and vector both have sticky ends and ligated with T4 DNA ligase. The ligation reaction was performed at 25 °C for 10 min followed by instant chilling in ice flakes and then transformed into competent *E. coli* cells. The ligation mixture composition is mention under table A6 (appendix).

2.2.13 Competent cells preparation

The competent cells were prepared from *E.coli* /DH5α/BL21 (DE3) pLysS cells through method reported by Cheung *et al.*, (1989). In brief, a single bacterial colony was isolated from LB agar plate, transferred into 5 ml LB broth aseptically, and kept for overnight growth at 37 °C, 180 rpm. Following which, 1 % of the primary culture was inoculated into 5 ml fresh LB broth and grown at the same condition until an optical density (O.D) of 0.4 - 0.5 is reached at $\lambda_{600\ nm}$, which is, belongs to the exponential growth phase of the microbes. Then bacterial cells were pelleted down at 2500 x g for 10 min at 4 °C. The bacterial pellet was resuspended into ice-cold transformation and storage solution (TSS) (Table A3, appendix). Aliquots of 100 µl volume was prepared by resuspending the bacterial competent cells and stored at -80 °C.

2.2.14 Transformation of competent cells

The competent cells aliquot was supplemented with 10 µl of ligation mixture and gently mixed with pipettes followed by incubation on ice for 30 min. The cells were subjected to heat shock at 42 °C in a water bath for 1.5 min followed by instant cooling on ice for 10-15 min. The mixture was suspended in 900 µl of LB broth and incubated at 37 °C for 1 h with shaking. After incubation, the transformed cells were pelleted by centrifugation at 2500 x g for 10 min at °C. The supernatant was discarded and pellet was resuspended in 100 µl fresh LB broth. The resuspended cells were spread on LB agar plates supplemented with proper concentration of antibiotic corresponding to the antibiotic resistance gene present in the recombinant plasmid. The positive clones with desired inserts were selected through restriction digestion after an overnight incubation of transformed cells at 37 °C.

2.2.15 Cloning of *PfGDH* and *HGDH genes*

The *PfGDH* open reading frame (ORF) was amplified from *P, falciparum 3D7* asynchronous cDNA. The amplified ORF was ligated into pGEMT easy vector through TA cloning kit as describe earlier. The positive clones were digested with *BamHI/XhoI* restriction enzyme and confirm by agarose electrophoresis.

The dissected bands were eluted from gel and ligated with *BamHI/XhoI* digested pET28a vector. The ORF for *H*GDH gene was PCR amplified and sub cloned into *NdeI/XhoI*

digested *pCOLD-II* vector. The recombinant vectors pET28a and pCOLD-II carrying *PfGDH, H*GDH *genes* respectively were used to transform into *E coli* DH5α competent cells. The transformed cells were selected over selective LB agar plate containing appropriate antibiotics (Kanamycin for pET28a, Ampicillin for pCOLD-II) after overnight incubation at 37 °C. The recombinant clones were further confirmed by restriction digestion resulting in release of appropriate size of insert and vector. The single isolated colony of selected clones for *PfGDH* or *HGDH* were confirmed by sequencing and the recombinant plasmids (insert+ vector) were then transformed into *E.coli* BL21 (DE3) pLysS cells for higher expression yield of the recombinant proteins.

2.2.16 Sequence analysis of cloned inserts

Sequence analysis of the clones was get done at Bioserve, India, using 96 capillary high throughput sequencer, ABI 3730 XL following Sanger sequencing protocol.

2.2.17 Expression of His tagged *PfGDH* and *H*GDH in *E. coli* BL21 (DE3) pLysS

The *E. coli* BL21 (DE3) pLysS /pET28a/*Pf*GDH clone was induced with 1mM IPTG for expression at 37 °C for 12 h and *E. coli* BL21 (DE3) pLysS /pCOLD II/*H*GDH clone was induced by cold shock at 15 °C for 30 min, followed by 1 mM IPTG for expression at 25 °C for 12 h. After the incubation, bacterial cells were pelleted down by centrifugation (5000 x g). The cells were resuspended in lysis buffer (table A3, appendix) followed by sonication using an ultrasonic processor (Hielscher) at 25 % amplitude with 0.5 cycle at 4 °C till the lysate appeared clearer. The sonicated sample was centrifugated at 13000 x g for 30 min at 4 °C and the collected supernatant was filtered through 0.45 µm pore size filter.

2.2.18 Purification of His tagged *Pf*GDH and *H*GDH protein

The supernatant was passed through Ni-NTA column at a rate of 0.5 ml min^{-1}. The adsorbed proteins in the column was then washed with 20 bed volumes of washing buffer-1 for *Pf*GDH and washing buffer 2 for *H*GDH at a flow rate of 0.5 ml min^{-1}. The purified *Pf*GDH protein was dialyzed in 50 mM PBS for overnight for renaturation of protein. The purified recombinant *H*GDH was dialysed against 50 mM Tris, pH 7.4 for overnight, where urea concentration was step-down from 8 M to 0 M in a step of 1 M difference. The composition of solutions used for protein purification has been listed in

table A3 (appendix).

2.2.19 Sodium dodecyl sulphate polyacrylamide gel electrophoresis (SDS PAGE)

The protein purified by Ni-NTA affinity chromatography was analysed through SDS PAGE electrophoresis following the protocol of Laemmli (Laemmli, 1970). An amount of 1 - 2 µg of recombinant protein or crude cell lysate was mixed with 2X SDS Loading dye and denatured by heating in boiling water bath for 10 min. The denatured sample along with pre-stained protein ladder (Broad range NEB ladder, USA) was loaded into SDS-PAGE gel. The electrophoresis was performed over a discontinuous buffer system with a 5 % stacking on top of a 10 % separating gel, with a thickness of 0.75 mm at a constant voltage of 100 V in a MiniVE vertical electrophoresis unit (GE Healthcare). The separated protein bands visualized over gel by using "Blue silver staining" protocol of Candiano *et al.*, 2004, where colloidal Coomassie G-250 (Sigma Aldrich, USA) (Table A3, appendix) was the staining dye.

2.2.20 Western blotting

The purified recombinant proteins were visualized in 10 % SDS PAGE and then electro blotted at constant voltage 25 V, 300 mA for 3 - 4 h at 4 °C in blot module (GE healthcare) over PVDF membrane to proceed with western blotting. The transfer of protein from gel to PVDF membrane was confirmed by staining with Ponceau reagent (Sigma Aldrich, USA), which was later washed away with washing buffer [PBS, pH 7.4 with 0.1 % Tween 20 (PBS-T)]. Before the addition of primary antibody over PVDF membrane it was blocked with 3 % BSA solution in PBS for overnight to prevent nonspecific binding. For western blotting anti His primary antibody was used in dilution of 1:1000 in 1 % BSA in PBS-T for 2 h at RT, followed by repetitive washing (3 times) for 10 min each with PBST and the blot was developed with anti-mouse IgG (Fab specific)-peroxidase secondary antibody (Sigma Aldrich, USA) in a dilution of 1:5000 in 1 % BSA in PBS for 1 h at RT followed by washing 3 time with PBS-T 10 min each. The membrane was developed with peroxidase substrate 3, 3'-Diaminobenzidine tetrahydrochloridehydrate (DAB) (Amresco, USA) at concentration of 0.4 $mg.ml^{-1}$ in PBS supplemented with 10 µl hydrogen peroxide (30 %). The image was captured with a gel documentation system (ChemiDoc XRS+ Imaging System, BIO RAD). Details of the solutions/buffers used are given in table A3, appendix.

2.2.21 Circular dichroism (CD) spectroscopy

CD spectra were recorded on Jasco J - 815 spectropolarimeter (Japan) at RT in 1 cm path length cuvette. The spectra were recorded in continuous mode with bandwidth of 1 nm and resolution of 1nm between 200 to 300 nm at a scan rate of 100 nm min^{-1}. The buffer influence was removed from the recorded spectra and smoothened by Savitsky-Golay algorithm through Origin 8.0 software. For the measurement, 0.5 μM of recombinant proteins (*Pf*GDH, *H*GDH) were used. The analysis of secondary structure was performed using the Dichroweb secondary structure estimation program by uploading generated data from the instrument.

2.2.22 Sedimentation velocity study

An analytical ultracentrifuge (Beckman XL-A/XL-I) with 50 - Ti rotor and 12 - mm double sector charcoal epon centerpiece with quartz windows was used for sedimentation velocity experiment. In the experiment, 100 absorbance profiles were recorded at 1,42,249 x g at 20 °C. The scan profiles were analysed by using SEDFIT program (Schuck *et al.*, 2002). The experiment was performed as described by Jain *et al.*, (2016). The additional specifications of *Pf*GDH like, partial specific volume, buffer density and viscosity were analysed by using Sednterp (Laue *et al.*, 1992).

2.2.23 Matrix- assisted laser desorption ionization- mass spectroscopy (MALDI-MS)

Intact mass of the recombinant *Pf*GDH protein was confirmed by MALDI-MS (4800 plus MALDI TOF/TOF (time of flight) Analyzer, AB SCIEX, USA) analysis. The high molecular weight hexameric *Pf*GDH protein with ~300 kDa size however, was not in a suitable range for the matrix (Sinapinic Acid - 10 to 150 kDa) for MALDI analysis. Because of this the subunits of the protein was separated first by denaturing it with the help 0.5 M DTT and 10 % SDS. The as prepared content with the monomeric form of the protein was mixed with saturated solution of sinapinic acid and then the spectra were collected in a positive mode with each spectrum being an averaged for 100 shots.

2.2.24 Determination of Isoelectric point (p*I*)

The p*I* of the purified recombinant *Pf*GDH was measured by Zeta potential study on Zetasizer nano series (Malvern Instruments limited, U.K). The zeta potential of *Pf*GDH

was measured in 50 mM appropriate buffers covering pH range from 2 to 10 in capillary cell (DTS1070 - Malvern instruments limited) equipped with gold platted Beryllium/Copper electrode. A graph was plotted between the measured zeta potential values and the corresponding pH values. The p*I* of *Pf*GDH was identified from the pH scale at which zeta potential is zero.

2.2.25 Enzyme kinetics studies

Enzyme kinetic studies for recombinant *Pf*GDH and *H*GDH were performed spectrophotometrically by monitoring the change in absorbance of NADPH (ε = 6220 M^{-1} cm^{-1}) at λ_{340} nm. The oxidative deamination of L- glutamate was followed in the presence of 100 µM NADP in 50 mM PBS, (pH 8.0) at 25 °C. The reaction was studied with L-glutamate as substrate in a concentration range of 5 – 100 mM and 1 µM of the enzyme protein. The enzyme inhibition kinetics study was performed with 10 mM Isopathalic acid (Himedia, India). The Michaelis-menten constant, K_m and V_{max} value for the enzyme catalysis were calculated from Lineweaver – Burk plots. A double beam spectrophotometer (Agilent, USA) was used for analysis and each assay was performed in triplicate.

2.3 Results and discussion

2.3.1 *Pf*GDH Sequence analysis and comparison

Multiple sequence analysis of *Pf*GDH with *H*GDH and *Pv*GDH were done using information about the length of the domains from the protein database with help of clustal Omega software. The *Pf*GDH sequence alignment result (Figure 2.1) showed 23 % sequence identity with HGDH and 69 % identity with *Pv*GDH indicating these protein sequence wise significantly different from each other. Sequence of the *P. falciparum 3D7* NADP specific glutamate dehydrogenase (E.C 1.4.1.4) protein of interest was located in the BRENDA database listed as Ontology ID 0004354.

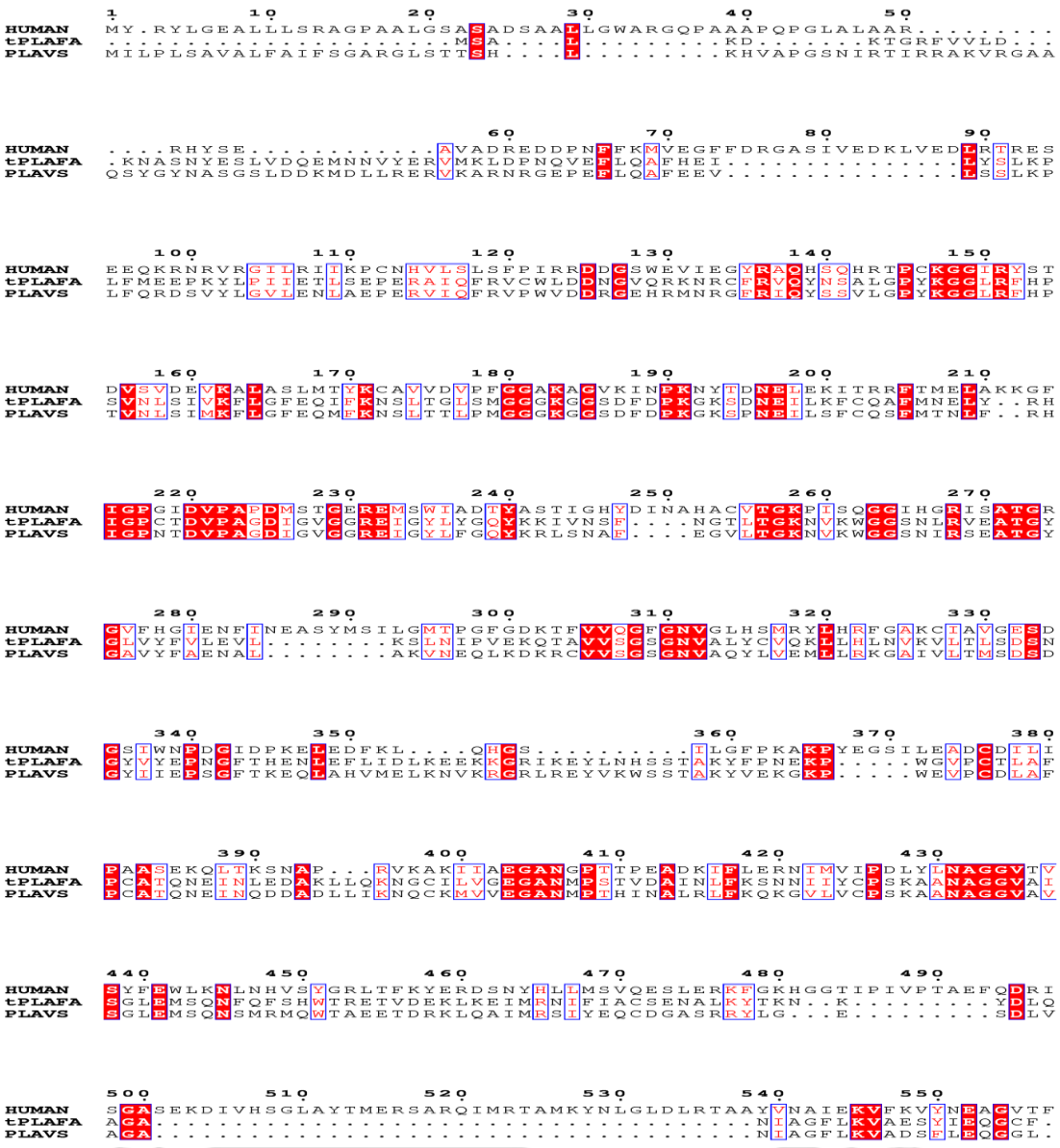

Figure 2.1: Multiple sequence alignment in Clustal Omega showing conserved regions of GDH from different species of *P. (vivax, falciparum*) and Human origin. The highlight in red indicates conserved in all the three spices and in blue box represents conserved between any two species.

The protein has a GenBank Acession number 14_0164 and is 470 amino acid residues long. The protein sequence was analysed for putative domains using the BLAST tool hosted on the NCBI website. BLAST result highlighted the presence of *Pf*GDH. The protein data bank (PDB) database set that was chosen for delta BLAST, for rest of the parameters default options were set. According to blast result *Pf*GDH have two type of conserved domain superfamily.

The *Pf*GDH amino acid sequence from 77 to 207 shows ELFV dehydrogenase superfamily specific to facilitate dimerization. The amino acid sequence from 215 - 469 shows conserved domain for short chain dehydrogenase reductase superfamily (SDR). The SDR family is functionally diverse family of oxidoreductase that have single domain with structurally conserved Rossmann fold (α / β folding pattern) with a central β - sheet.

2.3.2 Cloning and purification of *Pf*GDH and *H*GDH

The strategy used for *PfGDH* and *HGDH* genes cloning has been depicted in figure 2.2. The *Pf*GDH and *H*GDH ORF were amplified from cDNA and recombinant plasmid as template, respectively with prefabricated enzyme restriction site.

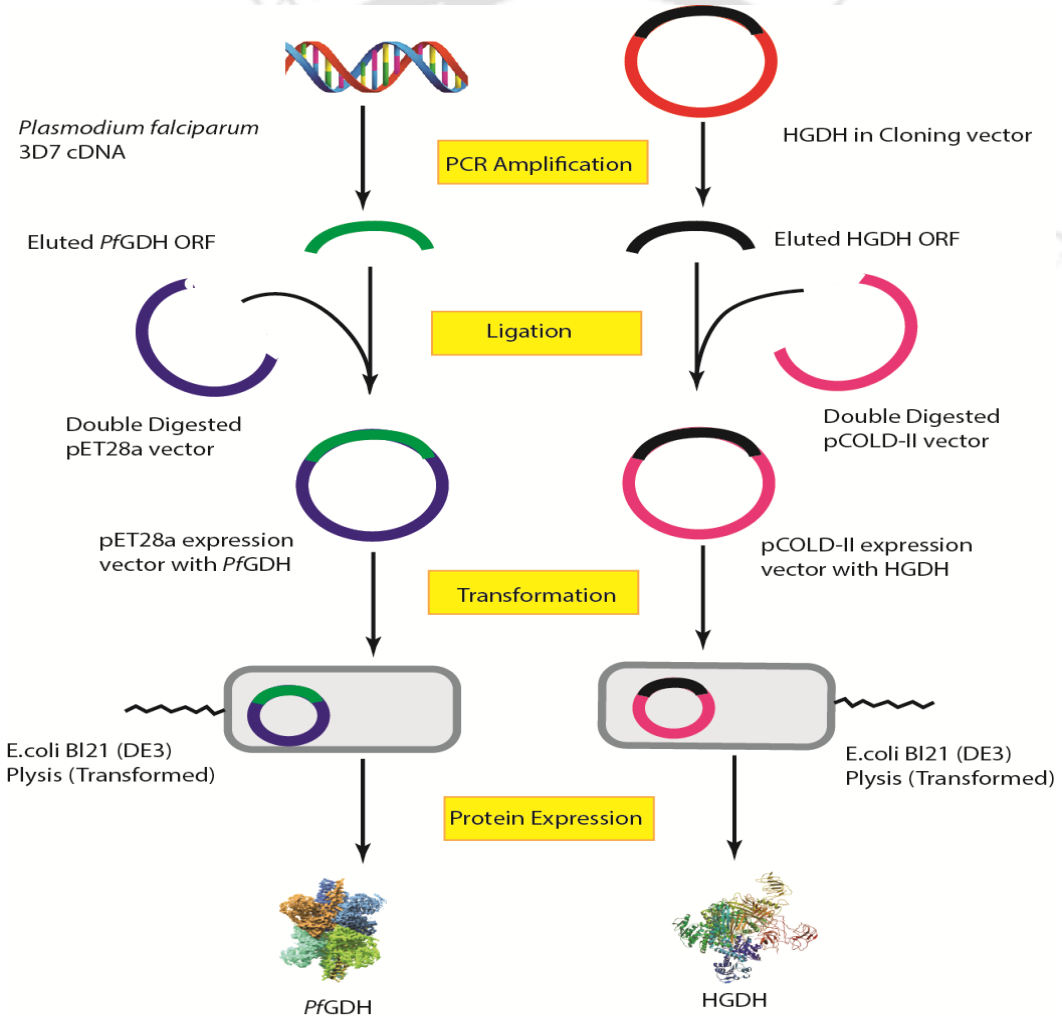

Figure 2.2: Schematic representation of the cloning strategy used in the present work.

The *Pf*GDH and *H*GDH amplification resulted in an amplified band ~1.5 kb and 1.6 kb, respectively, corresponding to appropriate sizes of the genes (Figure 2.3 A, B). This PCR amplified bands have poly A (adenine) tail towards 3' end of gene. The amplified fragments were ligated with prelinearized pGEMT easy vector flanking with 5' T (thymine) region with help of ligase enzyme followed by transformation in *E. coli* DH5α cells. The positive *Pf*GDH clone was selected through pair of restriction enzymes *BamHI/XhoI*. The restriction digestion result after gel electrophoresis indicated release of desired ~1.5 kb *Pf*GDH insert along with 3 kb size of pGEMT vector (Figure 2.3 C).

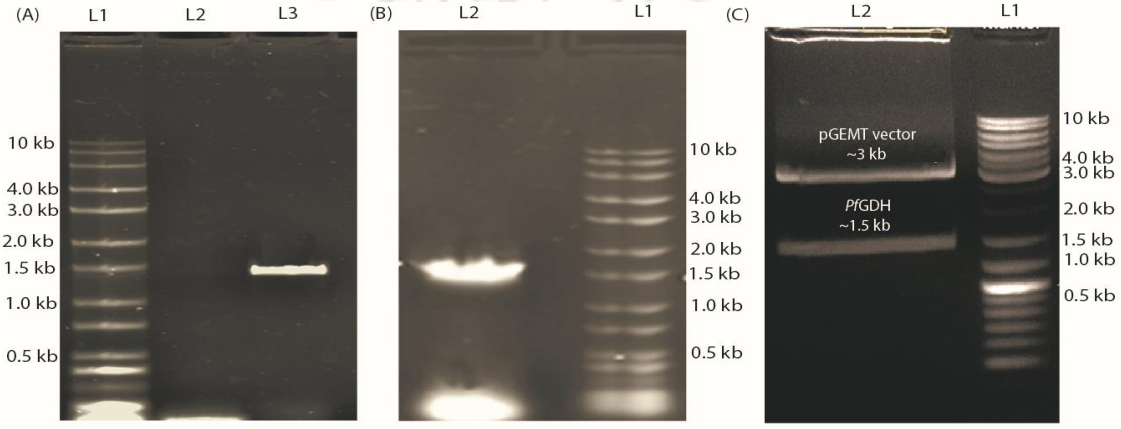

Figure 2.3: PCR amplification of (A) *PfGDH* (~1.5 kb) (B) *HGDH* (~1.6 kb) observed in 0.8 % agarose gel after staining with ethidium bromide (EtBr). Recombinant pGEMT easy vector (C) digested in Lane 2, Wide range DNA ladder- L1.

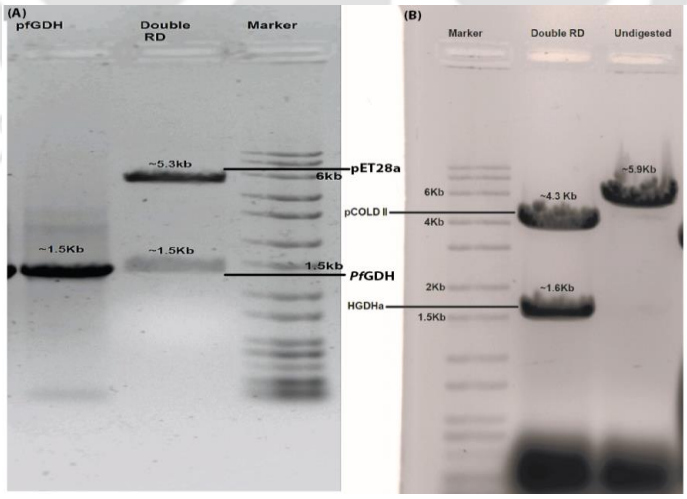

Figure 2.4: Confirmation of recombinant plasmids by restriction digestion of *pET28a_PfGDH* (A), *pCOLD*-II_*HGDH* (B) clones and release desired size insert. Marker: Wide range DNA ladder.

The *Pf*GDH and *H*GDH genes were eluted from the gel, ligated with pre-digested pET28a and pCOLD-II vectors followed by transformation into *E coli* BL21 (DE3) pLysS cells. The positive clones were confirmed by restriction digestion of recombinant plasmid isolated from single colony (Figure 2.4 A, B). Further these clones were confirmed through sequencing. The *H*GDH is very complex protein and difficult to express with bacterial cell system. Initially, we cloned it into pET28a vector system but the expression was very low because of retention of the major fraction of the expressed protein in the inclusion bodies. Hence, we cloned the insert in pCOLD-II vector, which consists of csp-A (cold shock protein A) promoter facilitating high expression of the insert protein (cloned gene) at low temperature with selective suppression of bacterial host protein with low protease activity. The confirmed *E coli* BL21 (DE3) pLysS / *Pf*GDH/pET28a and *E coli* BL21 (DE3) pLysS cells/pCOLD-II/*H*GDH clones were considered for protein expression (Figure 2.5).

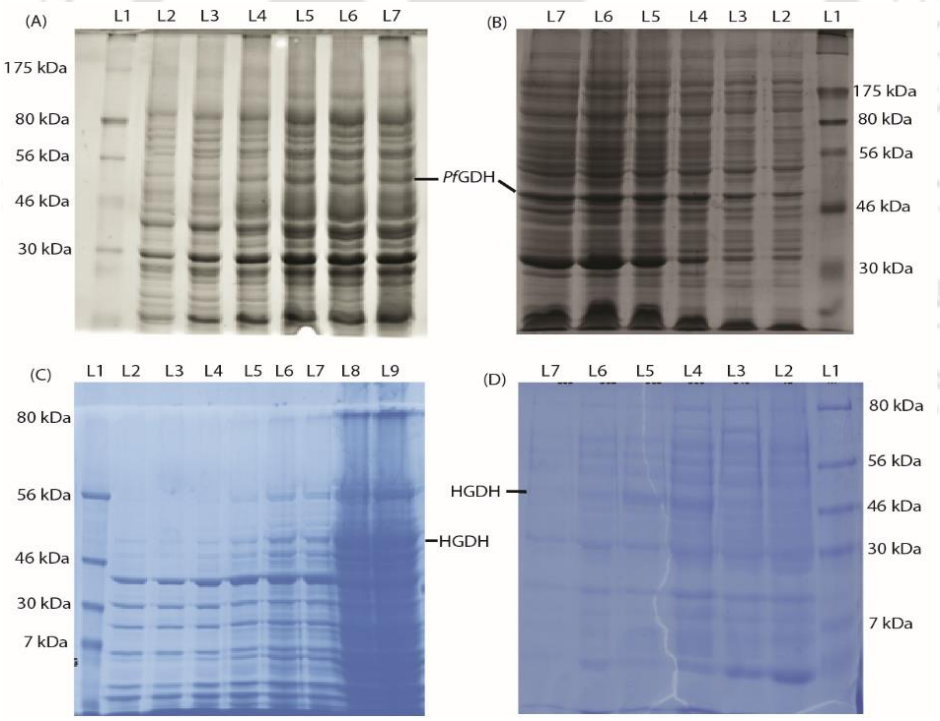

Figure 2.5: SDS PAGE (10 % gel stained with comassie brilliant blue). (A) Time optimization for *Pf*GDH expression L 2 - 0 h to L7 - 10 h with interval of 2 h (B) Temperature optimization for *Pf*GDH expression L2- 15 °C to L7- 40 °C with interval of 5 °C. (C) Time optimization for *H*GDH expression L 2-0 h to L 9- 14 h with interval of 2 h. (D) Temperature optimization for *H*GDH expression L 2- 15 °C to L 7- 40 °C with interval of 5 °C. L1 is protein ladder in all images.

The expression profile of these recombinant proteins were studied in the soluble supernatant fraction of lysed recombinant *E. coli* cells. The optimum temperature and incubation time were studied for both the proteins for the expression. The study revealed that the average incubation time for both the proteins was 10-12 h (Figure 2.5 A, B) and optimum temperature for *Pf*GDH and *H*GDH were 37 °C and 30 °C, respectively. The concentration of IPTG being used as inducer was 1 mM for both the proteins (Figure 2.5 C, D). The 6X His tagged recombinant *Pf*GDH and *H*GDH were purified through Ni-NTA affinity chromatography. For both the protein, cell lysate along with elute fractions were analysed over SDS PAGE (Figure 2.6 A, B). The purification yield for *Pf*GDH and *H*GDH were ~ 12 mg L^{-1} and ~ 3 mg L^{-1}, respectively as calculated from Bradford assay. The purified proteins were further confirmed through western blotting with anti-His monoclonal antibody (Figure 2.6 C, D).

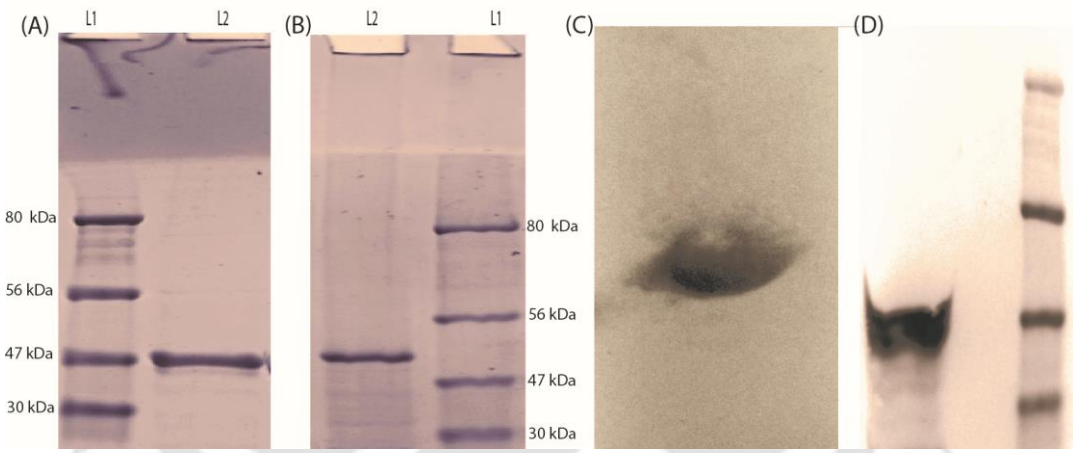

Figure 2.6: The purified *Pf*GDH (A) and *H*GDH (C) expressed in *E.coli* with 1mM IPTG induction and Incubation temperature 37 °C and 20 °C, respectively for 10 h in 10% SDS-PAGE gel stained by coomassie staining. Western blot of recombinant *Pf*GDH (C) and *H*GDH (D) with anti His antibody (1:5000 dilution) over PVDF membrane. L1 is protein ladder in all images.

2.3.3 Characterization of *Pf*GDH

The *Pf*GDH is homohexameric proteins consisting of six identical subunits joint together and form apozyme. The monomeric mass of single subunit is ~47.5 kDa as confirmed by MALDI mass spectroscopy (Figure 2.7 A). The molecular weight of the recombinant *Pf*GDH with 6X His tag was found to be ~54 kDa by MALDI-TOF mass spectrometry

that is consistent with the molecular weight of (~ 47.5 kDa) predicted on the basis of the encoded amino acid sequence. The MALDI-TOF m/z ratio shows ambiguity in molecular weight of the protein in presence of SDS (Jeannot *et al.*, 1998; Rodríguez-Acosta 1991). The reason is ascribed to the abnormal binding of SDS with the highly charged protein (Williams *et al.*, 1986; Yoo and Albanesi, 1990; Thomas *et al.*, 1991; Gast *et al.*, 1995). The p*I* of recombinant *Pf*GDH was discerned from a graph obtained by plotting zeta potential values versus corresponding pH values (Figure 2.7 B).

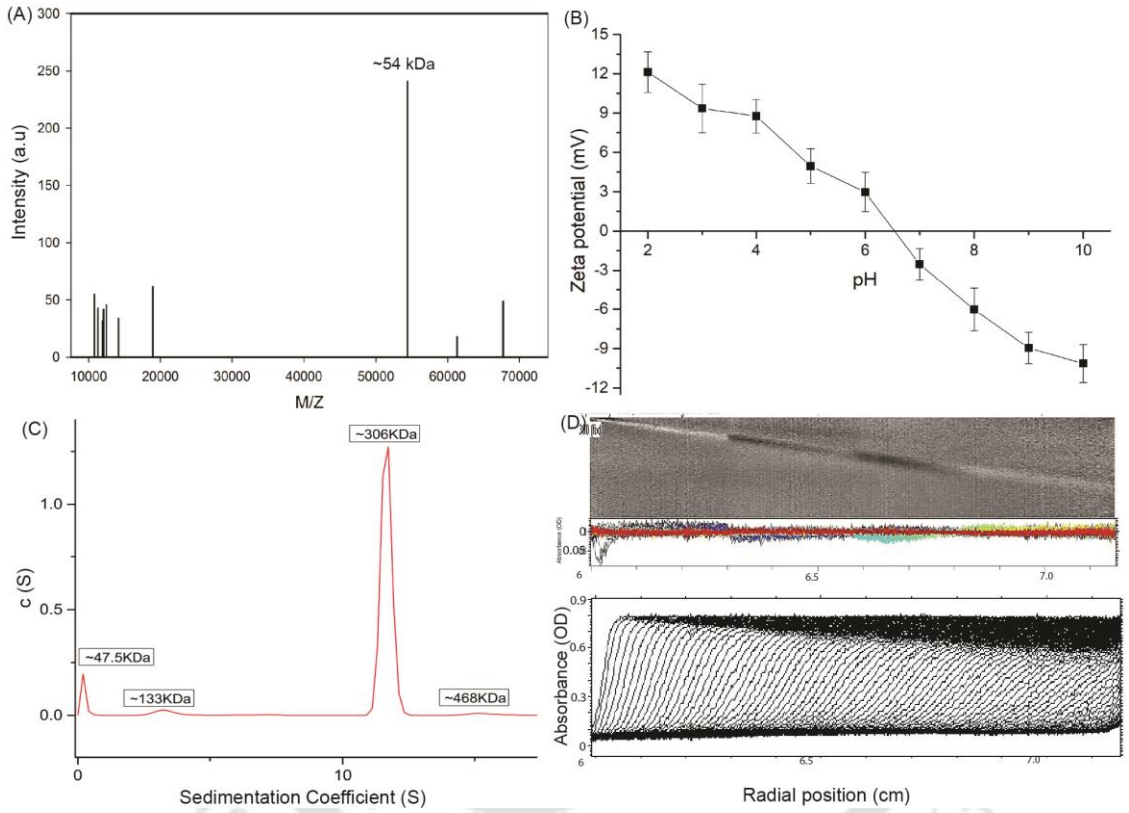

Figure 2.7: MALDI-MS Analysis of *Pf*GDH. The *Pf*GDH was denatured in the presence of 0.5 M DTT and 10 % SDS prior to the analysis (A). Zeta potential of recombinant *Pf*GDH at various pH values (B). Sedimentation velocity profile (C) of *Pf*GDH (0.5 $mg.ml^{-1}$) in 10 mM PBS, pH 8.0, 20 $^{\circ}C$ with (D) residual bitmap images.

As depicted in figure, is revealed that the recombinant *Pf*GDH had net intrinsic positive charge at acidic pH range because of protonation of carboxylic and amino groups. Likewise, a net negative charge in basic pH range was detected due to deprotonation of carboxylic and amino groups of the protein (Uskokovic *et al.*, 2010). The p*I* of the recombinant *Pf*GDH was found ~ 6.6. The result was distantly corroborated with

theoretically calculated p*I* (~ 7.4) of *Pf*GDH (Wagner *et al.*, 1998). The protein in solution exist as zwitterion, and the total number of net charged amino and carboxylic groups (NH_3^+, COO^-) at defined pH determined the surface charge present over the protein. The p*I* is the pH at which protein molecule carries equal number of positive $(NH_3)^+$ and negative (COO^-) charge leading to its void net surface charge.

The homohexameric *Pf*GDH protein expressed in monomeric form from the clone was later assembled into the hexameric form in 50 mM PBS, pH 8.0. The integrity of the oligomeric form of *Pf*GDH was confirmed by sedimentation velocity study (Figure 2.7 C, D). The *Pf*GDH sample was found to be largely homogeneous in nature with the major fraction (~ 95 %) accounted by the homohexameric form (~ 306 kDa) of the protein. A minor heterogeneity obtained was roughly corresponding to the monomeric form of the *Pf*GDH protein (~ 47.5 kDa).

2.3.4 Determination of structural and kinetic parameters of *Pf*GDH and *H*GDH

To study the structural integrity of the expressed *Pf*GDH and *H*GDH proteins, CD analysis was performed for both the recombinant proteins (Figure 2.8 A). The analysis showed that *Pf*GDH constitutes ~28 % α helix, ~5 % β sheet, 30 % turns and 37 % random coil, whereas HGDH constitutes ~27 % α helix, ~58 % β sheet, ~15 % random coil. The results correlate well with the previous reports (Wells, 1975; Yang *et al.*, 2003). The spectral contribution of NADP cofactor over the *Pf*GDH/*H*GDH was not taken into account because amount of cofactor binds with apoenzyme was not known.

In case of *Pf*GDH, low percentage of α and β structures appeared due to the forfeiture of it integrity or retained hidden under the hydrophobic milieu in aqueous environment. The intramolecular interaction between β - sheet structures are very fragile in presence of aqueous environment. Protection of these structures from water varies from protein to protein to their shielding mechanism (Das *et al.*, 2000). The K_m values for the substrate L-glutamate discerned for the recombinant *Pf*GDH and *H*GDH using Michaelis-Menten plot were 6.9 ± 0.38 mM, and 4.36 ± 0.18 mM, respectively (Figure 2.8 B, C). The activity of recombinant enzymes is in fair agreement with previously reported K_m values 1.05 ± 0.25 and 10.8 ± 3.3 for *Pf*GDH and *H*GDH, respectively (Wagner *et al.*, 1998; Shashidharan *et al.*, 1994). The results confirmed that both the expressed proteins were well folded and enzymatically active. The isophathalic acid (IPA) is a competitive

inhibitor for *Pf*GDH, which specifically blocked the enzymatic activity of *Pf*GDH but not of *H*GDH. The *Pf*GDH competitive inhibition was measured spectrophotometrically by following the change in absorbance at $\lambda_{340\ nm}$. The forward reaction (deamination of glutamate) was followed in the presence of 100 µM NADP in assay buffer (50 mM PBS), pH 8.0, and glutamate 10 mM. The reaction was started by adding 5 mM IPA to final concentration of 40 mM with presence of 1 µM enzyme concentration (Figure 2.8 D).

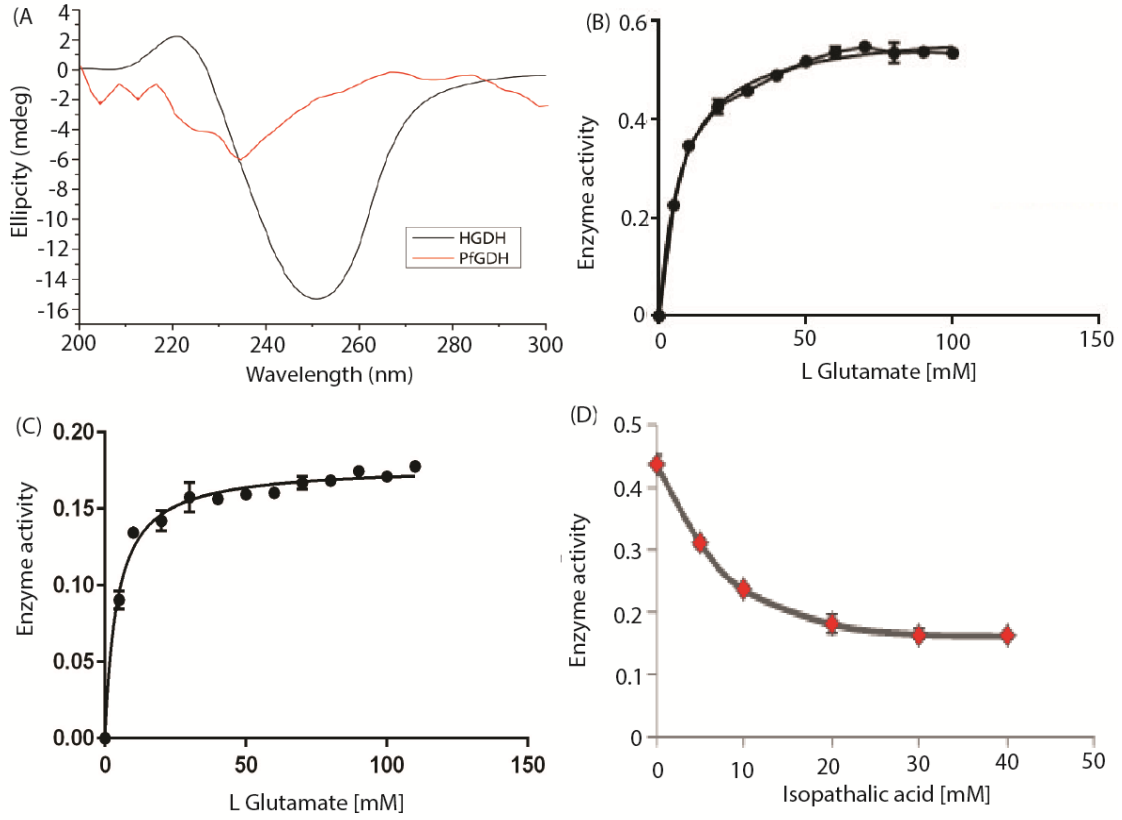

Figure 2.8**:** CD spectra of *Pf*GDH and *H*GDH (1 mg. ml^{-1}) in 10 mM phosphate and Tris buffer respectively (A). Michalis Manton plot for *Pf*GDH (B) and *H*GDH (C). Competitive Inhibition of *Pf*GDH in presence of Isophathalic Acid (D).

2.4 Conclusion

The target *Pf*GDH and *H*GDH genes were successfully cloned into a suitable expression vectors and confirmed the clones through restriction digestion and sequence analysis. The expression conditions for the proteins were optimized. The recombinant proteins were purified through Ni-NTA chromatography and characterised the purified proteins for their structural integrity through different techniques such as, CD, analytical

ultracentrifugation, and zeta potential studies. The enzyme kinetics studies were performed to check functional integrity of recombinant enzyme. This study proves that both the enzymes were successfully cloned, expressed and purified in appropriate structural, functional and enzymatically active form.

Chapter 3

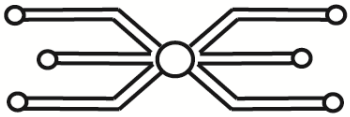

Development of Aptamer Specific for PfGDH and its Characterization

Chapter 3

Development of an Aptamer Specific for *Pf*GDH and its Characterization

3.1 Overview

Various recognition systems as alternative to antibody for point of care malaria diagnosis have been reported (Chakma *et al.,* 2016; Lee *et al.,* 2014; Gulka *et al.,* 2014). However, each of these systems has its own merits and demerits such as, low specificity, poor sensitivity and technical complexity of the methods. Among the new generation of biorecognition systems, aptamers have drawn special attention owing to their certain properties that fare well over the conventional antibody based systems for developing biosensors and bio detection systems. The advantages commonly being attributed to aptamers over antibodies are their easy synthesis, thermal stability, high shelf life, scope for modification to enhance the target selectivity, and wider target range from metal ions to macromolecules (Hicke and Stephens, 2000). The term aptamer has its origin from Latin word “aptus” meaning “to fit” and Greek “meros” meaning “location”. The nucleic acid aptamers are single-stranded oligonucleotides that are selected through an enrichment technique from a pool of oligonucleotide library in presence of the target following a widely acclaimed process called SELEX. The selected aptamers are amplified by PCR, cloned, sequenced and then characterized by different techniques to finally identify the best one in terms of specificity (Kakoti and Goswami, 2017). The aptamer has capability to bind to their specific target in the presence of various competitive and non-competitive binders. The aptamer has tendency to adapt three dimensional shape and bind with their targets via combination of various forces such as van der Waals forces, hydrogen bonding, electrostatic interactions and π-π system interaction (Kakoti and Goswami, 2016). Over the past decade, several attempts have been made to develop malaria diagnosis methods and techniques using aptamer as recognition molecule. These reports are mostly relied upon different target antigens such as, *P*LDH (Jain *et al.,* 2016) and *Pf*HRP-II (Chakma *et al.,* 2016), etc. However, the *Pf*GDH as target antigen for developing aptamer based malaria diagnosis methods and techniques are not yet adequately known. This chapter describes development of an aptamer specific for *Pf*GDH through SELEX procedure. The *Pf*GDH and *H*GDH proteins purified in the previous chapter (I) were used as target and control protein, respectively to develop the aptamer.

The PVDF membrane was used as matrix for protein immobilization. The structural characteristic, specificity and binding affinity of the developed aptamers were analysed through various methods. A detailed account on the findings of this work is included in this chapter.

3.2 Experimental procedures

3.2.1 Materials

A single stranded DNA library (10^{14} - 10^{15}) was procured from IDT technology (USA). The library was constructed from random oligonucleotide sequences containing a region of random 40-nucleotides (**N40**) (5'-CACCTAATACGACTCACTATAGCG GATCCGA-**N40**-CTGGCTCGAACAAGCTTGC-3') flanked by conserved primer binding site for amplification. The primer sequences used for the amplification are listed in table A4 (appendix). The compositions of various buffers used in this work are listed in table A3, appendix. The primers were synthesized by Bioserve (India). Restriction enzymes and streptavidin coated magnetic beads were obtained from New England Biolabs. SYBR Gold (10000X) from Invitrogen (USA). PVDF membrane (Hybond P) was procured from Amersham. Starting blocking buffer, H_2SO_4 and Top 10 competent cells were procured from Thermo Fisher. Dibasic/mono basic phosphate buffer, $MgCl_2$, NaCl, KCl, PCR kit, streptavidin magnetic beads and human serum albumin (HSA) were procured from Sigma Aldrich. The molecular weight cutoff filters from Sartorius and pGEMT easy vector from Promega were purchased.

3.2.2 *In vitro* selection of aptamers using SELEX

SELEX was performed to select specific ssDNA aptamers against *Pf*GDH protein using aptamer library as mentioned above. Before use, 5 nmole of ssDNA was suspended in 1 ml of the binding buffer and heated for 10 min at 90 $^{\circ}$C and then cooled to RT. PVDF membrane was used as support material for immobilization of the *Pf*GDH protein. The membrane of size 5 mm diameter was first prepared by punching technique and then it was activated in methanol for 10 min followed by equilibration in binding buffer for 15 min at RT. The *Pf*GDH protein (1mg. ml^{-1}) was then immobilized on the membrane in the binding buffer for 1 h in a centrifuge tube followed by washing with the binding buffer for 1 min and stored at 4 $^{\circ}$C. The immobilized net protein over the membrane was quantified by Bradford assay. Prior to the first round of positive selection, heat treated

ssDNA library was kept for immobilization over PVDF membrane for 10 min as a negative selection and then the unbound aptamer was used for the first round positive selection against *Pf*GDH. The stringency of aptamer binding with *Pf*GDH/ PVDF membrane was increased by decreasing the binding time, from 60 min to 10 min with a depreciation of 5 min for each cycle, from 6^{th} to 17^{th} cycle.

The immobilization of protein and aptamer over PVDF membrane were established by morphology analysis using Atomic force microscopy (AFM) on an ambient air scanning probe microscope (Agilent Technologies 5500, USA) coupled with a silicon nitride probe. Images were recorded with non-contact mode using Picoscan 5 software. Elution of bound aptamer after membrane washing with binding buffer was performed in PCR grade water by heating the membrane at 90 ^{o}C for 5 min and crushing with a sterile microtip. Bound ssDNAs were PCR amplified by using Taq Red DNA polymerase (Sigma) and the aptamers primers with initial denaturation at 95 ^{o}C for 10 min, followed by 20 cycles of 95 ^{o}C for 15 s, 68 ^{o}C for 15 s, 72 ^{o}C for 3 s, and final extension at 72 ^{o}C for 3 s were used in the PCR. The amplified PCR product was then incubated with 25 µl streptavidin magnetic beads in coupling buffer at RT for 1 h. The beads were then washed with coupling buffer and ssDNA strands were separated from biotinylated strands using 100 µl of 100 mM NaOH. The separated strands were used for the next round of cycle. A total of 17 SELEX cycles were performed out of which 3 against PVDF membrane as counter SELEX after (6^{th}, 8^{th}, 10^{th}cycle) and 2 against *H*GDH as negative SELEX at the end of 13^{th}, 15^{th} cycles. After the 17 cycle of SELEX, amplified product was proceed for cloning.

3.2.3 Cloning of enriched aptamer candidates

At the end of 17^{th} positive SELEX cycle the probable aptamer candidates were cloned into pGEMT easy vector and transformed into *E.coli* DH5α cells. The transformed cells were selected by blue-white screening and restriction digestion. The positive clones were sequenced and candidates were analyzed through Clustal X2 alignment software for comparison.

3.2.4 Electrophoretic mobility shift assay (EMSA)

Proteins at various concentrations (0 µM to 2.4 µM) and 0.25 nM of the aptamer candidate were mixed in the binding buffer (20 µL) and incubated at RT for 1 h. The protein–ssDNA complexes were loaded onto a 6 % PAGE tris-borate-EDTA (TBE) gel and separated at 100 V for 6 h at 4 $^{\circ}$C. After electrophoresis, the gel was stained with SYBR gold I for 5 minutes and coomassie brilliant blue for visualization of ssDNA and protein, respectively.

3.2.5 Prediction of secondary structure and G-quadruplex mapping

The secondary structure was predicted through Mfold online software (Zuker *et al.*, 2003). The ionic condition was selected as 2.5 mM $MgCl_2$ and 50 mM NaCl at RT. The QGRS (**Q**uadruplex forming **G-R**ich **S**equences) mapper software was used for prediction of quadruplex forming region based on sequence analysis (Kikin *et al.*, 2006). The default parameters were used with maximum 30 sequences of QGRS length, minimum G-group of 2 and loop size between 0-36 nucleotides.

3.2.6 Determination of dissociation constant (K_d) of aptamer- *Pf*GDH interaction

A surface plasmon resonance (SPR) study was performed for the measurement of the K_d value in immobilized state of the developed aptamer against *Pf*GDH using a Reichert SPR 7000DC (USA) dual channel flow spectrophotometer at 25 °C over 50 nm gold coated chips (Reichert Technology, USA). The SPR chip was first cleaned with piranha solution (3:1 H_2SO_4: H_2O_2) for 20 s, then washed with milli-Q water (18.2 MΩ.cm, Millipore, UK) for 5 min followed by purging with N_2 gas jet for drying. The chip was then incubated overnight with thiolated aptamer (1 µM) along with 6-mercapto 1-hexanol (MCH, Sigma) in a ratio of 1:100 in binding buffer, followed by backfilling the surface with 1 mM MCH for 1 h (Aliakbarinodehi *et al.*, 2017; Green *et al.*, 2000). All the protein solutions and buffer were filtered through a 0.2 µm filter and degassed for 2 h. After obtaining a stable binding buffer SPR line, different concentrations of *Pf*GDH and control protein were flowed over the aptamer modified SPR chip at 25 µl min^{-1} for 10 minutes, followed by 5 min of a dissociation step with buffer to remove any unbound proteins. The CD study was performed for the measurement of binding affinity of the aptamer to the

target protein in solution state. The CD spectra were recorded on Jasco J-815 spectropolarimeter (Japan) at RT in 1 cm path length cuvette. The spectra were recorded in continuous mode with bandwidth of 1 nm and resolution of 1nm between λ_{200} to λ_{250} nm at a scan rate of 100 nm min^{-1}. Induced CD (ICD) spectra were recorded for K_d measurement of the aptamers after their binding of the aptamer candidate with *Pf*GDH protein at increasing concentration. The buffer influence was removed from the recorded spectra and smoothened by Savitsky-Golay algorithm through Origin 8.0 software. The K_d value of the aptamer was calculated by plotting a graph of peak intensity versus concentration gradient of *Pf*GDH and fitted in single ligand binding model of Sigma plot. For the measurement, 4 µM of aptamer was heated at 95 ^{o}C for 10 min and then incubated at 4 ^{o}C for 30 min followed by incubating the aptamers solution with *Pf*GDH for 1 h. The buffer used for the present work is presented in the Appendix A3.

3.3 Results and discussion

3.3.1 Development of specific aptamer against *Pf*GDH

Specific aptamer against *Pf*GDH was selected from an ssDNA library through SELEX process. The schematic presentation of SELEX methodology is represented in figure 3.1.

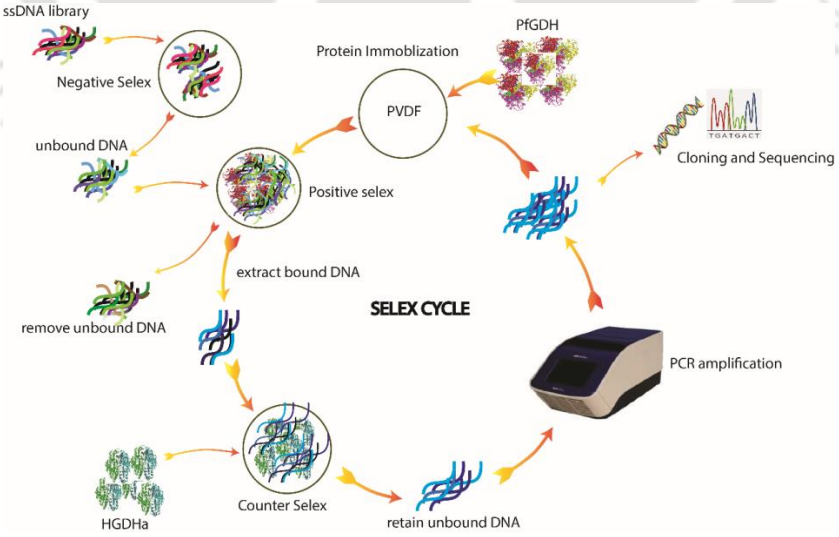

Figure 3.1: Schematic representation of SELEX performed to develop aptamer against *Pf*GDH.

To perform the SELEX, the protein (*Pf*GDH or *H*GDH) was immobilized on PVDF membrane. The reason for selecting PVDF membrane was based on the fact that the proteins get immobilized on this membrane in a non-uniform manner through various combination of weak forces (Matsudaira, 1987), which enhances the probability of forming a wider array of ‘‘aptatopes’’ for increased interactions with the potential aptamer candidates. The surface modification of PVDF membrane by protein and aptamer binding was characterized by AFM (Figure. 3.2).

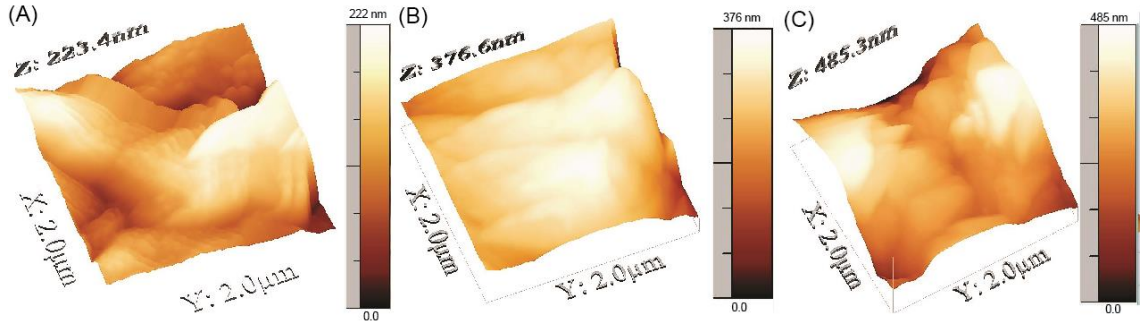

Figure 3.2: AFM images on the surface morphology of the modified PVDF membrane: (A) blank PDVF membrane, (B) Protein immobilization on PVDF membrane, and (C) after immobilization of protein and then aptamer on PVDF membrane.

The bare PVDF membrane was uneven with a root mean square (RMS) roughness factor of ~46 nm. The surface morphology of the membrane was shifted to more uneven state following the interactions. The average RMS roughness factors of ~50 nm and ~85 nm were detected for the immobilized *Pf*GDH and its interactions with the ssDNA candidates, respectively. The membrane thickness was also increased to ~ 376 nm and ~ 485 nm from ~223 nm of the blank membrane following the immobilization of the protein alone and its interaction with the ssDNA candidate, respectively. The amount of the proteins loaded on the membrane was ~ 0.12-0.15 mg cm^{-2}.

A total 17 rounds of SELEX cycle was performed, out of which 5 cycles were performed for the blank PVDF membrane and *H*GDH protein to prevent enrichment of non-specific aptamer candidates against the target. Following each positive cycle, a gradual enrichment of aptamer candidates was occurred as visible from the increased in band intensity in the gel (Figure 3.3 A). The enriched candidates were cloned, transformed into competent cells and then screened for the positive insert through blue white screening protocol. The positive clones were digested with *EcoR1* and then analyzed in gel (Figure 3.3 B).

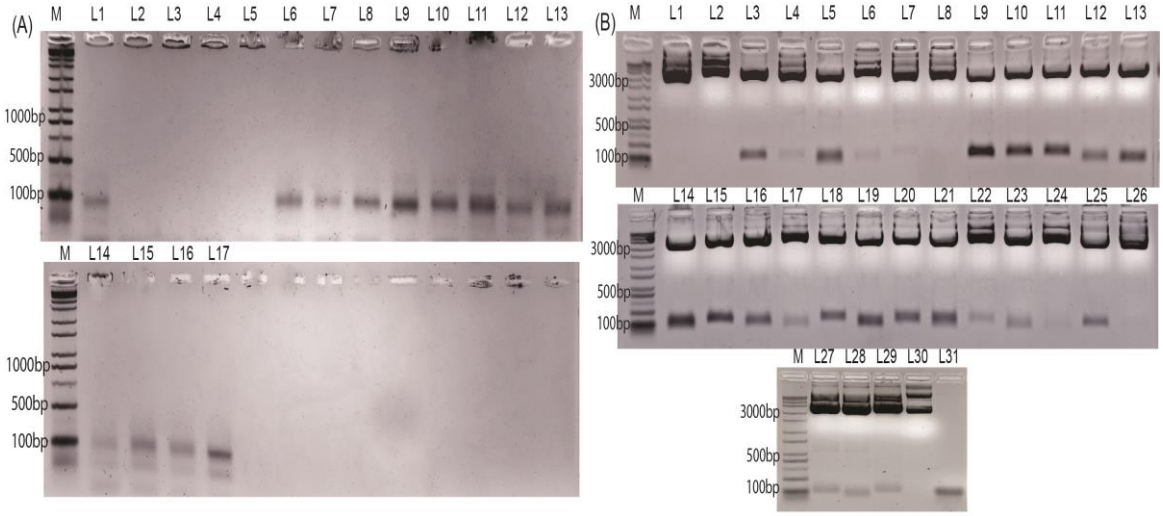

Figure 3.3: Amplified bands at the end of SELEX cycle L1−L17, respectively. The bands on counter SELEX against PVDF after L6, L8, L10 and negative SELEX against HGDH after L13, L15 are seen (A). Screening of TA clones of restriction digested (with *EcoR1*) products are seen at ~100 bp (B). Control digestion product of plasmid from a blue colony L30, and aptamer library in L31, M: marker.

The intense bands from the gel were isolated, and sequenced. The sequencing result revealed that out of 22 positive clones only 16 clones carried the proper aptamer insert. Analysis of the selected sequences by clustal X2 unveiled that two types of sequences were enriched better than the rest of the aptamer candidates out of which the candidates NG3 and NG51 were selected for further studies (Figure 3.4). The alignment studies of these sequences did not display any conservation in the random regions of the sequences.

```
NG37   GACCACGGCCAGCTCACCACGCTCCTCCCCCCCTCCCCCGC
NG46   ----------CCCCACTCACTGCTCGGACTCTCCCCCTCCCCGC-----
NG51   ----------CCCCACTCACTGCTCGGACTCTCCCCCTCCCCGC-----
NG53   ----------CCCCACTCACTGCTCGGACTCTCCCCCTCCCCGC-----
NG3    TCCGAGCCGGGGGTGTTCTGTTGGCGGGGGCGG--TGGGCGGG
NG55   TCCGAGCCGGGGGTGTTCTGTTGGCGTGGGCGGGGGTGGGCGGG
NG9    TCCGAGCCGGGGGTGTTCTGTTGGCGGGGGCGGGGGTGGGCGGG
NG36   TCGAGTGGCCTGGGCGTGTGGGGGGTGGGGGGGGTGGGCGCGGC
NG4    CCGATTCCCCCCCCCGCACCTCACCCTACCATGCCCGCCTCCCGC
NG15   TCGACCCCCCCCTCCTGTGCTCGTCGTG-GCTCTTCCATTCCGGC-
NG11    TCCGAACCCCACGAAGTGTGCTGGCTCTT-CTTGACCCATTCCG
NG24   GCCGACACCCGGGTTTCCCATCCGTTCCCCCGCTCCCCCCGGC-
NG29   ACCGAGGGG-GGGTGGGTGGTTCCTCCCGCCGCTCCCCCTTGGC
NG18   -------CG-TGATGCTCTCTCTCCTCCCGCCGCTCCCCCTTGGC--------
NG21   AGCGACAACAGCCACCCCCCACCCCGGACAACTCCCTGCTCGGC
NG35   CGCGACCTATC---CCCCTTCCCGGTTCTCCTTCTGGTCTCGTCGGC
```

Figure 3.4: Grouping of aptamer sequences on the basis of percentage sequence matches is presented where, comparatively more enriched sequences grouped in red and black boxes are indicated.

3.3.2 Electrophoretic mobility shift assay (EMSA)

The specificity of the NG3 and NG51 were evaluated by EMSA and the results validated specific binding of NG3 to *Pf*GDH as visible from the increase in intensity of the aptamer-protein complex band with increasing concentrations of the *Pf*GDH protein. There was no reactivity of both the aptamers with *H*GDH protein (Figure 3.5). A control study was also performed in the presence of random unrealted 90 bp nucleotide binding with *Pf*GDH and result showed no interaction with the protein. On the basis of EMSA results aptamer NG3 and NG51 were selected for further study.

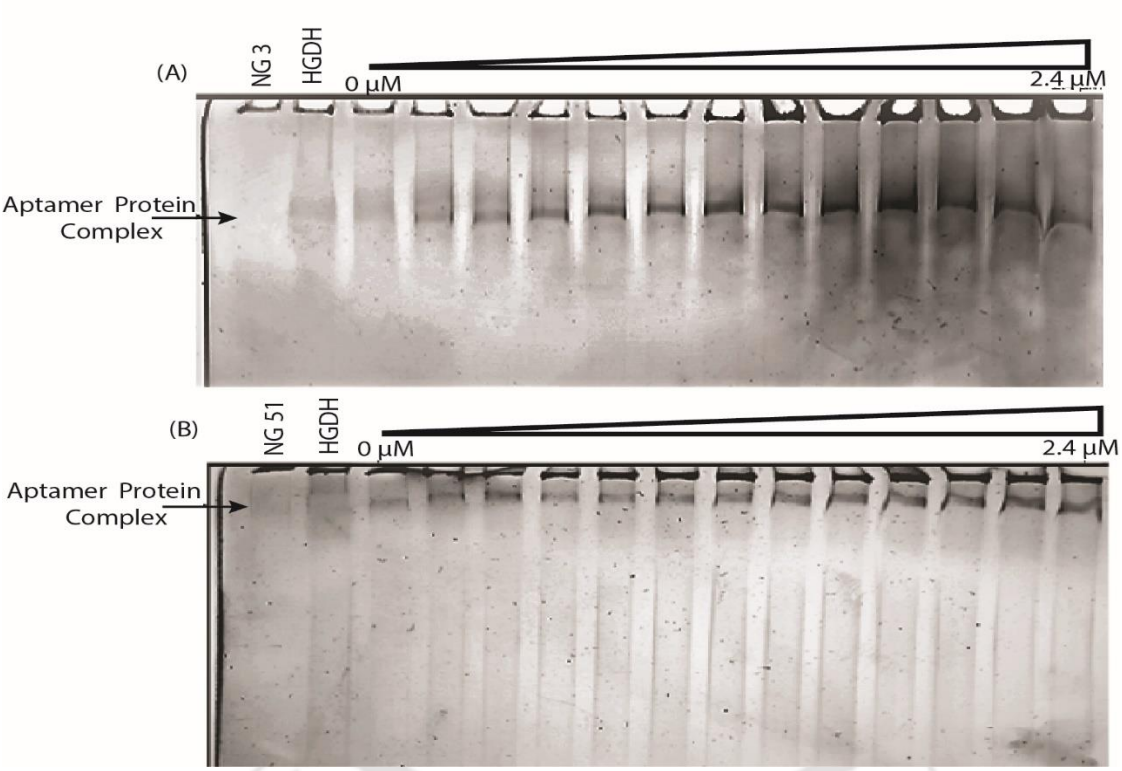

Figure 3.5: EMSA for NG3 (A) and NG51 (B). The concentration of *Pf*GDH used was in the range of 0 µM to 2.4 µM; and the concentration of each aptamer was 0.25 nM. Cyber gold was used to stain the gel. *H*GDH (1 µM) was used as negative control.

3.3.3 Prediction of aptamer strucuture

The secondary structures of NG3 and NG51 were predicted by using Mfold. The ΔG values for NG3 and NG51 were deduced as -7.99 Kcal mole^{-1}and -4.68 Kcal mole^{-1}, respectively. NG3 has two big loops with four small stem loop structures, connected through single straight long arm; whereas, NG51 has one big loop structure with three small stem loop structures, connected through the small arm (Figure 3.6 A, B).

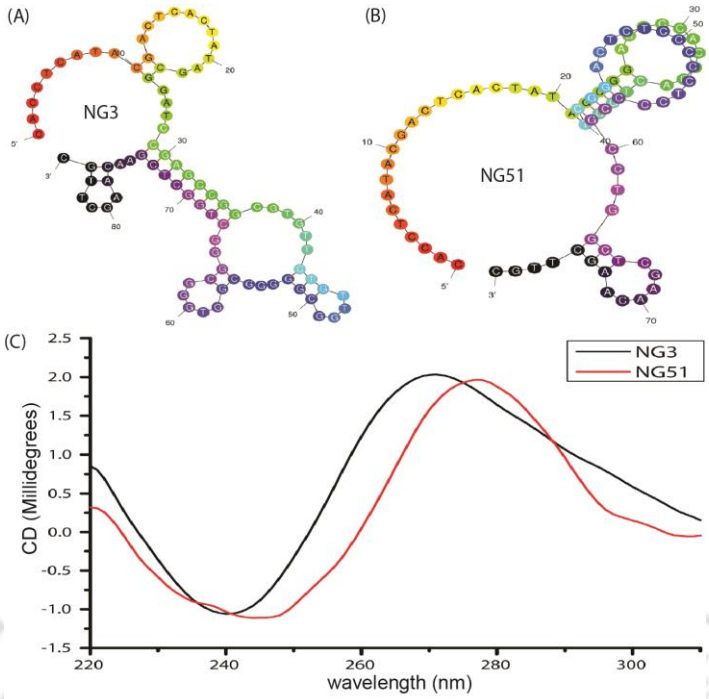

Figure 3.6: Secondary structures of NG3 (A) and NG51 (B) aptamers predicted by mfold software. CD spectra of NG3 and NG51 in 10 mM binding buffer (C).

Analysis of NG3 and NG51 aptamer sequence (Table 3.1) revealed the presence of various repeats of guanine (G) nucleotide which may contribute to the formation of G-quadruplex. The QGRS mapper analysis predicted the presence of two quadruplex forming regions in NG3 (Table. 3.2); while it was absent in NG51. The QGRS mapper results were braced with CD spectroscopy study. The CD spectra of NG3 exhibit a positive peak at ~ λ_{265} nm and negative peak at ~ λ_{240} nm which are characteristic of a antiparallel G qudraplex structure (Nagatoishi *et al*, 2007). Further, such observations were absent in NG51 (Figure 3.6 C). The ΔG value and G qudraplex forming capability indicate that aptamer NG3 has higher stability as compare to NG51.

Table 3.1: Sequence profile of selected aptamer candidates.

Aptamer	**Sequences (5'→3')**
NG3	TCA CCT CAT ACG ACT CAC TAT AGC GGA TCC GAG CCG GGG TGT TCT GTT GGC GGG GGC GGT GGG CGG GCT GGC TCG AAC AAG CTT GC
NG51	TCA CCT CAT ACG ACT CAC TAT AGC GGA CCC CAC TCA CTG CTC GGA CTC TCC CCC TCC CCG CCT GGC TCG AAC AAG CTT GC

Table 3.2: G qudruplex structure prediction of the developed aptamers.

Aptamer	Position	Length	QGRS	G-Score
NG3	24 57	30 14	GGATCCGAGCCGGGGTGTTCTGTTGGCGGG GGTGGGCGGGCTGG	13 21

3.3.4 Effect of ionic strength and pH on aptamer structure

Salt ions concentration is a crucial factor to maintain suitable structure of DNA. Therefore, the effects of various salt ions on the native confirmation of the developed aptamers were examined in presence of the binding buffer supplemented with salts at 100 mM (Figure 3.7 A, B). In case of NG3 spiked in milli-Q water we have observed the spectral shift from λ_{266} nm to λ_{278} nm compare to spike in binding buffer. Hence it proves that certain amounts of salts concentration are required to maintain structural integrity.

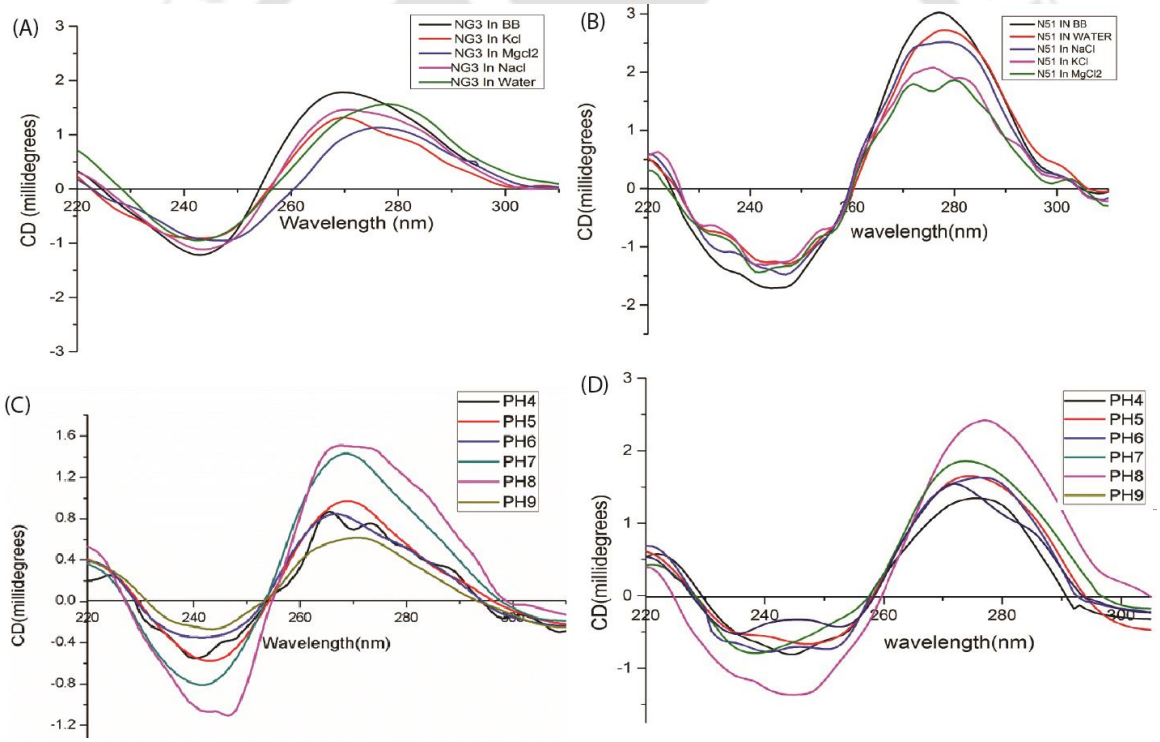

Figure 3.7: Effect of various salts on the structure of NG3 (A) and NG51 (B). Effect of pH on the structure of NG3 (C) and NG51 (D) in SELEX binding buffer (BB).

However, in the presence of high concentration of salt, there was a slight change in the CD spectra of NG3 aptamer. The change was more prominent in case of $MgCl_2$ most probably due to ionic interaction between Mg^{2+} ion and PO_4^{2-} backbone of ssDNA. We

also performed same experiment with NG51 to examine its structured integrity in presence of salt and observed major hypochromic shift when solvent changed from water to ionic liquid salt ($MgCl_2$). The result validate the effect of ionic interaction on the structure of aptamer. A similar study was done to find out the effect of different pH conditions on the structural folding of the aptamer (Figure 3.7 C, D). At acidic conditions, the CD spectra displayed reduced peak intensity at $\lambda_{266\ nm}$ and $\lambda_{278\ nm}$ for NG3 and NG51, respectively with a corresponding peak shift from ~ $\lambda_{278\ nm}$ to $\lambda_{275\ nm}$ was observed for NG51. For NG3, the peak intensity at $\lambda_{266\ nm}$ was increased in the order of pH 9 < pH 4 < pH 5 < pH 6 < pH 7 < pH 8 with the peak shape being slightly disordered at pH 4. Similarly for NG51 the peak intensities at $\lambda_{278\ nm}$ and $\lambda_{235\ nm}$ were similar for pH 6, pH 7 and pH 9 whereas at pH 8 the aptamer showed maximum peak intensities at both these wavelengths. At pH 4 and pH 5, the peak intensities at both $\lambda_{278\ nm}$ and $\lambda_{235\ nm}$ were reduced. This study suggests that the aptamers were comparatively stable at neutral and slightly acidic conditions as compared to alkaline conditions.

3.3.5 Binding affinity and specificity of aptamer-protein interactions

The aptamer-target interaction depends on proper 3D confirmation of aptamer. We have analyzed the aptamer binding affinity and specificity under the free state in solution through CD spectroscopy and surface immobilized state over solid substrate through SPR spectroscopy.

3.3.5.1 In-solution binding affinity and specificity of the developed aptamers

The binding affinities of the two positive aptamer candidates with the target and control proteins (*Pf*LDH, *Pf*HRP-II and HSA) were investigated by CD. Both the aptamers could change the ellipticity of the *Pf*GDH protein following their interactions validating the conclusive binding functions of the aptamers. The aptamers however, did not significantly change the ellipticity of the control proteins (*Pf*LDH, *Pf*HRP-II and HSA) indicating their specific nature (Figure 3.8).

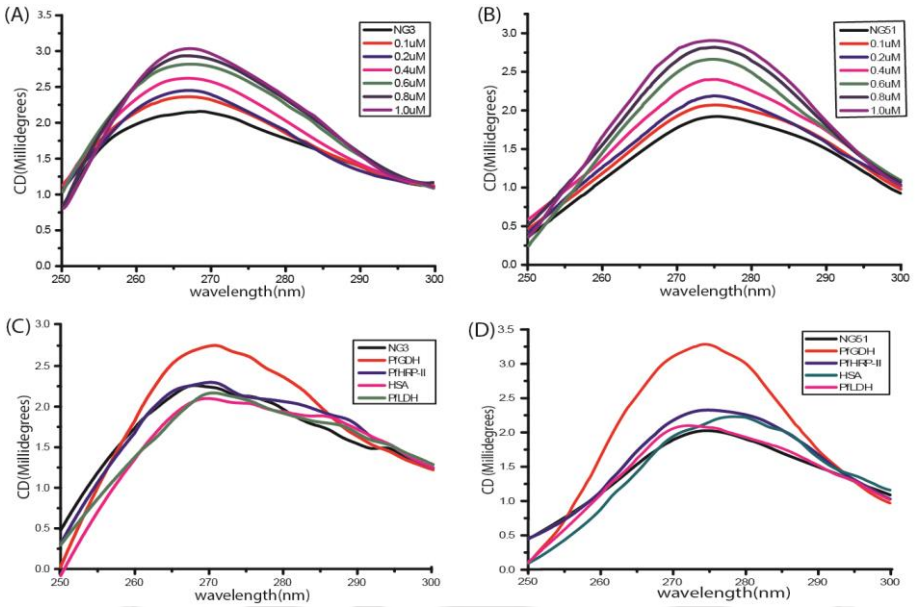

Figure 3.8: CD spectra of (A) NG3 and (B) NG51 in the presence of the target protein *Pf*GDH (0−1.0 μM). CD spectra of (C) NG3 and (D) NG51 in the presence of *Pf*GDH and negative control proteins HSA, HRP-II, and *Pf*LDH.

An increase in CD peak intensity on the binding of the aptamers with the increasing concentrations of *Pf*GDH was observed and the phenomena was utilized to determine the K_d of the aptamers. An increase in ICD signal upon increase in protein concentration is a direct indication of protein aptamer interaction (Garbett *et al.*, 2007). The determined K_d were 0.5 ± 0.04 μM and 1.1 ± 0.20 μM for NG3 and NG51, respectively (Figure 3.9). Taking into account the above findings and the lower K_d values, the aptamer NG3 was considered for further studies.

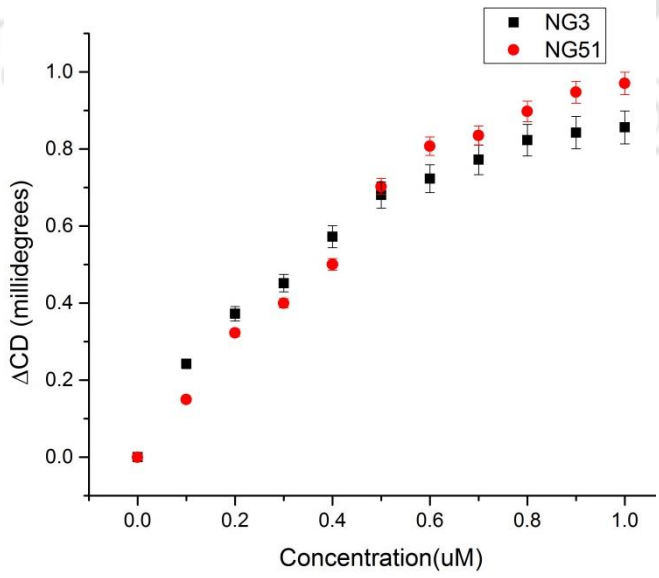

Figure 3.9: Curve fitting plots for K_d calculation using data from CD measurements.

3.3.5.2 Binding affinity and specificity of surface immobilized aptamer

The selected 5' end thiol modified aptamers (NG3, NG51) were immobilized (~200 nmol) over SPR chips followed by backfilling the chip with MCH. The prepared chips were then utilized for detection of different concentration of *Pf*GDH and other non-specific proteins. The binding of *Pf*GDH over the gold chip surface led to an increase in SPR angle, reaching a stabilization plateau within less than 10 min. After binding, buffer solution was passed over the surface to remove loosely bound protein from the surface. The amount of *Pf*GDH attached to the SPR chip was calculated by recording the difference between the final and initial SPR angle (Figure 3.10).

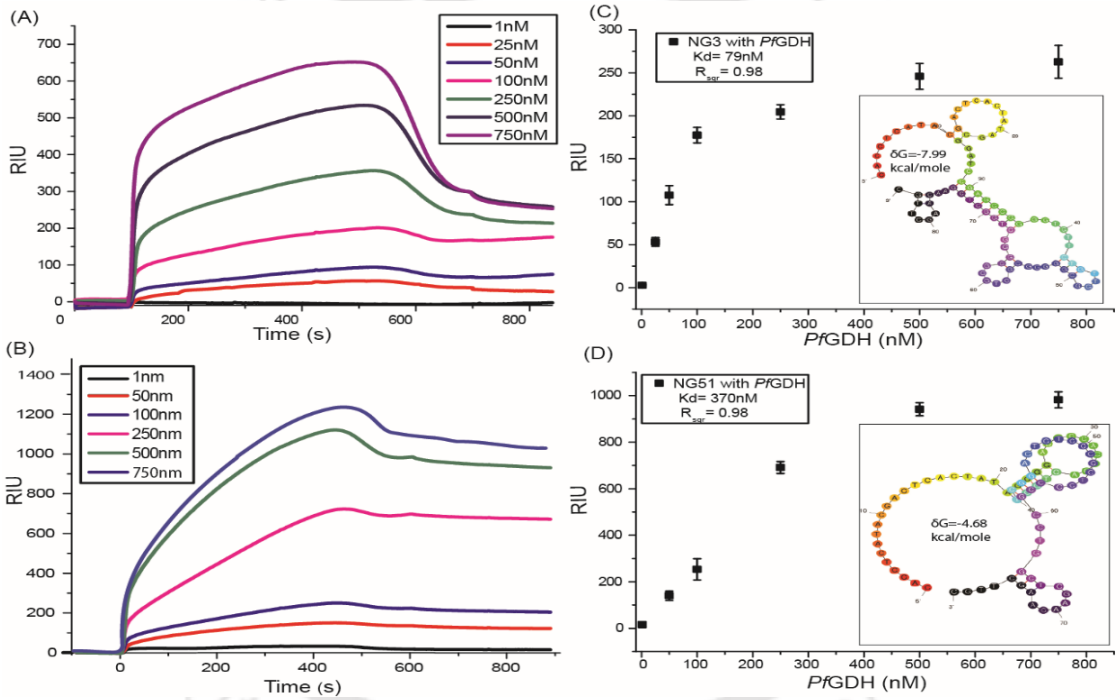

Figure 3.10: SPR sensogram for NG3 (A) and NG51 (B) with different concentration of *Pf*GDH. Plotting of sensogram response against different concentrations of *Pf*GDH to determine the K_d for (C) NG3 and (D) NG51. Inset secondary structure of NG3 and NG51 aptamer along with ΔG values.

The binding affinities of the developed aptamers were calculated using the single ligand binding site equation in 1:1 interaction mode, X+Y=XY, where X is injected target protein and Y is immobilized aptamer molecule, XY is aptamer–protein complex formed over the SPR chip. The formation of aptamer–protein complex (XY) is directly proportional to the response unit (RIU) of SPR (Scarano *et al.*, 2010). The K_d values for the aptamers were calculated using the equation RIU = RIU_{max}*c/ (K_d+c), where c is the

protein concentration. The K_d values were determined to be 79.16 ± 1.58 nM and 370 ± 14.39 nM for NG3 and NG51, respectively. The Gibbs energy, $\Delta G = - RT \ln K_a$, where R is the universal gas constant, T is temperature and association constant (K_a) = $1/K_d$, was also calculated for the NG3 and NG51 aptamers at 298 K and found to be - 56.9 kJmol^{-1} and - 36.7 kJ/mol^{-1}, respectively. The negative Gibbs energy values indicate the prompt interaction of *Pf*GDH with aptamer over the solid surface of the SPR chip, and found to be superior for NG3 candidate. The specificities of the developed aptamers were analysed by testing with control proteins (HGDH, *Pf*LDH, HSA), which showed negligible changes in SPR angle for both the NG3 and NG51 aptamers (Figure 3.11). Based on the higher binding affinity against *Pf*GDH and lower Gibbs energy change, NG3 was considered for further study.

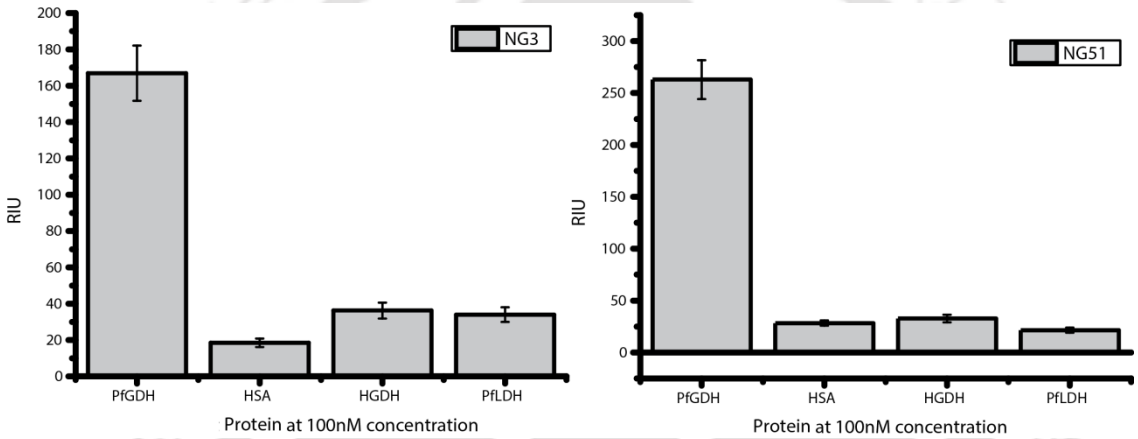

Figure 3.11: Interference study of the developed aptamers (NG3 and NG51) against different analogous and homologous protein at 100 nM concentration over SPR detection platform.

3.4 Conclusion

We have developed two novel aptamers (NG3, NG51) against the malarial antigen, *Pf*GDH through SELEX procedure. Both the aptamers showed slight change in structure in presence of high salt, high acidic and basic pH conditions. The binding affinity and specificity of the developed aptamers were qualitatively validated by EMSA. The dissociation constant and specificity of the developed aptamers in solution and surface immobilized states were discerned by CD and SPR spectroscopy, respectively. The K_d values in solution and surface immobilized conditions are summarized in table 3.3.

The results confirmed that both the aptamers do not exhibit cross - reactivity with analogous proteins.

Table 3.3: Comparison of K_d in free and immobilized state of developed aptamer through CD and SPR spectroscopy.

S. No	Name of Aptamer	Free/ Immobilized	Instrument	Dissociation Constant (K_d)
1.	NG3	Free	CD Spectroscopy	0.5 ± 0.04 µM
2.	NG3	Immobilized over gold chip	SPR Spectroscopy	79.16 ± 1.58 nM
3.	NG51	Free	CD Spectroscopy	1.1 ± 0.20 µM
4.	NG51	Immobilized over gold chip	SPR Spectroscopy	370 ± 14.39 nM

Chapter 4

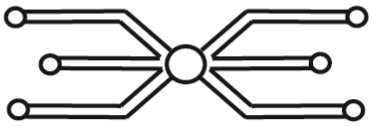

Protein-Induced Fluorescence Enhancement Based Detection of PfGDH Using Aptamer-Carbon Dot

Chapter 4

Protein-Induced Fluorescence Enhancement Based Detection of *Pf*GDH Using Aptamer-Carbon Dot as Detection Probe.

4.1 Overview

Search for efficient recognition system to detect malarial biomarker is one of the on-going research activities aggressively being pursued globally to design and develop flawless malaria detection system for deployment in POC settings in resource limiting malaria-infested regions (Jain *et al.*, 2014). One of the most critical requirements in developing rapid detection tests is the generation of noise free decipherable signal from the specific interaction of the bio recognition element with the target of interest. These interactions could be transduced to different signal forms among which, the optical signal systems have received intensive interest in the field of portable diagnostics and rapid detection tests due to their high sensitivity, scope for real-time analysis of the target in complex mixtures, and requirement of small sample volumes (Yue *et al.*, 2015). Of late, the fluorescence based optical detection systems are infusing to the portable sensors and biosensors segments for onsite and POC applications due to the recent advances in state-of-art on scaling down the size of the fluorescence monitoring devices (Malic and Kirk, 2006). Additionally, the fluorescence based method are reaching new heights with the invention of various highly efficient fluorophores for various applications (Zheng and Lavis., 2017). Cdot is a recent development on this field and is evolved as a universal fluorophore with a unique luminescent property. Among the various positive traits, carbon dots possess high quantum yield, broad excitation wavelength, less toxicity, easy surface modification, resistance against photo bleaching and simple green synthesis process that could be utilized for optical applications. The recent study on Cdots showed its broad application potential starting from bio imaging, ion sensing to protein detection (Zuo *et al.*, 2015).

Herein, we report application of a novel aptamer specific to *Pf*GDH selected through SELEX process as described in the previous chapter to develop a fluorescence-based detection of the biomarker. Following a simple chemistry, the aptamer was chemically conjugated to Cdots, which were synthesised following a straightforward pyrolysis method from a widely available amino acid. The synthesised Cdot-aptamer was then used as biorecognition cum fluorescence reporter assembly for quantitative detection of

*Pf*GDH protein in serum sample following the protein induced fluorescence enhancement (PIFE) phenomena. A schematic presentation of PIFE based detection of *Pf*GDH is depicted in figure 4.1.

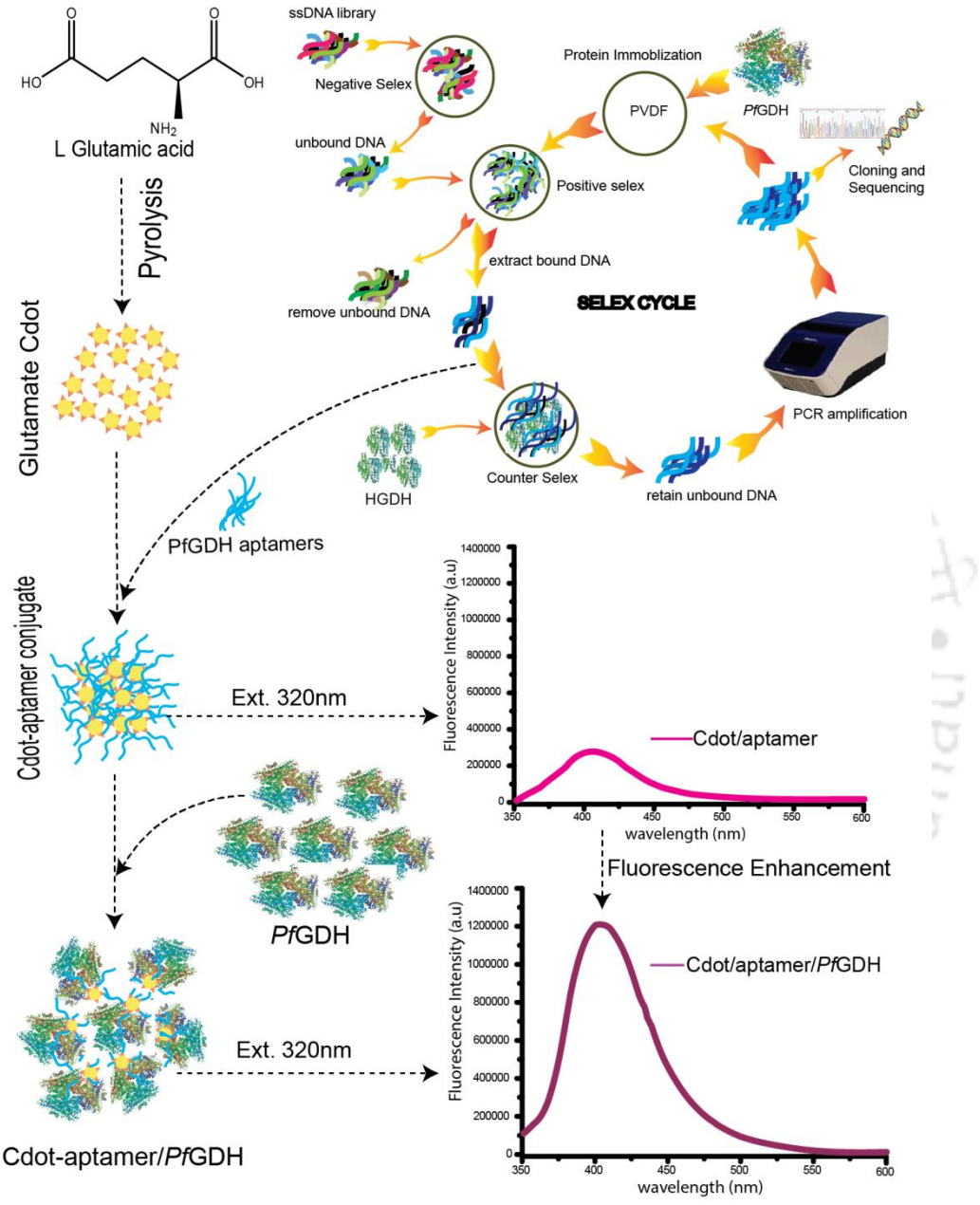

Figure 4.1: Schematic illustration of the fabrication of Cdot/aptamer conjugate and PIFE based detection.

The results showed that the fluorescence intensity is directly proportional to the protein concentrations in solution in a wide protein concentration range. The limit of detection (LOD) offered by the method was down to a nano - molar range. A detailed account on the findings is incorporated in this chapter.

4.2 Experimental Procedure

4.2.1 Materials

The monosodium glutamate and L-glutamic acid were obtained from Himedia, India. The transmission electron microscope (TEM) grid was procured from Sigma Aldrich, USA. The 5'-NH_2 modified NG3 aptamer was synthesised by Bioserve biotechnologies, India, pvt ltd. All the proteins (*Pf*LDH and *Pf*HRP-II) used in the present investigation were cloned, expressed and characterised as discussed in the previous chapter. Human blood was obtained from healthy person and kept at RT to clot and later centrifuged at 4000 rpm for 20 minutes to separate serum from clotted blood. All other chemicals used in the experiments were of analytical grade.

4.2.2 Experimental approaches

The current study was permitted and ethically approved by the Institute Human Ethics Committee (IHEC) of the Indian Institute of Technology Guwahati, India.

4.2.3 Carbon dot (Cdot) synthesis and characterizations

Cdots were synthesized from monosodium L-glutamate through pyrolysis bottom up process (Wu *et al.*, 2013) with some modifications. Two grams of monosodium L-glutamate was briefly heated at 180 $^{\circ}$C until the solution turned yellow. Following a brief incubation for 30 s at the same temperature the content was dissolved in 10 ml of Milli-Q water (18.1 MΩ.cm) with moderate magnetic stirring for 1 h at RT. The formed Cdots were separated by centrifugation at 13000 x g for 30 min.

The quantum yield (Φ) of the Cdot was measured with respect to fluorescein (Φ = 92% in 0.1N NaOH) as reference dye. The Φ was calculated with following equation (i):

$$\Phi x = \phi ref * \frac{\eta x2}{\eta ref2} * \frac{Ix}{Iref} * \frac{Aref}{Ax} \quad \text{.....(i)}$$

$$\tau_{avg} = \Sigma(Ai * \tau)^2/\Sigma(Ai+\tau)^2 \text{.....(ii)}$$

Where, annotation (x) and (*ref)* stand for sample and reference, respectively, I is integrated fluorescence intensity and absorbance at excitation wavelength is denoted with A. The refractive index (ηx^2, ηref^2) for PBS is 1.33. The Cdot was excited at λ_{320nm} and

emission was observed from λ_{350nm} to λ_{600nm}. The life time was measured with Picosecond Time-resolved cum Steady State Luminescence Spectrometer (Eddinburg Instruments, UK) with $\lambda_{308\ nm}$ LED excitation source. The colloidal milk powder was used as reference solution. The average life time was calculated from equation (ii). Where Ai is distribution of particle and τ is measured life time.

4.2.4 Preparation of Cdot-aptamer conjugates

The Cdots were covalently linked to 5'- amine modified aptamer using EDC-NHS covalent chemistry. The Cdots ($1mg.ml^{-1}$) were incubated with 0.1 M morpholino-ethanesulfonic acid (MES) buffer, pH 6.0 along with 2 mM EDC {1-ethyl-3-(3-dimethylamino propyl) carbodiimide} and 5 mM NHS (N-hydroxysulfo succinimide) reagents for 30 mins with gentle mixing followed by addition of binding buffer slowly into the system. Then 0.5 µM 5' NH_2-aptamer from stock solution of 100 µM was added to the solution and incubated for 2 h. Before the attachment of Cdot, the aptamer was heat treated to 90 °C for 10 min followed by incubation in ice for 4 minutes. To block the free carboxylic groups, the solution was treated with 1 % ethanolamine for 1 h at 4 °C. The Cdot-aptamers conjugates were then purified by 5 kDa cut-off centrifugation filter to remove uncoupled Cdot and excess chemical reagents.

4.2.5 Detection of *Pf*GDH through Cdot-aptamer conjugates

The *Pf*GDH samples, either dissolved in the binding buffer or spiked in 4-fold diluted human serum, were added to 100 µl of Cdot-aptamer conjugate and then made-up the volume to one ml with binding buffer. The mixture was incubated for different time intervals and then the fluorescence was recorded (excitation at $\lambda_{320\ nm}$ and emission at $\lambda_{350\ nm} - \lambda_{600\ nm}$) in Fluoromax-4 (Horiba USA). The specificity of the assay was also checked with different analogous potential interfering proteins. Each measurement was performed in triplicates to estimate the standard deviation of the results**.**

4.2.6 Docking of aptamer-protein for Interaction studies

The 3D structure of the aptamer was analysed through RNA composer software (Popenda *et al.,* 2012) by using mfold dot bracket annotation as input considering the fact that the 3D confirmation folding of ssDNA takes place almost the same way as for RNA folding (Kakoti and Goswami, 2016). Docking of *Pf*GDH (PDB ID: 2BMA) and 3D structure of

aptamer was performed through Autodock online server based on shape complementary principle (Schneidman-Duhovny *et al.*, 2005) and visualization and the analysis was performed by PyMOL software. The surface interaction between amino acid and nucleotide was analysed by protein ligand interaction programme (Salentin *et al.*, 2015).

4.3 Results and discussion

4.3.1 Characterization of Cdots

Transmission electron microscopy (TEM) analysis of the synthesized Cdots revealed homogenously distributed spherical particles with average diameter of 2 - 4 nm (Figure 4.2 A). XRD analysis of the synthesized carbon dot exhibited a broad peak at ~ 21^{o} with a lattice spacing of '002' indicating disordered carbon atoms conforming to the previous report (Liu *et al.*, 2016) (Figure 4.2 B).

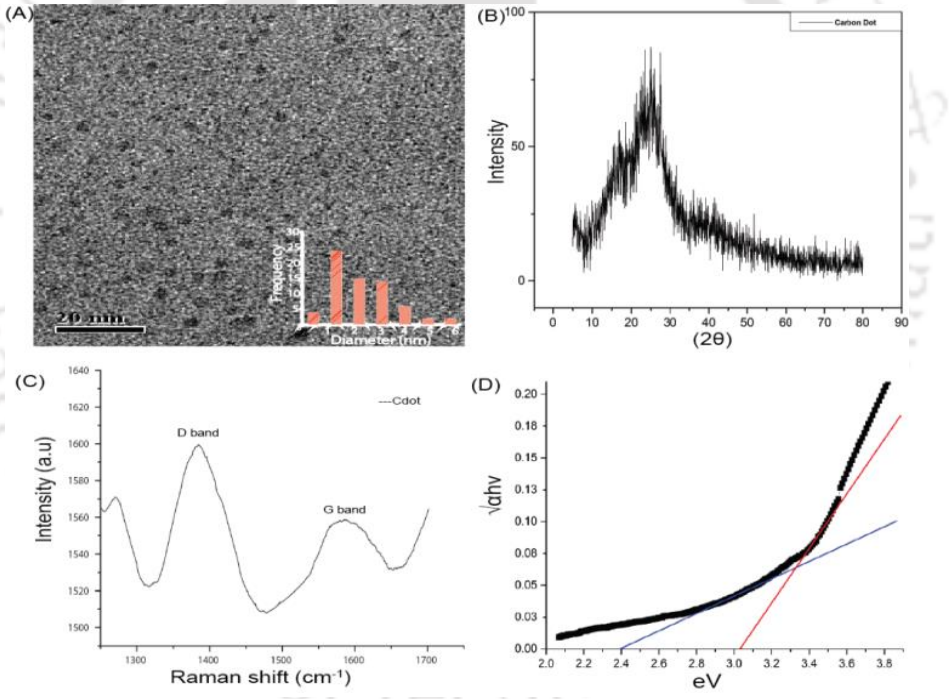

Figure 4.2: **(A)** TEM image of Cdots with inset indicating size distribution of the particles. **(B)** X-ray diffraction spectra of the Cdot in powder form. **(C)** Raman spectra of the Cdots. (D) Band gap measurment of Cdot with Tauc plot.

Raman spectra of the Cdots showed two typical peaks designated as D band at 1385 cm^{-1} due to out of plane vibration of sp^2 carbon atoms and G band at 1580 cm^{-1} as a result of in-plane vibrations of sp^2 carbon atoms. The intensity ratio of D/G was 1.03, which showed that some of the sp^2 bonds broke and turned into new sp^3 bond (Figure 4.2 C).

The band gap (Eg) of the Cdot and its aptamer conjugated product was measured following the Tauc equation, $(\alpha h\nu)^{1/n} = A (h\nu - Eg)$. Where α is the absorbance coefficient, h is the Planck constant and hν stand for incident photon energy. The nature of transition of electron between conductance and valence is defined by (n) the indirect electronic transition n = 2. The optical band gap of Cdot was measured with Tauc plot by extrapolating the linear part of $\alpha h\nu^{1/2}$ verses hν curve to energy axis where $\alpha h\nu^{1/2} = 0$. The average value of band gap for Cdot was 2.8 eV assuming indirect electronic transition (Figure 4.2D). FTIR spectra confirmed the presence of different surface oriented functional groups on the synthesized dots (Figure 4.3 A). A broad peak at ~3400 cm^{-1} in the spectra implied vibrational stretching of carboxylic –OH and amine –NH. Some additional bands exhibited by the Cdots at ~1680 cm^{-1} indicated the presence of C=O group because of COO^- vibration.

4.3.2 Characterization of Cdot-aptamer conjugates

The FT-IR absorbance peaks of NG3 at ~1620 cm^{-1} and ~3400 cm^{-1} can be assigned to N-H stretching of primary amine and –OH group, respectively (Figure 4.3 A).

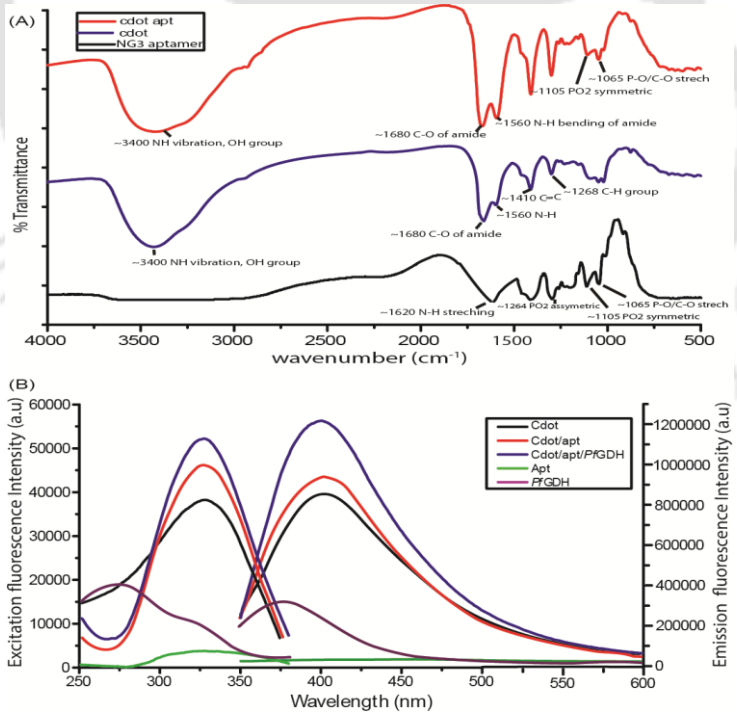

Figure 4.3: FTIR spectra of NG3 aptamer (black) Cdot (blue) and Cdot-aptamer conjugate after EDC/ NHS activation covalent linkage (red) (A). Excitation and emission spectra of Cdot, aptamer, *Pf*GDH, Cdot - aptamer and Cdot - aptamer/ *Pf*GDH complex in binding buffer (B).

The interaction of the amine modified NG3 aptamer with Cdot was confirmed by characteristic amide bond peak at ~1680 cm^{-1} (C=O group of amide) and ~1560 cm^{-1} (-NH bending vibration of amine) which established the covalent interaction between Cdot and NG3 aptamer. The presence of aptamer stretching vibration at ~ 1065 cm^{-1} and ~1105 cm^{-1} were assigned to the respective functional groups P-O/C-O, and PO_2^- symmetric bonds originated from aptamer phosphodiester backbone in the Cdot-aptamer assembly that confirmed the coupling of aptamer with Cdot. Besides the covalent binding between Cdot and aptamer some other interactions that support the carbon dot-aptamer binding in buffer condition such as, dipole bond, hydrogen bond and ionic/electrostatic interaction can't be ruled out. The band gap of the conjugate however, was not deviated from the value detected for the pure Cdot.

4.3.3 FRET-based detection of *Pf*GDH using Cdot-aptamer conjugate in buffer

Fluorescence resonance energy transfer (FRET) is a widely used sensing technique in which two fluorescence molecules are required, one act as a donor while the other act as an acceptor of the light energy at a defined distance. Application of FRET for detection of protein is difficult due to the complex and inefficient methods available for protein tagging and selection of acceptor and donor partner (Hwang and Myong, 2014). Herein, a protein induced fluorescence enhancement (PIFE) phenomenon for the Cdots was achieved due to which searching of the matching fluorophore and its labeling to the *Pf*GDH protein molecules could be avoided. The synthesized Cdot exhibited strong fluorescence in the spectral range of $\lambda_{350\ nm}$ - $\lambda_{600\ nm}$ with the peak intensity centered on ~ $\lambda_{410\ nm}$ when it was excited at $\lambda_{320\ nm}$. The characteristic excitation and emission wavelengths were not altered even when the Cdots were chemically coupled to the aptamers to produce the Cdot-aptamer assembly; which indicates that the chemical surface modification of Cdot for linking the aptamer did not affect the optical properties of this carbon based nanomaterial. Interestingly, the fluorescence intensity of the Cdot-aptamer assembly was markedly enhanced by their interaction with the target *Pf*GDH proteins in solution. Notably, the intrinsic fluorescence of the target protein was observed at a shorter wavelength (~ $\lambda_{385\ nm}$) with very low intensity and quantum yield (6 %); hence the observed enhancement of fluorescence intensity of the Cdot-aptamer assembly excludes the intrinsic fluorescence of the *Pf*GDH protein (Figure 4.3 B). The Quantum yield of the Cdot was 34 %, which did not significantly changed in Cdot-aptamer

assembly. However, in presence of *Pf*GDH the quantum yield of Cdot-aptamer increased to 40 %. A clear enhancement of fluorescence of Cdot-aptamer assembly on its interaction with the *Pf*GDH is visible from the spectra, which is attributed to the PIFE phenomenon. Optimum binding time for Cdot-aptamer with *Pf*GDH was analyzed and discerned as 30 mins (Figure 4.4).

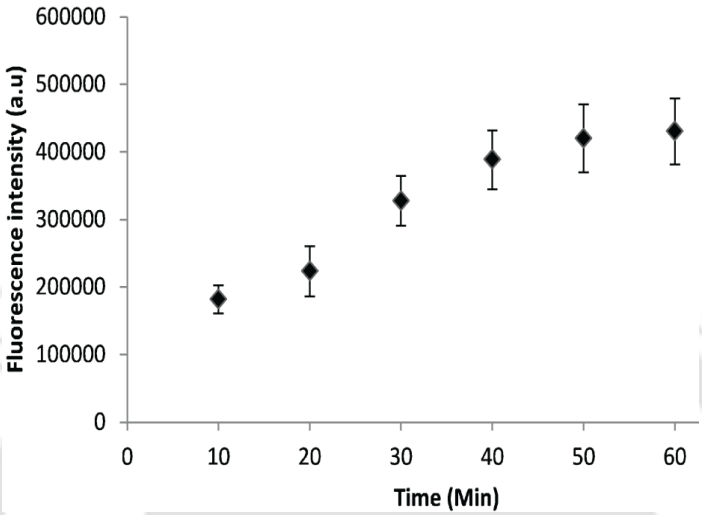

Figure 4.4: Time optimization study for PIFE of Cdot-aptamer/*Pf*GDH complex.

Based on this result, the Cdot-aptamer assembly was used to detect *Pf*GDH by monitoring the fluorescence emission at $\lambda_{410\ nm}$ at the excitation of $\lambda_{320\ nm}$. The PIFE in terms of relative fluorescence of Cdot-aptamer complex was studied with varying concentrations of spiked *Pf*GDH in binding buffer (Figure 4.5A).

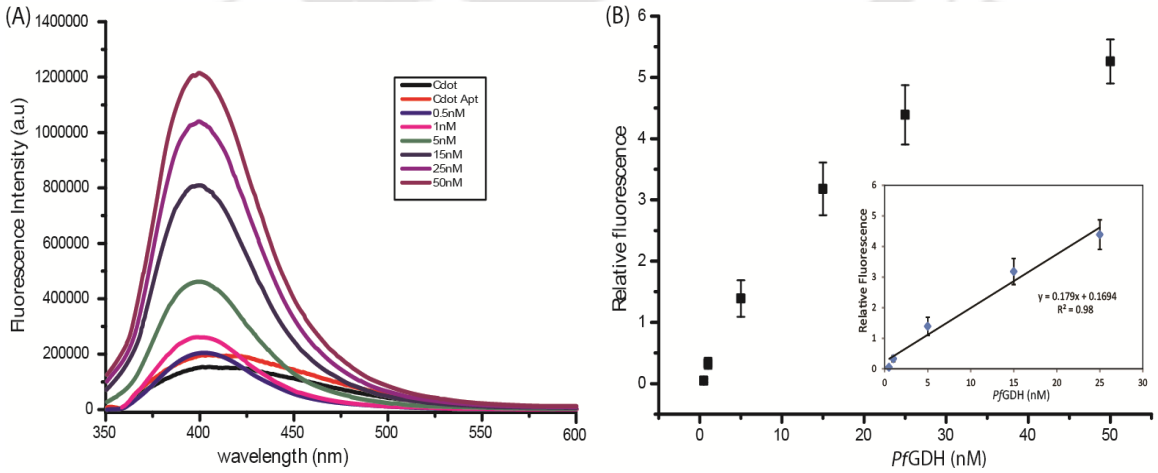

Figure 4.5: PIFE of Cdot-aptamer conjugate with increasing concentration of *Pf*GDH protein spiked in binding buffer (A). Calibration plot for PIFE response with *Pf*GDH protein spiked in binding buffer (B).

The relative fluorescence intensity was calculated by using the relation: $(F_t\text{-}F_b/F_b)$ where F_t is the fluorescence intensity of the conjugate (Cdot-aptamer/*Pf*GDH), and F_b is the fluorescence intensity of the Cdot-aptamer complex (as blank). From the calibration curve (Figure 4.5B) a linear detection range of 0.5 nM – 25 nM and a limit of detection {LOD= 3x Standard deviation (SD)/slope} of 0.48 nM for *Pf*GDH (R^2 = 0.98) were discerned in buffer.

4.3.4 Interference studies and analysis in serum sample

The detection of *Pf*GDH in serum sample was also analysed by spiking different concentration of *Pf*GDH (1 nM to 25 nM) in the 4-fold diluted serum (Figure 4.6 A) and discerned LOD of 2.85 nM (R^2 = 0.98) with a linear dynamic range of 1 nM - 25 nM (Figure 4.6 B).

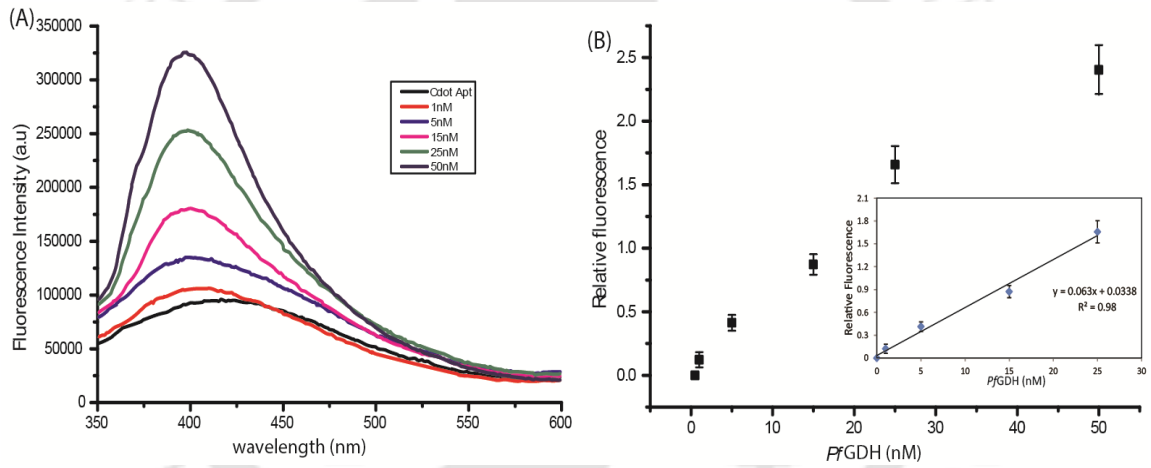

Figure 4.6: PIFE of Cdot-aptamer conjugate with increasing concentration of *Pf*GDH protein spiked in diluted serum (A). Calibration plot for PIFE response with *Pf*GDH protein spiked in diluted serum (B).

The high LOD in the serum has been attributed to its complex nature containing abundant amount of different proteins and ions, which is likely to interfere the fluorescence signal. Nevertheless, the level of sensitivity detected falls within the range (2 to 16 nM) of *Pf*GDH present in malaria patient (Li*et al.*, 2005).

The G-quadruplex structure of the aptamer provides a hydrophobic microenvironment to the conjugated Cdot, which facilitates the binding and sheltering of the Cdot-aptamer complex in the hydrophobic pocket of *Pf*GDH as reported for other cases (Cao *et al.*, 2011; Li *et al.*, 2010). This sheltering might support surface stabilization of Cdot by partial passivation and enabling more efficient radiative recombination between electron

and holes, the primary reason for Cdot fluorescence property (Liu *et al.*, 2012, 2016; Mondal *et al.*, 2012). This hypothesis was supported by the time-resolved fluorescence analysis. The Cdots lifetime of 2.69 ± 0.55 ns was correspondingly increased to 2.85 ± 0.67 and 3.32 ± 0.52 ns, following its interaction with aptamer and *Pf*GDH (Figure 4.7 A, Table 4.1).

Table 4.1: Florescence life time (**τ**) of Cdot, Cdot-aptamer and Cdot-aptamer-*Pf*GDH with excitation at $\lambda_{308\ nm}$.

Sample	τ_{ex1}	τ_{ex2}	τ_{ex3}	τ_{Avg}
Cdot	3.23	2.17	2.43	2.61±0.55
Cdot-aptamer	3.59	2.28	2.68	2.85±0.67
Cdot-aptamer-*Pf*GDH	3.93	2.95	2.95	3.32±0.52

The florescence lifetime increased in less polar environment because the lower dipole moments of surrounding molecule lead to decrease the efficiency of energy transfer (Elana *et al.*, 2015). The specificity of Cdot-aptamer was analysed in the presence of analogous malarial marker proteins *Pf*LDH, *Pf*HRP-II and other two nonspecific human proteins, HSA and HGDH at a concentration of 10 nM for each in the sample (Figure 4.7 B).

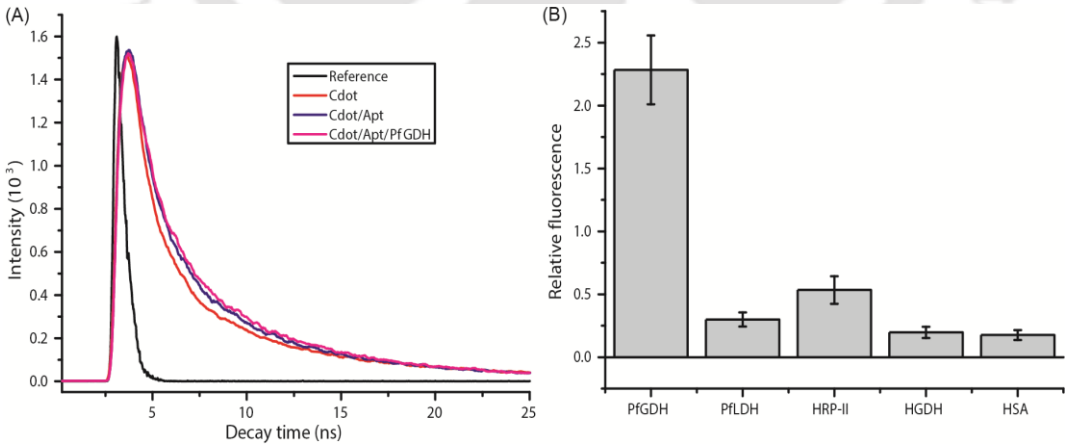

Figure 4.7: Picosecond Time-resolved fluorescence spectra with excitation at $\lambda_{308\ nm}$ obtained by using LED light source and colloidal milk solution as reference (A). PIFE response of Cdot-aptmer conjugate with different nonspecific malaria (*Pf*LDH, *Pf*HRP-II) and human (HSA, HGDH) proteins each at a concentration of 10 nM spiked in binding buffer (B).

The signal to noise ratio calculated with equation (iii). Fluorescence intensities of Cdot-aptamer/protein and Cdot-aptamer were considered as target and background signal, respectively.

$$\frac{\text{Signal (S)}}{\text{Noise (N)}} = \frac{\Delta\text{Target and background fluorescence intensity}}{\sqrt{\text{background signal}}} \quad \text{.....(iii)}$$

The S/N was found to be 1138.29, 141.17, 266.25, 97.98 and 87.65 for *Pf*GDH with corresponding proteins *Pf*LDH, *Pf*HRP-II, HGDH and HAS. This indicates a highly selective PIFE response of the Cdot-aptamer conjugate for the target *Pf*GDH protein.

4.3.5 Docking of aptamer-protein for interaction studies

The confinement of Cdot-aptamer into hydrophobic pocket of *Pf*GDH was also supported by the molecular docking studies (Figure 4.8).

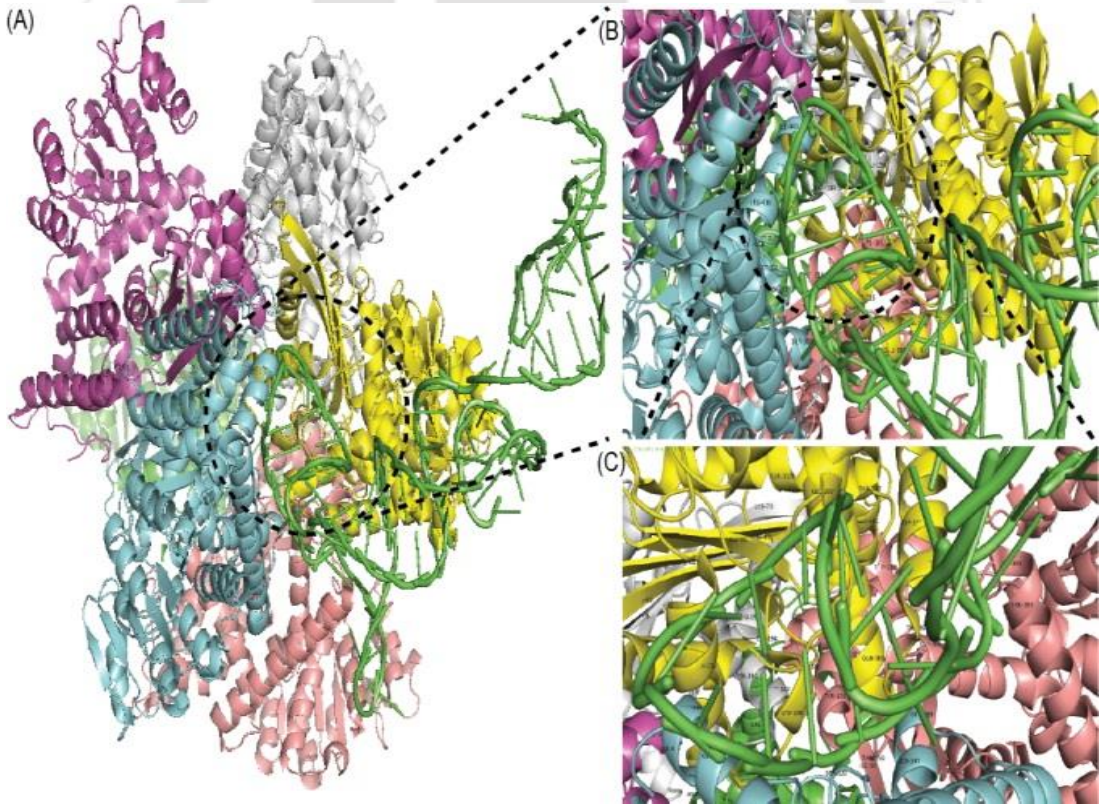

Figure 4.8: (A**)** Docking of NG3 aptamer with *Pf*GDH (PDB. ID.2BMA) for binding surface analysis with patch dock online software and visualize through PyMol software. Each subunit of the hexameric protein is shown in different color. The ssDNA aptamer is shown in green color in the binding pocket. (B) The hydrophobic binding pocket with the docked aptamer in expanded view. (C) Further enlargement of binding pocket of aptamer with surrounding amino acid.

The dock result revealed that NG3 aptamer was involved inside the hydrophobic side pocket of *Pf*GDH surrounded by hydrophobic amino acids, Meth 384(H.I 74), Leu 119 (H.I 97), Trp 195 (H.I 97) , Ile 397 (H.I 99), Phe 297 (H.I 100), Cys 446 (H.I 49), Tyr 211, 419 (H.I 63) and Val 296 (H.I 76). The relative hydrophobic index (H.I) of the amino acids shown in the parentheses was considered with respect to glycine at pH 7.0, which act as neutral amino acid (Monera *et al.*, 1995). Moreover, these amino acids constituted the binding domain involved in the interaction with the aptamer (Table 4.2). Protein Ligand Interaction Profiling (PLIP) study showed that 19 Hydrogen bonds, 15 salt bridges and 3 hydrophobic bonds were involved in the interaction between the Cdot-aptamer conjugate and *Pf*GDH leading to a strong binding between the protein and NG3 aptamer.

Table 4.2: Interacting forces and amino acid residues involved in binding NG3 with *Pf*GDH protein.

	Name of amino acid and position		
Hydrophobic Pocket	Meth 384, Leu 119, Trp 195, Ile 397,Phe 297,Cys 446, Tyr 211, 419 and Val 296.		
Interacting Amino acid: Nucleotides	**Salt Bridges**	**Hydrophobic Interaction**	**Hydrogen Bond**
	41Lys:48G, 205Arg:46T 205Arg:45G, 255Lys:83T 274His:43C, 282 Asp:48G 286Glu:48G, 395Arg:44T 396Glu:53G, 418Lys:50C 437Lys:52G,440Glu:49G 429Lys:48G,429Lys:47T	299Ser:28C, 313Pro:81C 396Glu:56C	41Lys:42G, 203Asn:52G 203Asn:53G, 205Arg:45G 211Tyr:43C, 232Thr:43C 232Thr:82T, 253Asn:65G 255Lys:82T, 270Asn:83T 300Thr:28C, 395Arg:44T 396Glu:56C, 400Glu:56C 415Glu:39T, 416Asn:51G 419Tyr:49G, 440Glu:45G 444Glu:46T, 429Lys48G

Underline amino acid are hydrophobic in nature.

4.4 Conclusion

The specific ssDNA aptamer (NG3) developed against the *Pf*GDH protein was chemically conjugated to a Cdot, which was chemically synthesized from monosodium L-glutamate through a bottom up approach. The Cdot-aptamer assembly was successfully employed to sensitively detect *Pf*GDH by using a principle of protein-induced fluorescence enhancement (PIFE). The detection approach was further validated in human serum sample with spiked *Pf*GDH. The proposed detection method holds promise for sensitive detection of *P. falciparum* malaria as the dynamic range obtained in this study covers the pathological concentration of *Pf*GDH present in the serum of malaria patient. The presence of potential interfering proteins namely, *Pf*LDH, *Pf*HRP-II, HGDH, and HSA showed lack of or poor influence on the response. The mechanism involved in PIFE has been elucidated and ascribed to the interaction of Cdot with the hydrophobic cohort comprising of G-quadruplex structure of the conjugated aptamer and surrounding molecular environment in the hydrophobic pocket of the target multimeric *Pf*GDH protein. The investigation also explored the key amino acid moieties of the *Pf*GDH protein that participated in binding with the aptamer. The key moieties involved in the interaction also emboldened the proposed hypothesis for PIFE response. The detection method proposed here has the potential to be developed into a sensitive, selective and rapid diagnosis method for malaria.

Chapter 5

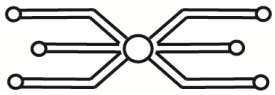

Development of Capacitive Aptasensor for Detection of PfGDH

Chapter 5

Development of capacitive aptasensor for detection of *Pf*GDH

5.1 Overview

Electrochemical impedance spectroscopy (EIS), either in Faradaic or non-Faradaic modes, has recently received enormous interest in the field of biosensors due to its highly sensitive signal transduction feature (Wang *et al.*, 2017; Rohrbach *et al.*, 2012). The Faradic impedance spectroscopy however, relies on an indirect method where a redox species is used to investigate the bio interaction at the electrode interface (Liu *et al.*, 2017). Hence, the method requires an additional design strategy or step to incorporate the redox species in the detection device, which intricate the system and thus discourage it for point of care (POC) applications. In contrast, non-Faradaic EIS measurements do not require any external redox probe, allowing direct measurement of the target molecule in the sample that makes the system suitable for POC applications (Arya *et al.*, 2018, Luo *et al.*, 2013). In non-Faradaic EIS measurements, variations in interfacial capacitance developed by dislocating water molecules and ions away from a bio-functionalised electrode surface following its binding to the target molecule is used for sensor application (Tkac and Davis, 2009). In this chapter, a *Pf*GDH ssDNA aptamer selected through SELEX process as described in a previous chapter has been used to develop a capacitive aptasensor (Figure 5.1) for the *Pf*GDH malaria antigen.

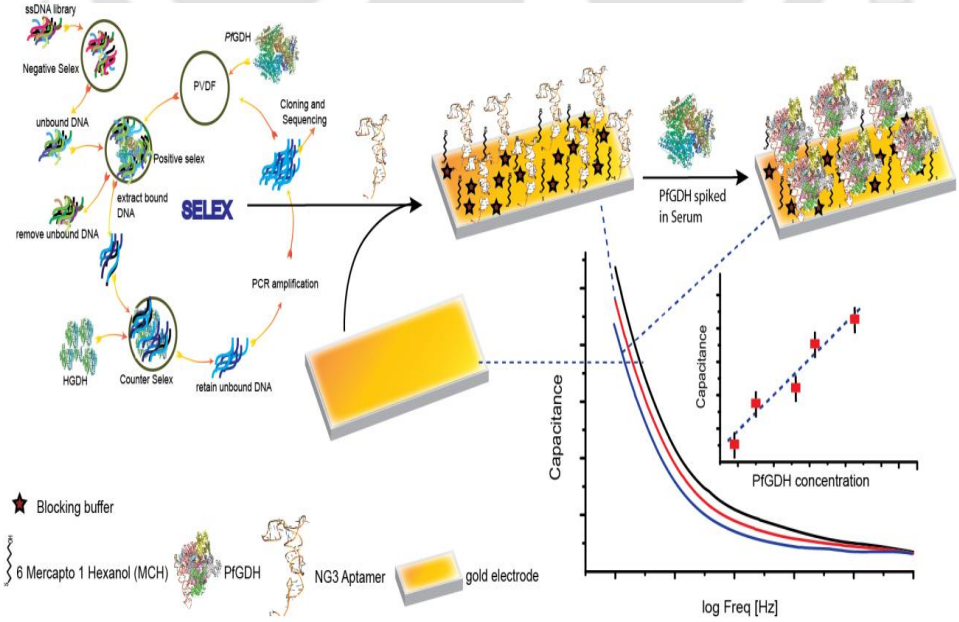

Figure 5.1: Fabrication of electrode with aptamer developed through SELEX and detection of *Pf*GDH.

The aptamer was first immobilized chemically over an electrode surface through a self-assembled technique as shown in the figure 5.1 then it was utilized for detecting *Pf*GDH directly in serum samples using non-Faradaic EIS technique. The aptasensor exhibited high sensitivity, selectivity and a wide dynamic range for the *Pf*GDH in blood serum.

5.2 Experimental procedures

5.2.1 Materials

Various reagents such as PBS, $MgCl_2$, NaCl, KCl, alumina powder (50 nm coarse sizes), HSA and human serum from AB positive male were procured from Sigma Aldrich, USA. The Starting blocking buffer and H_2SO_4 were procured from Thermo Fisher (UK). The single stranded random N40 oligonucleotide DNA library with conserved primer binding site and primer were received from IDT technology (USA). All the proteins (*Pf*LDH and *Pf*HRP-II) used in the present investigation were cloned, expressed and characterised as described in the previous chapter. Thiolated HPLC grade purified *Pf*GDH aptamer NG3 and NG51 (Table 5.1) were get synthesised from Sigma (UK). The experiments on human blood serum samples were ethically cleared and approved by the Institute Human Ethics Committee of IIT Guwahati, India and University of BATH, UK.

Table 5.1: Thiolated NG3 and NG51 aptamer sequences.

Aptamer	Sequences (5'→3')
NG3	SH-***$(CH_2)_6$-TTT*** TCA CCT CAT ACG ACT CAC TAT AGC GGA TCC GAG CCG GGG TGT TCT GTT GGC GGG GGC GGT GGG CGG GCT GGC TCG AAC AAG CTT GC
NG51	SH-***$(CH_2)_6$-TTT*** TCA CCT CAT ACG ACT CAC TAT AGC GGA CCC CAC TCA CTG CTC GGA CTC TCC CCC TCC CCG CCT GGC TCG AAC AAG CTT GC

Sequences in italics and bold added as linker region, to avoid restricted movement of aptamer

5.2.2 Sensor fabrication

Bare gold disc electrodes of 3 mm diameter (CHI Instruments, USA) were cleaned with piranha solution (3:1 ratio of H_2SO_4: H_2O_2) for 30 s, followed by mechanical polishing with 50 nm course size alumina slurry (Sigma) for 5 min over a polishing pad (BASi, USA). The electrodes were then sonicated in absolute ethanol and milli-Q water for 5 min each, sequentially. Thereafter, electrodes were electrochemically cleaned in 0.5 M H_2SO_4

by cycling the potential between -0.5 and +1.3 V *versus* Hg/Hg_2SO_4 till a stable characteristic reduction current peak of bare gold was observed. The electrodes were rinsed with ample amounts of milli-Q water and then dried in N_2 gas jet steam.

The aptamers were then grafted to the clean gold electrodes following a previously reported method (Jolly *et al.*, 2017). In brief, 100 mM of MCH was first prepared in absolute ethanol as stock solution and then diluted to 1 mM in binding buffer. The aptamer was heat treated at 90 °C for 5 min, then cooled down to room temperature (RT) for 15 min before initiating the sensor fabrication. The clean electrodes were incubated in 200 µl of *Pf*GDH specific aptamer: MCH in a 1:100 ratio and left overnight in a humidity chamber. After the immobilization, electrodes were rinsed with milli-Q water to remove unbound aptamers. To ensure proper coverage, the electrodes were further treated with 1 mM MCH for 1 h. The electrodes were again washed with milli-Q water and dried with N_2 steam and blocked with starting blocking buffer (Thermo Fisher, UK) for 30 minutes to prevent non-specific attachment of proteins over the electrodes.

5.2.3 Atomic force microscopy (AFM) study

The topological characterization of the fabricated aptamer-IDµE was performed by AFM in continuous tapping mode using Multimode Nanoscope with IIIa controller (Bruker, Germany) in combination with control software (version 6). The AFM images were captured using 10 nm diameter AFM ContAl-G tips (Budget Sensors®, Bulgaria), and then analyzed with WsxM version 5 software.

5.2.4 Cyclic voltammetry (CV) studies

The layer by layer fabrication of the aptasensor was characterized by means of Faradic CV measurements in a three-electrode configuration with Ag/AgCl as reference and Platinum wire as counter electrodes. The measurements were performed in 10 mM PBS pH 8 with 10 mM ($K_3Fe(CN)_6/K_4Fe(CN)_6$) as redox probe using a µAutolab III / FRA2 potentiostat/galvanostat (Metrohm, The Netherlands) at equilibrium potential with 25 mV amplitude in the frequency range 100 kHz to 100 mHz.

5.2.5 EIS measurements

Non-Faradaic EIS measurements were performed using a µAutolab III / FRA2 potentiostat (Metrohm) in a two-electrode setup consisting of aptamer functionalised gold disc as working electrode and Ag/AgCl as reference electrode. The measurements were

performed in binding buffer, applying a 10 mV a.c. amplitude voltage in the frequency range of 1 MHz - 100 MHz. After obtaining a stable signal in the measurement buffer, the electrodes were incubated with varying concentrations of *Pf*GDH protein in 200 µl binding buffer for 30 min, following which the EIS spectra were recorded after washing the electrodes with buffer. Further, to examine the applicability of the sensor for real sample analysis, blocked/ NG3 aptamer/gold electrodes were tested in undiluted human serum samples spiked with *Pf*GDH following the similar conditions. The specificity of the developed aptasensor was examined by challenging the aptasensor with other malaria biomarker proteins namely, *Pf*LDH, *Pf*HRP-II and analogous human GDH (*H*GDH) and HSA in serum sample.

5.3 Results and discussions

5.3.1 Sensor Surface characterization

The sensor fabrication process over the bare gold electrodes was characterized by AFM and CV studies. The results of AFM characterization were done in continuous tapping mode. The topographic average roughness analysis using Wsxm 5.0 software showed gradual decrease of roughness from the bare gold (1.52 nm) to aptamer modified gold electrode (1.41 nm) and blocked aptasensor electrode (1.33 nm). This was accompanied by an increase in the average height of the surface modified electrodes, indicating the binding of aptamer and blocking reagents over the electrode (Figure. 5.2 A-C). CV was performed to investigate the layer by layer modification on the electrode surface. The results depict the quasi reversible cyclic voltammogram of $[Fe(CN)_6]^{3-/4-}$ with a decrease in oxidation and reduction currents of the modified electrodes compared to the blank gold electrode (Figure. 5.2 D). The formation of a self-assembled monolayer of aptamer-MCH over the gold electrode led to an increase in ΔEp (difference between oxidation and reduction potentials) and lowered the redox current. This could be attributed to the charge repulsion caused by the negative phosphate backbone of the aptamer (Bang *et al.*, 2005) as well as the passivation of the electrode hindering the electron transfer. The results suggest successful assembly of the aptamer over the electrode surface. After blocking of aptamer/MCH electrode with the starting blocking buffer, a further decrease in redox current was observed due to void spaces of gold and/or MCH being occupied by non-conducting moieties of the blocking buffer.

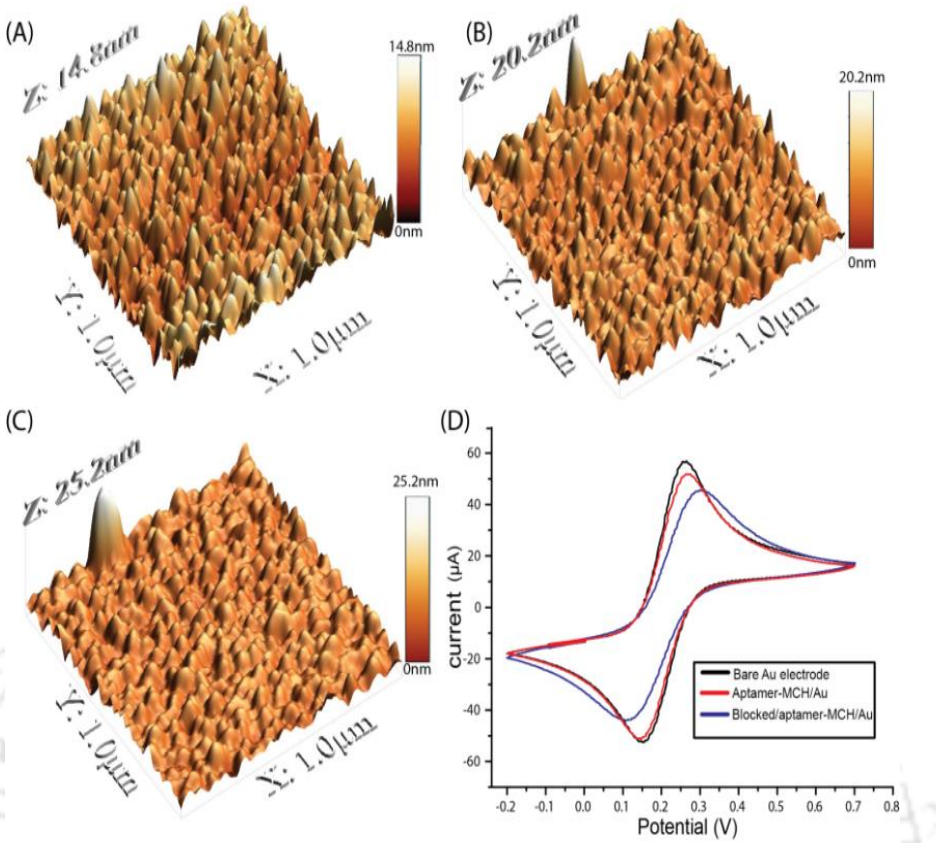

Figure 5.2: AFM images of (A) bare gold electrode (B) surface assembled monolayer with aptamer-MCH over gold electrode (C) surface blocking with MCH and blocking buffer over aptamer modified electrode. (D) CV of the electrodes recorded by using Ag/ AgCl as reference electrode. Scan rate of 50 mV/s in 10 mM potassium hexacyanoferrate solution prepared in PBS.

5.3.2 Detection of *Pf*GDH in spiked buffer sample

The NG3 aptamer (K_d 79.16 ± 1.58 over solid surface as discussed earlier in chapter 3) was used for *Pf*GDH sensing following non-Faradaic impedance measurements without using any redox marker in the solution. In this mode, high values of impedance were observed and variations in the capacitance of the system that occurred due to the binding of the aptamer with the target protein were measured. The capacitive response of the sensor was discerned by measuring $1/\omega Z''$, where ω is the angular frequency and Z'' the imaginary part of the impedance of the system. A maximum in the phase angle was observed at ~2 Hz, indicating maximum capacitive response at this frequency (Figure 5.3 A). This frequency was thus used for plotting the dose dependent response of the capacitive signal change. The reduction in capacitance with increasing concentrations of

*Pf*GDH indicates successful binding of the target molecule with the NG3 aptamer (Figure. 5.3 B, C). The change in capacitance is attributed to the alteration in dielectric properties of the biolayer through the replacement of solvated ions and water molecules by the protein, as well as due to the increase in thickness of the biolayer upon protein binding (Arya *et al.*, 2018; Liu *et al.*, 2017).

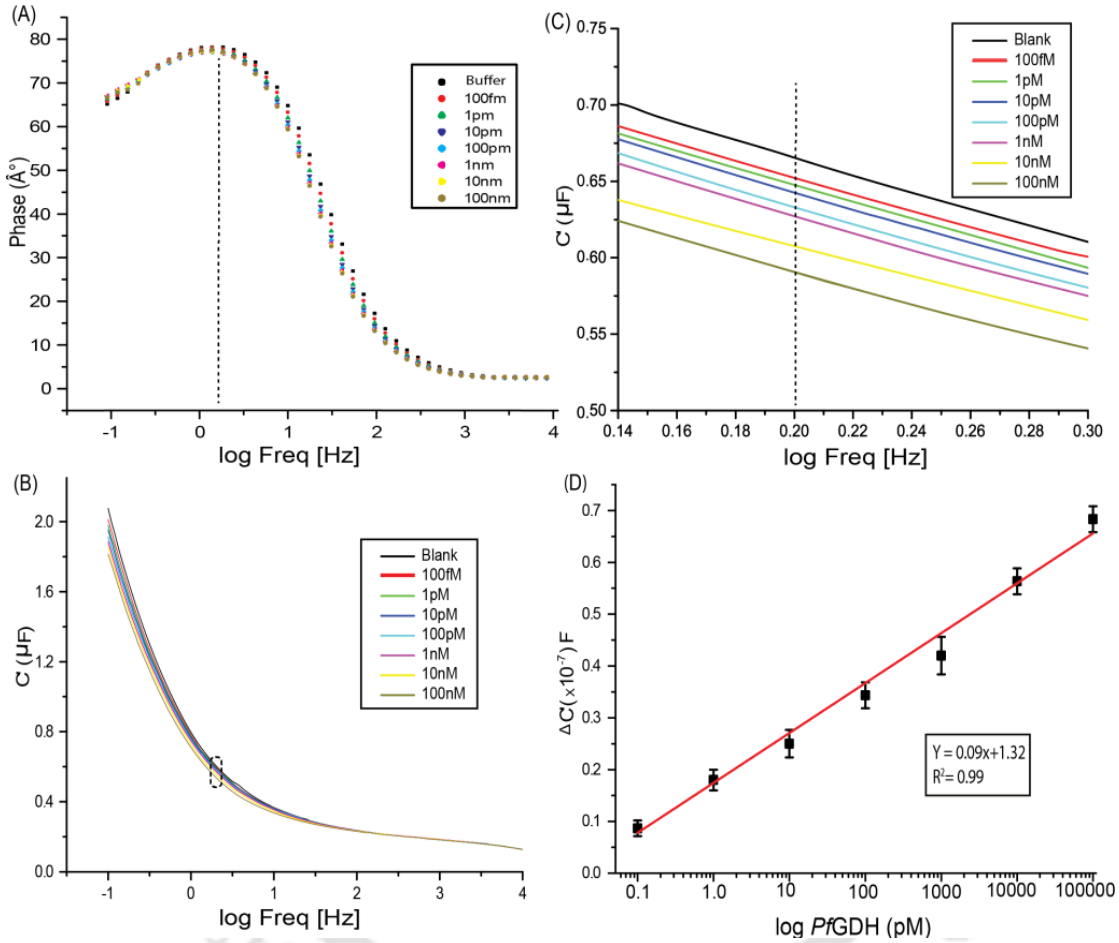

Figure 5.3: Non-Faradaic measurement in buffer (A) Phase response vs frequency, (B) Capacitance response of NG3 aptamer-*Pf*GDH with circled enlarged image in inset. (C) Enlarged image of circled region of capacitance responses. (D) Calibration curve of capacitance response at 2 Hz versus log *Pf*GDH concentrations spiked in buffer.

The limit of detection (LOD) (3x standard deviation of blank/slope of calibration curve) of *Pf*GDH was found to be 0.43 pM in the buffer, with a linear (in log scale) detection range of 100 fM - 100 nM (Figure. 5.3 D). The sensitivity of the developed capacitive aptasensor was compared with NG3 immobilized SPR sensor by analysing *Pf*GDH at concentrations of 1nM and 100 nM in buffer medium (Figure 5.4). The sensitivity of both

the aptasensor was comparable at higher concentration (100 nM) of the antigen. However, at lower concentration (1 nM) of *Pf*GDH, the sensitivity of the SPR sensor was negligible, while at this concentration the capacitive aptasensor exhibited ~ 62 % of the sensitivity at 100 nM of *Pf*GDH. The results confirmed the higher sensitivity of the capacitive aptasensor than the SPR aptasensor at lower concentration range of the antigen.

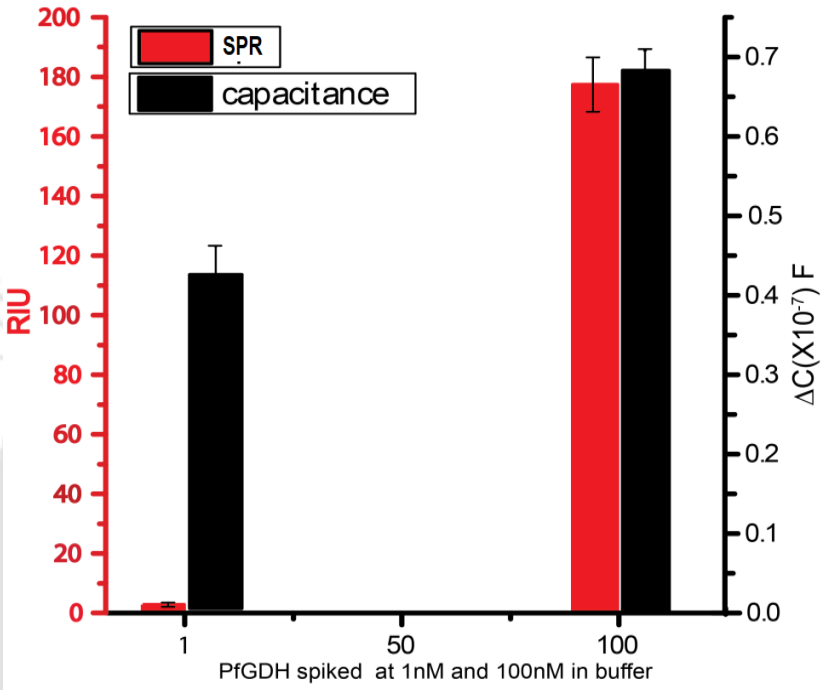

Figure 5.4: A comparison between SPR and capacitive response for spiked *Pf*GDH in buffer with NG3 aptamer/gold bio electrode.

5.3.4 Detection of *Pf*GDH in spiked undiluted human serum

The capacitive aptasensor was then tested directly in undiluted blood serum with spiked *Pf*GDH. The *Pf*GDH protein with different concentrations that fall within the dynamic range obtained in the buffer medium (100 fM - 100 nM) was used in the undiluted serum (Figure 5.5). This range covers the previously reported *Pf*GDH concentrations used (2 to 16 nM) for malaria diagnosis through an immuno-chromatographic dipstick based method (Djadiad *et al.*, 2014; Li *et al.*, 2005). Like in buffer, a maximum phase angle was observed at ~2 Hz during the measurement of *Pf*GDH protein in serum samples (Figure 5.5 A). The capacitance at 2 Hz was therefore considered further for generating the calibration curve (Figure 5.5 B). The detection of *Pf*GDH in serum also followed a linear

dependency of its concentration in the range with the capacitance signal and an LOD of 0.77 pM for *Pf*GDH was discerned (Figure 5.5 C).

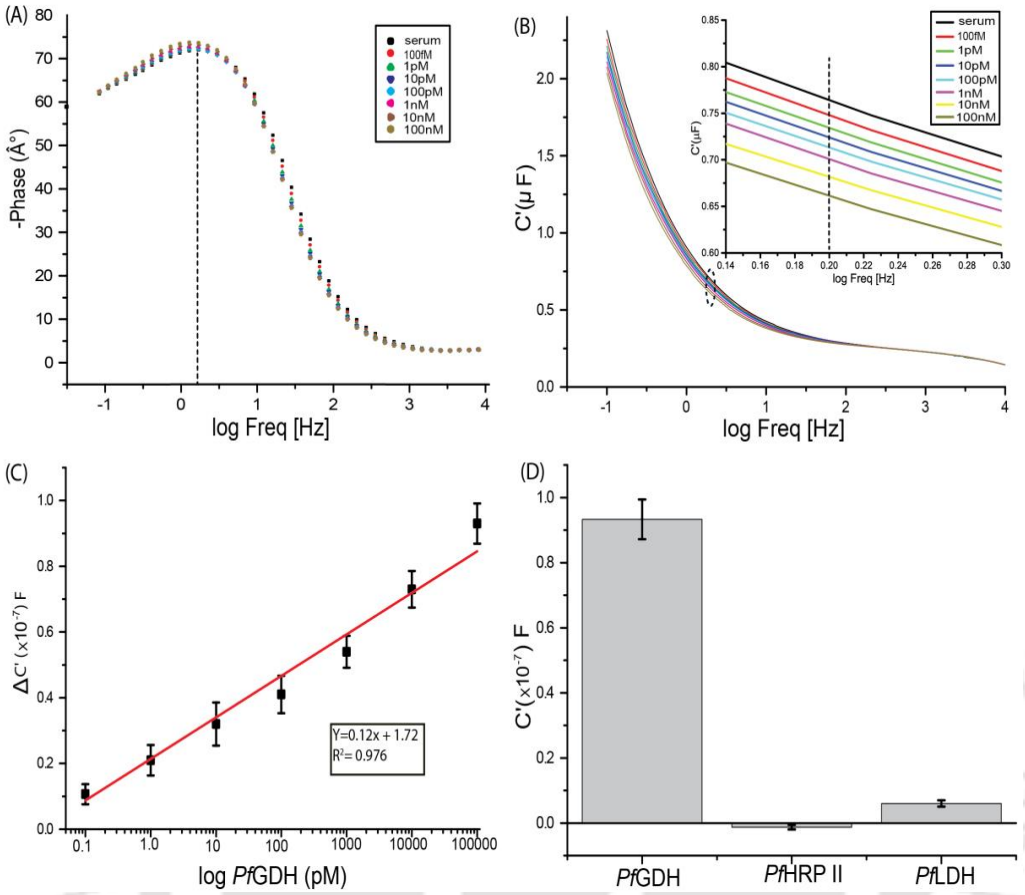

Figure 5.5: (A) Non-Faradaic measurements in undiluted serum Phase response vs frequency. (B) Capacitance response of NG3 aptamer-*Pf*GDH with circled enlarged image in inset. (C) Calibration curve of capacitance response at 2 Hz verses log *Pf*GDH concentrations spiked in undiluted serum. (D) Response of NG3 aptamer with analogue proteins each with 100 nM spiked in serum.

The sensitivity of the aptasensor as derived from the slopes of the calibration curves in serum and buffer samples were 0.12 (10^{-7}F)/ log ([*Pf*GDH] pM) and 0.09 (10^{-7}F)/ log ([*Pf*GDH] pM), respectively. The results indicate a comparable signal sensitivity of the aptasensor between samples in buffer and serum media, which validate a conducive microenvironment for the interaction of the aptamer with the target antigen protein in the serum medium (Park *et al.*, 2012). The binding between *Pf*GDH and NG3 aptamer over the electrode surface is likely to be facilitated by the interaction between some positively charged *Pf*GDH amino acid residues and the negatively charged ssDNA aptamer. The net

surface charge of aptamer-protein complex governed the dielectric property over the sensing surface of electrode which was not affected by the ionic microenvironment in serum in the present case (Cole and Cole, 1941; Pethig and Kell, 1987). There are limited reports on the malaria diagnostic device targeting the *Pf*GDH antigen (Seol *et al.*, 2017). An antibody based immuno chromatographic technique exploiting gold nanoparticles as optical probe could offer a detection range of 0.62 – 5 µg. ml^{-1} for *Pf*GDH (Li *et al.*, 2005). Hence, the present aptasensor exhibited superior performance both in terms of LOD and dynamic range than the previous reports.

5.3.5 Interference studies for developed capacitive aptasensor

The interferences from the other prominent malaria biomarker proteins (*Pf*LDH and HRP-II) that are likely to be secreted during the diseased condition were examined by spiking these proteins in undiluted serum (Figure. 5.5 D). The responses were 6.5 % (*Pf*LDH) and 0.5 % (*Pf*HRP-II) of the control protein (*Pf*GDH) for the corresponding proteins shown in the parentheses. The result indicates only a minor non-specific interaction of the sensor with the *Pf*LDH protein. The sensitive response profile obtained directly on the serum sample indicates that the serum components including *H*GDH and the predominant serum protein, HSA do not significantly interfered the aptasensor function.

5.4 Conclusion

A capacitive aptasensor for selective detection of the malaria biomarker, *Pf*GDH in undiluted human serum samples has been developed following the scheme shown in the figure 5.1. The aptasensor generated a non-Faradaic EIS signal following its binding with the target antigen (*Pf*GDH). The capacitive signal change was linearly correlated with a wide concentration range of the antigen (100 fM - 100 nM). The aptasensor offered an LOD for the antigen in picomolar level. This is the first report on *Pf*GDH aptasensor exploiting non-Faradaic impedance as sensing signal. The chemical technique adapted here for the immobilization of the aptamer over the electrode surface facilitated easy and reproducible fabrication of the aptasensor. This label-free aptasensor with ultra - low LOD has great application potential for diagnosis of asymptomatic malaria and for monitoring the regression of malaria during treatment regime with antimalarial drugs. We envisioned that with the advent of advance state-of-art electrochemical technology, the

instrument for measuring the capacitance could be scaling down to an appropriate size for converting the developed aptasensor to a hand-held device suitable for application in POC settings and resource limited environments.

Chapter 6

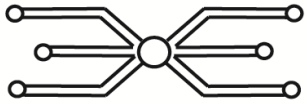

Development of Aptamer based Field Effect Transistor (aptaFET) Biosensor for Detection of PfGDH in Serum Sample

Chapter 6

Development of aptamer based field effect transistor (aptaFET) biosensor for detection of *Pf*GDH in serum sample

6.1 Overview

Malaria is a curable disease if diagnosed and treated promptly and correctly. There are many reliable laboratory based methods available for malaria diagnosis. However, these methods are time-consuming, expensive and require skilled operators and hence, are not applicable for point of care diagnosis of malaria (Tangpukdee *et al.*, 2009). Over the last decade there has been a continuous strive to replace antibodies and other labile biorecognition elements with stable recognition systems for developing various diagnostic and detection devices (Thiviyanathan and Gorenstein., 2012). Among them, nucleic acid based aptamers are emerging as an efficient and viable alternative (Kakoti and Goswami, 2017). The binding affinity of ssDNA aptamers is usually comparable to antibodies. Moreover, there is a scope for enhancing the selectivity of the DNA aptamers by chemical means (Song *et al.,* 2012). There are few reports on developing aptamer-based malaria detection methods (Cheung *et al.,* 2013; Jain *et al.,* 2016). These proof-of-concepts are mostly based on optical principles, while a few of them exploited electrochemical principles such as amperometry, voltammetry and impedance spectroscopy (Lee *et al.,* 2012; Miranda *et al.,* 2018; Chakma *et al.,* 2018). However, each of these methods have their own merits and demerits as discussed in these reports. The focus of the current work is to explore a detection platform, amenable for integration into a portable device that complies well with the ASSURED (Affordable, Sensitive, Specific, User-friendly, Rapid and robust, Equipment free and Deliverable to end-users) mandate of WHO for application in developing and underdeveloped countries (Kunte and Kunwar, 2011). The use of field effect transistor (FET) as a sensing platform has gained enormous attention in diagnosis of various diseases (Estrela and Migliorato, 2007; Estrela *et al.,* 2010; Formisano *et al.,* 2016; Aliakbarinodehi *et al.,* 2017). The major motivations for using FETs as biosensing platform are their high sensitivity, rapid response time, small size, and cheap fabrication process using integrated circuit technology. The FET system provides a sensitive and simple non-Faradic electrochemical measurement to monitor reactions occurring at the gate electrode surface, without using any redox marker (Park *et al.,* 2012). In its simplest form, the FET measures variations in the open circuit

potential that occur at the electrode interface. The extended gate FET (EgFET) was introduced to further increase the sensitivity and to overcome any instability issues that may occur during contact of FETs with biological liquids (Kaisti, 2017). In the EgFET structure, the gate of the transistor is extended away from the semiconductor and immersed in a solution for the measurement process, which gives an advantage to modify the surface of the extended gate chip as per the need of various sensing applications.

The *Pf*GDH is cytosolic protein and its NADP-specific activity present in the human serum with good detectable amounts during the infection (Acosta *et al.*, 1998; Seol *et al.*, 2017). The *Pf*GDH catalytic product of the reaction could be set in protonated form (α-ketoglutarate) using glutamate as the substrate which may furnish additional signal on the potentiometric platform once it is captured by the biorecognition element on the gate surface. Herein, we proposed an EgFET based detection of *P. falciparum* malaria using a selective aptamer as the biorecognition element against the biomarker, *Pf*GDH. The aptamer was immobilized via gold-thiol chemistry on inter digitated gold microelectrode (IDμE) connected to the gate of transistor (Figure 6.1). A detailed account on the interesting findings is incorporated in this chapter.

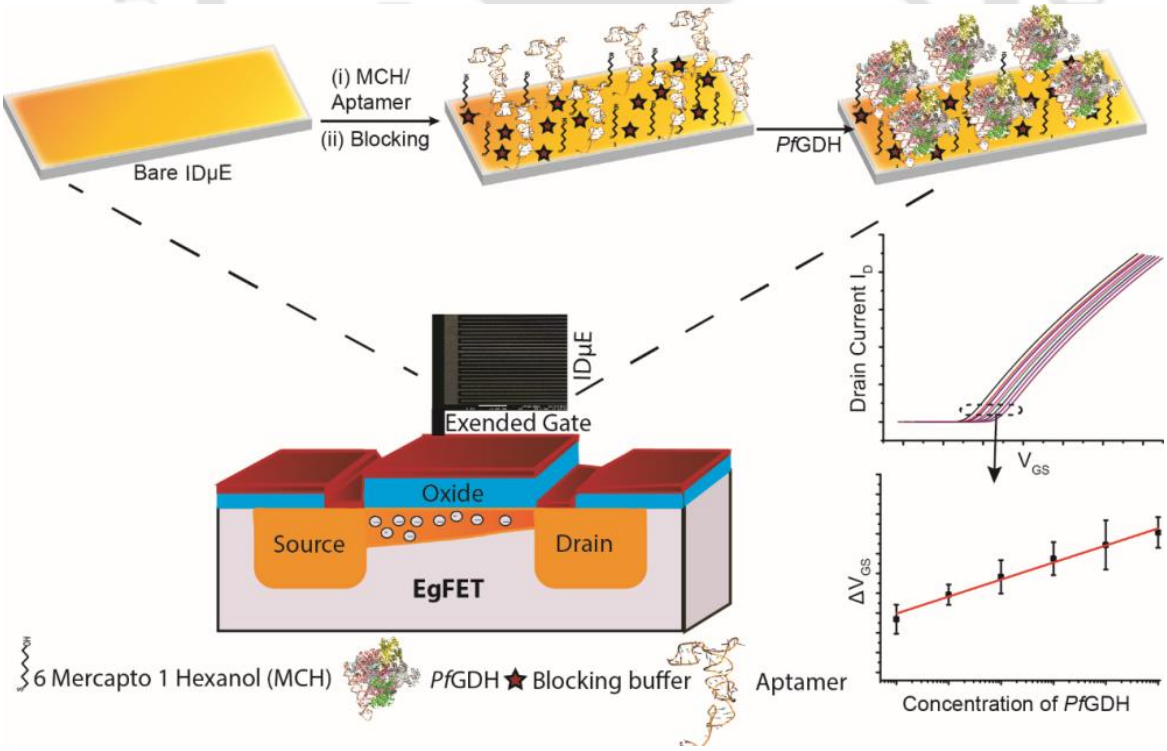

Figure 6.1: Fabrication scheme of aptaFET for detection of *Pf*GDH in blood serum.

6.2 Experimental procedure

6.2.1 Materials

The selected thiolated NG3 aptamer (SH-$(CH_2)_6$-5'-TTT TCA CCT CAT ACG ACT CAC TAT AGC GGA TCC GAG CCG GGG TGT TCT GTT GGC GGG GGC GGT GGG CGG GCT GGC TCG AAC AAG CTT GC-3' was synthesized by Sigma-Aldrich (UK). The starting blocking buffer containing a proprietary protein formulation in phosphate-buffered saline at pH 7.5 was obtained from Thermo Fisher (USA). The human serum from clotted whole blood type AB was received from Sigma Aldrich. The proteins, *Pf*LDH and *Pf*HRP-II were cloned, expressed and characterised as described in the chapter 3. The interdigitated gold microelectrode (IDμE) was procured from ASTAR, (Singapore). All other chemicals and reagents were of analytical grade and used as received. The compositions of all the buffers used in the current work are presented in Appendix A3.

6.2.2 Electrode preparation

An IDμE with dimension of 5 μm × 3200 μm for each fingers and 10 μm inter-spaces between the fingers was connected to a FET silicon oxide surface over an area of 0.8 cm × 1.6 cm following a reported design (Figure 6.2) (Pui *et al.*, 2013).

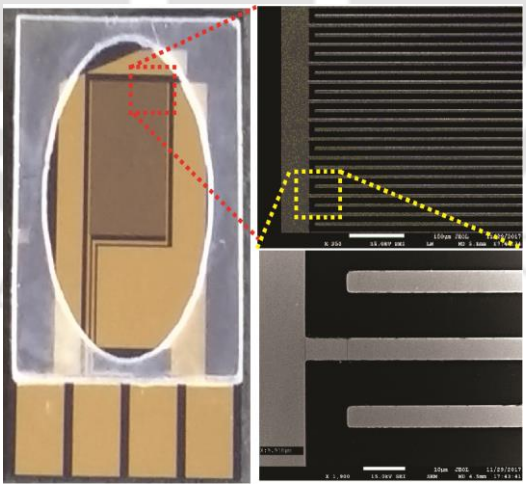

Figure 6.2: IDμE electrode image with normal camera, further enlargement of surface capture with SEM (LEO 1430 VP, ZEISS, Germany) to show interdigitated region present over electrode surface.

The microelectrodes were UV-ozone cleaned for 30 minutes and then washed with streams of acetone, isopropanol and ethanol for 30 seconds each sequentially and

followed by washing with ample amounts of mili-Q water (18.2 MΩ cm). The sample holding region with a holding capacity of 50 µl over the microelectrode was prepared by sealing the edges with molding tape. The fabrication of the biolayer over the cleaned gold electrode was performed by following a reported method (Jolly *et al.*, 2016). Briefly, 100 mM solution of 6 mercapto 1 hexanol (MCH) was prepared in absolute ethanol, which was further diluted to 1 mM in the binding buffer. The cleaned microelectrode surface was then incubated with 50 µl solution of thiolated aptamer: MCH in 1:100 ratio for 12 h in a humidity chamber. Prior to the immobilization over the electrode, the aptamer was treated at 90 °C for 5 minutes followed by cooling at 4 °C for 10 minutes to ensure that the aptamer is free from any hybridization. Following the immobilization procedure, the fabricated aptamer-IDµE was first cleaned with mili-Q water to remove unbound aptamer from the electrode surface and then it was further treated with 1 mM MCH for 1 h to ensure backfilling of any free spaces in the microelectrode. The electrode was further washed with mili-Q water and stem jet dry with nitrogen gas. Before analysis of samples, the aptamer/MCH gold microelectrode was treated with starting blocking buffer for 30 minutes to minimize the probability of non-specific interactions over the electrode surface.

6.2.3 EgFET Fabrication

The aptamers immobilized IDµE was connected to a home-designed n-type complementary metal oxide semiconductor (CMOS) field-effect transistor (MOSFET).

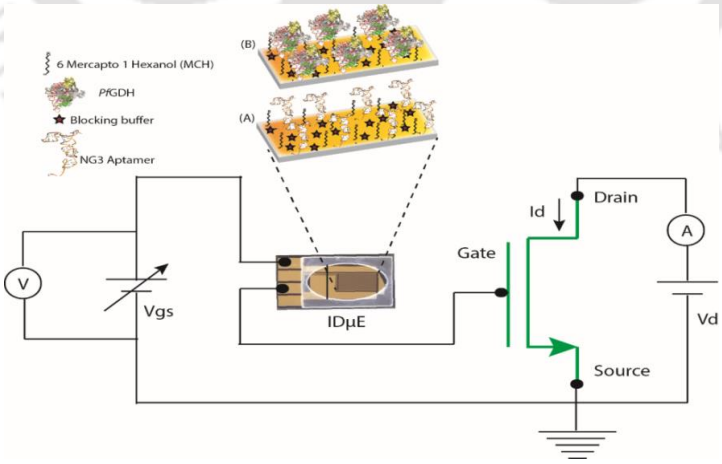

Figure 6.3: Working circuit of aptaFET biosensor. An interdigitated gold electrode (IDµE) with pseudo reference electrode connected to the gate of n type MOSFET. The aptamer target binding reaction carried out on surface of IDµE and FET system transduced this binding event into electrical signal.

The design, specification, and fabrication process of the MOSFET have been previously reported (Formisano *et al.*, 2016) (EgFET circuit diagram in Figure 6.3). In brief, single crystalline n-type MOSFETs were fabricated by using 0.7 µm CMOS technology with electrostatic discharge (ESD) protection circuits on the contact pads.

6.2.4 Atomic force microscopy (AFM) study

The topological characterization of the fabricated aptamer-IDµE was performed by AFM in continuous tapping mode using Multimode Nanoscope with IIIa controller (Bruker, Germany) in combination with control software (version 6). The AFM images were captured using 10 nm diameter AFM ContAl-G tips (Budget Sensors®, Bulgaria), and then analyzed with WsxM version 5 software.

6.2.5 Electrochemical impedance spectroscopy (EIS) study

The layer by layer fabrication of the aptasensor was characterized by means of Faradic EIS measurements in a three-electrode configuration with on-chip 2 mm gold as pseudo reference and counter electrodes. The measurements were performed in 10 mM PBS pH 8 with 10 mM ($K_3Fe(CN)_6/K_4Fe(CN)_6$) as redox probe using a µAutolab III / FRA2 potentiostat/galvanostat (Metrohm, The Netherlands) at equilibrium potential with 25 mV amplitude in the frequency range 100 kHz to 100 mHz. The Z- view software (Scribner associates) was used for curve fitting.

6.2.6 Debye length calculations

The Debye length for FET measurement buffer was calculated by the following equations:

$$\kappa^{-1} = (\varepsilon_r \varepsilon_o k_B T / 2N_A e^2 I)^{1/2} \ldots\ldots\ldots \text{(i)}$$

$$I = 1/2 \sum_{ion}^{n} C_{ion} Z_{ion}^2 \ldots\ldots\ldots \text{(ii)}$$

The Debye length κ^{-1} was calculated using equation (i) where ε_r is the relative permittivity, ε_o dielectric constant, k_B Boltzmann constant, T temperature, e elementary charge, N_A Avogadro number and I is the ionic strength of solution. The ionic strength was calculated to be ~ 43.3 mM for 10 mM PBS, pH 8.0 and by considering the concentrations of mono and di basic components using equation, (ii) with the additives of measurement buffer (5 mM NaCl, 5 mM KCl, 2.5 mM $MgCl_2$). In the above calculation, we have assumed that all the species are in their ionized form in water The relative

permittivity of FET measurement has been taken as 80, assuming it is equivalent to relative permittivity of PBS. Measurement temperature of 328 K was used for the calculation. The calculated Debye length was found to be approximately ~1.5 nm for FET measurement buffer.

6.2.7 EgFET measurements

The aptaFET measurement was performed by using a semiconductor device analyzer B1500A HR CMU (Agilent, USA). The EgFET was connected to an external IDμE and the measurement was performed over IDμE integrated with pseudo reference and working electrode. The FET transfer characteristics (drain current, I_D, vs. gate-to-source voltage, V_{GS}) were measured at a drain-to-source voltage (V_{DS}) of 50 mV varying the V_{GS} from 0 to 3 V. These settings protect the device from heating and reduce the risk of false measurements by the FET system. The aptamer-IDμE was incubated in FET measurement buffer until a stable signal was obtained. The electrode was then incubated in the binding buffer or diluted human serum (10 fold) spiked with different concentrations of *Pf*GDH protein for 30 minutes and washed with measurement buffer prior to the measurement. To ensure the interaction between aptamer and protein within the Debye length limitation, low ionic strength PBS solution or 10 fold diluted serum with PBS was used as measurement buffer (Chan *et al.*, 1980; Stern *et al.*, 2007).

All data presented here are the mean of at least three independent experiments performed with independent devices that are fabricated and investigated under similar conditions while the error bars represent the standard deviations. The statistical analysis was performed with Origin 8.0 software.

6.3 Results and discussion

6.3.1 Characterization of aptamer IDμE

AFM studies of the fabricated electrodes revealed that the average height of the IDμE surface increased from ~1.35 ± 0.18 nm to ~1.48 ± 0.27 nm and ~1.71 ± 0.38 nm following immobilization of the aptamer/MCH layer and subsequent binding of the target protein, respectively. The surface root mean square roughness (R_{rms}) of the bare electrode increased from ~0.41 nm to ~0.53 nm following formation of the self-assembled monolayer (SAM) of aptamer/MCH which was however, reduced to ~0.47 nm after binding with the target protein. The surface topographical analysis of AFM images with peak distribution is shown in figure. 6.4 A-C.

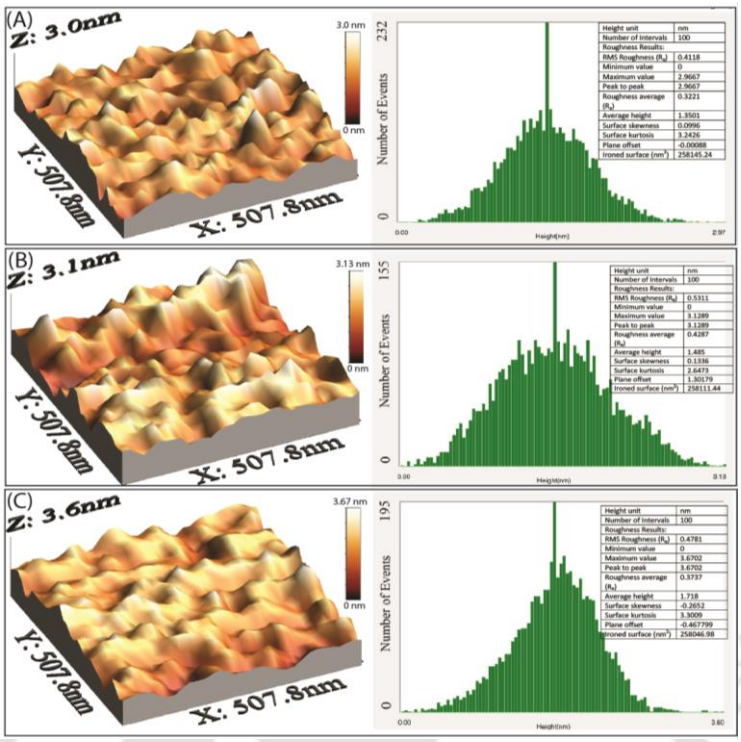

Figure 6.4: AFM topographical analysis (inset table) and peak distribution of bare IDμE (A), aptamer-IDμE surfaces (B) and target/aptamer- IDμE surfaces (C) (scanned area~0.5 x 0.5 μm^2)

The surface modification was further characterized by EIS and obtained Nyquist plots were fitted with Randles- Ershler equivalent circuit model (inset of Figure 6.5 A) where R_s represents the solution resistance at higher frequency, C_{dl} the double layer capacitance formed at electrode-electrolyte interface, W is the Warburg impedance indicative as tail at lower frequency accounting for diffusion of charge from solution to electrode and R_{ct} the charge transfer resistance represented by the diameter of semicircle. Typical fitted values of these parameters for electrode modification are mention in Table 6.1.

Table 6.1. Typical Randles–Ershler equivalent circuit values.

S.No	Electrodes/SAM	R_s (Ω)	R_{ct} (Ω)	C_{dl} (μF)	W ($\Omega s^{-1/2}$)
1.	IDμE	144.27	118.5	17.1	885.66
2.	IDμE/Aptamer/MCH	151.14	620.23	2.56	848.74
3.	IDμE/Aptamer/MCH/Blocking	155.76	1778.1	1.34	825.34

The R_{ct} value increased from ~ 118 ± 13 Ω for bare electrode to ~ 620 ± 47 Ω after co-immobilization of aptamer/ MCH and to ~ 1778 ± 68 Ω following subsequent treatment

with MCH and starting blocking buffer. The reason for the increase in R_{ct} value following aptamer immobilization is attributed to the charge repulsion from the electrode surface caused by the negatively charged phosphate backbone of the DNA aptamer; further increase in R_{ct} value following the blocking step is ascribed to the accommodation of non-conducting protein in free areas of the gold electrode surface. The stepwise increase in impedance value confirmed the successful immobilization of the aptamer over the SAM layer on the IDμE surface.

6.3.2 Stability of aptaFET Sensor

Before starting the aptaFET detection of *Pf*GDH, the stability of the aptamer-IDμE was checked in FET measurement buffer by applying V_{GS} potentials from 0 to 3 V. A slight drift was observed, which was stabilized after 30 min of incubation (Figure 6.5 B). This change in response can be attributed to buried oxide site in surface assembled monolayer and which was reached to equilibrium by protonation/deprotonating of this oxide layer through the applied potential over time.

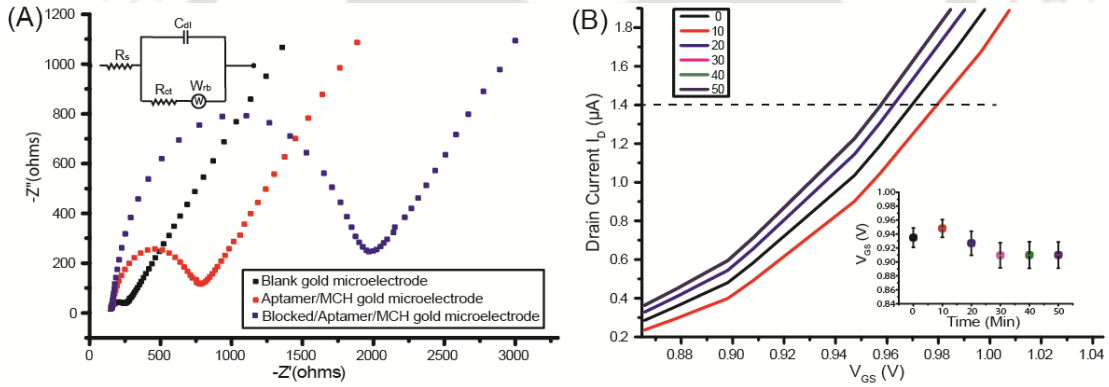

Figure 6.5: EIS characterization of blank and modified IDμEs (A). AptaFET stability studies in binding buffer from the plot of drain current (I_D) versus gate voltage (V_{GS}) at different incubation time (B). Inset plot depicts gate voltage at fixed drain current verses different incubation time.

6.3.3 Detection of *Pf*GDH using aptaFET

The aptaFET measurement was performed at low ionic strength buffer to screen the probe-target interactions from the solution ions for gaining better sensitivity of the measurement as the presence of high counter ions in solution may shield the surface charge of the target protein. The negatively charged phosphate backbone of aptamer and the complementary positively charged amino acid moieties in protein induced complex

formation between the target protein and the aptamer (Pethig and Kell, 1987). The net balanced charge produced on the electrode surface conferred by the target protein due to formation of the complex influenced the electric field in the FET. The developed surface charge could be detected within the electrical double layer (Goda and Miyahara., 2013), because the aptamer (NG3)–target (*Pf*GDH) interaction in the present case took place adjacent to the electrode surface due to smaller dimension of the aptamer. The relationship among the change in charge density (ΔQ), change in gate voltage (ΔV_{GS}), the number of bound proteins (N) bearing an effective electric charge per molecule (q), and the electric double layer capacitance (C_{dl}) effective within the Debye length may be projected as $\Delta V_{GS} = \Delta Q/C_{dl} = Nq/C_{dl}$ (Goda and Miyahara, 2012). Notably, the small size of the folded aptamer helps to overcome the Debye length limitation, which is normally exists with antibodies, thus provides freedom of using these DNA based recognition elements in FET measurements (Chu *et al.,* 2017). The average distance of the aptamer from the electrode surface (average height of SAM layer - Average height of blank electrode) was calculated to be ~0.14 nm (Figure 6.4). This proximal distance facilitated the biointeraction closer to electrode surface. A characteristic Debye length of ~ 1.5 nm was calculated from the equation (i) for FET measurement. The aptamers known to undergo conformational change on their binding with the target molecules, and increase the charge density closer to electrode surface (Kakoti and Goswami, 2017; Aliakbarinodehi *et al.,* 2017; Formisano *et al.,* 2015). Thus, the interaction of the surface grafted aptamer with the target protein falls within the calculated Debye length limit. The *Pf*GDH is ~ 300 kDa size globular protein however; the spherical structure of the globular proteins is normally not sustained following their adsorption over the electrode surface because of the rearrangements through a multistep process (Goda and Miyahara, 2012). This modification promotes the orientation of their anionic domain toward the contact phase on the positively charged surface. Therefore, the charge induced at the adsorbed protein surface falls within the Debye length facilitating the FET measurement as discuss below.

In the FET measurement, when the applied gate voltage (with respect to the source contact) is higher than the threshold voltage of the transistor, a conducting bridge is formed between drain and source. Under this condition when the voltage between drain and source become higher than zero (V_{DS} >0), the flow of current through the channel under the influence of the electric field across the gate dielectric is initiated. In the

operation of the EgFET, the change in magnitude of charge at the gate surface leads to a change in the threshold voltage, as seen by a shift on the drain current versus gate voltage (I_D *vs.* V_{GS}) (Chi *et al.*, 2000). For the aptaFET measurement, the aptamer - IDµE was incubated with target *Pf*GDH protein spiked in diluted serum or binding buffer for 30 min. The response characteristics of the aptaFET are shown in figure 6.6, displaying incremental positive shifts of V_{GS} with the binding of *Pf*GDH protein in increasing concentrations, both in binding buffer (Figure 6.6 A) and in diluted serum (10 fold) (Figure 6.6 C) pH 8.0.

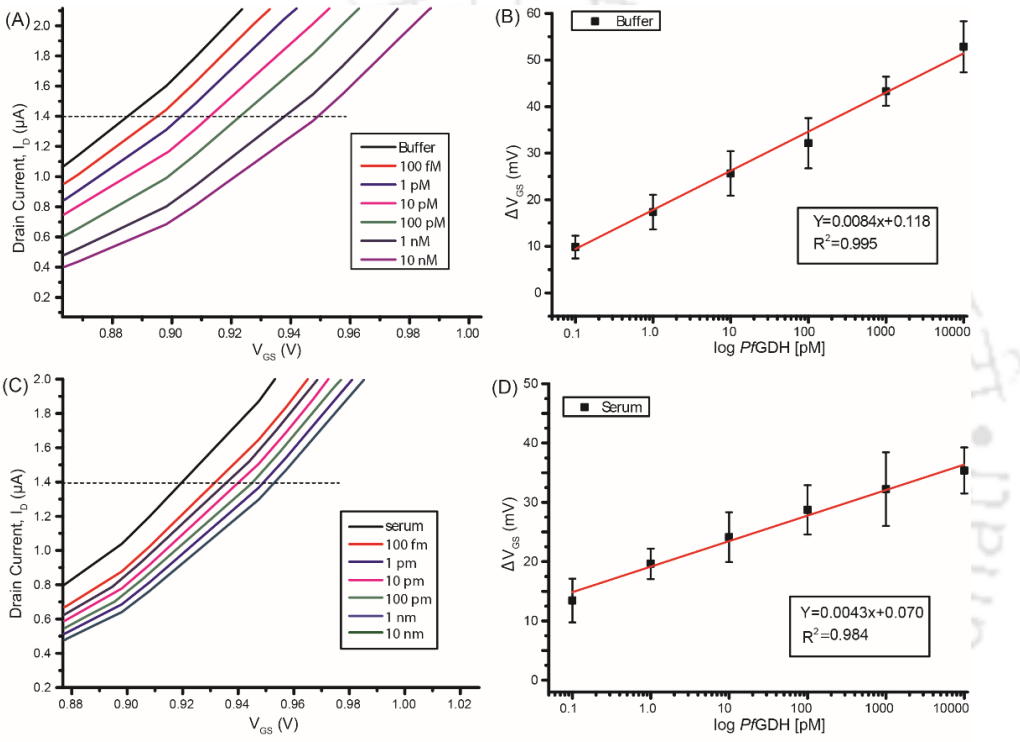

Figure 6.6: AptaFET response against different concentrations of *Pf*GDH protein spiked in buffer (A) and serum (C) with corresponding calibration plots (B) and (D).

This positive shift of gate voltage may be attributed to the increase in negative charge on the gate surface caused by the interaction of the negatively charged *Pf*GDH protein (p*I* of 6.6) with the folded aptamer within the Debye length as discussed above (for p*I* figure 2.11). The calibration curves were generated by plotting varying concentrations of *Pf*GDH spiked in buffer and serum solutions against V_{GS} shift at a constant 1.4 µA drain current (Figure. 6.6 B, D). A linear detection range of 100 fM – 10 nM for *Pf*GDH in both buffer and diluted serum was discerned. The aptaFET therefore offered *Pf*GDH detection towards much lower concentration range than the existing immune chromatographic dipstick method, which known to offers a detection range of 2 nM to 16 nM for malaria

diagnosis (Li *et al.*, 2005). The limits of *Pf*GDH detection (LOD = 3 × SD of blank/ slope of calibration curve) discerned from the corresponding calibration plots were 16.7 pM and 48.6 pM in buffer and diluted serum, respectively. The sensitivities of the aptaFET sensor were calculated from the calibration plots (Figure. 6.6B, D) and found to be 8.40 X 10^{-6} V/log ([*Pf*GDH] pM) (R^2 = 0.99) in buffer solution and 4.30 X 10^{-6} V/ log ([*Pf*GDH] pM) (R^2 = 0.98) in diluted serum. A minor reduction in sensitivity and increase in LOD value in serum medium have been attributed to the complex nature of the chemical environment in serum samples causing hindrance to aptamer-*Pf*GDH interaction. Moreover, the presence of extra solvated ions in serum is affecting the Debye screening length and hence, lowering the effective charge of the biomolecules. The minor reduction of these performances however, may not have much effect on the diagnosis of malaria considering the serum concentration level of this biomarker under the diseased conditions (Li *et al.*, 2005).

6.3.4 Selectivity of the developed aptaFET biosensor

The selectivity of the developed aptaFET biosensor analyzed in 10 nM each of the analogous human proteins (HGDH, HSA) and malaria proteins (*Pf*LDH, *Pf*HRP-II) spiked in buffer, showed much weaker signal (ΔV_{GS}) as compared to the target (*Pf*GDH) protein (Figure. 6.7 A, B).

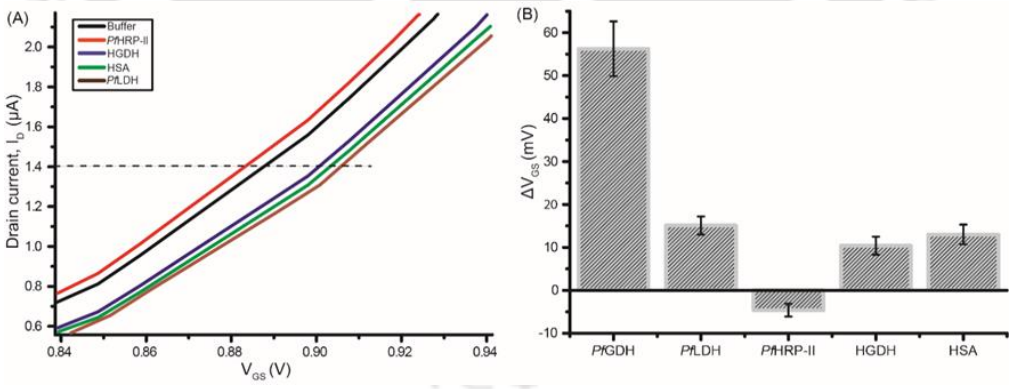

Figure 6.7: (A) AptaFET response against different potential interfering proteins. The analysis was performed in FET measurement buffer with 30 minutes of incubation time; shift in gate voltage (V_{GS}) was monitored at 1.4 μA drain current (I_D). (B) Selectivity of the aptaFET biosensor for analogous proteins. Mean data with standard deviations from triplicate experiments are presented.

The results validated high selectivity of the developed aptaFET biosensor suitable for analysis of real sample for malaria diagnosis. Overall, the results validated the application

potential of the developed aptaFET for diagnosis of both symptomatic and asymptomatic malaria.

6.4 Conclusion

Herein, a novel aptaFET biosensor for selective detection of *P. falciparum* specific biomarker *Pf*GDH in serum sample has been reported. The device utilized an interdigitated gold micro electrode connected with extended gate of transistor offering easy immobilization of the DNA-aptamer over it and sensitive detection of the target biomarker in solution without impairing the FET functions. The aptaFET biosensor offered response time in seconds (~5 s), detection limit down to pico molar level (48.6 pM), and detection range in lower concentration region (0.1 pM to 10,000 pM) in diluted serum samples. This detection capability of the aptaFET biosensor would be suitable for its application in diagnosis of symptomatic as well as asymptomatic malaria including the analysis of parasitemia level during regression of parasitic load under medication. Notably, the minimum *Pf*GDH concentration in serum of malaria patients including in asymptomatic malaria, usually lies in nanomolar range (Li *et al.*, 2005). We compared the response of the aptaFET with other reported portable biosensors (Table 6.2), and found that the presented biosensor exhibited superior detection range under lower concentration region, lower response time and comparable LOD values for *Pf*GDH. This FET-based potentiometric sensor offered reliable results with the sufficiently diluted serum samples that minimized the screening effect of the sample ions on the gate potential. We validated the function of the device well ≤ 10 mM of the sample salts, which may be attained by diluting the serum by ~ 10 folds. This miniaturized aptaFET with extended IDμE delivered label free detection capability through direct readout of the intrinsic net charge of the capture target molecule (*Pf*GDH) making the measurement easy and swift. Further integration of the developed device with a portable electrochemical system for data measurement will make this aptaFET suitable for implementing in POC settings.

Table 6. 2: Comparison between the present work and state-of-art sensors suitable for POC.

Technique	Surface and Probe	Detection range	Target Antigen	Response time	LOD	References
Colorimetric	Paper µPAD Murexide dye-Ni Ions)	10-100 nM	*Pf*HRP-II	~5 min	30 nM	Chakma *et al.*, (2016)
Electrochem-ical phone based Immuno-sensor	Poly dimethyl siloxne µPAD Antibody	10.8- 27.5 nM	*Pf*HRP-II	~15 min	432.43 pM	Lillehoj *et al.*, (2013)
Colorimetric	Magnetic beads Antibody	25 nM-2 µM	*Pf*LDH	~45 min	25.7 pM	Markwalter *et al.*, (2016)
Colorimetric	Paper Aptamer	3.5 nM-35 µM	*Pf*LDH	~45 min	36 pM	Dirkzwager *et al.*, (2016)
Opto-Magnetic	-	100 nM-5.0 µM	Hemozoin	~1 min	~2 nM	Newman *et al.*, (2008)
Immune chromato-graphic	Gold nanoparticle Antibody	2-16 nM	*Pf*GDH	10-20 min	N/A	Li *et al.*, (2005)
RDT*	Paper µPAD Antibody	0.7- 91 pM	*Pf*HRP-II	20 Min	23 pM	Jimenez *et al.*, (2017)
		3.9 pM-39 nM	*Pv*LDH	20 Min	195 pM	Jimenez *et al.*, (2017)
EgFET	IDµE Aptamer	100 fM-10 nM	*Pf*GDH	~5 sec	48.6 pM	Present work

* Based on analytical performance of best malaria rapid diagnostic tests (RDTs) in market.

Chapter 7

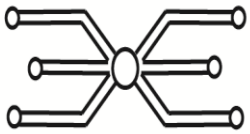

Development of laboratory and portable format based detection system for pan malaria and P. falciparum species

Chapter 7

Development of laboratory and portable format based detection systems for pan malaria and *P. falciparum* species

7.1 Overview

There are many malaria diagnosis methods and techniques available in the global market (Jain *et al*., 2014). However, portable and simple diagnostic kits and devices for specific detection of *P. falciparum* malaria for deployment in point of care (POC) and resource limited settings are limited. Currently, the rapid diagnostic tests (RDTs) for detection of *P. falciparum* as well as pan specific malaria are widely used which involved immune-chromatographic test strip with antibodies as biorecognition molecules. For specific detection of *P. falciparum* species, *P. falciparum (Pf)* Histidine Rich Protein II (*Pf*HRP-II) has been used as target antigen. However, several reports claimed variable results on the use of RDT against *Pf*HRP-II (Mason *et al.*, 2002). WHO has recommended exploring other alternative methods and biomarker for detection of *P. falciparum* (World Health Organization, 2017). In this regards, *Pf*GDH (EC no. 1.4.1.4) has received increasing attention over the last few years as a specific biomarker for *P. falciparum* (Vander Jagt et al., 1982; de Dominguez and Rodriguez-Acosta, 1996). The characteristics and similarity of *Pf*GDH with other malaria biomarker have already been described under the chapter 1. This homohexameric *Pf*GDH protein (M_w = 49.5 kDa, Uniprot gene- GluDH) shares only 23 % overall amino acid sequence identity with the human counterpart (HGDH, Uniprot gene - GLUD1), 69 % identity with *Pv*GDH (Uniprot gene-PVX_085005), and 85 % identity with *Pk*GDH (Uniprot gene-PKH_133070). Moreover, the *H*GDH is not present in the human erythrocyte where *Pf*GDH is primarily released. This particular protein is present in significant quantity in the blood stream of the malaria patient.

The *P*GDH based RDT functioning with immune-chromatographic principle is also limited (Seol *et al.,* 2017). For diagnosis of pan malaria infections *Plasmodium* lactate dehydrogenase (*P*LDH) and aldolase as the target antigens in the patients serum have been commonly used in the RDTs (Jain *et al.,* 2014, Tanijaki *et al.,* 2014). The *P*LDH protein exhibited ~ 90 % sequence identity with different *Plasmodium* species and less than 30 % sequence identity with the human lactate dehydrogenase (HLDH) (Dunn *et al.,* 1996, Brown *et al.,* 2004). Hence, *P*LDH has been considered suitable pan specific

malarial biomarker (Shin *et al.,* 2013; Kim and Searson, 2017). This immune-chromotographic principle based RDTs have though contributed a lot towards global malaria management, certain limitations of these antibody based detection devices such as, poor stability in hot and humid climates, batch to batch variations of results, and non-quantitative in nature, prompted to explore robust, stable and efficient recognition systems for developing malaria diagnostics (Jorgensen *et. al,* 2006, Erdman and Kain, 2008).

Herein, we report a novel strategy to detect both pan specific and *P. falciparum* malaria following a dye based chromogenic reaction. For the detections, two different DNA aptamers specific to the corresponding target antigens *P*LDH and *Pf*GDH in the serum samples were used. The aptamer captured biomarker enzymes were then detected through substrate dependent chromogenic reactions. The DNA aptamers as bio recognition molecules were considered here due to their higher thermal stability than the conventional antibodies, low cost as they can be produced economically in a large scale following standard chemical synthesis protocol, and comparable selectivity with the antibodies to the target analytes. All these properties are conducive for their deployment in malaria infested hot and humid climate (Claudia *et al.,* 2008; Cho *et al.*, 2009; Chakma *et al.*, 2016). The chromogenic reaction has been implemented here to determine malaria following two different strategies, one is through instrument-based analytical technique for application in laboratory set-ups while the other one is through instrument –free paper based analytical technique for POC settings and resource limited environments. The instrument based technique has the choice to read the results in both colorimetric as well as fluorometric platforms. Whilst, the paper-based technique generates the results through simple pixel based data forms. Notably, there has been an intensive study over the last couple of years on the paper based diagnostic platforms owing to its several advantages coined as ASSURED (Affordable, Selective and Specific, User-friendly, Rapid and robust, Equipment –free and Deliverable) by WHO (Kosack *et al.,* 2017). Paper based fluidics give access for rapid, simple, low cost and accurate diagnosis as a vital aspect of global health problems. The chromatography paper increasingly used for point of care diagnosis due to its defined pore size, uniform structure, white background facilitates visible readout of response, wicking ability which enables a sample to transport, filter or get entrapped and result indicate by visible readout (Chakma *et al.,* 2016; Dirkzwager *et al.,* 2016). Notably, there has been an intensive study over the last couple of years on the use of paper as diagnostic platform. However poor physical adsorption of molecules over

paper surface has an inevitable drawback that sometime could not able to offer reproducible results (Credou *et al.*, 2013). In order to significantly improve the adsorption via covalent binding over paper need to functionalize with surface modifiers such as long chain flexible polysaccharides, polypeptide for paper based sensor application to enhanced signal response (Araujo *et al.*, 2012; Wang *et al.*, 2012). The paper microfluidic patterning was expensive and time consuming to create 2D-3D print, hydrophobic/hydrophilic pattern that restricted it use over broad conditions (Li *et al.*, 2012). Till date many researcher have made great effort to capture and separate biomarker from human blood or serum (Markwalter *et al.*, 2016; Fraser *et al.*, 2018; Dirkzwager *et al.*, 2016). A detailed account on the developed technique and device and their advantages for malaria diagnosis are discussed in this chapter.

7.2 Experimental procedure

7.2.1 Materials

The aptamers NG3 (dissociation constant, K_d 79 nM) as described in chapter 3 and P38 (K_d 0.35 µM) as reported from this laboratory by Jain *et al.*, (2016a) that bind with high affinity to malaria biomarker *Pf*LDH and *Pf*GDH, respectively were used in this investigation. The sequences of the aptamers are shown in table. 7.1. The recombinant enzymes, *Pf*GDH, *P*LDH, *H*LDH, *Pf*HRP-II and *H*GDH for the present work were expressed in *E. coli* strain BL21(DE3) PlysS and purified through Ni-NTA (HiTrap) affinity chromatography column as reported by Jain *et al.*, (2016a) and Chakma *et al.*, (2016) for *P*LDH and *Pf*HRP-II, respectively. The biotinylated NG3 and P38 aptamers were fabricated with linker region (*Italics*) in the sequences to avoid movement restriction in adaptation of proper confirmation after attachment to the magnetic beads, synthesised from IDT Singapore. The AMG™ streptavidin coated magnetic beads (1 µm) were purchased from Anteo diagnostics (Australia). The starting block buffer (SB) was procured from Thermo fisher scientific (USA). The reagents like Resazurin, Phenazine ethosulphate (PES), Acetylpyridine adenine (APAD), Nicotinamide adenine dinucleotide phosphate (NADP), chitosan and diethyl amino ethyl (DEAE)-cellulose were procured from Sigma Aldrich. The sodium glutamate, lactic acid, sodium chloride, potassium chloride, magnesium chloride and potassium phosphate buffer obtained from Himedia, India. The human blood (B^{+ve}) obtained from a healthy person was allowed to clot at 25 °C and then centrifuged at 1800 x g for 20 min to separate the serum from clotted blood. All other chemicals used in

the experiments were of analytical grade. The buffer compositions used in current work mention in table A3 under appendix section.

Table.7.1: Biotinylated aptamer sequence.

S. No.	Name	Sequence of Aptamer (5'-3')	Target
1.	P38	5'(**Biotin**)*TTTT*CACCTAATACGACTCACTATAGCGG ATCCGACAATAATACACTTTGCTCCCCTGTGGCTT TTCGCACTCGCCTGGCTCGAACAAGCTTGC-3'	*P*LDH
2.	NG3	5'(**Biotin**)*TTTT*CACCTCATACGACTCACTATAGCGG ATCCGAGCCGGGGTGTTCTGTTGGCGGGGGCGGT GGGCGGGCTGGCTCGAACAAGCTTGC-3'	*Pf*GDH

Text in italics is linker region of aptamer

7.2.2 Preparation of aptamer coated magnetic beads

The streptavidin coated magnetic beads were washed thrice with coupling buffer at RT for 1 minute in each wash. The beads (100 µg) were then incubated for two hours with different amount of aptamer (P38 or NG3) in defined aptamer: bead ratio (1:10, 1:20, 1:30, 1:40, 1:50) in binding buffer. Prior to the binding, aptamers were heat treated at 90 °C for 10 min and then cooled at RT for 5 min to maintain the native conformation of the aptamers. The aptamer-bead conjugate was then separated from the incubated solution by using a magnet (12-15 Gauss) followed by washing with binding buffer. Further, to prevent nonspecific binding, the aptamer-bead complex was treated with starting blocking buffer (SB) for 30 min. As prepared aptamer-bead assembly was stored at 4 °C for future use. The amount of bound aptamer over magnetic bead was quantified through following relation: ssDNA concentration = 33 µg/mL × OD_{260} of net bound aptamer × dilution factor. Net amount of captured protein on aptamer-bead complex was quantified by Bradford assay by measuring OD at $\lambda_{595\ nm}$.

7.2.3 Procedure for capturing biomarkers from sample on aptamer coated magnetic beads.

A total of 200 µg of aptamer (NG3 or P38) coated on streptavidin magnetic bead conjugate was incubated in 0.5 ml of binding buffer or human blood serum containing *Pf*GDH or *P*LDH protein with gentle shaking for 30 min at room temperature in a 1.5 ml centrifuge tube. Following capture of the biomarkers, the beads were concentrated inside the tube with the help of an external magnet (12-15 Gauss), decant the solution from the tube and then washed the retained beads with binding buffer to remove the non-specifically attached

proteins and other components. The captured target enzyme/aptamer/bead complex in the tube was suspended in the cocktail buffer for 1 hour to catalysed captured enzyme based reaction. The developed enzyme/aptamer/bead response with cocktail buffer was then used to employ either for instrument (UV-Visible or fluorescence spectrophotometer) based or equipment free techniques for quantitative detection of the biomarkers through optical signals (Figure 7.1).

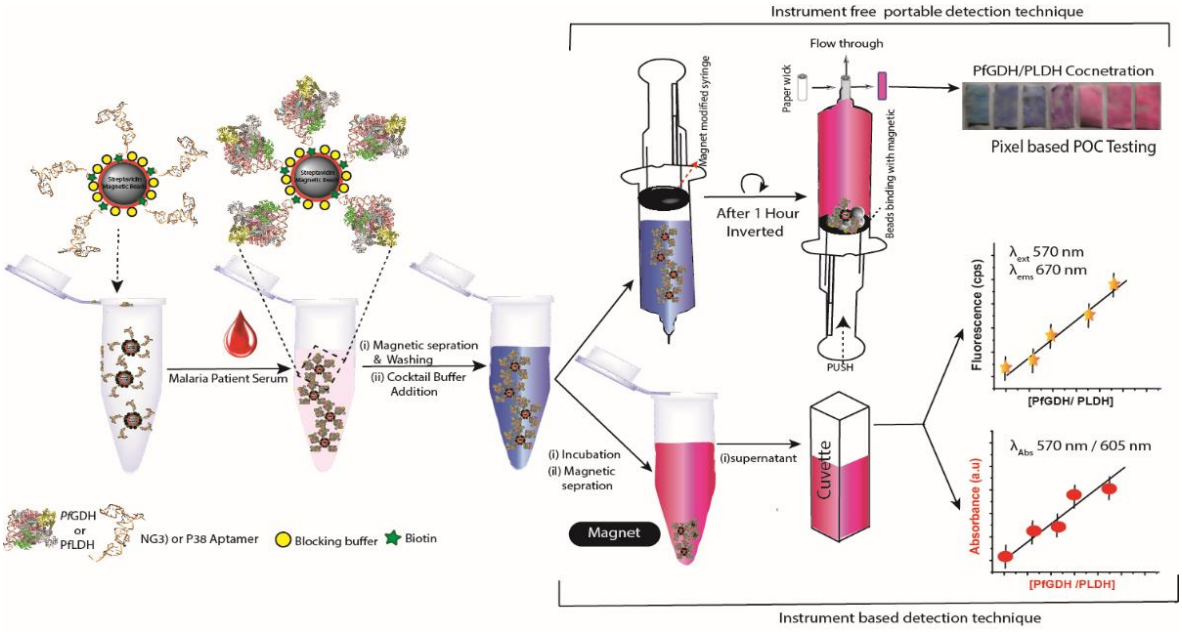

Figure 7.1: Schematic of the Instrument based and Instrument free analytical procedure for detection of malaria biomarkers.

7.2.4 Syringe modification with paper wick and magnet

The Nipro, 5 ml (24GX1", 0.55 mm X 25 mm), syringe was modified with magnet as shown in figure 7.2. The syringe piston was mounted with Ni coated magnet (5 mm X 5 mm X 2 mm, magnetic field 2-3 Gauss) within the rubber valve. The syringe needle was removed and the exposed syringe hose was used as holding support for a chromatographic paper roll (Whatman grade-1) made from a paper wick (10 mm X 15 mm). The roll was then covered with the syringe needle at the time of operation.

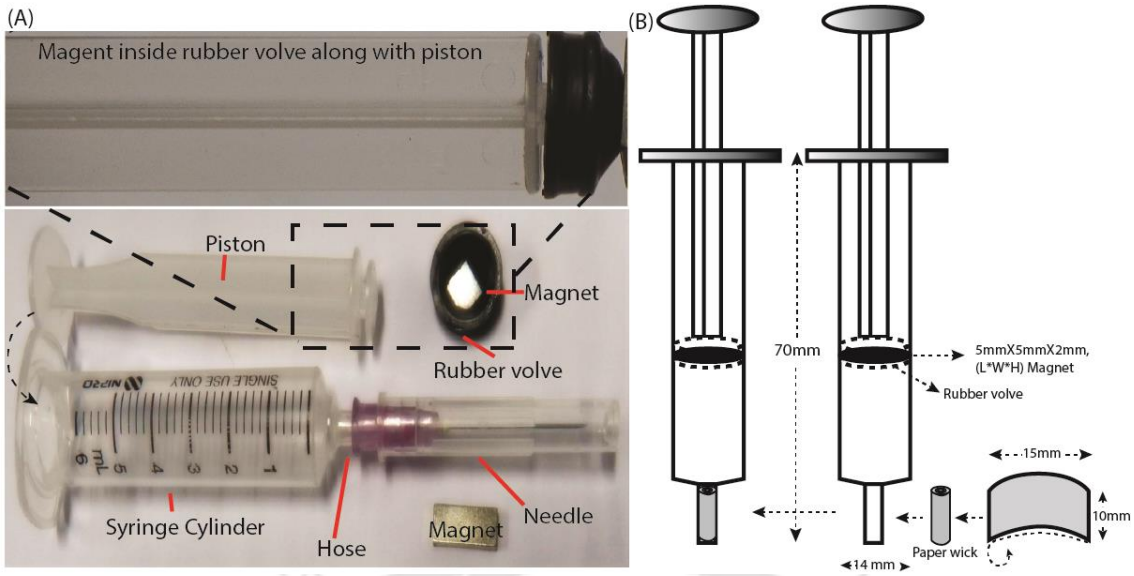

Figure 7.2: Fabrication of modified syringe (A) real image with its components (B) Drawings of fabricated syringe.

7. 2.5 Preparation of polysaccharide/polypeptide coated paper

For the improvement in sensitivity, normal filter paper was surface modified with polysaccharides (chitosan, DEAE-cellulose) and polypeptide (sericine) as surface modifiers to improve the entrapment efficiency of dye over paper surface. The carboxylic functional group present over Whatman filter paper was activated through EDC/ NHS chemistry as previously described by Cao and co-workers (Cao *et al.*, 2015). In brief equimolar (0.1 M) mixture of EDC/ NHS uniformly spread over paper and kept at RT for 1 h followed by washing with water. Subsequently, activated paper was treated with chitosan, DEAE-cellulose and sericine (silk protein) 1 % w/v aqueous solution in BB. The sericine protein extracted from *Antheraea mylitta* cocoons through degumming process (Dash *et al.*, 2007). The respective solutions were uniformly spread over the activated paper surface and dried at RT for 2 h followed by final drying at 40 °C for 10 min in oven.

The surface topography of modified paper was characterized through field emission scanning electron microscopy (FESEM). This surface modified (SM) paper was cut in specific dimension and turned into wick for instrument free technique as describe above with syringe. The net entrapped dye over paper surface was calculated with Beer-Lambert law ($C = A_{570nm}/ \varepsilon L$) where ε is molar extinction coefficient of resorufin (73 mM in PBS), A is absorbance and L path length. The pixel intensity calculated from colour developed on paper.

7.2.6 Set-up for instrument-free detection of biomarkers

The procedure for detection of malaria biomarkers through instrument free technique using modified syringe is shown in figure 7.1. After suspending the enzyme-bound magnetic bead in cocktail buffer (0.5 ml) in a centrifuge tube as mentioned under section 7. 2.3, the content was immediately siphoned into a syringe and incubated for 1 hour at room temperature. After the incubation, a rolled paper wick made from Whatman grade-1 filter paper was placed inside the syringe hose and then it was capped with the syringe needle. The enzyme-captured beads from the reaction mixture were arrested by the magnet in rubber valve in the piston leaving the dye in solution. The dye content was absorbed and concentrated on the paper wick when the piston was gently pressed to pass the solution through it. The paper was removed from the syringe hose, unfurled and then kept it for air-drying at room temperature for 5 min. The color formed in the paper was captured by Nikon L830 coolpix camera in uniform light, distance conditions. After that, the image was transformed into RGB format through adobe illustrator and processed through Image J software to measure the pixel intensity of the color.

7.2.7 Statistical analysis of data

All the experiments performed in triplicate and mean of data with standard deviation as error bars are represented in this work. The Origin 8.0 software was used for statistical analysis. The limit of detection (LOD) for analytical response was calculated from slope of calibrations curve (fluorometric/ colorimetric) for both the enzymes by using the relation, LOD = 3 x standard deviation (SD) of blank/ slope of calibrations curve. The LOD over paper platform was calculated with formula LOD = LOB + 1.65 x SD of lowest concentration, where limit of blank (LOB) = mean of blank + 1.65 x SD of blank.

7.3 Results and discussion

7.3.1 Principle for detection of aptamer captured malarial biomarker

The reaction principle for detection of the malarial biomarkers, *P*LDH and *Pf*GDH is summarized in the figure 7.3 A. Herein, two different selective aptamers, P38 and NG3 were used to capture the corresponding enzymes, *P*LDH and *Pf*GDH from the buffer or serum samples. The captured enzymes were then detected through substrate dependent chromogenic reactions.

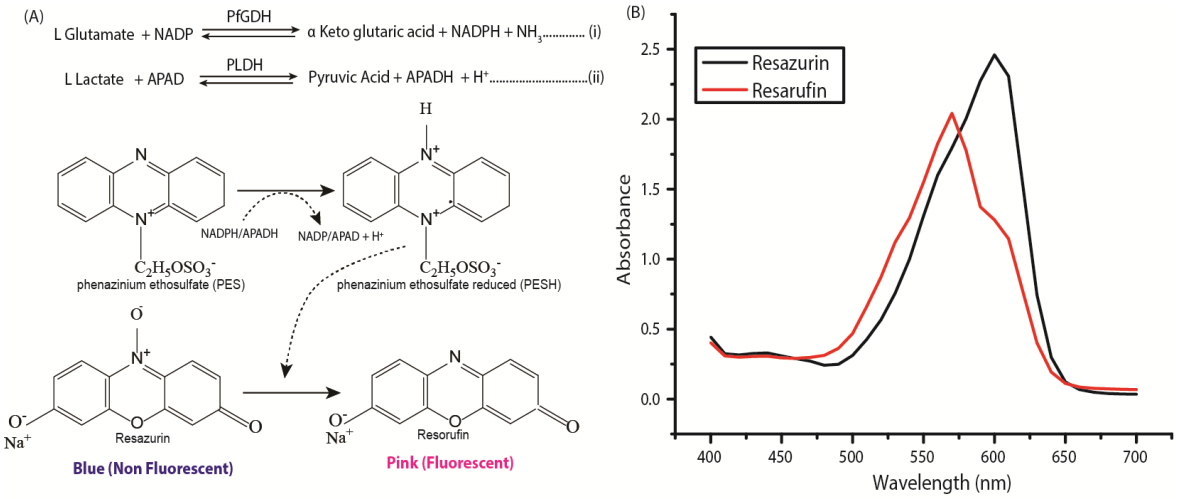

Figure 7.3: Reaction scheme used for substrate dependent detection of malarial biomarker enzymes *Pf*GDH and *P*LDH (A). Absorbance spectra of resazurin and resorufin in cocktail buffer (B).

The enzymes *P*LDH and *Pf*GDH catalysed the reactions in presence of their respective substrates-cofactors, lactate-APAD and glutamate-NADP supplemented together with resazurin dye and co-activator PES in a cocktail buffer. The reduced cofactors (APADH/NADPH) formed in the reaction converted the blue coloured (absorption at ~$\lambda_{605\ nm}$) non-fluorescent resazurin dye (Gloeckner *et al.*, 2001) into a pink coloured (absorption at ~$\lambda_{570\ nm}$) fluorescent resorufin dye, (Figure 7.3 B) (Candeias *et al.*, 1998), which exhibits excitation at ~ $\lambda_{570\ nm}$ and emission at ~$\lambda_{660\ nm}$ (Figure 7.4).

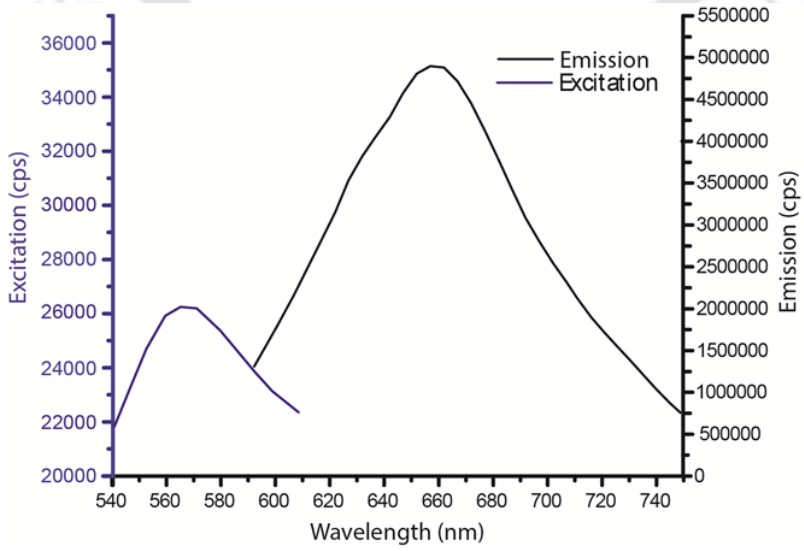

Figure: 7.4: Excitation and Emission spectra of resazurin and resorufin in cocktail buffer.

The red shift of resorufin emission to ~$\lambda_{660\ nm}$ in cocktail buffer from $\lambda_{610\ nm}$ in phosphate buffer (Choi *et al.*, 2013) may be attributed to the possible ionic effect of the dye in the cocktail buffer. The two ionic terminals with partial negative charge on oxygen atoms in the molecule render it as a potential candidate for various ionic interactions (Flamigni *et al.*, 1989). The phenazine ethosulphate (PES) was used as an electron transfer mediator (ETM) for transferring the reductive equivalents from the reduced co-factors to resazurin leading to the formation of resorufin (Davis and Thornalley, 1983). The choice for the PES was based on its higher aqueous stability than the other commonly used ETMs, such as, phenazine methosulphate (Ghosh and Quayle, 1979). The biomarkers captured by the aptamer coated magnetic beads could therefore be monitored optically following colorimetric measurement of absorbance as well as fluorimetric analysis. In the colorimetric approach, a ratio metric analysis using $\lambda_{570\ nm}$/ $\lambda_{605\ nm}$ was used for quantitative detection of the targets. The reaction could be customized either for specific detection of *P. falciparum* malaria or for detection of pan malaria. For species-specific detection of *P. falciparum*, only the NG3 coated magnetic beads were used. For pan malaria detection without being laid any interest of retrieving species specific information, the P38 coated magnetic beads alone or its combination with the NG3 coated magnetic beads could be used considering the fact that P38 reacts with multiple *Plasmodium* LDHs (Jain *et al.*, 2016).

To develop an interference-free format for monitoring the reaction, the aptamer captured biomarker enzymes were separated from the blood serum with the help of aptamer coated magnetic beads. It may be mentioned that blood serum is a highly complex cocktail of various organic, inorganic and organometallic compounds hosting various redox and chromogenic compounds such as, haem proteins and various forms of bilirubin (Basu and Kulkarni, 2014; Lightson *et al.*, 2018). These complex environment stands as a challenge in selective and interference-free detection of specific compound of interest through chromogenic reaction based optical transduction principle. In general, the effort to extrapolate the results from the standard buffer conditions to the serum samples is not always successful in analytical studies. The strategy frequently adapted to reduce the interference is to dilute the serum samples sufficiently before being analysed (Chakma *et al.*, 2016). However, it involves an additional step and marginalizes the chance to detect the target under dilute condition for the methods which are less sensitive.

7.3.2 Optimisation of aptamer: magnetic bead ratio and time

A suitable aptamer density over the bead surface is important for a better analytical performance. While, overcrowding of aptamers over the beads may cause steric hindrance in the binding, this might also reduce the efficiency of the aptamers to capture the target (Jolly *et al.*, 2017). The surface coverage and spacing among the surface coated aptamer molecules depend on the concentration ratio between aptamers and magnetic beads. Therefore a range of ratio was spectroscopically studied to obtain the optimum detection response. The biotin modified aptamers were mixed with streptavidin coated magnetic bead at different concentration ratios (Figure 7.5 A, B).

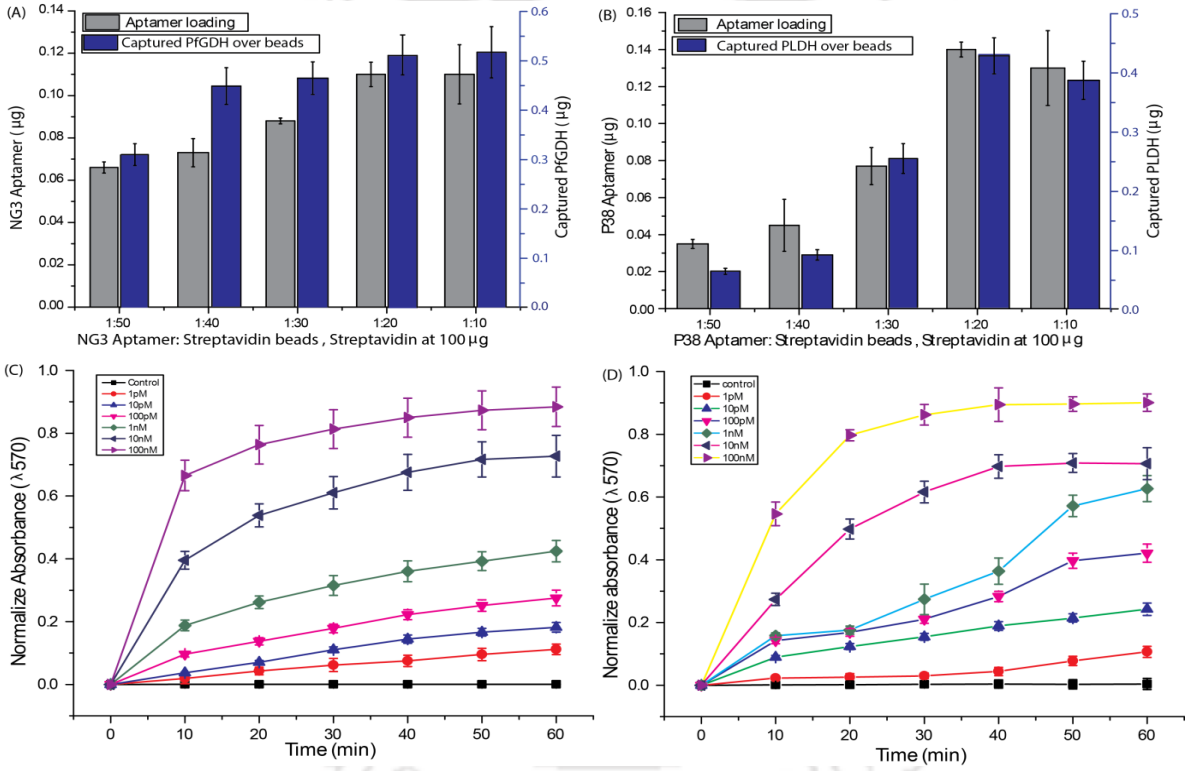

Figure 7.5: Optimization of the binding ratio of biotin modified aptamers with enzyme capture efficiency with streptavidin coated magnetic beads for maximum aptamer and protein loading efficiency for (A) NG3/*Pf*GDH and (B) P38/*P*LDH time optimization study for optimum absorbance intensity at different concentrations of the target enzyme proteins for the captured (C) *Pf*GDH (D) *P*LDH.

It can be seen that the bead surface gets saturated with the ratio of 1:20 (5 µg aptamer to 100 µg beads) for both the aptamers. To further highlight this target capture response is hugely affected by the density of surface-bound aptamer over the bead but after increasing

the aptamer concentration from 1:20 to 1:10 it is slightly affected instead it suppressing the capturing efficiency in case of P38/*P*LDH. Among all the ratios, 1:20 ratio (5 µg of aptamer with 100 µg of magnetic beads) provided better response compared to higher aptamer density at 1:10 ratio.

A study was performed to identify the optimum time for monitoring the assay using the optimum ratio of aptamer: bead (1:20) with 200 µg of aptamer bead complex (Figure 7.5 C, D). As expected, higher the concentration of the enzymes shorter was the reaction time to attain the saturation level with concomitant increase in slop of the response curve. To obtain an optimum signal with a broad detection range we chose 1 h reaction time for the detection. As depicted in figure 7.5 C, D, different concentrations of captured *P*LDH and *Pf*GDH over magnetic beads displayed a particular gradient of colour response between blue to pink corresponding to specific concentration. This has been attributed to the fact that following 1 h of incubation different percentage of resazurin gets converted to resorufin in response to various concentration of captured enzyme. The formation of resorufin was calculated by using Beer Lambert law (A = εcl) where A is absorbance recorded at $\lambda_{570\ nm}$, ε is molar extinction coefficient of Resorufin (73 mM in PBS), c is concentration of analyte in solution. The concentration of resorufin was measured after 1 h of reaction as listed in table- 7.2. The progress of the reaction against different concentration of the target enzyme (*P*LDH or *Pf*GDH) would thus be expressed by using ratiometric analysis of dyes i.e., ($\lambda_{570\ nm}$/ $\lambda_{605\ nm}$).

Table.7.2: Percentage of resorufin formed from resazurin in response to different concentration of enzymes.

Concentration* Over aptamer magnetic beads	**Percentage of resorufin formed by *P*LDH**	**Percentage of resorufin formed by *Pf*GDH.**
1 pM	3.64	3.82
10 pM	8.30	6.25
100 pM	14.94	9.40
1 nM	21.45	14.55
10 nM	24.20	24.90
100 nM	30.85	30.30

* Spiked solution concentration used for capture efficiency testing of aptamer/magnetic beads.

7.3.3 Paper surface functionalization for dye entrapment

In the instrument free technique, Whatman paper acts as sensing surface and was responsible for entrapment of resazurin/resorufin dye from the solution. The dye adsorbed over paper surface was indirectly used for identification and quantification of *P*LDH or *Pf*GDH. Hence, effective adsorption of dye over paper surface is crucial part for sensor sensitivity. As reported by various researchers, the various functional groups such as, hydroxyl and carboxyl molecules that exist over paper surface and further functionalization with polysaccharides and polypeptide, can potentially facilitate better adsorption of various molecules from solution (Cao *et al.,* 2015; Kongdee *et al.,* 2005). Under this study, two kinds of polysaccharides viz. chitosan, diethyl amino ethyl (DEAE)-cellulose and polypeptide (sericine protein) were utilized for paper modification by adsorption through covalent chemistry over paper surface as surface modifiers. The amount of resorufin dye adsorbed over normal filter paper was considered as control and compared with modified paper surfaces (Figure 7.6).

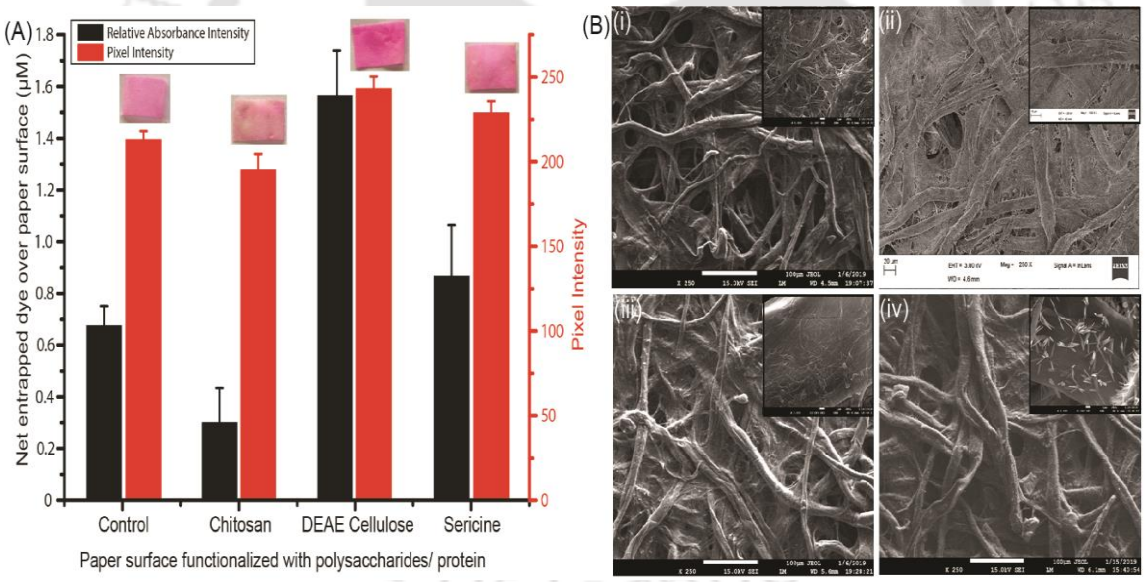

Figure: 7.6: Dye entrapment efficiency of Whatman filter paper (control) and the paper modified with compound (A). The surface topography of modified paper (B), control (i), chitosan treated (ii), sericine treated (iii) DEAE treated (iv) at 250 x magnification and inset respective image magnified at 5000 x.

As depicted in figure 7.6 A, DEAE cellulose modified (DSM) paper has better entrapment capacity for dye followed by sericine, while chitosan modified paper showed poor entrapment efficiency towards dye compared to control. The improved adsorption of

dye with DSM and sericine paper are ascribed to the unique electrostatic interaction between the functional groups deposited on paper and the dye. The electrostatic interaction is possibly driven by adsorption with positively charged (amines) functional groups and partially negatively charged resorufin dye. Besides the electrostatic interaction, covalent coupling via Schiff reaction with amino group may also play significant role in interaction chemistry. While chitosan (pKa ~ 6.5) carries negative charge in basic medium (Bajaj *et al.*, 2012), which countenance ionic repulsion with negatively charged resorufin dye, and hence a poor binding ability. The surface topography after modification was confirmed through FESEM study (Figure 7.6 B). As depicted under inset image, it is plausible to observe that the porous structure present over cellulose paper was completely coated with chitosan and sericine in the form of thin layer. Beside this microstructure of DEAE treated paper was exposed presence of specific porous structure along with presence of whipped structure over it. This result reveals that DSM paper has better entrapment efficiency in comparison to normal paper which further facilitates to enhance the sensitivity of instrument free technique for malaria detection.

7.3.4 Quantitative detection of *Pf*GDH and *P*LDH

The aptamer decorated magnetic beads were used to capture the respective biomarker enzymes from the binding buffer and undiluted human serum samples. The enzyme-captured beads were mixed with the cocktail buffer in a centrifuge tube. The samples were then analysed by instrument based system and instrument free potable detection technique as described below. For the analysis, each of the marker enzymes was studied in a broad concentration range of 1 pM to 100 nM. This range fairly covers the previously reported dynamic range for *P*LDH (3.9 pM to 39 nM) offered by the immune-chromatographic RDTs available in the market (Jimenez *et al.*, 2017) and for *Pf*GDH (2 to16 nM) offered by the immuno-chromatographic dipstick test (Li *et al.*, 2005).

7.3.4.1 *Instrument-based analytical technique*

The analysis was first performed in buffer samples spiked with *P*LDH or *Pf*GDH. The reaction mixture containing the enzyme captured beads and the cocktail buffer was incubated for one h at RT. The reaction supernatant was then separated from the mixture following the method described above. The supernatant was then subjected to absorbance

and fluorescence spectral analyses for *P*LDH (Figure 7.7 A, B), *Pf*GDH (Figure 7.7 C, D) spiked in buffer and *P*LDH (Figure 7.8 A, B), *Pf*GDH (Figure 7.8 C, D) spiked in serum.

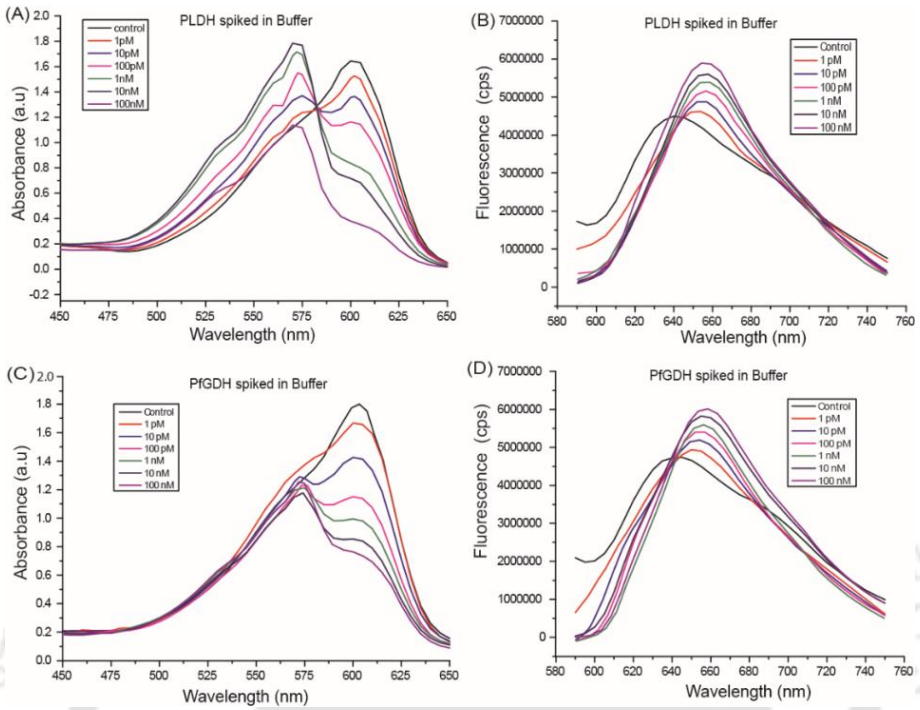

Figure: 7.7: (A) Absorbance spectra of *P*LDH (A), *Pf*GDH (C) and fluorescence spectra of *P*LDH (B), *Pf*GDH (D) response with different concentrations spiked in binding buffer.

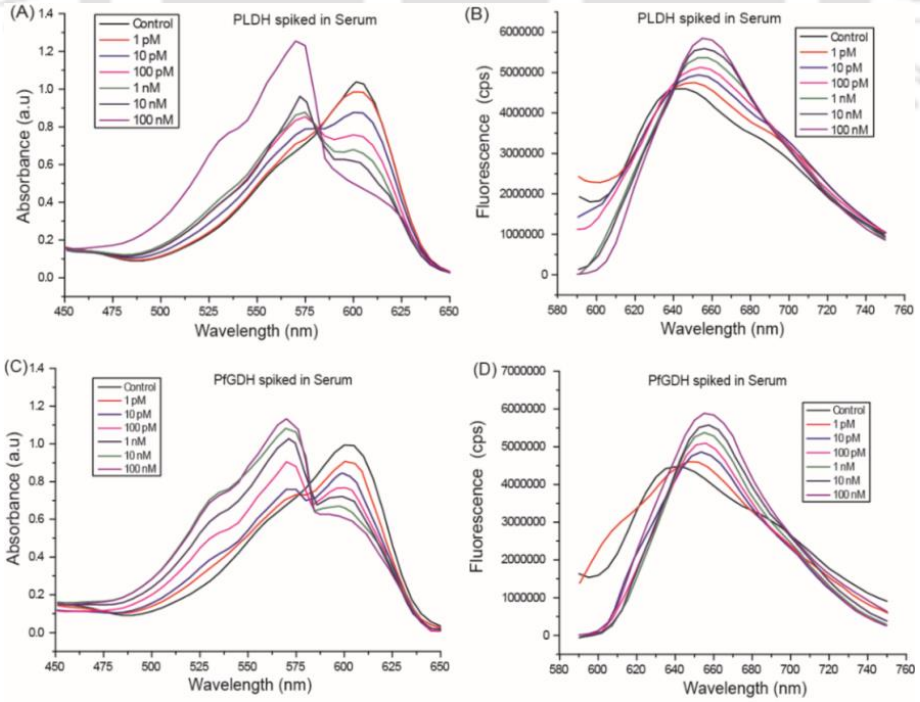

Figure: 7.8: (A) Absorbance spectra of *P*LDH (A), *Pf*GDH (C) and fluorescence spectra of *P*LDH (B), *Pf*GDH (D) response with different concentrations spiked in serum.

With the increasing concentration of the captured enzymes, the absorption peak at ~λ_{605nm} of the enzyme free mixture shifted to ~λ_{570nm} along with the appearance of a fluorescent peak at $\lambda_{660\ nm}$ (excitation at ~$\lambda_{570\ nm}$). The calibration plots for the respective enzymes were constructed from the spectral absorbance and fluorescence intensity for binding buffer solution (Figure 7.9 A, B) and serum samples (Figure 7.9 C, D). For absorption spectra based calibration plot, the ratio metric ($\lambda_{570nm}/\lambda_{605nm}$) response was considered to improve the sensitivity of the method (Sun *et al.*, 2012). The LODs (3 σ/s) calculated for *P*LDH from the corresponding absorbance and fluorescence intensity based calibrations curves in binding buffer were 0.41 ± 0.07 pM and 1.63 ± 0.14 pM and in serum were 0.55 ± 0.09 pM and 1.72 ± 0.13 pM, respectively. Whereas, the LOD for *Pf*GDH from the corresponding absorbance and fluorescence intensity based calibrations curves in binding buffer were 1.14 ± 0.12 pM and 0.81 ± 0.10 pM and in serum were 1.34 ± 0.12 pM and 1.43 ± 0.14 pM, respectively.

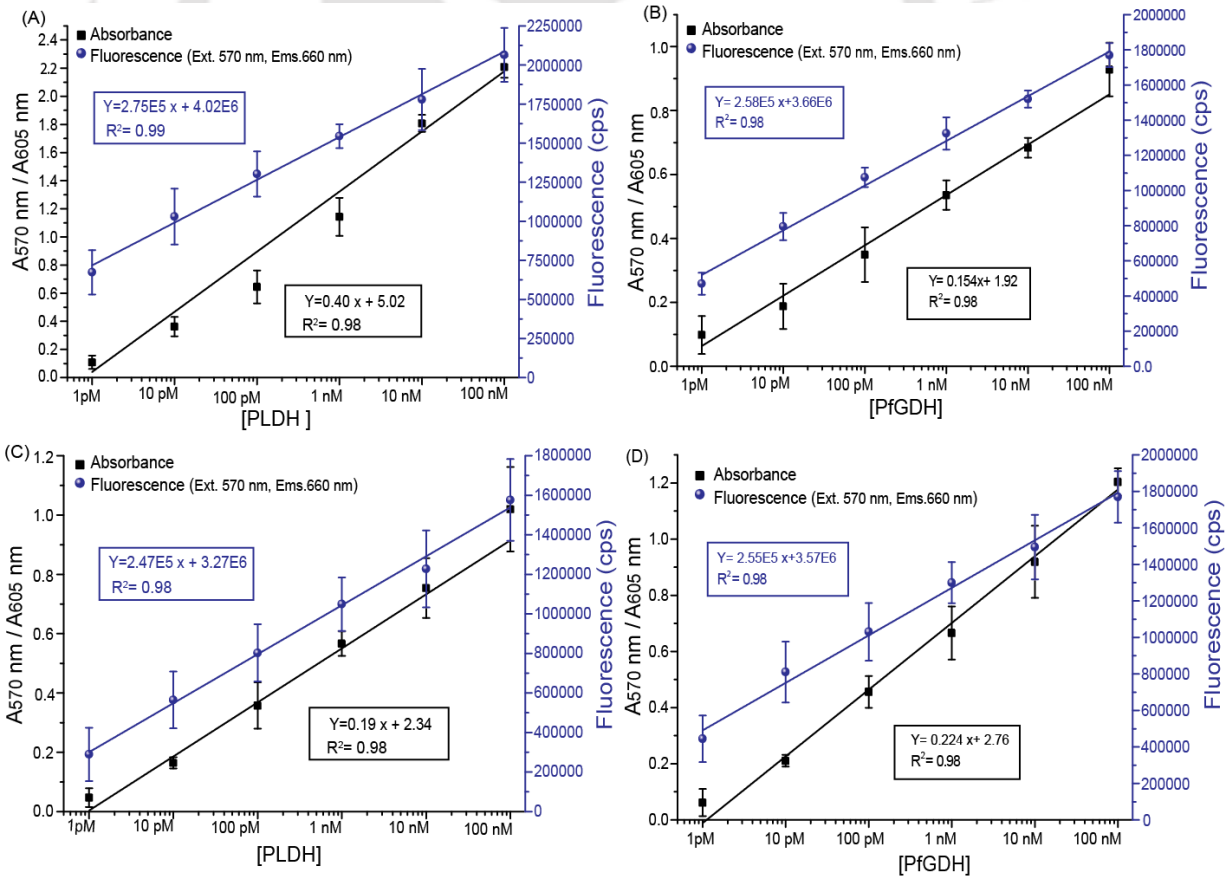

Figure: 7.9: Calibration plots derived from absorbance and fluorescence characteristics for (A) *P*LDH and (B) *Pf*GDH in binding buffer and (C) *P*LDH and (D) *Pf*GDH in serum.

Overall, the absorbance spectroscopy offered superior LODs for the biomarkers than the corresponding fluorescence based determination indicating higher sensitivity of the ratio metric absorption response than the single wavelength-based fluorescence response. The discerned LOD values were far superior than 30.45 ± 47.65 nM for *P*LDH and 1-16 nM for *Pf*GDH, which are considered to be in the clinically significant range for malaria diagnosis (Li *et al.*, 2005; Jang *et al.*, 2013).

The performance of the method was also examined for co-activity of the enzymes using an equimolar mixture of P38 and NG3 coated magnetic beads in binding buffer spiked with different concentrations of *P*LDH and *Pf*GDH. Subsequently the reaction was performed by mixing the enzyme captured beads and cocktail buffer following the procedure described above. Calibration plots were constructed for both absorbance ($\lambda_{570nm}/\lambda_{605nm}$) and fluorescence (emission at λ_{660nm}) signals (Figure 7.10 A) as well as for instrument free technique (Figure 7.10 B), which will be discussed below. As evident from the graphs, the linear response for both the instrument based and instrument free methods was identified to be 1 pM to a maximum of ~100 pM with R^2 (co-efficient of determination) value 0.95. Since beyond this concentration of 100 pM, the R^2 values of the regression line were significantly reduced.

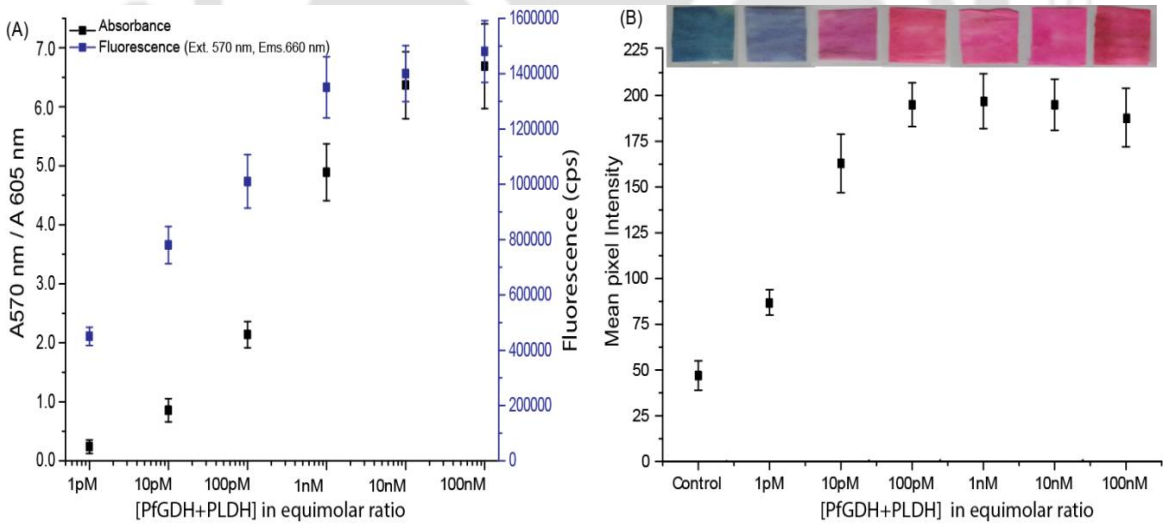

Figure 7.10: (A) Absorbance and fluorescence (Excitation λ_{570}, Emission λ_{660}) response and (B) colour (pixel) response of the reaction with different concentration of each enzyme (*Pf*GDH and *P*LDH) co-spiked in binding buffer.

7.3.4.2 *Instrument-free portable detection technique*

For the instrument free method, the reaction mixture in the eppendorf tube containing the enzyme captured beads and the buffer was immediately siphoned into the modified syringe and then incubated for 1 hour. The reaction supernatant from the syringe was then passed through a DSM paper wick fixed inside the syringe hose. The dye got adsorbed in the DSM paper wick displaying increase in pink colour response with increasing concentration of the captured *P*LDH or *Pf*GDH in the buffer or serum samples allowing visual detection of the biomarker enzymes in serum samples (top panel in figure 7.11).

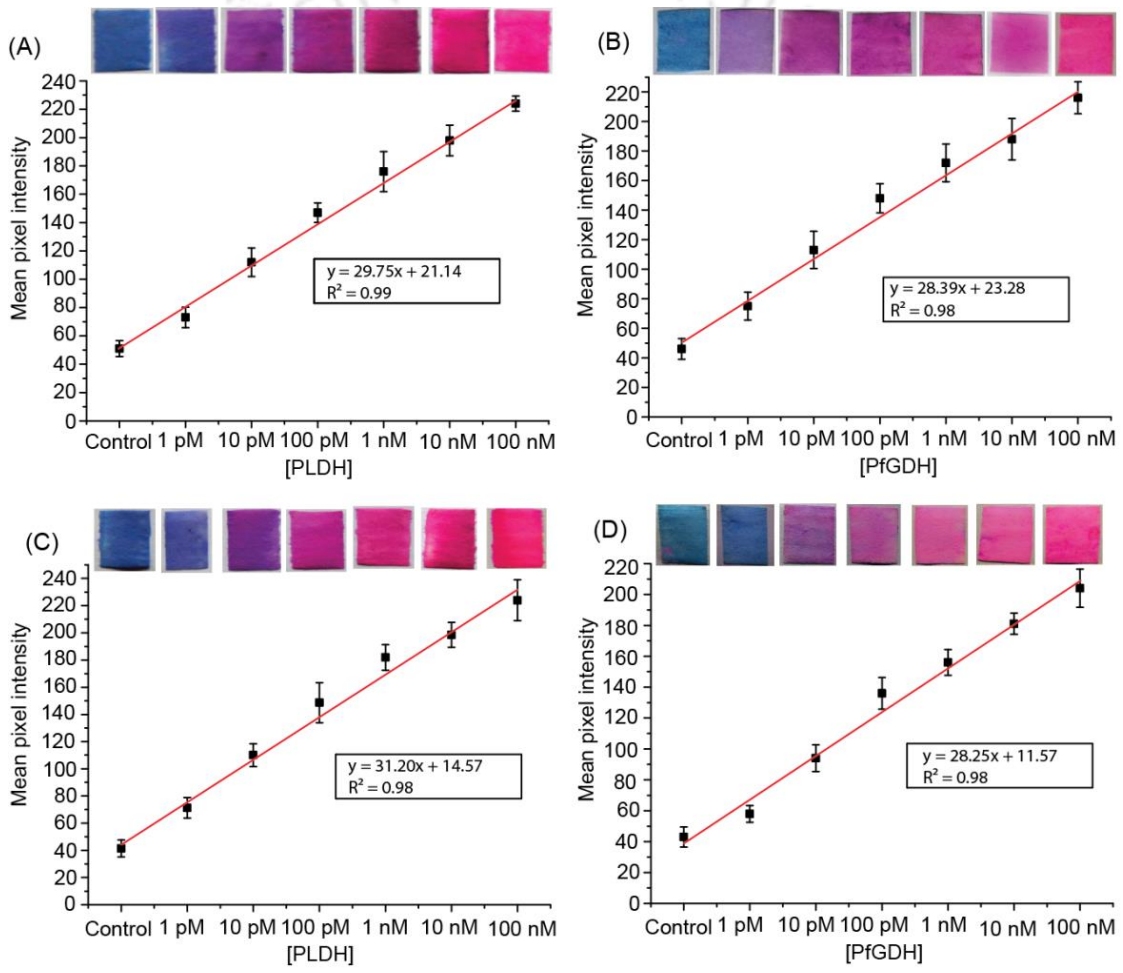

Figure: 7.11: Calibration plots derived from the pixel intensity of the colour developed on DSM paper against different concentration of (A) *P*LDH, (B) *Pf*GDH spiked in binding buffer and (C) *P*LDH, (D) *Pf*GDH spiked in serum.

The calibration plots were constructed by measuring colour intensity on the paper versus different concentration of *P*LDH (Figure 7.11 A) and *Pf*GDH (Figure 7.11 B). The

calibrations curve for both the enzymes exhibits a linear response within the range of 1 pM to 100 nM. The LODs discerned were 61.50 ± 6.43 pM and 63.97 ± 7.24 pM for *P*LDH and *Pf*GDH, respectively in spiked buffer solution.

The value of LOB was taken into account while calculating LOD for the assay over the paper surface considering the high background noise of the pixel based colorimetric detection over paper platform (Shrivastava *et al.,* 2011). Like the buffer samples, the dynamic range for the serum samples was also identified as 1 pM to 100 nM for both the enzymes (7.11 C and D). The LODs calculated for *P*LDH and *Pf*GDH in the serum sample were 69.25 ± 8.22 pM, and 68.75 ± 7.64 pM, respectively. A minor lower sensitivity observed in serum than the buffer condition has been attributed to the complex nature of the serum causing hindrance to the aptamer-target interactions. Furthermore, we performed the co-activity test on paper following similar reaction conditions and molar concentrations of the ingredients enzymes used for instrument based method. Like instrument-based method, the linear response was limited within the early concentration of the enzymes (Figure 7.10 B with colour response in top panel). We propose similar reason as discussed under the instrument based method.

7.3.5 Interference study

Any potential interference by the blood serum of healthy person on the detection of the malaria biomarkers following the approach presented here was void as evident from the results discussed above. We further investigated any interference from some relevant proteins that may be co-expressed in the parasite and host counterparts during the diseased conditions. For the study, we selected *H*LDH, *Pf*GDH, *Pf*HRP-II for P38 coated beads being used to capture *P*LDH (Figure 7.12 A) and *H*GDH, *P*LDH, *Pf*HRP-II for NG3 coated beads being used to capture *Pf*GDH (Figure 7.12 B). In independent reactions, each of these proteins were used at a concentration of 100 nM in the binding buffer keeping other constituents of the reaction mixture same as discussed above. The colour intensity developed with these non- specific proteins were either low or negligible as compared to the target proteins indicating good selectivity of the detection device. The proposed instrument free technique therefore, has high potential for malaria diagnosis with high sensitivity for the target biomarker enzymes.

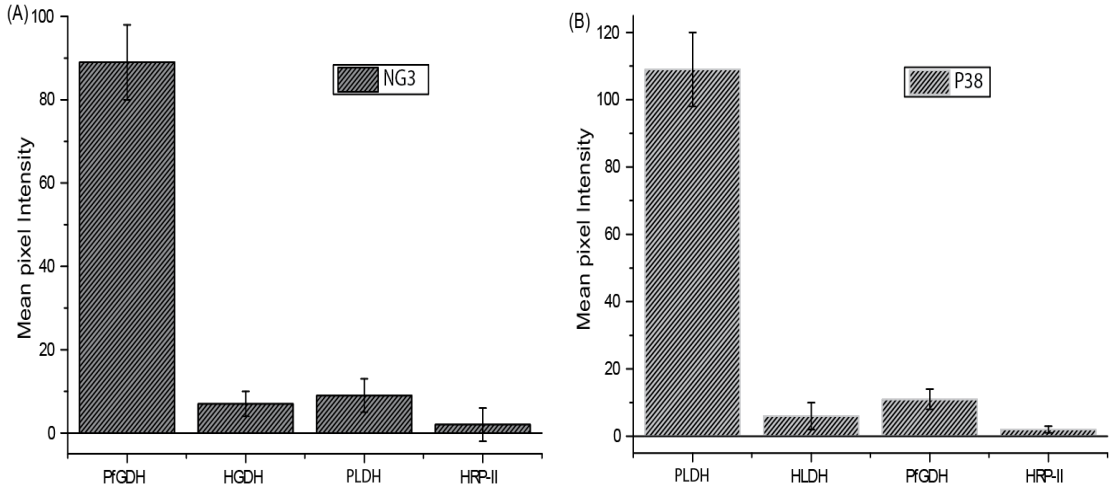

Figure 7.12: Response signal in the paper based instrument free technique with respect to aptamers (A) NG3 (B) P38 against the potential interfering analogous proteins each of which at 100 nM concentration spiked in buffer.

7.4 Conclusion

A novel approach for detection of pan specific and *Pf* specific malaria has been developed by using a chromogenic reaction catalysed by the corresponding biomarkers *P*LDH and *Pf*GDH. Using specific aptamers coated over magnetic beads these enzymes could be captured and isolated from the blood serum to perform the reaction. This strategy greatly excluded the potential interferences caused by the complex milieu of blood serum. We demonstrated that the approach could be implemented both in laboratory instrument based analytical platform and in an instrument-free paper based solid platform. The portable paper based device exploited a medical syringe modified through a novel design of integrating magnet inside to separate the biomarker-enzyme captured on aptamer coated magnetic beads from the reaction mixture, which could then be passed through a chromatographic origami to absorb the colour product formed from the reaction. The colour developed on the paper may be used either for qualitative detection following yes/no format through visual observation or for quantitative detection following color pixel based response with the aid of camera integrated suitable software. The DEAE cellulose treated paper was used in place of normal chromatographic paper for better colorimetric response with improved sensitivity of the method.

Table 7.3: Comparison between the present work and colorimetric sensors suitable for POC.

Technique	Surface and Probe	Detection range	Target Antigen	Response time	LOD	Reference
UV-Visible spectroscopy or Instrument free	Paper µPAD, murexide dye-Ni Ions	10-100 nM	*Pf*HRP-II	~5 min	30 nM	Chakma *et al.*, 2016
UV-Visible spectroscopy	Gold nanoparticle, Aptamer	N/A	*P*LDH	~10 min	445 pM	Cheung *et al.*, 2013
UV-Visible spectroscopy or Instrument free	Magnetic beads, Antibody	25 nM- 2 µM	*Pf*LDH	~45 min	25.7 pM	Markwalter *et al.*, 2016
UV-Visible spectroscopy or Instrument free	Paper µPAD, Aptamer	3.5 nM- 35 µM	*Pf*LDH	~45 min	36 pM	Dirkzwager *et al.*, 2016.
Instrument free	Immune chromate-graphic, Antibody	2-16 nM	*Pf*GDH	10-20 min	N/A	Li *et al.*, 2005
UV-Visible spectroscopy	Functionalized paper, Antibody	N/A	*Pf*HRP-II	25 min	0.32, 0.15, 6.9 , 6.2 nM for paper Functionalized by enzyme / metal/ polymer	Lathwal and Sikes, 2016
Instrument free	Paper µPAD Antibody	0.7- 91 pM	*Pf*HRP-II	20 Min	23 pM	Jimenez *et al.*, 2017
		3.9 pM- 39 nM	*Pv*LDH	20 Min	195 pM	Jimenez *et al.*, 2017
Instrument based UV-Visible spectroscopy	Magnetic beads aptamer	1 pM- 100 nM	*P*LDH and *Pf*GDH	60 min	0.55 pM, 1.34 pM for *P*LDH and *Pf*GDH respectively	Present work
Instrument based Fluorescence spectroscopy					1.72 pM, 1.43 pM for *P*LDH and *Pf*GDH respectively	
Instrument free					69.25, 68.75 for *Pf*GDH and *P*LDH respectively	

The linear detection range and the LODs offered by both the instrument based and instrument free detection systems are comparable (Jimenez *et al.*, 2017) and even, superior (Chakma *et al.*, 2016) than some of the previously reported methods (Table 7.3). Flexible detection capability of pan specific and *Pf* specific malaria, low cost, and interference free detections of the biomarker enzymes from serum samples are the major advantages offered by the developed approaches. Further, the paper-based portable device has a great potential for its application in POC and resource limited environment due to its low cost (~ 0.10 $

per test) and stable reaction components (aptamers, magnetic beads, dyes) that can withstand in hot and humid malaria endemic regions. For quantitative applications of the paper based device, suitable custom made software loaded in a camera integrated device such as, smart phone, will simplify capture of the pixel response, and transduction of the generated response to a digital form for determination of the biomarker concentration and its linked parasitaemia level. The results confirmed that the aptamer coated magnetic beads with the dye based reaction could be used successfully for sensitive determination of *P*LDH and *Pf*GDH in undiluted serum samples. The simple and sensitive equipment free technique has high application potential in point of care settings for diagnosis of malaria.

Conclusion and Future directions

Science is the process that takes us from conclusion to understandings....

- Brian Green

Conclusion and future scope

The major goal set for the current work was to develop aptamer based detection of *Pf*GDH in human serum sample for malaria diagnosis. To accomplish this goal functionally active *Pf*GDH and *H*GDH enzymes were cloned and expressed in *E. coli* following the standard molecular biology techniques and protocols. The expressed proteins were then purified by affinity chromatography. The purity of the recombinant enzymes was established by western blotting and MALDI-MS. The structural and functional integrity of the recombinant enzymes were confirmed through analytical ultracentrifuge, CD spectroscopy and enzyme kinetics studies. Following the structural and functional confirmation of *Pf*GDH and *H*GDH proteins, the major focus was laid on aptamer development.

The aptamers were developed through SELEX procedure by using PVDF as immobilization matrix for the target protein, *Pf*GDH. To enhance selectivity of the enriched aptamers candidates counter SELEX cycles against PVDF membrane, negative SELEX cycles against *H*GDH protein along with the cycles with low interaction time were performed. The enriched aptamer candidates were identified by cloning, screening and sequence analysis. The sequence alignment study revealed that among the 26 positive clones two aptamer sequences, named as NG3 and NG51, showed higher enrichment compared to other sequences. The stability of both the aptamers was not much affected in solutions of high ionic strength and wide pH range. The K_d of the developed aptamers was calculated in free state and surface immobilised state via CD and SPR spectroscopy, respectively. The combination of both the studies revealed superiority of NG3 over NG51.

Using the developed aptamer (NG3) as recognition molecule we proposed four different "proof of concept" for diagnosis of malaria. (1) Protein induced fluorescence based detection of *Pf*GDH by using aptamer functionalised Cdots; (2) Development of capacitive aptasensor based detection of *Pf*GDH; (3) Development of aptaFET based sensor for detection of *Pf*GDH over extended gate field effect transistor; (4) Dye coupled aptamer-captured enzyme catalysed reaction for detection of pan malaria and *P. falciparum* species in laboratory set-up and instrument–free paper based format.

In the first approach, the aptamer (NG3) was chemically conjugated to a Cdot, which was synthesized from monosodium L-glutamate through a bottom up approach. The Cdot-aptamer assembly was successfully employed to sensitively detect *Pf*GDH by using a

principle of protein-induced fluorescence enhancement (PIFE). The detection approach was further validated in human serum sample with the spiked *Pf*GDH. The proposed detection method holds promise for sensitive detection of *P. falciparum* malaria as the dynamic range obtained in this study covers the pathological concentration of *Pf*GDH in malaria patient. The presence of potential interfering proteins namely, *Pf*LDH, *Pf*HRP-II, *H*GDH, and HSA showed lack of or poor influence on the response. The mechanism involved in PIFE was ascribed to the interaction of the Cdot with the hydrophobic cohort comprising of G-quadruplex structure of the conjugated aptamer and surrounding molecular environment in the hydrophobic pocket of the target *Pf*GDH protein. The investigation also explored the key amino acid moieties of the *Pf*GDH protein that participated in the binding with the aptamer. The key moieties involved in the interaction also emboldened the proposed hypothesis for PIFE response. The detection method proposed here has the potential to be developed as a sensitive and selective diagnosis method for malaria.

A capacitive aptasensor for selective detection of *Pf*GDH in undiluted human serum samples was developed as a part of the 2nd proof of concept. The aptasensor generated a non-Faradaic EIS signal following its binding with the target antigen (*Pf*GDH). The capacitive signal change was linearly correlated with a wide concentration range of the antigen (100 fM-100 nM). The aptasensor offered an LOD for the antigen in picomolar level. This is the first report on *Pf*GDH aptasensor exploiting non-Faradaic impedance as sensing signal. The chemical technique adapted here for the immobilization of the aptamer over the electrode surface facilitated easy and reproducible fabrication of the aptasensor. This label-free aptasensor with ultra-low LOD has great application potential for diagnosis of asymptomatic malaria and for monitoring the regression of malaria during treatment regime with antimalarial drugs. We proposed that with the advent of advance state-of-art electrochemical technology, the instrument for measuring the capacitance could be scaling down to an appropriate size for developing a hand-held aptasensor suitable for onsite applications.

In the third approach, we have developed a highly sensitive portable malaria biosensor by using extended gate field effect transistor (BioFET) with interdigitated micro gold electrodes with pseudo reference electrode for the detection of *Pf*GDH. The thiolated NG3 was co immobilised over IDμE and blocked with blocking buffer for selective capture of *Pf*GDH from a 10 fold diluted human serum over the aptaFET platform. The intrinsic surface net charge of the captured protein, combined with the folding of the

aptamer, induces shifts in the gate potential of the device, which could be correlated to the concentration of captured protein. The device could generate a dynamic detection range of 100 fM – 10 nM. The efficiency of the aptaFET sensor was further tested in diluted serum samples and was found to perform well within and beyond the relevant clinical range. The high selectivity of the sensor for *Pf*GDH was verified by testing relevant analogous human and parasitic proteins in the device. Overall, the results validated the potential application of the developed aptaFET for diagnosis of both symptomatic and asymptomatic malaria.

In our final proof of concept, we report a novel detection strategy for pan malaria and *P. falciparum* species using a dye based reaction catalysed by the biomarker enzymes *P*LDH and *Pf*GDH, respectively. For the detection, we additionally used an ssDNA aptamers specific to *P*LDH that was developed previously in our laboratory. The aptamer-captured enzymes were detected through a substrate dependent reaction coupled with the conversion of resazurin (blue, ~ $\lambda_{605\ nm}$) to resorufin (pink, ~ $\lambda_{570\ nm}$) dye. The reaction was monitored by measuring the fluorescence intensity ($\lambda_{660\ nm,}$ at excitation ~ $\lambda_{570\ nm}$) of resorufin, absorbance ratio ($\lambda_{570\ nm}$/ $\lambda_{605\ nm}$) and change in color (blue to pink). The detection approach was customized to spectrophotometer-based laboratory technique and instrument-free device. For both the approaches, the biomarker enzymes were captured from the serum samples with the help of aptamer coated magnetic beads prior to the analysis to exclude potential interferences from the serum. For the instrument free device, a medical syringe (5 ml) was prefabricated with a magnet for *in-situ* separation of the enzyme-captured beads from the reaction supernatant, which was then passed through a rolled paper wick assembled in the syringe hose. The paper wick was treated with DEAE cellulose to enhance the adsorption of dye. The presence of biomarkers could be discerned qualitatively and quantitatively based on the formation of the color and pixel intensity, respectively on the paper surface. The developed methods offered LOD in a range of 0.55 - 121 pM and detect the target enzymes in a dynamic range of 1 pM – 100 nM. Flexible detection capability, low cost, interference-free detections, and portable nature (for instrument-free devices) are the major advantages offered by the developed techniques.

Finally we attempted to perform a comparative analysis based on few performance factors among the developed biosensing platforms as shown in Table C1.

Table C.1: Comparison between different developed detection platforms.

Technique	Surface/ Probe	Sample	Linear Detection range	Target Antigen	Detection /Response time	LOD
PIFE	Cdots/ Aptamer	4 fold diluted serum	1-25 nM	*Pf*GDH	30 min/ ~10 sec	2.85 nM
Capacitance	Gold electrode/ Aptamer	Undiluted serum	100 fM-100 nM	*Pf*GDH	30 min/ ~10 min	0.77 pM
AptaFET	IDµE/Apta-mer	10 fold diluted serum	100 fM-10 nM	*Pf*GDH	30 min/ ~5 sec	48.6 pM
Absorbance based	Dye coupled reaction: Magnetic beads/ Aptamer	Undiluted serum	1 pM-100 nM	*P*LDH and *Pf*GDH	60 min/~10-30 sec	0.55 pM, 1.34 pM for *P*LDH and *Pf*GDH respectively
Fluorescence based						1.72 pM, 1.43 pM for *P*LDH and *Pf*GDH respectively
Instrument free						69.25 pM, 68.75 pM for *Pf*GDH and *P*LDH respectively

As it is clear from the table C1, the dynamic range for all the developed method are in clinically relevant range. The capacitance based aptasensor showed very broad detection range with highest sensitivity attained in term of LOD in undiluted serum conditions. The aptaFET sensor displayed very fast response time (~ 5 sec) and good sensitivity and has potential for using in POC settings. The dye based instrument free detection platform was designed focusing on low cost, portable and sensitive technique suitable to deploy in malaria endemic regions with poor health care facility. This method is based on cheap reagents and simple syringe design to avoid dependence on any kind of expensive instruments. The optical response generated over paper platform when compared with standard colour chart bar may provide tentative information about parasitic load.

Scope for future work

The investigations carried out in this thesis work is the first of its kind on aptamer based platform for detection of *Pf*GDH. However, in order to translate the proof of concepts embodied in this thesis to commercially viable products we would like to propose some points to be addressed in the next steps of research as delineated below.

(a) The exact chemical interaction between the aptamer and the target *Pf*GDH protein that confers specificity to the aptamer is to be elucidated. This information will help to set a rational design for linking the aptamer to the support materials for the proposed detection methods and techniques. The potential techniques that may be utilized to decipher the linkage chemistry are X-ray crystallography, NMR spectroscopy and Mass spectrometry among others.

(b) Our hypothesis for the PIFE on the interaction between the aptamer-Cdots conjugate and *Pf*GDH was formulated based on time resolved fluorescence and computational docking studies. The proposition needs to be validated through an in-depth investigation. The result may be helpful in optimizing the parameters for the fluorescence response.

(c) The label-free capacitance based aptasensor with ultra-low LOD has great application potential for diagnosis of asymptomatic malaria and for monitoring the regression of malaria during treatment regime with antimalarial drugs. For developing this device for commercial application, the instrument for measuring the capacitance should be scaling down to an appropriate size as a hand-held device suitable for on field applications.

(d) This miniaturized aptaFET with extended IDμE delivered label free detection capability through direct readout of the intrinsic net charge of the capture target molecule (*Pf*GDH) making the measurement easy and swift. The developed aptaFET however, needs to be integrated to a suitable miniature portable electrochemical system for recording the response and converting the data to a readable form for implementing in POC settings.

(e) The flexible detection capability of the dye coupled reaction strategy as included in the chapter 7 offers detection of both pan-malaria and *P. falciparum* specific malaria at low cost and negligible interference. However, for quantitative applications of the paper based

instrument free device, a suitable custom-made software loaded in a camera-integrated device such as, smart phone, is important that will simplify capture of the pixel response, and translation of the generated response to a digital form for determination of the biomarker concentration and its linked parasitemia level. Further, to reduce the cost of the device, the magnetic beads purchased from the company may be replaced with *in-situ* prepared magnetic nanoparticles for functionalisation with the aptamer.

Bibliography

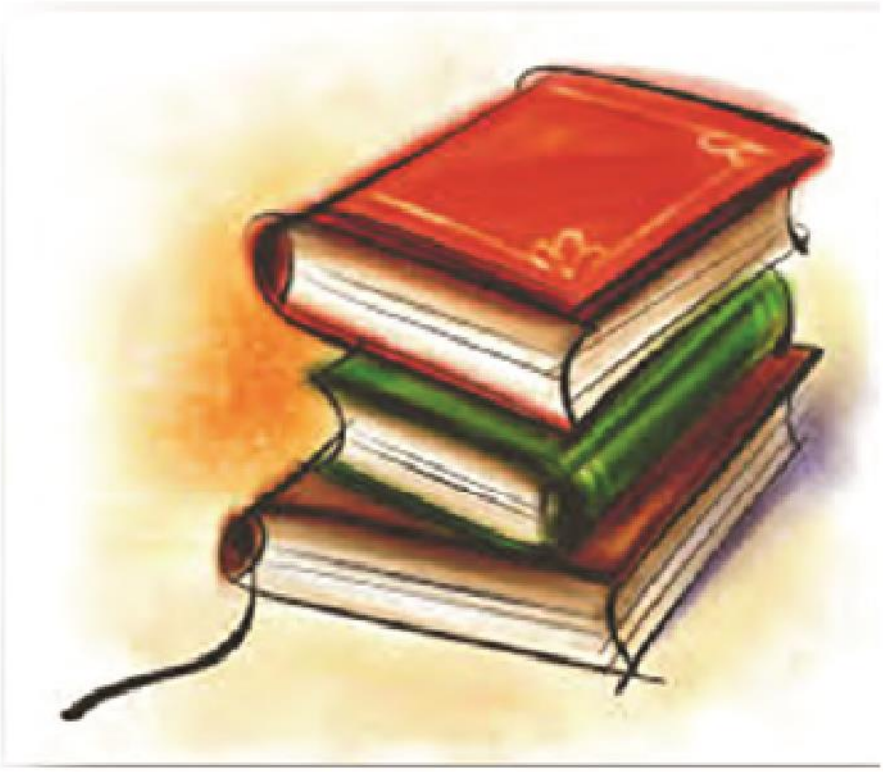

Either write something worth reading or do somthing worth writing....

- Benjamin Franklin

Bibliography

Acosta R, Domínguez., N.G., Aguilar., Girón, M. E., Characterization of *Plasmodium falciparum* glutamate dehydrogenase-soluble antigen. Braz. J. Med. Biol. Res. 31(9) 1149-1155, (1998).

Abeku, T., Kristan, M., Jones, C., Beard, J., Mueller, D., *et al.* Determinants of the accuracy of rapid diagnostic tests in malaria case management: evidence from low and moderate transmission settings in the East African highlands. Malar. J. 7, 202, (2008).

Aliakbarinodehi, N., Jolly, P., Bhalla, N., Miodek, A., De Micheli, G., Estrela, P., Carrara, S., Aptamer-based field-effect biosensor for tenofovir detection. Sci. Rep. 7, (2017).

Alias, A., Afifi, S. B., Zuraidah, R., Shukri, A., Khairul, A. A., Malaria diagnosis by quantitative buffy coat technique. Med J Malaysia. 51 (2), (1996).

Alnasser Y., Ferradas C., Clark T., Calderon M., Gurbillon A., Colorimetric Detection of *Plasmodium vivax* in Urine Using MSP10 Oligonucleotides and Gold Nanoparticles, PLOS Neglected Tropical Diseases | DOI:10.1371/journal.pntd.0005029, (2016).

Aparicio, I. M.,Marin, M., Bell, A., Engel, P. C., Susceptibility of *Plasmodium falciparum* to glutamate dehydrogenase inhibitors–apossible new antimalarial target. Mol Biochem Parasitol .172:152–5 (2010).

Araujo, A. C., Song, Y., Lundeberg, P. L. S., Brumer, H., Activated Paper Surfaces for the Rapid Hybridization of DNA through Capillary Transport. Anal. Chem. 84, 3311-3317, (2012).

Armah, H. B., Wilson, N. O., Sarfo, B.Y., Powell, M. D., Bond, V. C., *et al.* Cerebrospinal fluid and serum biomarkers of cerebral malaria mortality in Ghanaian children. Malar. J. 6, 147, (2007).

Arya, S. K., Zhurauski, P., Jolly, P., Batistuti, M. R., Mulato, M., Estrela, P., Capacitive aptasensor based on interdigitated electrode for breast cancer detection in undiluted human serum, Biosens. Bioelectron. 102, 106–112, (2018).

Avendano, A., Deluna, A., Olivera, H., Valenzuela, L. and Gonzalez, A., GDH3 encodes a glutamate dehydrogenase isozyme a previously unrecognized route for glutamate biosynthesis in *Saccharomyces cerevisiae*. J. Bacteriol., 179, 5594–5597, (1997).

Avila, P.E., Kirchgatter, K., Brunialti, K. C. S., Oliveita, A.M., Siciliano, R. F., *et al.* Evaluation of a rapid dipstick test, Malar-CheckTM, for the diagnosis of *Plasmodium falciparum* malaria in Brazil. Revista do Instituto de Medicina Tropical de São Paulo 44, 293–296, (2002).

Bajaj, G., Alstine, W. G., Yeo, Y., Zwitterionic Chitosan Derivative, a New Biocompatible Pharmaceutical Excipient, Prevents Endotoxin-Mediated Cytokine Release PLoS One, 7, e30899, (2012).

Baker, P. J., Britton, K. L., Engel, P. C., Farrants, G. W., Lilley, K. S., Rice, D. W., Stillman, T. J. Subunit assembly and active site location in the structure of glutamate dehydrogenase, Proteins: Structure Function, and Genetics 12,75286, (1992).

Baker, J., McCarthy, J., Gatton, M., Kyle, D. E., Belizario, V., *et al.* Genetic diversity of *Plasmodium falciparum* histidine rich protein 2 (PfHRP2) and its effect on the performance of *Pf*HRP2 based rapid diagnostic tests. J. Infect. Dis. 192, 870 –877, (2005).

Bang, G. S., Cho, S., Kim, B., A novel electrochemical detection method for aptamer biosensors. Biosens. Bioelectron, 21, 863–870, (2005).

Barbas III F. C., Burton R. D., Scott K. J., Silverman J. G., Quantitation of DNA and RNA, General Procedures, Appendix 3, Phage Display, Cold Spring Harbor Laboratory Press, Cold Spring Harbor, NY, USA, (2001).

Bendezu, J., Rosas, A., Grande, T., Rodriguez, H., Llanos-Cuentas, A., *et al.* Field evaluation of a rapid diagnostic test (ParascreenTM) for malaria diagnosis in the Peruvian Amazon. Malar. J. 9, 154, (2010).

Bergveld, P., Development of an ion-sensitive solid-state device for neurophysiological measurements. IEEE Trans. Biomed. Eng. BME-17, 70–71, (1970).

Berggren, C., Bjarnason, B., Johansson, G., capacitive biosensor, Electroanalysis, 13, 173–180 (2001).

Bhattacharya, J., Methods for the detection and diagnosis of malaria using an electrochemical sensor, US patent, US20130008785A1, (2011).

Bhatt, S., Weiss, D.J., Cameron, E., Bisanzio, D., Mappin, B., Dalrymple, U., Battle, K.E., Moyes, C.L., Henry, A., Eckhoff, P.A., Wenger, E.A., Briët, O., Penny, M.A., Smith, T.A., Bennett, A., Yukich, J., Eisele, T.P., Griffin, J.T., Fergus, C.A., Lynch, M., Lindgren, F., Cohen, J.M., Murray, C.L.J., Smith, D.L., Hay, S.I., Cibulskis, R.E., Gething, P.W., The effect of malaria control on *Plasmodium falciparum* in Africa between 2000 and 2015. Nature 526, 207–211, (2015).

Bjorkman, A. and Martensson, A., Risks and Benefits of Targeted Malaria Treatment Based on Rapid Diagnostic Test Results. Clin. Infect. Dis. 51(5):512–514, (2010).

Bhalla, N., Jolly, P., Formisano, N., Estrela, P., Introduction to biosensors, Essays Biochem. 60(1), 1–8, (2016).

Bharti, P. K., Chandel, S. H., Ahmad, A., Krishna, S., Kumar, U. V., Singh, N., Prevalence of pfhrp2 and/or pfhrp3 Gene deletion in *Plasmodium falciparum* population in eight highly endemic states in India. journal.pone.0157949, (2016).

Bontidean, I., Berggren, C., Johansson, G., Csoregi, E., Mattiasson, B., Lloyd, J. A., Jakeman, K. J., Brown, N. L., Detection of Heavy Metal Ions at Femtomolar Levels Using Protein-Based Biosensors. Anal. Chem. 70, 4162, (1998)

Bozdech, Z., Llinás, M., Pulliam, B. L., Wong, E. D., Zhu, J., *et al.* The transcriptome of the intraerythrocytic developmental cycle of *Plasmodium falciparum*. PLoS Biol. 1, e5, (2003).

Brince, P. K., Kumar, S., Tripathy, S., Vanjari, S. R. K., Singh, V., Singh, S. G., A highly sensitive self assembled monolayer modified copper doped zinc oxide nanofiber interface for detection of *Plasmodium falciparum* histidine-rich protein-2: Targeted towards rapid, early diagnosis of malaria. Biosens Bioelectron. 15 (80), 39-46, (2016).

Brown, W. M., Yowell, C. A., Hoard, A., Vander Jagt, T. A., Hunsaker, L. A., *et al.* Comparative structural analysis and kinetic properties of lactate dehydrogenases from the four species of human malarial parasites. Biochem. 43, 6219–6229, (2004).

Cao, L., Meziani, M. J., Sahu, S., Sun, Y. P., Photoluminescence properties of graphene versus other carbon nanomaterials. Acc. Chem. Res. 46, 171–180, (2013).

Cao, R., Guan, L., Li, M., Tian, J,, Shen, W., A zero-step functionalization on paper-based biosensing platform for covalent biomolecule immobilization. Sens. and Bio-Sens. Res, 6, 13–18, (2015).

Candiano, G., Bruschi, M., Musante, L., Santucci, L., Ghiggeri, G. M., *et al.* Blue silver: a very sensitive colloidal Coomassie G-250 staining for proteome analysis. Electrophoresis. 25,1327-33 (2004).

Candeias, L. P., MacFarlane, D. P. S., McWhinnie, S. L. W., Maidwell, N. L., Roeschlaub, C. A., Sammes, P. G., Whittlesey, R., The catalysed NADH reduction of resazurin to resorufin. J. Chem. Soc. Perkin Trans. 2 2333, 2333–2334, (1998).

Chakma, B., Jain, P., Singh, N. K., Goswami, P., Development of an indicator displacement based detection of malaria targeting HRP-II as biomarker for application in Point-of-Care Settings. Anal. Chem. 88 (20), 10316−10321, (2016).

Chakma, B., Jain, P., Singh, N. K., Goswami, P., Development of electrochemical impedance spectroscopy based aptasensor for malaria using HRP-II as target biomarker, Electroanal. 30, 1839-1846, (2018).

Chaikuad, A., Fairweather, V., Conners, R., Joseph-Horne, T., Turgut-Balik, D., *et al.* Structure of lactate dehydrogenase from Plasmodium vivax: Complexes with NADH and APADH. Biochem. 44, 16221–16228, (2005).

Chansuda, W., Rapid diagnostic techniques for malaria control. Trends Parasitol. 17, 307– 309, (2001).

Chan, D. C., Pashley, R. M., White, L. R., A Simple Algorithm for the Calculation of the Electrostatic Repulsion between Identical Charged Surfaces in Electrolyte. Journal of Coll. and Inte. Sci. 77 (1), 283–285, (1980).

Chen F., Flaherty B. R., Cohen C. E., Peterson D. S., Zhao Y., Direct detection of malaria infected red blood cells by surface enhanced Raman spectroscopy, Nanomedicine: Nanotechnology, Biology, and Medicine, 12, 1445–1451, (2016a).

Chen K., Yuen C., Aniweh Y., Preiser P., Liu Q., Towards ultrasensitive malaria diagnosis using surface enhanced Raman spectroscopy, Scientific Reports, 6:20177, (2016b).

Cheesman, S. J., The topoisomerases of protozoan parasites. Parasitol. Today. 16(7): 277-281 (2000).

Chen, M. M., Shi, L., Sullivan Jr., D.J., Haemoproteus and Schistosoma synthesize heme polymers similar to *Plasmodium* hemozoin and β-hematin. Mol. Biochem. Parasitol. 113, 1–8, (2001).

Chen K., Chou L. Y. T., Song F., Chan W. C. W., Fabrication of metal nano shell quantum-dot barcodes for bio molecular detection, Nano Today8, 228—234, (2013).

Cheung, Y.W., Kwok, J., Law, A., W., Watt, R., M., Kotaka, M., *et al.* Structural basis for discriminatory recognition of *Plasmodium* lactate dehydrogenase by a DNA aptamer PNAS. 110, 15967-72, (2013).

Chiodini, P.L., Bowers, K., Jorgensen, P., Barnwell, J.W., Grady, K.K., *et al.* The heat stability of *Plasmodium* lactate dehydrogenase-based and histidine-rich protein 2-

based malaria rapid diagnostic tests. Trans. R. Soc. Trop. Med. Hyg. 101, 331–337, (2007).

Chi, L.L., Chou, J.C., Chung, W.Y., Sun, T.P., Hsiung, S.K., Study on extended gate field effect transistor with tin oxide sensing membrane. Mater. Chem. Phys. 63, 19–23, (2000).

Cho, S. W., Lee, J., Choi S. Y., Two soluble forms of glutamate dehydrogenase isoproteins from bovine brain. Eur. J. Biochem. 233, 340–346, (1995).

Cho, E.J., Lee, J.W., Ellington, A.D., Applications of aptamers as sensors. Annu. Rev. Anal. Chem. 2, 241–264, (2009).

Chu, C. H, Sarangadharan, I., Regmi, A., Chen, Y. W., Hsu, C. P., Chang, W. H., Lee, G. Y., Chyi J. I., Chen, C. C., Shiesh, S. C., Lee, G. B, Wang, Y. L., Beyond the Debye length in high ionic strength solution: direct protein detection with field-effect transistors (FETs) in human serum, Sci. Rep. 7, 5256, (2017).

Chung, C. T., Niemela, S. L., Miller, R. H. One-step preparation of competent *Escherichia coli*: Transformation and storage of bacterial cells in the same solution. Proc Natl Acad Sci. 86, 2172-2175 (1989).

Centers for disease control and prevention, (2016), (https://www.cdc.gov/immigrantrefugeehealth/pdf/malaria-overseas.pdf).

Claudia M. Dollins, Smita Nair, and B.A.S., Aptamers in immunotherapy 19, 443-449, (2008).

Conners, R., Schambach, F., Read, J., Cameron, A., Sessions, R.B., *et al.* Mapping the binding site for gossypol-like inhibitors of *Plasmodium falciparum* lactate dehydrogenase. Mol. Biochem. Parasitol. 142, 137–148, (2005).

Conroy, A., Lafferty, E., Lovegrove, F., Krudsood, S., Tangpukdee, N., *et al*. Whole blood angiopoietin-1 and -2 levels discriminate cerebral and severe (non-cerebral) malaria from uncomplicated malaria. Malar. J. 8,295, (2009).

Colon, A., Plaitakis, A., Perakis, A,, Berl, S. & Clarke, D. D., Purification and characterization of a soluble and a particulate glutamate dehydrogenase from rat brain. J. Neurochem. 46, 1811-3829, (1986).

Cole, K. S., Cole, R. H., Dispersion and absorption in dielectrics I. Alternating current characteristics. J. Chem. Phys. 9 (4), 341-351, (1941).

Consalvi, V., Chiaraluce, R., Politi, L., Vaccaro, R., De Rosa, M., Scandurra, R., Extremely thermostable glutamate dehydrogenase from the hyperthermophilic archaebacterium *Pyrococcus furiosus*. Eur J Biochem. 202:1189-1196, (1991).

Credou, J., Volland, H., Dano, J., Berthelot, T. J., A one-step and biocompatible cellulose functionalization for covalent antibody immobilization on immunoassay membranes. J. Mater. Chem. B. 1, 3277– 3286, (2013).

Cunliffe, D., Leason, M., Parkin, D. & Lea, P., The inhibition of glutamate dehydrogenase by derivatives of isophthalic acid. Phytochemistry 22, 1357–1360, (1983).

Das, C., Nayak, V., Raghothama, S., Balaram, P., Synthetic protein design: construction of a four-stranded b-sheet structure and evaluation of its integrity in methanol±water systems. J. Peptide Res, 56, 307-317, (2000).

Dash, R., Ghosh, S. K., Kaplan, D. L., Kundu, S. C., Purification and biochemical characterization of a 70 kDa sericin from tropical tasar silkworm, *Antheraea mylittaComp*. Biochem Physiol B Biochem Mol Biol, 147: 129–34, (2007).

Dal-Bianco, M., Köster K., Kombila, U., Kun, J.F.J., Grobusch, M., *et al.* High prevalence of asymptomatic *Plasmodium falciparum* infection in Gabonese adults. Am. J. Trop. Med. Hyg. 77(5), pp. 939–942, (2007).

Daniels, J. S., Pourmand, N., Label-free impedance biosensors: Opportunities and challenges. Electroanalysis, 19 (12), 1239–1257, (2007).

Davis, G., Thornalley, P. J., 1983. Free radical production from the aerobic oxidation of reduced pyridine nucleotides catalysed by phenazine derivatives. BBA - Bioenerg. 724, 456–464, (1983).

de Dominguez, N., Rodriguez, A., Acosta, A., Glutamate dehydrogenase antigen detection in *Plasmodium falciparum* infections. Korean J. Parasitol. 34 (4), 239−46, (1996).

de Oliveira, A. M., Skarbinski, J., Ouma, P. O., Kariuki, S., Barnwell, J. W., Performance of malaria rapid diagnostic tests as part of routine malaria case management in Kenya. Am. J. Trop. Med. Hyg. 80, 470 –474, (2009).

de Souza Castilho, M., Laube, T., Yamanaka, H., Alegret, S., Pividori, M.I., Magneto immunoassays for *Plasmodium falciparum* histidine rich protein 2 related to malaria based on magnetic nanoparticles. Anal. Chem. 83, 5570–5577, (2011).

Delahunt C., Horning P. M., Wilson K. B., Proctor L. J., Hegg C. M., *et al.* Limitations of haemozoin-based diagnosis of *Plasmodium falciparum* using dark-field microscopy, Malar. J., 13:147, (2014).

Ding, Y., Ling, J., Wang, H., Zou, J., Wang, K., Xiao, X., Yang, M., Fluorescent detection of Mucin 1 protein based on aptamer functionalized biocompatible carbon dots and graphene oxide, Anal. Methods,7, 7792-7798 , (2015).

Dirkzwager, R.M., Kinghorn, A.B., Richards, J.S., Tanner, J.A., APTEC: aptamer tethered enzyme capture as a novel rapid diagnostic test for malaria. Chem. Commun. 51, 4697-700, (2015).

Dirkzwager M. R., Liang S., Tanner A. J., Development of Aptamer-Based Point-of-Care Diagnostic Devices for Malaria Using Three-Dimensional Printing Rapid Prototyping, ACS Sens. 1, 420−426, (2016).

Djadiad, N. D., Sedighion, F., Raj, A., Zakeri, S. Gold nanoparticle based dipstick nano biosensor for detecting *Plasmodium falciparum* and *vivax* and method. US patent. US 2014/0248629 A1, (2014).

Döbeli, H., Trzeciak, A., Gillessen, D., Matile, H., Srivastava, I.K., *et al*. Expression, purification, biochemical characterization and inhibition of recombinant *Plasmodium falciparum* aldolase. Mol Biochem Parasitol. 41(2):259-68, (1990).

Dunn, C. R., Banfield, M. J., Barker, J. J., Higham, C. W., Moreton, K. M., The structure of lactate dehydrogenase from *Plasmodium falciparum* reveals a new target for anti-malarial design. Nat. Struct. Mol. Biol. 3, 912–915, (1996).

Dutta, G., Lillehoj, P.B., An ultrasensitive enzyme-free electrochemical immunosensor based on redox cycling amplification using methylene blue. Analyst. 142, 3492-3499, (2017).

Dutta, G., Nagarajan, S., Lapidus, L.J., Lillehoj, P.B., Enzyme-free electrochemical immunosensor based on methylene blue and the electro-oxidation of hydrazine on Pt nanoparticles. Biosens Bioelectron. 92, 372-377, (2017).

Eisen, D. P., Saul, A., Disappearance of pan-malarial antigen reactivity using the ICT Malaria P.f/ P.v TM kit parallels decline of patent parasitaemia as shown by microscopy. Trans. R. Soc. Trop. Med. Hyg. 94, 169–170, (2000).

Elana, M. S., Ciuba, M. A., Lin, S., Levitus, M., Demystifying PIFE: The photophysics behind the protein-induced fluorescence enhancement phenomenon in Cy3. J. Phys. Chem. Lett. 6, 1819−1823, (2015).

Ellington, A. D., Szostak, J. W. In vitro selection of RNA molecules that bind specific ligands. Nature. 346, 818-822 (1990).

Estrela, P., Migliorato, P., Chemical and biological sensors using polycrystalline silicon TFTs. J. Mater. Chem. 17, 219-224, (2007).

Estrela, P., Paul, D., Song, Q., Stadler, L. K. J., Wang, L., Huq, E., Davis, J. J., Ko Ferrigno, P., Migliorato, P., Label Free Sub-picomolar Protein Detection with Field-Effect Transistors. Anal. Chem. 82, 3531-3536, (2010).

Formisano, N.; Bhalla, N.; Heeran, M.; Reyes Martinez, J.; Sarkar, A.; Laabei, M.; Jolly, P.; Bowen, C. R.; Taylor, J. T.; Flitsch, S.; Estrela, P., Inexpensive and fast pathogenic bacteria screening using field-effect transistors. Biosens. Bioelectron. 85, 103-109, (2016).

Feldman, A. B., Progress toward rapid malaria screening based on mass spectrometry. 2006, Lab Tech. Link: http://www.cli-online.com/fileadmin/artimg/progress-toward-rapidmalaria- screening-based-on-mass-spectrometry.pdf

Fernando, K. S., Sahu, S., Liu, Y., Lewis, W. K., Guliants., Jafariyan, A., Wang, P., Bunker, C. E., Sun, Y. P., Carbon Quantum Dots and Applications in Photocatalytic Energy Conversion. ACS Appl. Mater. Interfaces. 7, 8363–8376, (2015).

Fisher H. F., L glutamate dehydrogenase from bovine liver. Methods Enzymol.,113, 16-27, 1985.

Fitch, C. D., Kanjananggulpan, P., The state of ferriprotoporphyrin IX in malaria pigment. J. Biol. Chem. 262, 15552–15555, (1987).

Fleischer, B., Editorial: 100 years ago: Giemsa's solution for staining of *Plasmodia*. Trop. Med. Int. Health. 9, 755–756, (2004).

Föger, F., Noonpakdee, W., Loretz, B., Joojuntr, S., Salvenmoser, W., Thaler, M., Bernkop, S. A., Inhibition of malarial topoisomerase II in *Plasmodium falciparum* by antisense nanoparticles. Int. J. Pharm. 17;319(1-2):139-46, (2006).

Fogg, C., Twesigye, R., Batwala, V., Piola, P., Nabasumba, C., *et al.* Assessment of three new parasite lactate dehydrogenase (pan-pLDH) tests for diagnosis of uncomplicated malaria. Trans. R. Soc. Trop. Med. Hyg. 102, 25–31, (2008).

Forney, J.R., Magill, A.J., Wongsrichanalai, C., Sirichaisinthop, J., Bautista, C.T., *et al.* Malaria rapid diagnostic devices: performance characteristics of the ParaSight F device determined in a multisite field study. J. Clin. Microbiol. 39, 2884–2890, (2001).

Freyssinet, J.M., Cellular microparticles: what are they bad or good for. J. Thromb. Haemost. 1, 1655–1662, (2003).

Frank, R., Hargreaves, R., Clinical biomarkers in drug discovery and development. Nat. Rev. Drug Discov. 2, 566–580, (2003).

Francis, S. E, Sullivan, D. J., Goldberg, D. E., Hemoglobin metabolism in the malaria parasite *Plasmodium falciparum*. Annu Rev Microbiol 51: 97–123, (1997).

Fraser, L. A., Kinghorn, A. B., Dirkzwager, R. M., Liang, S., Cheung, Y. W., Lim, B., Shiu, S. C. C., Tang, M. S. L., Andrew, D., Manitta, J., Richards, J. S., Tanner, J. A., A portable microfluidic Aptamer-Tethered Enzyme Capture (APTEC) biosensor for malaria diagnosis. Biosens. Bioelectron. 100, 591–596, (2018).

Gallup, J. K., Sachs, J. D., The Economic Burden of Malaria, American Society of Tropical Medicine and Hygiene. Am. J. Trop. Med. Hyg. 64 (12), 85–96, (2001).

Gamboa, D., Ho, M.-F., Bendezu, J., Torres, K., Chiodini, P.L., *et al.* A large proportion of *P. falciparum* isolates in the amazon region of Peru lack pfhrp2 and pfhrp3: implications for malaria rapid diagnostic tests. PLoS ONE 5, e8091, (2010).

Gardner, M. J., Hall, N., Fung, E., White, O., Berriman, M., Hyman, R.W., Carlton, J. M., Pain, A., Nelson, K. E., Bowman, S., Paulsen, I. T, James, K., Eisen, J. A, Rutherford, K., Salzberg, S. L., Craig, A., Kyes, S., Chan, M. S, Nene, V., Shallom, S. J., Suh, B., Peterson. J., Angiuoli, S., Pertea, M., Allen, J., Selengut, J., Haft, D., Mather, M. W., Vaidya, A. B., Martin, D. M., Fairlamb, A. H., Fraunholz, M. J., Roos, D. S., Ralph, S.A., McFadden, G. I., Cummings, L. M., Subramanian G. M., Mungall, C., Venter, J. C., Carucci, D. J., Hoffman, S. L., Newbold, C., Davis R. W., Fraser, C. M., Barrell, B., Genome sequence of the human malaria parasite *Plasmodium falciparum*. Nature 2002, 419:498-511, (2012).

Garrett L. N., Sekine R., Dixon A. W. M., Tilley L., Bamberye R. K., *et al*. Bio-sensing with butterfly wings: naturally occurring nano-structures for SERS-based malaria parasite detection, Phys. Chem. Chem. Phys., 17, 21164, (2015).

Garbett, N. C., Ragazzon, P. A., Chaires, J. B., Circular dichroism to determine binding mode and affinity of ligand–DNA interactions. Nat. Protoc. 2, 3166–3172, (2007).

Gast, K., Damaschun, H., Eckert, K., Schulze-Forster, K., Maurer, H. R., Müller-Frohne, M., Zirwer, D., Czarnecki, J., & Damaschun, G., NACP, A Protein Implicated in Alzheimer's Disease and Learning, Is Natively Unfolded Biochemistry 34, 13211−13218, (1995).

Geldert K.A., Zhang, X., Zhang, H., Lim, C.T., Highly Sensitive and Selective Aptamer Based Fluorescence Detection of a Malarial Biomarker Using Single-Layer MoS2 Nanosheets, ACS Sens. 1, 1315−1321, (2016).

Gibson, L.E., Wright, D.W., Sensitive Method for Biomolecule Detection Utilizing Signal Amplification with Porphyrin Nanoparticles. Anal. Chem. 88, 5928–5933, (2016).

Givskov, A., Kristoffersen, E. L., Vands, K., Ho, Y. Pi., *et al*. Optimized Detection of *Plasmodium falciparum* Topoisomerase I Enzyme Activity in a Complex Biological Sample by the Use of Molecular Beacons. Sensors, 16(11), 1916, (2016).

Gikunoo E., Abera A., Woldesenbet E., A Novel Carbon Nanofibers Grown on Glass Microballoons Immunosensor: A Tool for Early Diagnosis of Malaria, Sensors, 14, 14686- 14699, (2014).

Goncalves, L., Subtil, A., de Oliveira, M.R., Rosario, V., Lee, P.W., *et al.* Bayesian latent class models in malaria diagnosis. Plos one. 7, e40633, (2012).

Goda, T., Miyahara, Y., Interpretation of protein adsorption through its intrinsic electric charges: A comparative study using a field-effect transistor, surface plasmon resonance, and quartz crystal microbalance. Lang. 28 (41), 14730–14738, (2012).

Goda, T., Miyahara, Y., Label-free and reagent-less protein biosensing using aptamer-modified extended-gate field-effect transistors. Biosen. And Bioelectr. 45, 89–94, (2013).

Godonoga M., Lin Y-T., Oshima A., Sumitomo K., Tang M., *et al.* A DNA aptamer recognising a malaria protein biomarker can function as part of a DNA origami assembly, Sci. Rep., 6:21266, (2016).

Guo S, Dong S. Biomolecule-nanoparticle hybrids for electrochemical biosensors. Trends Anal Chem 28:96-109, (2009).

Gulka, C. P., Swartz, J. D., Trantum, J. R., Davis, K. M., Peak, C. M., Denton, A. J., Haselton, F. R., Wright, D. W., Coffee rings as low- resource diagnostics: Detection of the malaria biomarker *Plasmodium falciparum* histidine-rich protein-II using a surface-coupled ring of Ni(II)NTA gold-plated polystyrene particles. ACS Appl. Mater. Interfaces. 6, 6257−6263, (2014).

Guirgis B. S. S., Cunha C. S., Gomes I., Cavadas M., Silva I., *et al.* Gold nanoparticlebased fluorescence immunoassay for malaria antigen detection, Anal Bioanal Chem, 402:1019–1027, (2012).

Green, M. R., Sambrook, J. Molecular Cloning: a laboratory manual-4th ed. Cold Spring Harbour Laboratory Press, Cold Spring Harbour, New York, USA (2012).

Green, R. J., Frazier, R. A., Kevin, M. S., Martyn, C. D., Clive J. R., Saul J. B. T., Surface plasmon resonance analysis of dynamic biological interactions with biomaterials. Biomaterials, 21 1823-1835, (2000).

Haest, C.W., Interactions between membrane skeleton proteins and the intrinsic domain of the erythrocyte membrane. Biochim. Biophys. Acta. 694, 331–352, (1982).

Hede, M. S., Fjelstrup, S., Lötsch, F., Zoleko, R. M., Klicpera, A., Groger, M., Mischlinger, J., *et al*. Detection of the Malaria causing *Plasmodium* Parasite in Saliva from Infected Patients using Topoisomerase I Activity as a Biomarker. Scie. Rep. 8, 4122, **(2018**).

Hemben, A., Ashley, J., Tothill, I.E., Development of an Immunosensor for *Pf*HRP 2 as a Biomarker for Malaria Detection. Biosensors. 7, 28-42. (2017).

Hicke, B. J., Stephens, A. W., Escort aptamers a delivery service for diagnosis and therapy. J. Clin. Invest. 106 (8), 923−928, (2000).

Howard, R.J., Uni, S., Aikawa, M., Aley, S.B., Leech, J.H., Secretion of a malarial histidine-rich protein (*Pf*HRP II) from *Plasmodium falciparum* infected erythrocytes. J. Cell Biol. 103, 1269–1277, (1986).

Hudson, R. C., Daniel, R. M., L-Glutamate dehydrogenases: distribution, properties and mechanism. Comp Biochem Physiol 106B, 767–792, (1993).

Hulka, B., Epidemiologic Studies Using Biological Markers - Issues for Epidemiologists. Cancer Epidemiol. Biomarkers Prev. 1, 13–19, (1991).

Hurdayal, R., Achilonu, I., Choveaux, D., Coetzer, T. H. T., Goldring, D. J. P., Antipeptide antibodies differentiate between *plasmodial* lactate dehydrogenases. Peptides. 31, 525–532, (2010).

Hwang, H., Myong, S., Protein induced fluorescence enhancement (PIFE) for probing protein–nucleic acid interactions. Chem Soc Rev. 21, 1221–1229, (2014).

Iqbal J, Sher A, Rab, A., *Plasmodium falciparum* histidine rich protein 2-based immunocapture diagnostic assay for malaria: cross-reactivity with rheumatoid factors. J. Clin. Microbiol. 38 (3): 1184–1186, (2000).

Iqbal, J., Sher, A., Rab, A., *Plasmodium falciparum* histidine rich protein 2-based immunocapture diagnostic assay for malaria: cross-reactivity with rheumatoid factors. J. Clin. Microbiol. 38, 1184–1186, (2002).

Iqbal, J., Siddique, A., Jameel, M., Hira, P.R., Persistent histidine rich protein 2, parasite lactate dehydrogenase and pan malarial antigen reactivity after clearance of *Plasmodium falciparum* monoinfection. J. Clin. Microbiol. 42, 4237–4241, (2004).

Jain, P., Chakma, B., Goswami, P., Potential Biomarkers and Their Applications for Rapid and Reliable Detection of Malaria. Biomed Res. Int. 2014, 852645, (2014).

Jain, P., Chakma, B., Singh, N.K., Patra, S., Goswami, P., Aromatic surfactant as aggregating agent for aptamer-gold nanoparticle based detection of *Plasmodium* lactate dehydrogenase. Mol. Biotechnol. 58, 497–508, (2016a).

Jain, P., Das, S., Chakma, B., Goswami, P., Aptamer-graphene oxide for highly sensitive dual electrochemical detection of *Plasmodium* lactate dehydrogenase. Anal. Biochem. 514, 32–37, (2016b).

Jain, P., Chakma, B., Singh, N.K., Patra, S., Goswami, P., Metal-DNA interactions improve signal in high resolution melting of DNA for species differentiation of *Plasmodium* parasite, Mol. Biotec. 59 (6), 179-191, (2017).

Jang, J. W., Cho, C. H., Han, E.T., An, S. S. A., Lim, C. S., 2013. *P*LDH level of clinically isolated *Plasmodium vivax* and detection limit of *P*LDH based malaria rapid diagnostic test. Malar. J. 12 (1), 12-18, (2013).

Jayant, K., Singhai, A., Cao, Y. Q., Phelps, J. B., Lindau, M., Holowka, D. A., Baird, B. A., Kan, E. C., Non-Faradaic Electrochemical Detection of Exocytosis from Mast and Chromaffin Cells Using Floating-Gate MOS Transistors Sci. Rep, 5, No. 18477, (2015)

Jensen, M.D., Conley, M., Helstowski, L.D., Culture of *Plasmodium falciparum*: The role of pH, glucose, and lactate. J. Parasitol. 69, 1060–1067, (1983).

Jeannot A. M., Zheng J., Li L., Observation of Sodium Gel-Induced Protein Modifications in Dodecylsulfate Polyacrylamide Gel Electrophoresis and Its Implications for Accurate Molecular Weight Determination of Gel-Separated Proteins by Matrix-Assisted Laser Desorption Ionization Time-of-Flight Mass Spectrometry, J Am Soc Mass Spectrom. 10, 512–520 (1998).

Jeon, W., Lee, S., Manjunatha, D., H., Ban, C., A colorimetric aptasensor for the diagnosis of malaria based on cationic polymers and gold nanoparticles. Anal. Biochem. 439, 11–16, (2013).

Jimenez, A., Channer, R., Perera, R., Gamboa, D., Chiodini, P. L., González, I. J., Mayor, A., Ding, X. C., Analytical sensitivity of current best-in-class malaria rapid diagnostic tests Malar. J. 16, 128, (2017).

John, C. C., Panoskaltsis-Mortari, A., Opoka, R. O., Park, G. S., Orchard, P. J., *et al.* Cerebrospinal fluid cytokine levels and cognitive impairment in cerebral malaria. Am. J. Trop. Med. Hyg. 78, 198 – 205, (2008).

Jorgensen, P., Chanthap, L., Rebueno, A., Tsuyuoka, R., Bell, D., Malaria rapid diagnostic tests in tropical climates: the need for a cool chain. Am. J. Trop. Med. Hyg. 74, 750–754, (2006).

Jolly, P., Formisano, N., Tkac, J., Kasák, P., Frost, C.G., Estrela, P., Label-free impedimetric aptasensor with antifouling surface chemistry: A prostate specific antigen case study Sens. Actuators B 209, 306–312, (2015).

Joshi, H., Markers for population genetic analysis of human *Plasmodia* species, P. falciparum and P. vivax, J. Vect. Borne. Dis, 40, 78–83, (2003).

Kang J., Liu Y., Xie M.X., Li S., Jiang M., *et al.* Interactions of human serum albumin with chlorogenic acid and ferulic acid, Biochim. Biophys. Acta. 1674, 205–214, (2004).

Kasetsirikul, S., Buranapong, J., Srituravanich, W., Kaewthamasorn, M., Pimpin, A., The development of malaria diagnostic techniques: a review of the approaches with focus on dielectrophoretic and magnetophoretic methods. Malar. J. 15, 358, (2016).

Kelly, A., Stanley, C. A., Disorders of glutamate metabolism. Ment Retard Dev Disabil Res Rev. 7:287-295, (2001).

Kemp, D. J., Coppel, R. L., Anders, R. F., Repetitive proteins and genes of malaria. Ann. Rev. Microbio. 181-208, (1987).

Keough, D. T., Ng, A. L., Winzor, D. J., Emmerson, B. T., de Jersey, J., Purification and characterization of *Plasmodium falciparum* hypoxanthine–guanine–xanthine phosphori- bosyltransferase and comparison with the human enzyme. Mol. Biochem. Parasitol. 98, 29–41, (1999).

Kichey, T., Gouis, J. L., Sangwan, B., Hirel, B., Dubois, F., Changes in the cellular and subcellular localization of glutamine synthetase and glutamate dehydrogenase during flag leaf senescence in wheat (*Triticum aestivum L*.) Plant Cell Physiol.;46:964–974, (2005).

Kikin, O., D'Antonio, L., Bagga, P. S. QGRS Mapper: a web-based server for predicting G quadruplexes in nucleotide sequences. Nucleic Acids Res.34, W676-682 (2006).

Kilejian, A., A unique histidine rich polypeptide from the malaria parasite, *Plasmodium lophurae*. J. Biol. Chem. 249, 4650–4655, (1974).

Kilejian, A., Histidine-Rich Protein as a Model Malaria Vaccine. Science. 201, 922–924, (1978).

Kim, H., Certa, U., Döbeli, H., Jakob, P., Hol, W. J., Crystal Structure of Fructose-1,6-bisphosphate Aldolase from the Human Malaria Parasite *Plasmodium falciparum.* Biochem. 30:37 (13), 4388-96, (1998).

Kim, C., Searson, P.C., Detection of *Plasmodium* Lactate Dehydrogenase Antigen in Buffer Using Aptamer-Modified Magnetic Microparticles for Capture, Oligonucleotide-Modified Quantum Dots for Detection, and Oligonucleotide-Modified Gold Nanoparticles for Signal Amplification. Bioconjug. Chem. 28, 2230–2234, (2017).

Kim, J. Y., Choi, K., Moon, D. I., Ahn, J. H., Park, T. J., Lee, S.Y., Choi, Y. K., Surface engineering for enhancement of sensitivity in an underlap-fet biosensor by control of wettability. Biosens. Bioelectron. 41, 867–870, (2013).

Kimoto, M., Yamashige, R., Matsunaga, K., Yokoyama, S., Hirao, I., Generation of high affinity DNA aptamers using an expanded genetic alphabet. Nat. Biotechnol. 31, 453- 457, (2013).

Kaisti, M., Field-effect based chemical and biological sensing: theory and implementation, Ph.D. thesis, University of Turku. (2016).

Kaisti, M., Detection principles of biological and chemical FET sensors, Biosen. Bioelec. 98, 437–448, (2017).

Kakoti A., Goswami P., Multifaceted analyses of the interactions between human heart type fatty acid binding protein and its specific aptamers, Biochim. Biophys. Acta. 1861(1), 3289– 3299, (2017).

Kakoti, A., Siddiqui, M.F., Goswami, P., A low cost design and fabrication method for developing a leak proof paper based microfluidic device with customized test zone. Biomicrofluidics. 9, 502-524, (2016).

Knapp, B., Hundt, E., Küpper, H. A., *Plasmodium falciparum* aldolase: gene structure and localization. Mol. Biochem. Parasitol, 40 (1),1-12, (1990).

Kongdee, A., Bechtold, T., Teufel, L. J., Modification of Cellulose Fiber with Silk Sericin. Appl. Poly. Sci, 96, 1421–1428, (2005).

Kraemer, S., Vaught, J. D., Bock, C., Gold, L., Katilius, E., *et al.* From SOMAmer based biomarker discovery to diagnostic and clinical applications: a SOMAmer-based, streamlined multiplex proteomic assay. PLos One. 6, e26332, (2011).

Klein, R., Lin, E., Zhang, B., Luster, A., Tollett, J., *et al*. Neuronal CXCL10 directs CD8 T-cell recruitment and control of west nile virus encephalitis. J. Virol. 79, 11457–11466, (2005).

Koita, O.A., Doumbo, O.K., Ouattara, A., Tall, L.K., Konaré, A., Diakité, M., Diallo, M., Sagara, I., Masinde, G.L., Doumbo, S.N., Dolo, A., Tounkara, A., Traoré, I., Krogstad, D.J., False-negative rapid diagnostic tests for malaria and deletion of the histidine-rich repeat region of the hrp2 gene. Am. J. Trop. Med. Hyg. 86, 194–198, (2012).

Kongdee, A., Bechtold, T., Teufel, L., Modification of cellulose fiber with silk sericin. J. Appl. Poly. Sci. 96, 1421–1428, (2005).

Kyabayinze, D., Tibenderana, J., Odong, G., Rwakimari, J., Counihan, H., Operational accuracy and comparative persistent antigenicity of HRP2 rapid diagnostic tests for Plasmodium falciparum malaria in a hyperendemic region of Uganda. Malar. J. 7, 221, (2008).

Kunte, R., Kunwar, R., WHO Guidelines for the treatment of malaria, MJAFI. 67 (4), 376, (2011).

Kumar, N., Pande, V., Bhatt, R.M., Shah, N. K., Mishra, N., Srivastava, B., Valecha, N., Anvikar, A. R., Genetic deletion of HRP2 and HRP3 in Indian *Plasmodium falciparum* population and false negative malaria rapid diagnostic test. Acta Trop. 125, 119–121, (2013).

Laemmli, U. K. Cleavage of structural proteins during the assembly of the head of bacteriophage T4. Nature. 227, 680–685, (1970).

Lane, A. N., Chaires, J. B., Gray, R. D., Trent, J. O., Stability and kinetics of G-quadruplex structures. Nucleic Acids Res. 36, 5482–5515, (2008).

Lau, Y.L., Fong, M.Y., Mahmud., R., Chang., P.Y., Palaeya, V., *et al.* Specific, sensitive and rapid detection of human *Plasmodium knowlesi* infection by loop mediated isothermal amplification in blood samples. Malar. J. 10,197, (2011).

Laue, T. M., Shah, B. D., Ridgeway, T. M., Pelletier, S. L. Analytical ultracentrifugation in biochemistry and polymer science (pp. 90–125). Cambridge: Royal Society of Chemistry, (1992).

Lathwal, S., Sikes, H.D., Assessment of colorimetric amplification methods in a paperbased immunoassay for diagnosis of malaria. Lab Chip. 16, 1374-82, (2016).

Lee, N., Baker, J., Andrews, K.T., Gatton, M.L., Bell, D., *et al.* Effect of sequence variation in *Plasmodium falciparum* histidine rich protein 2 on Binding of specific monoclonal antibodies: implications for rapid diagnostic tests for malaria. J. Clin. Microbiol. 44, 2773–2778, (2006a).

Lee, J.S.; Lytton-Jean, A.K.R.; Hurst, S.J.; Mirkin, C.A. Silver nanoparticle oligonucleotide conjugates based on DNA with triple cyclic disulfide moieties. Nano Lett. 7, 2112-2115, (2007).

Lee, P.W., Ji, D.D., Liu, C.T., Rampao, H.S., Rosario. V., *et al.* Application of loop mediated isothermal amplification for malaria diagnosis during a follow up study in Sao Tome. Malar. J.11, 408, (2012a).

Lee, S., Song, K.M., Jeon, W., Jo, H., Shim, Y.B., Ban, C., A highly sensitive aptasensor towards *Plasmodium* lactate dehydrogenase for the diagnosis of malaria. Biosens. Bioelectron. 35, 291–296, (2012b).

Lee, S., Manjunatha, H. D., Jeon, W., Ban, C., Cationic surfactant-based colorimetric detection of *Plasmodium* lactate dehydrogenase, a biomarker for Malaria, using the specific DNA aptamer. PLoS One. 9 (7), e100847, (2014).

Leech, J., Barnwell, J., Aikawa, M., Miller, L., Howard, R., *Plasmodium falciparum* malaria association of knobs on the surface of infected erythrocytes with a histidine-rich protein and the erythrocyte skeleton. J. Cell Biol. 98, 1256–1264, (1984).

Lew, V. L., Tiffert, T., Ginsburg, H., Excess hemoglobin digestion and the osmotic stability of *Plasmodium falciparum*–infected red blood cells. Blood, 101, 4189-4194, (2003).

Li, Y., Ning, Y.S., Li., L., Peng, D.D., Dong, W.Q., *et al.* Preparation of a monoclonal antibodies against *Plasmodium falciparum* glutamate dehydrogenase and establishment of colloidal gold-immunochromatographic assay. Di Yi Jun Yi Da Xue Xue Bao. 25(4):435-8, (2005).

Li, S., Guo, Z., Zhang, Y., Xue, W., Liu, Z., Blood Compatibility Evaluations of Fluorescent Carbon Dots. Appl. Mater. Interfaces. 7 (34), 19153–19162, (2015).

Li, Tao., Wang, E., Dong, D., Parallel G-Quadruplex-specific fluorescent probe for monitoring DNA structural changes and fabel-free detection of potassium ion. Anal. Chem. 82, 7576–7580, (2010).

Li, X., Ballerini, D. R., Shen, W., A perspective on paper-based microfluidics: Current status and future trends. Biomicrofluidics 6, (2012). doi:10.1063/1.3687398

Lightfoot, D. A., A. J. Baron, and J. C. Wootton., Expression of the *Escherichia coli* glutamate dehydrogenase gene in the *Cyanobacterium Synechococcus* PCC6301 causes ammonium tolerance. Plant Mol. Biol. 11:335– 344, (1988).

Lin, S. P., Vinzons, L. U., Kang, Y. S., Lai, T. Y., Non-Faradaic electrical impedimetric investigation of the interfacial effects of neuronal cell growth and differentiation on silicon nanowire transistors ACS Appl. Mater. Interfaces, 7, 9866, (2015).

Lillehoj, P.B., Huang, M.C., Truongc, N., Hod , C.M., Rapid electrochemical detection on a mobile phone. Lab Chip.13, 2950-2955, (2013).

Liu, J., Chisti, M.M., Zeng, X., General Signal Amplification Strategy for Nonfaradic Impedimetric Sensing: Trastuzumab Detection Employing a Peptide Immunosensor. Anal. Chem. 89, 4013–4020, (2017).

Liu, J., Liu, H., Li, Y., Wang, H., Probing the coordination properties of glutathione with transition metal ions (Cr2+, Mn2+, Fe2+, Co2+, Ni2+, Cu2+, Zn2+, Cd2+, Hg2+) by density functional theory. J. Biol. Phys. 40, 313-323**, (**2012).

Liu, B., Lu, L., Hua, E., Jiang, S., Xie, G., Detection of the human prostate- specific antigen using an aptasensor with gold nanoparticles encapsulated by graphitized mesoporous carbon. Microchim. Acta 178, 163–170, (2012).

Liu, J. M., Lin, L., Wang, X. X., Lin, S. Q., Cai, W. L., Zhang, L. H., Zheng, Z. Y., Highly selective and sensitive detection of Cu2+ with lysine enhancing bovine serum albumin modified-carbon dots fluorescent probe. Analyst. 137, 2637, (2012).

Liu, Z., Jiang, T., Wang, B., Ke, B., Zhou, Y., Du, L., Li, M., Environment-Sensitive Fluorescent Probe for the Human Ether-a-go- go-Related Gene Potassium Channel. Analytical Chemistry. 88 (3), 1511-1515, (2016).

Liu, Y., Wang, P., Fernando, K. S., LeCroy, G. E., Maimaiti, H., Miller, B., Lewis, W. K., Bunker K. E., Hau, Z., Sun, Y. P., Enhanced fluorescence properties of carbon dots in polymer films', Journal of Materials Chemistry C. 4(29), 6967–6974, (2016).

Luo, X., Davis, J. J., Electrical biosensors and the label free detection of protein disease biomarkers, Chem. Soc. Rev, 42, 5944-5962, (2013).

Lovegrove, F.E., Tangpukdee, N., Opoka, R.O., Lafferty, E.I., Rajwans, N., *et al.* Serum angiopoietin-1 and -2 levels discriminate cerebral malaria from uncomplicated malaria and predict clinical outcome in African children. PLoS ONE 4, e4912, (2009).

Lindblade, K.A, Steinhardt, L., Samuels, A., Kachur, S.P., Slutsker, L., The silent

threat: asymptomatic parasitaemia and malaria transmission. Expert Rev Anti Infect. 11, 623–39. (2013).

Lucchi, N. W., Jain, V., Wilson, N. O., Singh, N., Udhayakumar, V., and Stiles, J. K., Potential serological biomarkers of cerebral malaria. Dis. Markers 31, 327–335, (2011).

Lukianova-Hleb Y. E., Campbell M. K., Constantinou E. P., Braam J., Olson S. J., *et al.* Hemozoin-generated vapor nanobubbles for transdermal reagent- and needle-free detection of malaria, PNAS, 900–905, 111:3, (2014).

Lynn, A., Chandra, S., Malhotra, P., Chauhan, V.S., Heme binding and polymerization by *Plasmodium falciparum* histidine rich protein II: Influence of pH on activity and conformation. FEBS Lett. 459, 267–271, (1999).

Ma, K. S., Zhou, H., Zoval, J., Madou, M., DNA hybridization detection by label free versus impedance amplifying label with impedance spectroscopy. Sens. Actuators, B,114, 5, (2006).

MacRae, J. I., Dixon, M. W., Dearnley, M. K., Chua, H. H., Chambers, J. M., Kenny, S., Bottova, I., Tilley, L., and McConville, M. J., Mitochondrial metabolism of sexual and asexual blood stages of the malaria parasite *Plasmodium falciparum*. BMC Biol. 11, 67, (2013).

Malica, L., Kirk, A. G., Integrated miniaturized optical detection platform for fluorescence and absorption spectroscopy. Sensors and Actuators A: Physical.135 (2),515-524, (2006).

Martin, S.K., Rajasekariah, G.H., Awinda, G., Waitumbi, J., Kifude, C., Unified parasite lactate dehydrogenase and histidine-rich protein ELISA for quantification of *Plasmodium falciparum.* Am. J. Trop. Med. Hyg. 80, 516–522, (2009).

Martinez, A.W., Phillips, S.T., Whitesides, G.M. Diagnostics for the developing world: microfluidic paper-based analytical devices. Anal. Chem. 82, 3–10 (2010).

Martinez, A.W., Phillips, S.T., Carrilho, E., Iii, S.W.T., Sindi, H., Whitesides, G.M., Simple Telemedicine for Developing Regions : Camera Phones and Paper-Based Microfluidic Devices for Real-Time , Off-Site Diagnosis. Anal. Chem. 80, 3699–3707, (2008).

Malleret, B., Claser, C., Ong A.S.M., Suwanarusk,R., Sriprawat, K., *et al.* A rapid and robust tri-color flow cytometry assay for monitoring malaria parasite development. Scientific reports. 1,118, (2011).

Maltha, J., Gamboa, D., Bendezu, J., Sanchez, L., Cnops, L., *et al*. Rapid diagnostic tests for malaria diagnosis in the Peruvian Amazon: Impact of pfhrp2 gene deletions and cross reactions. PLoS ONE 7, e43094, (2012).

Maltha, J., Gillet, P., Bottieau, E., Cnops, L., Esbroeck, M. van, *et al.* Evaluation of a rapid diagnostic test (CareStartTM Malaria HRP-2/pLDH (Pf/pan) Combo Test) for the diagnosis of malaria in a reference setting. Malar. J. 9, 171, (2010).

Markwalter F. C., Davis M. K., Wright W. D, Immunomagnetic capture and colorimetric detection of malarial biomarker *Plasmodium falciparum* lactate dehydrogenase, Anal. Biochem., 493, 30e34, (2015).

Markwalter, C.F., Ricks, K.M., Bitting, A.L., Mudenda, L., Wright, D.W., Simultaneous capture and sequential detection of two malarial biomarkers on magnetic microparticle, Talanta. 161, 443–449, (2016).

Margaret A. P, Jeremy N. B., Rob H. H., Manyando, C., Wesley, C. V., Timothy N. W.,. Malaria. Nature Reviews Disease Primers. 3, (2017). doi:10.1038/nrdp.2017.50

Marangoni, K., Neves, A.F., Rocha, R.M., Faria, P.R., Alves, P.T., et al. Prostate specific RNA aptamer: promising nucleic acid antibody-like cancer detection. Sci. Rep. 5, 12090, (2015).

Mariette, N., Barnadas, C., Bouchier, C., Tichit, M., Menard, D., Country-wide assessment of the genetic polymorphism in *Plasmodium falciparum* and *Plasmodium vivax* antigens detected with rapid diagnostic tests for malaria. Malar. J. 7, 219, (2008).

Mason, D.P., Kawamoto, F., Lin, K., Laoboonchai, A., Wongsrichanalai, C., A comparison of two rapid field immunochromatographic tests to expert microscopy in the diagnosis of malaria. Acta Trop. 82, 51–59, (2002).

Matsudaira, P., Sequence from picomole quantities of proteins electroblotted onto polyvinylidene difluoride membranes. Biological Chemistry, 262(21), 10035–10038, (1987).

Mavrothalassitis, G., Tzimagiorgis, G., Mitsialis, A,, Zannis, V. I., Plaitakis, A., Papamatheakis, J. ,Moschonas, N. K., Isolation and characterization of cDNA clones encoding human liver glutamate dehydrogenase: evidence for a small gene family Proc. Nut1 Acud Sci. 85 (10), 3494-3498, (1988).

Mawili-Mboumba, D.P., Akotet, M.K.B., Ngoungou, E.B., Kombila, M., Evaluation of rapid diagnostic tests for malaria case management in Gabon. Diagn. Micr. Infec. Dis. 66, 162–168, (2010).

Mayxay, M., Pukrittayakamee, S., Chotivanich, K., Looareesuwan, S., White, N.J., Persistence of *Plasmodium falciparum* HRP-2 in successfully treated acute *falciparum* malaria. Trans. R. Soc. Trop. Med. Hyg. 95, 179–182, (2001).

Mirsky, V. M.; Riepl, M.; Wolfbeis, O. S., Capacitive monitoring of protein immobilization and antigen-antibody reactions on monomolecular alkylthiol films on gold electrodes Biosens. Bioelectron, 12, 977, (1997).

McBirney, S. C., Chen, D., Scholtz, A., Ameri, H., Armani, A. M., Rapid Diagnostic for Point-of-Care Malaria Screening, ACS Sens, 3, 1264−1270, (2018)

McKenzie, F.E., Prudhomme, W.A., Magill, A.J., Forney, J.R., Permpanich, B., Lucas, C., Gasser, Jr., R.A., Wongsrichanalai, C., White Blood Cell Counts and Malaria. J. Infect. Dis. 192, 323–330, (2005).

Melancon, M.P., Zhou, M., Zhang, R., Xiong, C., Allen, P., *et al.* Selective uptake and imaging of aptamer- and antibody-conjugated hollow nanospheres targeted to epidermal growth factor receptors overexpresses in head and neck cancer. ACS Nano. 8, 4530-4538, (2014).

McMorrow, M.L., Masanja, M.I., Kahigwa, E., Abdulla, S.M.K., Kachur, S.P., Quality assurance of rapid diagnostic tests for malaria in routine patient care in rural Tanzania. Am. J. Trop. Med. Hyg. 82, 151–155, (2010).

McKeague, M. and DeRosa, C.M., Challenges and Opportunities for Small Molecule Aptamer Development. J. Nucleic Acids.2012:748913, (2012).

Mens F. P., Matelon J. R., Nour Y. M. B., Newman M. D., Schallig H., Laboratory evaluation on the sensitivity and specificity of a novel and rapid detection method for malaria diagnosis based on magneto-optical technology (MOT), Malar. J., 9:207, (2010).

Miller L.H., Ackerman H.C., Su X.Z., Wellems T.E., Malaria biology and disease pathogenesis: insights for new treatments. Nat Med. 19(2):156-67. doi: 10.1038/nm.3073, (2013).

Min, K., Cho, M., Han, S.Y., Shim, Y.B., Ku, J., *et al.* A simple and direct electrochemical detection of interferon-γ using its RNA and DNA aptamers. Biosens. Bioelectron. 23, 1819–1824, (2008).

Miranda, F. G., Feng, L., Shiu, S.C.-C., Dirkzwager, R.M., Cheung, Y.-W., Tanner, J.A., Schöning, M.J., Offenhäusser, A., Mayer, D., Aptamer-based electro- chemical biosensor for highly sensitive and selective malaria detection with ad- justable dynamic response range and reusability. Sens. Actuators B Chem. 255, 235–243, (2018).

Miyashita, Y., Good A. G., Glutamate deamination by glutamate dehydrogenase plays a central role in amino acid catabolism in plants. Plant Signal. Behav. 3, 842–843, (2008).

Mfonkeu, P. J., Gouado, I., Fotso, K. H., Zambou, O., Zollo, A., *et al*. Elevated Cell-Specific Microparticles Are a Biological Marker for Cerebral Dysfunctions in Human Severe Malaria. PLoS ONE. 5(10), (2010).

Moody, A., Rapid diagnostic tests for malaria parasites. Clin. Microbiol. Rev. 15, 66–78, (2002).

Mondal, S., Thirupathi, R., Atreya, S. H., Carbon Quantum Dots as a Macromolecular Crowder. J. Name. 00, 1-3, (2012).

Monera, O. D., Sereda, T. J., Zhou, N. E., Kay, C. M., Hodges, R., Relationship of sidechain hydrophobicity and alpha-helical propensity on the stability of the single-stranded amphipathic alpha-helix.J. Protein Sci. 1: 319-329, (1995).

Morassin, B., Fabre, R., Berry, A., Magnaval, J.F., One year's experience with the polymerase chain reaction as a routine method for the diagnosis of imported malaria. Am. J. Trop. Med. Hyg. 66, 503–508, (2002).

Motaghi, H., Mehrgardi, M. A., Bouvet, P., Carbon Dots-AS1411 Aptamer Nanoconjugate for Ultrasensitive Spectrofluorometric Detection of Cancer Cells. Sci. Rep. 7, 10513, 2017

Mouatcho, J. C., and Goldring, J. P., Malaria rapid diagnostic tests: challenges and prospects. J. Med. Microbiol. 62, 1491− 505, (2013).

Mohammadi, S., Nikkhah, M., Hosseinkhan, S., Investigation of the effects of carbon-based nanomaterials on A53T alpha-synuclein aggregation using a whole-cell recombinant biosensor. Int J Nanomedicine.12, 8831–8840, (2017).

Murillo, S. C., Sheila, A. O., Joseph, F. A., Zuleima, P., Erika, D., Sandra. I., Curtis, S. H., Alexandre, M. O., David, B., Venkatachalam, U. K., Barnwell, J. W., Deletion of *Plasmodium falciparum* histidine-rich protein 2 (pfhrp2) and histidine-rich protein 3 (pfhrp3) genes in Colombian parasites. PLoS One 10 (7), e0131576, (2015).

Nagatoishi, S., Tanaka, Y., Tsumoto, K., Circular dichroism spectra demonstrate formation of the thrombin-binding DNA aptamer G-quadruplex under stabilizing-cation-deficient conditions. Biochem. Biophys. Res. Commun, 352, 812–817, (2007).

Nakatani, Y., Banner, C., Herrath, M. V., Schneider, M. E., Smith, H. H., Freese, E., Comparison of human brain and liver glutamate dehydrogenase cDNAS. Biochem Biophys Res Commun 149:405–410, (1987).

Nandineni, M. R., Laishram, R. S., Gowrishankar, J., Osmosensitivity associated with insertions in argP (iciA) or glnE in glutamate synthase-deficient mutants of *Escherichia coli*. J Bacteriol. 186:6391-6399, (2004).

National vector born disease control and prevention (NVBDCP) report on malaria, 2016 (http://nvbdcp.gov.in/Doc/Annual-report-NVBDCP-2014-15.pdf).

Newman, D. M., Heptinstall, J., Matelon, R. J., Savage, L., Wears, M. L., *et al.* A magneto-optic route toward the in vivo diagnosis of malaria: Preliminary results and preclinical trial data. Biophys. J. 95, 994–1000, (2008).

Newman, D. M., Matelon, R. J., Wears, M. L., Savage, L. B., The in vivo diagnosis of malaria: Feasibility study into a magneto-optic fingertip probe. IEEE J. Sel. Top. Quantum Electron. 16, 573–580, (2010).

Ng, E.W., Adamis, A.P., Anti-VEGF aptamer (pegaptanib) therapy for ocular vascular diseases. Ann. N. Y. Acad. Sci. 1082, 151-171, (2006).

Ngo H. T., Gandra N., Fales A. M., Taylor S. M., Vo-Dinh T., Sensitive DNA detection and SNP discrimination using ultrabright SERS nanorattles and magnetic beads for malaria diagnostics, Biosens. Bioelectron. 81, 8–14, (2016).

Nicastri, E., Bevilacqua, N., Schepisi, M.S., Paglia, M.G., Meschi, S., *et al.* Accuracy of malaria diagnosis by microscopy, rapid diagnostic test, and PCR methods and evidence of antimalarial overprescription in non-severe febrile patients in two Tanzanian hospitals. Am. J. Trop. Med. Hyg. 80, 712–717, (2009).

Noedl, H., Yingyuen, K., Laoboonchai, A., Fukuda, M., Sirichaisinthop, J., *et al.* Sensitivity and specificity of an antigen detection ELISA for malaria diagnosis. Am. J. Trop. Med. Hyg. 75, 1205–1208, (2006).

Noland, G.S., Briones, N., Sullivan Jr., D.J., The shape and size of hemozoin crystals distinguishes diverse *Plasmodium* species. Mol. Biochem. Parasitol. 130, 91–99, (2003).

Odijk, M., van der Wouden, E., Olthuis, W., Ferrari, M., Tolner, E., van den Maagdenberg, A., van den Berg, A., Microfabricated solid-state ion-selective electrode probe for measuring potassium in the living rodent brain: compatibility with dc-eeg recordings to study spreading depression. Sens. Actuators B: Chem. B 207, 945–953, (2015).

Ohnoa, R., Ohnukia, H., Wanga, H., Yokoyamaa,T., Endob, H., *et al.* Electrochemical impedance spectroscopy biosensor with interdigitated electrode for detection of human immunoglobulin A. Biosens. Bioelectron. 40.422-426, (2013).

Oliveira, M.F., Silva, J.R., Dansa-Petretski, M., Souza, W. de Lins, U., *et al*. Haem detoxification by an insect. Nature. 400, 517–518, (1999).

Olszewski, K.L., Llinás, M., Central carbon metabolism of *Plasmodium* parasites. Mol. Biochem. Parasitol. 175, 95–103, (2011).

Omodeo-Salè, F., Motti, A., Dondorp, A., Nicholas J. W., Taramelli, D., Destabilisation and subsequent lysis of human erythrocytes induced by *Plasmodium falciparum* haem products. Eur. J. Haematol. 74, 324–332, (2005).

Pagola, S., Stephens, P.W., Bohle, D.S., Kosar, A.D., Madsen, S.K., The structure of malaria pigment β-haematin. Nature. 404, 307–310, (2000).

Palmer, C.J., Lindo, J.F., Klaskala, W.I., Quesada, J.A., Kaminsky, R., *et al.* Evaluation of the OptiMAL test for rapid diagnosis of *Plasmodium vivax* and *Plasmodium falciparum* malaria. J. Clin. Microbiol. 36, 203–206, (1998).

Parekh, P., Kamble, S., Zhao, N.X., Portier, B.P., Zu, Y.L. Immunotherapy of CD30-expressing lymphoma using a highly stable ssDNA aptamer. Biomaterials. 34, 8909-8917, (2013).

Parra, M.E., Evans, C.B., Taylor, D.W., Identification of *Plasmodium falciparum* histidine-rich protein 2 in the plasma of humans with malaria. J Clin Microbiol. 29, 1629–1634, (1991).

Park, J. W., Saravan K. S., Niazi, J. H., Gurbuz, Y., Youn, B. S., Gu, M. B., Rapid and sensitive detection of Nampt (PBEF/visfatin) in human serum using an ssDNA aptamer-based capacitive biosensor. Biosens. Bioelectron. 38, 233–238, (2012).

Paul K. B., Kumar S., Tripathy S., Vanjari S. R. K., Singh V., *et al.* A highly sensitive self-assembled monolayer modified copper doped zinc oxide nanofiber interface for detection of *Plasmodium falciparum* histidine-rich protein-2: targeted towards rapid, early diagnosis of malaria, Biosens. Bioelectron. 80, 39–46, (2016).

Peng, Y., Wu, J., Wang, J., Li, W., Yu, S., Study and evaluation of Wondfo rapid diagnostic kit based on nano-gold immunochromatography assay for diagnosis of *Plasmodium falciparum*. Parasitol. Res. 110, 1421–1425, (2012).

Peng W. K., Kong T. F., Ng C. S., Chen L., Huang Y., *et al.*, Micromagnetic resonance relaxometry for rapid label-free malaria diagnosis, Nature Medicine 20, 1069–1073, (2014).

Pethig, R., Kell, D., The passive electrical properties of biological systems: their significance in physiology, biophysics and biotechnology. Phys. Med. Biol. 32, 933-970, (1987).

Pirnstill W. C., Coté L. G., Malaria diagnosis using a mobile phone polarized microscope, Sci. Rep., 5:13368, (2015).

Piper, R., Lebras, J., Wentworth, L., Hunt-Cooke, A., Houzé, S., *et al.* Immunocapture diagnostic assays for malaria using *Plasmodium* lactate dehydrogenase (pLDH). Am. J. Trop. Med. Hyg. 60, 109–118, (1999).

Pologe, L.G., Pavlovec, A., Shio, H., Ravetch, J.V., Primary structure and subcellular localization of the knob-associated histidine-rich protein of *Plasmodium falciparum*, Proc. Natl. Acad. Sci. U. S. A, 84, 7139–7143, (1987).

Popenda, M., Szachniuk, M., Antczak, M., Purzycka, K. J., Lukasiak, P., Bartol, N., Blazewicz, J., Adamiak, R. W., Automated 3D structure composition for large RNAs. Nucleic Acids Res. 40, 1–12, (2012).

Potyrailo, R.A., Murray, A.J., Nagraj, N., Pris, A.D., Ashe, J.M., *et al.* Towards maintenance-free biosensors for hundreds of bind/release cycles. Angew. Chem. Int. Ed. Engl. 54, 2174-2178, (2015).

Pui, T. S., Kongsuphol, P., Arya, S. K., Bansal, T., Detection of tumor necrosis factor (TNF-α) in cell culture medium with label free electrochemical impedance spectroscopy. Sens. Actuators B: Chem. 181, 494–500, (2013).

Queen, S. A., Vanderjagat, D., Ryes, P., Properties and substrate specificity of purine phosphorribosyl transferase from human malaria parasite *Plasmodium falciparum*, mole. And Biochem. Parsit. 30, 123-134, (1988).

Radom, F., Jurek, P.M., Mazurek, M.P., Otlewski, J., Jeleń, F., Aptamers: molecules of great potential. Biotechnol. Adv. 31, 1260-1274, (2013).

Rakotonirina, H., Barnadas, C., Raherijafy, R., Andrianantenaina, H., Ratsimbasoa, A., *et al.* Accuracy and reliability of malaria diagnostic techniques for guiding febrile outpatient treatment in malaria endemic countries. Am. J. Trop. Med. Hyg. 78, 217–221,(2008).

Ragavana, K. V., Kumar, S., Swaraj, S., Neethirajana, S., Advances in biosensors and optical assays for diagnosis and detection of malaria, Biosen. Bioele. 105, 188–210, (2018).

Raman, J., Ashok, C. S., Sujay, I. N. S., Anand, R. P., Senthamizh, T. S., Balram, H., *Plasmodium falciparum* hypoxanthine guanine phosphoribosyltransferase. J. FEBS, 272, 1900-1911, (2005).

Ranadive, N., Kunene, S., Darteh, S., Ntshalintshali, N., Nhlabathi, N., Dlamini, N., Chitundu, S., Saini, M., Murphy, M., Soble, A., Schwartz, A., Greenhouse, B., Hsiang, M.S., Limitations of rapid diagnostic testing in patients with suspected malaria: A diagnostic accuracy evaluation from Swaziland, a low-endemicity country aiming for malaria elimination. Clin. Infect. Dis. 64, 1221–1227, (2017).

Rebelo M., Sousa C., Shapiro M. H., Mota M. M., Grobusch P. M., *et al*. A Novel Flow Cytometric Hemozoin Detection Assay for Real-Time Sensitivity Testing of *Plasmodium falciparum*, Plos One, 8: 4, e61606, (2013).

Richardson, D.C., Ciach, M., Zhong, K.J.Y., Crandall, I., Kain, K.C., Evaluation of the Makromed dipstick assay versus PCR for diagnosis of *Plasmodium falciparum* malaria in returned travelers. J. Clin. Microbiol. 40, 4528–4530, (2002).

Rickert, J.; Gopel, W.; Beck, W.; Jung, G.; Heiduschka, P., A 'mixed' self-assembled monolayer for an impedimetric immunosensor. Biosens. Bioelectron. 11, 757, (1996).

Robert, W. S., Carlos, A. G., Abdisalan, M. N., Hla, Y. M., Simon I. H., The global distribution of clinical episodes of *Plasmodium falciparum* malaria. Nature, 434, 214-15, **(2005).**

Robert W. S., Global malaria eradication and the importance of *Plasmodium falciparum* epidemiology in Africa. BMC Medicine,13:23, (2015).

Rodríguez, A., Domínguez, N. G., Aguilar, I., Girón, M. E., Characterization of *Plasmodium falciparum* glutamate dehydrogenase-soluble antigen. Braz. J. Med. Biol. Res. 31, 1149–1155, (1998).

Rogier, E., Plucinski, M., Lucchi, N., Mace, K., Chang, M., Lemoine, J.F., *et al.* Beadbased immunoassay allows sub-picogram detection of histidine-rich protein 2 from *Plasmodium falciparum* and estimates reliability of malaria rapid diagnostic tests. PLoS One. 12, e0172139, (2017).

Rohrbach, F., Karadeniz, H., Erdem, A., Famulok, M., Mayer, G., Label-free impedimetric aptasensor for lysozyme detection based on carbon nanotube-modified screen-printed electrodes. Anal. Biochem. 421, 454–459, (2012).

Roth, E., *Plasmodium falciparum* carbohydrate metabolism - a connection between hostcell and parasite. Blood Cells. 16, 453–460, (1990).

Rothe, F. Jr., Calvin, M. C., Max-Audit, I., Rosa, J., Rosa, R., The enzymes of the glycolytic pathway in erythrocytes infected with *Plasmodium falciparum* malaria parasites.Blood 72, 1922–1925, (1988).

Rohrbach, F., Karadeniz, H., Erdem, A., Famulok, M., Mayer G., Label-free impedimetric aptasensor for lysozyme detection based on carbon nanotube-modified screen-printed electrode, Anal Biochem. 15;421(2):454-9, (2012).

Sachs, J.D., Malaney, P., The economic and social burden of malaria. Nature 415, 680–685, (2002).

Santero, E., Hervas A. B., Canasa I., Govantes F., Glutamate dehydrogenase Enzymology, Physiological role and Biotechnological relevance, DOI: 10.5772/47767. (2012).

Salentin, S., Schreiber, S., Haupt, V. J., Adasme, M. F., Schroeder, M. PLIP: fully automated protein–ligand interaction profiler. Nucleic Acids Res. 43, W443-447 (2015).

Schmidt, M.T., Schaechter, M., Topics and ecological and environmental microbiology. Academic press. p584, (2011).

Schuck P., Size distribution analysis of macromolecules by sedimentation velocity ultracentrifugation and Lamm equation modeling. Biophysical Journal, 78, 1606–1619, (2000).

Schneidman, D. D., Inbar, Y., Nussinov, R., Wolfson, H. J., PatchDock and SymmDock: Servers for rigid and symmetric docking. Nucleic Acids Res. 33, 363–367, (2005)

Schoning, M.J., Poghossian, A., Recent advances in biologically sensitive field effect transistors (biofets). Analyst 127, 1137–1151, (2002).

Shashidharan, P., Michaeiidis, T. M., Robakis, N. K., Kresovali, A., Papamatheakis, J. & Plaitakis, A., Novel human glutamate dehydrogenase expressed in neural and testicular tissues and encoded by an X-linked intronless gene. J. Bioi. Clzenz. 269, 16971-16976, (1994).

Schmidt, E., Schmidt, F. W., Glutamate dehydrogenase, in Methods of Enzymatic Analysis, Vol. 3, 3rd edit. Verlag Chemie, Weinheim , pp. 216-227, (1983).

Schneider E.L., Marletta M.A., Heme binding to the histidine-rich protein II from *Plasmodium falciparum*. Biochemistry. 44(3):979-86, (2005).

Scarano, S., Mascinia, M., Turner, A.P.F., Minunnia, M., Surface plasmon resonance imaging for affinity-based biosensors. Biosens. Bioelectron. 25 (5), 957–966, (2010).

Seol, B., Shin, H. I., Kim, J. Y., Jeon, B. Y., Kang, Y. J., Pak, J. H., Kim, T. S., Lee, H. W., Sequence conservation of *Plasmodium vivax* glutamate dehydrogenase among Korean isolates and its application in seroepidemiologyMalar. J. 16, 3, (2017).

Sessions, R.B., Dewar, V., Clarke, A.R. and Holbrook, J., A model of *Plasmodium falciparum* lactate dehydrogenase and its implications for the design of improved antimalarials and the enhanced detection of parasitaemia. Protein. Eng. 10,301-6, (1997).

Siegel, K. R. L., Müller, J. G., Lottspeich, F. & Schirmer, R. H. Glutathione reductase and glutamate dehydrogenase of *Plasmodium falciparum*, the causative agent of tropical malaria, Eur. J. Biochem. 235, 3452350, (1996).

Sikarwar B., Sharma P. K., Srivastava A., Agarwal G. S., Boopathi M., *et al.* Surface plasmon resonance characterization of monoclonal and polyclonal antibodies of malaria for biosensor applications, Biosens. Bioelectron. 60, 201–209, (2014).

Singh, N., Saxena, A., Awadhia, S.B., Shrivastava, R., Singh, M.P., Evaluation of a rapid diagnostic test for assessing the burden of malaria at delivery in India. Am. J. Trop. Med. Hyg. 73, 855–858, (2005).

Singh, N. K., Chakma, B., Jain, P., Goswami, P., Protein-Induced Fluorescence Enhancement Based Detection of *Plasmodium falciparum* Glutamate Dehydrogenase Using Carbon Dot Coupled Specific Aptamer. ACS Comb. Sci. doi:10.1021/acscombsci.8b00021, (2018a).

Singh, N. K., Arya, S. K., Estrela, P., Goswami, P., Capacitive malaria aptasensor using *Plasmodium falciparum* glutamate dehydrogenase as target antigen in undiluted human serum. Biosens. Bioelectron. doi:10.1016/j.bios.2018.06.022, (2018b).

Sharma J., Yeh H. C., Yoo H., Werner J. H., Martinez J. S., Silver nanocluster aptamers: in situ generation of intrinsically fluorescent recognition ligands for protein detection, Chem. Commun. 47, 2294–2296, (2010).

Sharma, M.K., Rao, V.K., Agarwal, G.S., Rai, G.P., Gopalan, N., *et al.* Highly sensitive amperometric immunosensor for detection of *Plasmodium falciparum* histidine rich protein 2 in serum of humans with malaria: comparison with a commercial kit. J. Clin. Microbiol. 46, 3759–3765, (2008).

Sharma, M.K., Rao, V.K., Merwyn, S., Agarwal, G.S., Upadhyay, S., *et al.* A novel piezoelectric immunosensor for the detection of malarial *Plasmodium falciparum* histidine rich protein-2 antigen. Talanta. 85, 1812–1817, (2011).

Shear, H.L., Wanidworanun, C.C., Nagel, R.L., Antisense oligonucleotides targeting

malarial aldolase inhibit the asexual erythrocytic stages of *Plasmodium falciparum*," Mol. Biochem Parasitol. 102, 91–101, (1999).

Sherman, I. W., Biochemistry of *Plasmodium (*malarial parasites). Microbiol Rev 43, 453–495, (1979).

Shin, H. I, Kim, J.Y., Lee, W.J., Sohn, Y., Lee, S.W., Kang, Y.J., Lee, H.W., Polymorphism of the parasite lactate dehydrogenase gene from *Plasmodium vivax* Korean isolates. Malar. J. 12, 1, (2013).

Shoemark, D.K., Cliff, M.J., Sessions, R.B., Clarke, A.R., Enzymatic properties of the lactate dehydrogenase enzyme from *Plasmodium falciparum*. FEBS J. 274, 2738–2748, (2007).

Song H.O., Lee, B., Bhusal, R.P., Park, B., Yu, K., *et al.* Development of a Novel Fluorophore for Real-Time Biomonitoring System, Plos One. 7, e48459, (2012).

Shoorideh, K., Chui, C. O., On the origin of enhanced sensitivity in nanoscale FET based biosensors. Proc. Natl. Acad. Sci. 111, 5111–5116, (2014).

Slater, A. F., Swiggard, W. J., Orton, B. R., Flitter, W. D., Goldberg, D. E., *et al.* An iron carboxylate bond links the heme units of malaria pigment. Proc. Natl. Acad. Sci. USA. 88, 325–329, (1991).

Smith, E. L., Austin, B. M., Blumenthal, K. M., Nyc, J. F., Glutamate dehydrogenase. In: Boyer, P.D. (Ed.), The Enzymes, vol. 11. Academic Press, New York, pp. 293–367, (1975).

Solomonov, I., Osipova, M., Feldman, Y., Baehtz, C., Kjaer, K., *et al.* Crystal nucleation, growth, and morphology of the synthetic malaria pigment β-hematin and the effect thereon by quinoline additives: The malaria pigment as a target of various antimalarial drugs. J. Am. Chem. Soc. 129, 2615–2627, (2007).

Srivastava, I.K., Schmidt, M., Certa, U., Döbeli ,H., Perrin, L.H., Specificity and inhibitory activity of antibodies to *Plasmodium falciparum* aldolase. J. Immunol. 144:1497– 503, (1990).

Stern, E., Wagner, R., Sigworth, F. J., Breaker, R., Fahmy, T. M., Reed, M. A., Importance of the Debye screening length on nanowire field effect transistor sensors. Nano Letters 7 (11), 3405–3409, (2007).

Stillman, T. J., Baker, P. J., Britton, K. L. & Rice, D. W. Conformational flexibility in glutamate dehydrogenase. Role of water in recognition and catalysis, J. Mol. Biol. 234, 1131-1139, (1993).

Stoltenburg, R., Nikolaus, N., Strehlitz, B., Capture-SELEX: Selection of DNA Aptamers for Aminoglycoside Antibiotics. J. Anal. Methods. Chem. 2012, 415697, (2012).

Storm, J., Perner, J., Aparicio, I., Patzewitz, E. M., Olszewski, K., Llinas, M., Engel, P. C., Müller, S., *Plasmodium falciparum* glutamate dehydrogenase a is dispensable and not a drug target during erythrocytic development. Malar. J. 10, 193, (2011).

Stoeva, S.I.; Lee, J.S.; Smith, J.E.; Rosen, S.T.; Mirkin, C.A. Multiplexed detection of protein cancer markers with biobarcoded nanoparticle probes. J. Am. Chem. Soc. 128, 8378- 8379, (2006).

Stryer, L., Berg, J. M., Tymoczko, J. L., Biochemistry (5th ed.), New York: W. H. Freeman, ISBN 0716746840, (2002).

Sui, Y., Potula, R., Dhillon, N., Pinson, D., Li, S., *et al.* Neuronal apoptosis is mediated by CXCL10 overexpression in simian human immunodeficiency virus encephalitis. Am. J. Pathol. 164, 1557–1566, (2004).

Sun, S.K, Tu, K.X., Yan, X.P., An indicator-displacement assay for naked-eye detection and quantification of histidine in human urine. Analyst. 137, 2124-8, (2012).

Sun, X., Lei, Y., Fluorescent carbon dots and their sensing applications, TrAC Trends Anal. Chem. 89,163-180, (2017).

Tangpukdee N., Duangdee C., Wilairatana P., Krudsood S., Malaria Diagnosis: A Brief Review. Korean J Parasitol. 47, No. 2: 93-102, (2009).

Tarasov, A., Gray, D.W., Tsai, M.-Y., Shields, N., Montrose, A., Creedon, N., Lovera, P., O'Riordan, A., Mooney, M.H., Vogel, E.M., A potentiometric biosensor for rapid on-site disease diagnostics. Biosens. Bioelectron. 79, 669–678, (2016)

Tesauro, C., Juul, S., Arnò, B., Nielsen, C. J., Fiorani, P., Frøhlich, R. F., Andersen, F.F., Desideri, A., Stougaard, M., Petersen, E., *et al*. Specific detection of topoisomerase I from the malaria causing *P. falciparum* parasite using isothermal Rolling Circle Amplification. Conference of the IEEE Engin. in Med. and Bio. Soc. (EMBC), (2012).

Thiviyanathan, V., Gorenstein, D.G., Aptamers and the next generation of diagnostic reagents. Proteomics Clin Appl. 6(0), 563–573, (2012).

Thomas, P. D., Basus, V. J., James, J., Protein solution structure determination using distances from two-dimensional nuclear Overhauser effect experiments: effect of approximations on the accuracy of derived structures. PNAS,88 (4), 1237-1241, (1991).

Tjitra, E., Suprianto, S., Dyer, M., Currie, B.J., Anstey, N.M., Field evaluation of the ICT malaria *P.f/P.v* immunochromatographic test for detection of *Plasmodium falciparum* and *Plasmodium vivax* in patients with a presumptive clinical diagnosis of malaria in Eastern Indonesia. J. Clin. Microbiol. 37, 2412–2417, (1999).

Tjitra, E., Suprianto, S., McBroom, J., Currie, B.J., Anstey, N.M., Persistent ICT malaria *P.f/P.v* panmalarial and HRP2 antigen reactivity after treatment of *Plasmodium falciparum* malaria is associated with gametocytemia and results in false positive diagnoses of Plasmodium vivax in convalescence. J. Clin. Microbiol. 39, 1025–1031, (2001).

Tkac, J., Davis, J. J., Engineering the Bioelectronic Interface: Applications to Analyte Biosensing and Protein Detection. The Royal Society of Chemistry, 193–224, (2009).

Trape, J. F, Pison, G., Spiegel, A., Enel, C., Rogier, C., Combating malaria in Africa, Trends Parasitol. 18, 224-30, (2002).

Trampuz A., Jereb M., Muzlovic I., Prabhu R.M., Clinical review: Severe malaria, Crit. Care, 7, 315-323, (2003).

Tuerk, C., Gold, L. Systematic evolution of ligands by exponential enrichment: RNA ligands to bacteriophage T4 DNA polymerase. Science. 4968, 505-510 (1990).

Uguen, C., Rabodonirina, M., De Pina, J.J., Vigier, J.P., Martet, G., *et al.* ParaSight-F rapid manual diagnostic test of *Plasmodium falciparum* infection. Bull World Health Organ. 73, 643–649, (1995).

Ullman, B., Carter, D., Hypoxanthine-guanine phosphoribosyl transferase as a therapeutic target in protozoal infections. Infect. Agents. Dis. 4, 29–40, (1995).

Uskoković, V., Castiglione, Z., Cubas, P., Zhu, L., Li, W., Habelitz, S., Zeta-potential and Particle Size Analysis of human amelogenins. J. Dent. Res. 89(2), 149–153, (2010).

Uthman, O. A., Saunders, R., Sinclair, D., *et al.* Safety of 8-aminoquinolines given to people with G6PD deficiency: protocol for systematic review of prospective studies. BMJ Open, 4:e004664, (2014).

Vaidya, A. B., Mather, M. W., Mitochondrial evolution and functions in malaria parasites. Annu. Rev. Microbiol. 63, 249–267 (2009).

Vander Jagt, D. L., Intress, C., Heidrich, J. E., Mrema, J. E. K., Rieckmann, K. H., Heidrich, H. G. Marker enzymes of *Plasmodium falciparum* and human erythrocytes as indicators of parasite purity, J. Parasitol. 68, 1068-1071, (1982).

Valle, M.R., Quakyi, I.A., Amuesi, J., Quaye, J.T., Nkrumah, F.K., *et al.* Detection of antigens and antibodies in the urine of humans with *Plasmodium falciparum* malaria. J. Clin. Microbiol. 29, 1236–1242, (1991).

Viana, G. R., Akinyi, O. S, Silva, F. L, Lima, B. D, Macedo, O. A, Goldman, I. F., Histidine-rich protein 2 (*pfhrp2*) and *pfhrp3* gene deletions in *Plasmodium falciparum* isolates from select sites in Brazil and Bolivia. PLoS ONE 12 (3), e0171150, (2017).

Wang, L., Veselinovic, M., Yang, L., Geiss, B. J., Dandy, D. S., Chen, T., A sensitive DNA capacitive biosensor using interdigitated electrodes. Biosens. and Bioel, 87, 646-653, (2017).

Wang, S., Ge, L., Song, X., Yu, J., Ge, S., Huang, J., Zeng, F., Paper-based chemiluminescence ELISA: lab-on-paper based on chitosan modified paper device and wax-screen-printing. Biosens. Bioelectron. 31, 212-218, 2012.

Wagner, J.T., Ludeman, H., Farber., P.M., Lottspeich, F., Krauth–Siegel, R.L., Glutamate dehydrogense, the marker protein of *Plasmodium falciparum* : cloning, expression and characterization of malarial enzyme. Eur. J .Biochem . 258, 813-819, (1998).

Wenisch, C., Spitzauer, S., Florris-Linau, K., Rumpold, H., Vannaphan, S., *et al.* Complement Activation in Severe *Plasmodium falciparum* malaria. Clin. Immunol. Immunopathol. 85, 166–171, (1997).

Werner, C., Stubbs, M. T., Krauth-Siegel, R. L., Klebe, G., The crystal structure of *Plasmodium falciparum* glutamate dehydrogenase, a putative target for novel antimalarial drugs. J. Mol. Biol. 349, 597−607, (2005).

Wellems, T.E., Howard, R.J., Homologous genes encode two distinct histidine-rich proteins in a cloned isolate of *Plasmodium falciparum*. Proc. Natl. Acad. Sci. USA 83, 6065–6069, (1986).

Wells, B. D., Circular Dichroism Estimate of Secondary Structure of Glutamate Dehydrogenase. J. Mol. Biol. 97, 391-394 391–394, (1975).

Williams, P., Brown, M. R. W., Influence of iron-restriction on growth and the expression of outer membrane proteins by Haemophilus influenza and H. para@uenzae. FEMS Microbio. Lett. 33, 153-157, (1986).

Wongsrichanalai, C., Barcus, M.J., Muth, S., Sutamihardja, A., Wernsdorfer, W.H., A review of malaria diagnostic tools: microscopy and rapid diagnostic test (RDT). The Am. J. Trop. Med. Hyg. 77, 119 –127, (2007).

World Malaria Report, 2016, (http://apps.who.int/iris/bitstream/10665/252038/1/9789241511 711-eng.pdf?ua=1).

World Malaria Report, 2017, (http://apps.who.int/iris/bitstream/handle/10665/259492/9789241565523eng.pdf;jsessionid=A4C5C23F098C4F9177749B660F842307?sequence=1).

Wu, Y. X., Young, J., Kwon, J., Aptamers: The "evolution" of SELEX, 106, 21-28, (2016).

Wu, X., Tian, F., Wang, W., Chen, J., Wu, M., Zhao, J. X., Fabrication of highly fluorescent graphene quantum dots using L-glutamic acid for in vitro/in vivo imaging and sensing. J. Mater. Chem. C. Mater. Opt. Electron. Devices. 1, 4676–4684, (2013).

Xiong, X.L., Lv, Y.F., Chen, T., Zhang, X.B., Wang, K.M., *et al.* Nucleic acid aptamers for living cell analysis. Annu. Rev. Anal. Chem (Palo Alto Calif). 7, 405-426 (2014).

Xiao Y., Patolsky F., Katz E., Hainfeld J. F., Willner I., "Plugging into enzymes": Nanowiring of redox enzymes by a gold nanoparticle. Science, 21, 1877-1881, (2003).

Yang, Q., Goldstein, I.J., Mei, H.Y., Engelke, D.R. DNA ligands that bind tightly and selectively to cellobiose. Proc. Natl. Acad. Sci. U S A. 95, 5462-5467 (1998).

Yang, S. J., Huh, J. W., Lee, J. E., Choi, S. Y., Kim, T. U., Cho, S.W., Inactivation of human glutamate dehydrogenase by aluminum. Cell. Mol. Life Sci. 2003, 60, 2538–2546, (2003).

Yeo S.J., Huong D.T., Han J.H., Kim J.Y., Lee W.J., *et al.* Performance of coumarin derived dendrimer-based fluorescence-linked immunosorbent assay (FLISA) to detect malaria antigen. Malar. J.13,266, (2014).

Yoo, S. H., Albanesi, J. P., Ca2(+)-induced conformational change and aggregation of chromogranin A. J. Biol. Chem. 265, 14414 –14421, (1990).

Yraola, A. H., Bakhit S.M., Franke P., Weise C., Schweiger M., Jorcke D., Ziegler M.,. Regulation of glutamate dehydrogenase by reversible ADP-ribosylation in mitochondria.EMBO J., 20. 2404–2412, (2001).

Yamauchi, K. The sequence flanking translational initiation site in protozoa, Nucleic Acids Res. 19,2715-2720, (1991).

Yue, Q., Hou, Y., Yue, S., Du, K., Shen, T., Wang, L., Xu, S., Li, H., Liu, J., Construction of an off-on fluorescence system based on carbon dots for trace pyrophosphate sensing. J Fluoresc. 25(3),585-94, (2015).

Yuen C., and Liu Q., Magnetic field enriched surface enhanced resonance Raman spectroscopy for early malaria diagnosis, Journal of Biomedical Optics 17(1), 017005, (2012).

Zaganas I., Kanavouras, K., Mastorodemos V., Latsoudis H., Spanaki C., Plaitakis A., The human GLUD2 glutamate dehydrogenase: localization and functional aspects Neurochem Int, 55, pp. 52–63, (2009).

Zaganas, I., Spanaki, C., Plaitakis, A., Expression of human GLUD2 glutamate dehydrogenase in human tissues: Functional implications. Neurochem. Int. 61, 455−462, (2012).

Zhang B., Chan Y., Lu B., Diamond M., Klein R., CXCR3 mediates region-specific antiviral T cell trafficking within the central nervous system during west nile virus encephalitis, J. Immunol,180:2641-2649, (2008).

Zheng, Q., Lavis, D. L., Development of photostable fluorophores for molecular imaging. Cur. Opin. Chem. Bio. 39:32–38, (2017).

Zuo, J., Jiang, T., Zhao, X., Xiong, X., Xiao, S., Zhu, Z., Preparation and Application of Fluorescent Carbon Dots. J. Nanomater. 787862, (2015).

Zuker M., Mfold web server for nucleic acid folding and hybridization prediction. Nucleic Acids Research, 31(13), 3406–3415, (2003).

Publications and Patents

Put your heart, mind and soul
into even your smallest acts.
This is the secreat of success....

- Swami S. Saraswati

List of Publications

Publications in refereed journals

Naveen K Singh, Sunil K Arya, Pedro Estrela, Pranab Goswami Capacitive malaria aptasensor using *Plasmodium falciparum* glutamate dehydrogenase as target antigen in undiluted human serum, Biosensors and Bioelectronics, https://doi.org /10.1016 /j. bios.2018.06.022 (2018).

Naveen K Singh, Babina Chakma, Priyamvada Jain, P Goswami*, Protein induced fluorescence enhancement based detection of *P. falciparum* glutamate dehydrogenase using carbon dot coupled specific aptamer. ACS Combinatorial Science, 20 (6), 350–357 (2018).

Naveen K. Singh, Phurpa Dema Thungoan, Pedro Estrela, Pranab Goswami, Development of an aptamer based BioFET sensor for quantitative detection of *Plasmodium falciparum* glutamate dehydrogenase in serum samples. Biosensor and Bioelectronics. https:// doi.org/10.1016/j.bios.2018.09.085

Naveen K. Singh, Priyamvada Jain, Smita Das, Pranab Goswami, Dye coupled aptamer-captured enzyme catalysed reaction for detection of pan specific and *P. falciparum* malaria in laboratory set-up and instrument–free paper based format. Under review in "Analytical Chemistry".

Somasekhar R. Chinnadayyala, Mallesh Santhosh, **Naveen K. Singh**, Pranab Goswami. Alcohol oxidase protein mediated *in-situ* synthesized and stabilized gold nanoparticles for developing amperometric alcohol biosensor. ***Biosens Bioelectron*** (2015) 69:155-161

Kuldeep Gupta, Rini Dhawan, Mithilesh Kajla, B Jnanasiddhy, Singh, **Naveen K. Singh,** Lalita Gupta. Molecular Identification and Colonization of Yellow Fever Mosquito *Aedes aegypti* (Diptera: Culicidae) Isolated from Rajasthan Region, India. **Journal of vector borne diseases** 53(2):149-155 · June 2016.

Mallesh Santhosh, Somasekhar R. Chinnadayyala, **Naveen K. Singh,** Pranab Goswami***.**Human serum stabilized gold nanocluster act as electron transfer bridge supporting specific electrocatalysis of Bilirubin useful for biosensing application. **Bioelectrochemistry**, 111, 7–14 (2016).

Priyamvada jain, Babina Chakma, **Naveen K. singh**, Pranab Goswami. Aptamer against Lactate dehydrogenase stablised nanoparticle for Malaria Diagnosis. **Molecular biotechnology**, 58 (7): 497–508 (2016)

R. Bhuvanasundar, R. N. Naresh Kumar, **Naveen K. Singh**, K. Coral, P. R. Deepa, K. N. Sulochana*. Physico - chemical characterization of human Lysyl Oxidase enzyme and study on its structural stability. (Communicated)

Babina Chakma, Priyamvada jain, **Naveen K. Singh**, Pranab Goswami. Development of indicator displacement based detection of malaria targeting HRP-II as biomarker for application in point of care and analystical settings. **Anal chem,** 88 (20): 10316-10321 (2016)

Priyamvada Jain, Babina Chakma, **Naveen K. Singh**, Sanjukta Patra, Pranam Goswami, Metal-DNA interactions improve signal in high resolution melting of DNA for species differentiation of *Plasmodium* parasite, Molecular Biotechnology. 59 (6), 179-191, DOI: 10.1007/s12033-017-0004-0 (2017)

Babina Chakma, Priyamvada Jain, **Naveen K. Singh**, P Goswami, Development of Electrochemical Impedance Spectroscopy Based Malaria Aptasensor Using HRP-II as Target Biomarker, Electroanalysis, https://doi.org/10.1002/elan.201800142 (2018).

Babina Chakma, **Naveen K. Singh**, Priyamvada Jain, and Pranab Goswami, Quantitative detection of histidine-rich proteins using silver nanoparticle-based sensitive competitive binding assay. (Under review).

Patents filed

Pranab Goswami, **Naveen Kumar Singh**, Priyamvada Jain, Babina Chakma (2016). Title of the invention: Dna aptamers specifically binding to *Plasmodium falciparum* glutamate dehydrogenase (PFGDHa). Application no. 201631025722.

Pranab Goswami, **Naveen Kumar Singh (2018)**, A novel syringe design to facilitate instrument free detection of NADP/NAD^+ based enzymatic reaction over paper platform following optical signal. Application no. 201831030902.

Abstracts published in conferences

Naveen K Singh, Phurpa D Thungon, Vinay B. "Development of *Plasmodium falciparum* glutamate dehydrogenase based sensor for Malaria" poster Presentation, 19-23 Feb 2017 at International Conference on Advances in Biological Systems and Material Science in NanoWorld (ABSMSNW-2017), IIT BHU.

Naveen K Singh, Vinay B and Pranab Goswami. Carbon dots as peroxidase mimetic catalyst for detection of H_2O_2 and cholesterol. International Conference on Advanced Nanomaterials and Nanotechnology (ICANN)-2017, Organised by Centre for Nanotechnology, IIT Guwahati during 18th Dec-21 Dec (2017).

Naveen K Singh, Pedro Estrela, Pranab Goswami. Development of simple, pragmatic and low cost aptasensor for malaria diagnosis. International Conference on Advancement in Science and Technology (ICAST-2018) 3-4 September, 2018 organized by JSPS society, Japan at Visva-Bharati, Santiniketan-731235,West Bengal, India.

Naveen K Singh, Pedro Estrela, Pranab Goswami, The aptaFET sensor for malaria diagnosis. Second International conference of engineering science and technology, ICONSEA-2018, 4-6 October, Jawaharlal Nehru Engineering and Technology, Hyderabad.

Pooja Rani Kuri, **Naveen K Singh**, Pranab Goswami. C Dots aptamer conjugate based detection of *Plasmodium falciparum* for malaria diagnosis. International Conference on Advancement in Science and Technology (ICAST-2018) 3-4 September, 2018 organized by JSPS society, Japan at Visva-Bharati, Santiniketan-731235,West Bengal, India.

Sanjeev Kumar, Lalita Gupta, Mithilesh Kajla, **Naveen K Singh**. Modulation of mosquito immunity during *Plasmodium* development**.** Poster (S1301M03) presented at the XXIV International Congress of Entomology (ICE 2012) held at Daegu Korea from 19th to 25th August, 2012.

Somasekhar R. Chinnadayyala**,** Mallesh Santhosh, **Naveen K Singh,** Pranab Goswami* (**2014**). National conference in New Advances and Horizons in Nanoscience and Nanotechnology, 20-21th December, held at IASST Guwahati, Assam, India

R.Bhuvansunder,M Arun, **Naveen K Singh**. Characaterization of Human Lysyl Oxidase (LOX) and development of novel peptides to inhibit its activity. Poster presented at International Confrence held at KIIT Bhubhenshwer.

Mallesh Santhosh**, Naveen K Singh**. HAS stabilized gold nanocluster supporting specific electrocatalysis of bilirubin useful for biosensing application.Poster presented at Reserch conclave, 17-20th March, IIT Guwahati.

Phurpa D Thungon, **Naveen K Singh**. "Study of peroxidase mimicking of nanoscience for development of alchohol biosensor" IUMRS-ICYRAN.

Babina Chakma, Priyamvada Jain, **Naveen. K. Singh** and P. Goswami*, Label-free colorimetric detection of histidine rich proteins using glutathione functionalized silver nanoparticles probe. International conference on sophisticated instruments in Modern Research, Organized by CIF, IIT Guwahati during 30th June-1stJuly,(2017)

Phurpa Dema Thungon, **Naveen K Singh**, Pranab Goswami, Study of Peroxidase mimicking agents/ Nanoenzymes for development of alcohol biosensors, IUMRS-International Conference of Young Researchers on Advanced Materials (IUMRS-ICYRAM 2016) organized by Materials Research Society of India (MRSI) and Indian Institute of Science Bangalore, held at Indian Institute of Science Bangalore, India, during December 11-15. Conference proceeding page No. 128

Awards and achievements

Selected for **Newton-Bhabha PhD placement grant-2017** organized by British council and Department of biotechnology, under part of PhD research work performed at **University of Bath, United Kingdom for 6 months under the supervison of Dr. Pedro Estrela.**

Received **Third prize** with prize money Rs 20,000 in **North East Bio start talent search contest,** conduct by Guwahati Biotech Park during 2018.

Received **travel grant** for **Shastri Indo Canadian International Conference** held in New Delhi, 7-8 July 2018.

Recevied **best poster award** in International Conference on Advancement in Science and Technology (ICAST-2018) 3-4 September, 2018 organized by JSPS society, Japan at Visva-Bharati, Santiniketan-731235,West Bengal, India.

Selected for **Third round (Expert selection committee) in Biotechnology ignition grant, BIG-13** organised by BIRAC India.

Technical article published in **North East Bioline magazine** 4th Edition by us.

Our work "capacitance based aptasensor for malaria detection" (doi.org /10.1016 /j. bios.2018.06.022) was highlighted in Current science magazine (October edition).

Appendix

Table A1: List of bacterial strains

Strain	Description
Escherichia coli DH5α (Novagen)	F'ϕ80dlacZΔM15 Δ (lacZYA-argF) U169 endA1 recA1 hsdR17 (rk^-mk^+) deoR thi-1 phoA supE44 λ^- gyrA96 relA1
Escherichia coli BL21 (DE3) (Novagen)	F^- ompT hsdSB ($rB^- mB^-$) gal dcm (DE3). Derivation of B834. (Parental strain: B834; Resistance: none)
Escherichia coli BL21 (DE3) pLysS(Novagen)	F-ompT gal dcm(DE3) hsdSB($rB^- mB^-$) pLysS(Cam^R)

Table A2: Culture medium for bacteria

Medium Composition	**Composition**
Luria Bertani broth (LB) (1 L)	Casein enzymic hydrolysate 10 g, Yeast extract 5 g, NaCl 10 g, pH 7.5 + 0.2
Luria Bertani Agar (LB) (1 L)	Casein enzymic hydrolysate 10 g, Yeast extract 5 g, NaCl 10 g, Agar 15 g, pH 7.5 ± 0.2

Table A3: Buffers and solutions

Table A 3.1: Solutions for plasmid isolation

Solution I	50 mM glucose, 25 mM Tris-Cl buffer, 10 mM EDTA, pH 8.0
Solution II	0.2 N NaOH, 1 % SDS
Solution III	5 M potassium acetate, pH adjusted to 4.8 with acetic acid

Table A 3.2: Buffer for agarose gel electrophoresis

TAE buffer (50X) 1L	242 g Tris base, 57.1 ml glacial acetic acid, 100 ml 0.5 M EDTA (pH 8), adjust final volume to 1L with water

Table A 3.3: Solution for competent cell preparation

Transformation and storage solution (TSS)	10 % (w/v) polyethylene glycol, 5 % (v/v) dimethyl sulfoxide and 50 mM $MgCl_2$ in LB broth, pH 6.5

Table A 3.4: Buffers for protein purification

Lysis Buffer	50 mM potassium phosphate buffer, 30 mM NaCl, 0.2 mg/ml Lysozyme pH 8 (for *Pf*GDH) 50 mM Tris, NaCl 50 mM , Urea 8 M, 1mM DTT, 1% Tween 20, 0.2 mg/ml Lysozyme, PMSF 1mM, pH 7.4 (for *H*GDH)
Washing buffer	50 mM potassium phosphate buffer, 30 mM NaCl, supplemented with varying concentration of imidazole (20 mM, and 50 mM), pH 8 (for *Pf*GDH) 50 mM Tris, NaCl 50 mM , Urea 8 M, 1mM DTT, 1% Tween 20, 10 mM Imdiazole, pH 7.4 (for HGDH)
Elution buffer	50 mM potassium phosphate buffer, 30 mM NaCl, 300 mM imidazole (for *Pf*GDH) 50 mM Tris, NaCl 50 mM , Urea 8 M, 300 mM Imdiazole, pH 7.4 (for HGDH)

Table A 3.5: Buffers/solutions for SDS-PAGE

30 % acrylamide-bisacrylamide gel solution (100 ml)	29.2 g acrylamide, 0.8 g bisacrylamide
Tris-HCl, pH 6.8, 0.5 M (100 ml)	6.06 g Tris base, pH adjusted to 6.8 with 2 N HCl
Tris-HCl, pH 8.8, 1.5 M (100 ml)	18.18 g of Tris base, pH adjusted to 8.8 with 2 N HCl
Gel running buffer (10X)	30.0 g of Tris base, 144.0 g of glycine, and 10.0 g of SDS in 1000 ml of water.
SDS gel loading buffer (2X)	100 mM Tris/HCl (pH 6.8), 4 % (w/v) SDS, 0.2% (w/v) bromophenol blue dye, 20 % (v/v) glycerol, 200 mM DTT or β-mercaptoethanol
Staining solution (blue silver	10 ml ortho phosphoric acid, 10 g w/v ammonium

staining) (100 ml)	sulfate, 0.12 g w/v

Table A 3.6: Composition of Biuret solution

Biuret solution	1.50 g of cupric sulfate pentahydrate ($CuSO_4.5H_2O$) with 6.0 g sodium potassium tartrate tetrahydrate ($NaKC_4H_4O_64.H_2O$) in 500 ml of H_2O. Add 300 ml 10 % (w/v) NaOH and make the volume to 1 litre with water

Table A 3.7: Solutions for SELEX

Binding buffer	50 mM potassium phosphate buffer, pH 8.0, 50 mM NaCl, 5 mM KCl, 2.5 mM $MgCl_2$
Coupling buffer	20 mM Tris HCl, pH 7.5, 0.5 M NaCl, 1 mM EDTA
TBE buffer (5X)	54 g of Tris base, 27.5 g of boric acid, 20 mL of 0.5 M EDTA (pH 8.0)
10 % acrylamide bisacrylamide Gel solution (75:1), 15 ml	5 ml of 30 % acrylamide-bisacrylamide solution (75:1), 3 ml, TBE buffer (5X), 105 µl 10 % APS, 10 µl TEMED, 6.8 ml water

Table A 3.8: FET Measurement Buffer

FET measurement Buffer	10 mM Potassium phosphate buffer, 5 mM NaCl, 5 mM KCl and 2.5 mM $MgCl_2$, pH 8.0

Table A 3.9: Buffers used for DECAMAL

Coupling Buffer	10 mM TrisCl, 100 mM NaCl, pH 7.5,
Binding Buffer	50mM potassium phosphate buffer, 5mM NaCl, 5mM KCl, 2.5mM $MgCl_2$, pH 8.0
Cocktail Buffer	Lactate-50mM, Glutamate-10mM, APAD-1mM, NADP-0.2mM, Resazurin-0.40mM, Phenazinetho sulphate- 0.37mM in 50mM potassium phosphate buffer

Table A4: List of primers

Name	Sequence (5'-3')
F1	CACCTAATACGACTCACTATAGCGGA
R1	GCAAGCTTGTTCGAGCCAG
R1-biotin	biotin-GCAAGCTTGTTCGAGCCAG
*Pf*GDH (forward)	CCG*GGATCC*ATGAGTGCTCTTAAAGACAAAACG
*Pf*GDH (reverse)	CCG*CTCGAG*TTAAAAACAACCTTGTTCAATATATGATTC
HGDH (forward)	TA*CATATG*ATGTACGCTACCTGGGCGAAG
HGDH (reverse)	TCGA*CTCGAG*CTATGTGAAGGTCACACCG

Table A5: PCR reaction mixture

Reaction mixture components	volume used
2X Taq Red Mix	12.5 µl
Forward primer	1 µl
Reverse primer	1 µl
DNA template	20-30 ng
Nuclease free water	For solution to make final volume 25 µl

Table A 5.1: PCR reaction condition

PCR steps	Temperature and Time for *Pf*GDH	Temperature and Time for HGDH	Cycle
Initial denaturation	95 °C for 5 min	95 °C for 5 min	1
Denaturation	94 °C for 1 min	94 °C for 5 min	35
Annealing	47 °C for 1 min	59 °C for 1.15 min	35
Extension	60 °C for 1.5 min	72 °C for 1.5 min	35
Final extension	72 °C for 10 min	72 °C for 10 min	1
Store	4 °C for ∞ min	4 °C for ∞ min	

Table A6: Components ligation and digestion setup for cloning

Reaction mixture components	Volume used
2X Rapid ligation buffer	5 µl
pGEMT easy vector	50 ng
PCR product	50 ng
T4 DNA ligase (3 weiss unit)	1 µl
Nuclease free water for volume makeup	10 µl

Components of digestion mixture	Amount
Cut smart buffer	5 µl
Restriction endonuclease (20 units.µl^{-1})	1 µl
Restriction endonuclease (20 units.µl^{-1})	1 µl
DNA template	~1 µg
Nuclease free water	50 µl to make final volume

Component of ligation reaction	Amount
Insert DNA (~1 kb)	32.5 ng (0.06 pmole)
Linearized Plasmid DNA,5.4 kb (pET 28a, vector Novagen)	65.2 ng (0.02 pmole)
2 x Quick ligation buffer	12.5 µl
T4 DNA ligase	1 µl
Nuclease free water	To make final volume 25 µl

Figure B1: Cloning and expression vector map